

Dynamic effect of Young's modulus on attachment and differentiation of mouse embryonic stem cells

Shahzad Ali

2015

University College London

Thesis submitted for the degree of Doctor of Philosophy (PhD) in
Biochemical Engineering

Declaration

'I, Shahzad Ali confirm that the work presented in this thesis is my own. Where information has been derived from other sources, I confirm that this has been indicated in the thesis.'

A handwritten signature in black ink, appearing to read "Shahzad Ali".

Abstract

Embryonic stem cells have generated much interest due to their ability to differentiate into any cell type within the body. This ability could potentially allow for scientists and engineers to develop a number of therapies for diseases, which currently have no cure such as Parkinson's disease, Alzheimer's disease and diabetes. However, the differentiation process itself is one of the major bottlenecks in developing potential therapies. Currently protocols involve the use of mixtures of growth factors in order to create a suitable soluble microenvironment for differentiation. These growth factors are often expensive, thereby limiting the potential for scale-up of cell bioprocesses. Much interest has thus been generated into other elements of the microenvironment that could improve differentiation efficiency. The field of mechanobiology in particular, has developed rapidly in recent years.

The aim of this thesis was to investigate the effect of Young's modulus on neuronal differentiation of mouse embryonic stem cells (mESC's). Instead of treating differentiation as one long process, the decision was made to split the process into three stages. The first, involved the formation of neural precursors from mESC's. This was followed by the formation of immature neurons from neural precursors. The final stage was to allow the immature neurons to develop into a mature neuronal subtype. The impact of Young's modulus was split into three effects. One was the initial attachment of cells. The second was the expansion of cells into colonies. The third was the effect of Young's modulus on enrichment of neuronal cells.

It was found that physiologically soft materials favoured the formation of all three neuronal cell types (precursor, immature and mature). However, the exact effect of differentiation varied over the course of differentiation. Over the first and second stages, soft substrates favoured the initial attachment of cells without affecting enrichment. Over the final stage, however, soft substrates directly favoured maturation of immature neurons, without having a significant effect upon their attachment. Thus the effect of Young's modulus on neuronal differentiation changes according to the level of cellular maturity.

There have not been any previous studies, which have tried to characterise the effect of the mechanical microenvironment on differentiation in a stage-by-stage manner. These findings have many important implications in terms of regenerative medicine bioprocessing. Firstly the optimal conditions for cellular attachment are not always the same as the optimal conditions for increasing cell enrichment. By carefully fine-tuning the mechanical properties at each stage of differentiation, both cell yields and final enrichment could be increased substantially. Furthermore, different cell types will require different optimisation strategies. Finally, by better understanding the interaction between cells and their mechanical environment, these findings could allow for better future design of tissue engineering biomaterials for implantation of cells into target areas for cell therapies.

Acknowledgements

I would like to thank my primary supervisor Dr Farlan Veraitch (Dept. of Biochemical Engineering, University College London, London, UK) for his invaluable help and advice throughout my project. I would also like to thank my secondary adviser Dr Ivan Wall (Dept. of Biochemical Engineering, University College London, London, UK) for his support. Furthermore, I would like to thank Dr Andrew Pelling (The Pelling Lab, University of Ottawa, Ottawa, Canada) for providing the GXG substrate synthesis method and Young's modulus data.

Furthermore, I would like to give my most heartfelt appreciation to all the members of the regenerative medicine laboratory, including Kate, Tristan, Rui, Amelia, Owen, Giulia, John, Vishal, Zuming, Carlotta, Iwan and Ben.

Above all, I would like to thank Nathalie, my parents and Azeem for their constant, unwavering support and love throughout my time at UCL.

On a separate note, I would like to thank Drake, Lana Del Rey and the many other artists on my music playlists. Without their creativity and inspiration, long hours of data analysis would not have been nearly the same.

This work was supported by the Engineering and Physical Sciences Research Council (EPSRC) and Innovative Manufacturing Research Centre (IMRC).

Table of Contents

Acknowledgements.....	5
List of Figures.....	10
Nomenclature.....	13
<i>1.1 Embryonic Stem Cells</i>	14
<i>1.2 Neuronal Differentiation</i>	16
1.2.1 In Vertebrate Development	16
1.2.1.1 Neural Induction and Formation of the Neural Tube	16
1.2.1.2 Dorsal-Ventral Patterning.....	17
1.2.1.3 Antero-Posterior Patterning.....	18
1.2.1.4 Neuronal Migration	18
1.2.2 Neurogenesis in Adult Brain	19
1.2.3 Neuronal Development <i>in vitro</i>	19
1.2.3.1 Neuronal Development in Adherent Monoculture.....	20
1.2.3.2 Effect of microenvironment upon neuronal differentiation	21
<i>1.3 Mechanotransduction</i>	22
1.3.1 Known Mechanotransduction Mechanisms and Associated Components	25
1.3.1.1 Integrins and Focal Adhesions	25
1.3.1.2 Actin Cytoskeleton	26
1.3.1.3 Non Muscle Myosin II.....	27
1.3.1.4 Rho/ROCK and ERK Regulation.....	27
1.3.1.5 Microtubules.....	28
1.3.1.6 Intermediate Filaments	28
1.3.1.6 Ezrin/Radixin/Moesin (ERM)	28
1.3.1.7 Cytoskeletal-Nuclear Interaction.....	29
<i>1.4 Effect of material properties on cells</i>	30
1.4.1 Effect of material properties on fibroblasts.....	30
1.4.2 Effect of material properties upon mesenchymal stem cells	31
1.4.3 The effect of material properties upon cardiomyocytes	32
1.4.4 Effect of material properties upon myoblasts.....	33
1.4.5 Effects of material properties upon endothelial cells	34
1.4.7 Effect of material properties on bone.....	34
1.4.8 Effect of material properties upon the malignant phenotype	35
1.4.9 Effect of material properties on neural development and growth	35
1.4.9.1 Effect of material properties on neural stem cells and neural precursor cells	36
1.4.9.2 The effect of material properties on primary neuronal cultures.....	37
1.4.9.3 Effect of material properties on glial cells	38
1.4.9.4 Effect of extracellular matrix stiffness upon neuroblastoma differentiation.....	39
1.4.10 Effect of material properties on pluripotent stem cells	39
1.4.11 Materials Used in Studies.....	41
1.4.12 GXG	41
<i>1.5 Aims and Objectives of Investigation</i>	43
2 Materials and Methods.....	45
<i>2.1 Cell Culture.....</i>	45
2.1.1 Mouse Embryonic Stem Cells (MESC's)	45
2.1.2 Mouse Embryonic Fibroblasts	46
2.1.3 Human EB Retinal Differentiation	46

2.2 GXG Preparation	47
2.3 Neuronal Differentiation	49
2.3.1 MESC	49
2.3.2 Partially-differentiated Cells	51
2.4 Attachment and Expansion Studies	52
2.4.1 Phase Contrast Microscopy.....	52
2.4.2 Image Analysis.....	53
2.5 Immunocytochemistry Analysis	53
2.5.1 Preparation – Fixation, Permeabilisation and Blocking.....	53
2.5.2 Antibody Staining.....	54
2.6 Flow Cytometry	56
2.6.1 Preparation.....	56
2.6.2 Analysis.....	57
2.7 qPCR.....	58
2.8 Blebbistatin and Nocodazole Inhibition	65
2.8.1 Blebbistatin.....	65
2.8.2 Nocodazole	65
2.9 Rate of Spreading	65
2.10 Statistics	66
3 GXG and Protocol Development	67
3.1 Aims.....	67
3.2 How does medium composition affect attachment of mESC's in neuronal differentiation medium?	68
3.3 How does seeding density affect attachment of mESC's in neuronal differentiation medium?	73
3.4 Validation of starting cell populations and neuronal differentiation marker expression	75
3.5 Assay validation for flow cytometry and qPCR.....	81
3.5.1 PSA-NCAM negative control	81
3.5.2 qPCR Internal Control Gene Selection	83
3.6 The effect of GXG Young's modulus on attachment of mouse fibroblasts	85
3.7 Effect of Young's modulus on attachment and phenotype of human embryoid bodies in neuronal differentiation medium	87
3.8: Effect of Young's modulus on mESC attachment and expansion in normal pluripotent growth medium and undirected differentiation medium	90
3.8.1 Effect of Young's modulus on mESC attachment and expansion in normal pluripotent growth medium.....	90
3.8.2 Effect of Young's modulus on attachment and expansion of mESC's in spontaneous differentiation medium	94
3.9 Summary of Findings	97
4 Does Young's modulus affect attachment and phenotype of mouse embryonic stem cells?.....	98
4.1 Aims.....	98
4.2 Does Young's modulus influence attachment and early expansion of mESC'S?	99
4.2.1 Does Young's modulus influence attachment of mESC's in neuronal differentiation medium?	99

4.2.2 Does Young's modulus influence expansion of mESC's in neuronal differentiation medium?	102
4.3 Does Young's modulus affect the morphology or phenotype of cells formed after four days of mouse embryonic stem cell differentiation in N2B27 medium?	105
4.3.1 Does Young's modulus affect the morphology of cells formed after four days of mESC differentiation in N2B27 medium?	105
4.3.2 Does Young's modulus affect neural precursor or immature neuron formation from mESC's in neuronal differentiation medium?	111
4.3.3 Does Young's modulus enrich populations of neural precursors during mESC differentiation in N2B27 medium?	119
4.3.4 Does Young's modulus affect gene expression during mESC differentiation in N2B27 medium?	122
4.4 Is the favourable attachment of mESC's on soft materials dependent on stress fiber stabilization or microtubule formation?	128
4.5 Summary of Findings	135
5 Does Young's modulus affect attachment and phenotype of partially-differentiated mouse embryonic stem cells differentiated in N2B27 medium?	136
5.1 Aims	136
5.2 Does Young's modulus influence attachment and early expansion of partially-differentiated cells?	137
5.2.1 Does Young's modulus affect attachment of partially-differentiated cells in N2B27 medium?	138
5.2.2 Does Young's modulus affect expansion of partially-differentiated cells in N2B27 medium?	140
5.3 Does Young's modulus affect the initial rate of spreading of partially-differentiated cells?	144
5.4 Does Young's modulus affect the phenotype of cells formed after four days of neuronal precursor differentiation in N2B27 medium?	147
5.4.1 Does Young's modulus affect the formation of immature neurons from partially-differentiated cells in N2B27 medium?	147
5.3.2 Does Young's modulus affect yield of PSA-NCAM positive cells following differentiation in N2B27 medium?	149
5.4.3 Does Young's modulus influence mature neuronal gene expression in partially-differentiated cells after four days of differentiation in N2B27 medium?	152
5.5 Is the attachment of partially-differentiated cells influenced by inhibition of stress fiber stabilization or microtubule formation?	157
5.5.1 Is the improved attachment of partially-differentiated cells on soft materials related to F-actin stress fiber polymerization?	157
5.4.2 Is the improved attachment of partially-differentiated cells on soft materials related to microtubule formation?	162
5.5 Does Young's modulus affect the attachment and expansion of partially-differentiated neurons maturing in N2B27 medium?	165
5.5.1 Does Young's modulus affect the attachment of partially-differentiated neurons maturing in N2B27 medium?	166
5.4.2: Does Young's modulus influence the expansion of partially-differentiated neurons undergoing maturing in N2B27 medium?	168
5.5 Does Young's modulus affect the maturation of partially-differentiated neurons in N2B27 medium?	170
6 Conclusions and Future Work	174
6.1 Conclusions	174

<i>6.2 Future Work</i>	178
7 References	181

List of Figures

Figure 1.1: Outline of the known early, mid and late neural markers used for phenotype determination.....	22
Figure 1.2: Elasticities of various mammalian tissues.....	24
Figure 1.3: A comparison between GXG and other materials, based upon their preparation and components.....	42
Figure 2.1: Media components for normal mESC culture.....	45
Figure 2.2: The relationship between gelatin concentration and Young's modulus of GXG.....	47
Figure 2.3: Medium components used to formulate 200 mL of N2B27 neuronal differentiation medium.....	49
Figure 2.4: Primary antibodies used for immunocytochemistry analysis.....	55
Figure 2.5: Primer assays used for qPCR analysis.....	64
Figure 3.1: Comparison of cell attachment and 96h expansion in three different medium formulations.....	69
Figure 3.2: The effect of serum concentration on attachment and expansion.....	72
Figure 3.3: Comparison of cell concentration at two different seeding densities.....	74
Figure 3.4: Immunocytochemistry analysis of starting populations for key pluripotency markers.....	76
Figure 3.5: Time-lapse immunocytochemistry analysis for validation of neuronal differentiation in N2B27 medium.....	78
Figure 3.6: PSA-NCAM Flow cytometry analysis in undifferentiation mESC's.....	82
Figure 3.7: qPCR internal control gene stability test.....	84
Figure 3.8: Phase contrast and confluency analysis for fibroblasts seeded on GXG	86
Figure 3.9: Human EB's seeded on three different GXG materials.....	88
Figure 3.10: Confluency at 24h and 72h for mESC's seeded on GXG in GMEM with LIF.....	91

Figure 3.11: Confluence at 24h and 72h for mESC's seeded on GXG in GMEM without LIF.....	96
Figure 4.1: Phase contrast images and confluency measurements at 24h for mESC's seeded on GXG in N2B27 medium.....	101
Figure 4.2: Confluency at 72h for mESC's seeded on GXG in N2B27.....	104
Figure 4.3: Phase contrast images showing cell morphology at day four on GXG	106
Figure 4.4A: Relating D4 morphologies to Nestin immunocytochemistry.....	107
Figure 4.4B: Relating D4 morphologies to Sox17 immunocytochemistry.....	109
Figure 4.4C: Relating D4 morphologies to T-Brachyury immunocytochemistry.....	110
Figure 4.5: Time course analysis for pluripotent markers on GXG.....	112
Figure 4.6: Immunocytochemistry analysis for Ki67.....	115
Figure 4.7: Time course analysis for neural markers on GXG.....	117
Figure 4.8: Total cell concentration at day four on GXG in N2B27.....	121
Figure 4.9: Flow cytometry analysis and PSA-NCAM(+) cell yield on GXG.....	123
Figure 4.10: Changes in gene expression with Young's modulus.....	126
Figure 4.11: Effect of blebbistatin on mESC attachment in N2B27 medium.....	129
Figure 4.12: Immunocytochemistry analysis for F-actin in mESC's.....	130
Figure 4.13: Immunocytochemistry analysis for F-actin with and without blebbistatin inhibition on GXG.....	131
Figure 4.14: Effect of nocodazole on mESC attachment in N2B27 medium.....	133
Figure 4.15: Immunocytochemistry analysis for α-tubulin with and without nocodazole inhibition.....	134
Figure 5.1: Phase contrast images and confluency measurements at 24h for partially-differentiated cells seeded on GXG in N2B27 medium.....	139
Figure 5.2: Confluency at 72h for partially-differentiated cells seeded on GXG.....	142
Figure 5.3: Rate of spreading for partially-differentiated cells seeded on GXG for 6h.....	145

Figure 5.4: Immunocytochemistry analysis for b-III tubulin in partially-differentiated cells on GXG.....	146
Figure 5.5: Total cell concentration at day four on GXG in N2B27.....	148
Figure 5.6: Flow cytometry and PSA-NCAM(+ve) cell yield.....	151
Figure 5.7: Gene expression of mature neuronal and glial markers.....	153
Figure 5.8: Effect of blebbistatin treatment on attachment of partially-differentiated cells on GXG.....	158
Figure 5.9A): Morphological changes with blebbistatin treatment in partially-differentiated cells.....	159
Figure 5.9B-D): Immunocytochemistry analysis for F-actin in partially-differentiated cells with and without blebbistatin on GXG.....	159
Figure 5.10: Effect of nocodazole treatment on attachment of partially-differentiated cells on GXG.....	163
Figure 5.11: Immunocytochemistry analysis for α-tubulin in partially-differentiated cells with and without nocodazole on GXG.....	164
Figure 5.12: Phase contrast images and confluency at 24h for partially-differentiated neurons seeded on GXG in N2B27 medium.....	167
Figure 5.13: Confluency at 72h for partially-differentiated neurons seeded on GXG in N2B27 medium.....	169
Figure 5.14: Immunocytochemistry analysis for b-III tubulin and MAP2 in partially-differentiated neurons differentiated for a further six days on GXG in N2B27.....	174
Figure 5.15: Phase contrast images of partially-differentiated neurons replated from GXG to GXG.....	172

Nomenclature

ANOVA = Analysis of Variance
BMP = Bone Morphogenetic Protein
DAPI = 4',6-Diamidino-2-Phenylindole
DMSO = Dimethyl Sulfoxide
EB = Embryoid Body
ECM = Extracellular Matrix
ERK = Extracellular Signal-Regulated Kinases
ESC = Embryonic Stem Cell
FBS = Fetal Bovine Serum
FGF = Fibroblast Growth Factor
GABA = γ -Aminobutyric Acid
GAD2 = Glutamate Decarboxylase 2
GFAP = Glial Fibrillary Acidic Protein
GMEM = Glasgow Minimum Essential Medium
GXG = Gelatin Crosslinked with Glutaraldehyde
hESC = Human Embryonic Stem Cell
HUVEC = Human Umbilical Vein Endothelial Cell
iPSC = Induced Pluripotent Stem Cell
LIF = Leukemia Inhibitory Factor
MAP2 = Microtubule-Associated Protein
MEF = Mouse Embryonic Fibroblast
mESC = Mouse Embryonic Stem Cell
MSC = Mesenchymal Stem Cell
NaBH₄ = Sodium Borohydride
NMMII = Non-Muscle Myosin II
OCT4 = Octamer-Binding Transcription Factor
PA = Polyacrylamide
PBS = Phosphate Buffer Saline
PDMS = Polydimethylsiloxane
PGK1 = Phosphoglycerokinase
PSA-NCAM = Polysialylated-Neural Cell Adhesion Marker
qPCR = Quantitative Polymerase Chain Reaction
RHB-A = Rory's Home Brew
RN18 = 18S Ribosomal RNA
SGZ = Sub-Granular Zone
Shh = Sonic Hedgehog
SVZ = Sub-Ventricular Zone
TBP = TATA Box Binding Protein
TCP = Tissue Culture Polystyrene
TH = Tyrosine Hydroxylase
UTF1 = Undifferentiated Embryonic Cell Transcription Factor 1
vmlPN = Variable Moduli Interpenetrating Polymer Networks

1 Introduction

1.1 Embryonic Stem Cells

Embryonic stem (ES) cells are capable of unlimited self-renewal *in vitro* (Evans & Kaufman, 1981) and differentiation into any cell lineage from each of the three germ layers (endoderm, ectoderm and mesoderm). Embryonic Stem Cells are derived in culture by the removal and *in vitro* replating of the inner cell mass of blastocysts, 8 days post-fertilisation (Thomson et al., 1998). These cells can then be expanded as a monolayer in adherent culture (on gelatin in the case of mouse ES cells or mitomycin-treated mouse embryonic fibroblasts in the case of human ES cells). When expanded in a suspension culture without gelatin or feeders, embryonic stem cells form cellular aggregates termed embryoid bodies (Itskovitz-Eldor et al, 2000). Embryoid bodies (EB's) contain a mixture of differentiated cells from the three germ layers.

Regenerative medicine is the replacement or generation of cells, tissues and organs damaged by disease in order to restore or establish normal function (Mason & Dunnill, 2008). The ability of embryonic stem cells to differentiate into multiple cell types has generated much interest into potential regenerative medicine applications, including potential therapies for Parkinson's disease (Morizane et al, 2008; Lee et al, 2000; Frilling et al. 2009), diabetes (Soria et al, 2000; Lumelsky et al, 2001) and cardiovascular disease (Kehat et al, 2001; Kehat et al, 2002; Westfall et al, 1998; Min et al, 2002). In the case of Parkinson's disease for example, stem cells could be used to replace populations of dopaminergic neurons, which die in large numbers during the progress of the disease.

The ability of embryonic stem cells to differentiate into any cell type (other than extra-embryonic tissue such as placenta) is termed pluripotency. This is in contrast to multipotency, where cells such as adult stem cells have the potential to form a more limited variety of cells restricted to certain lineages. For example, haematopoietic stem cells, which are isolated from bone marrow (Gunsilius et al, 2001) and used in haematopoietic stem cell transplantation (HSCT), form into blood cells (Lewis &

Trobaugh, 1964). Similarly adult mesenchymal stem cells can only form into a limited range of cell types, including neurons, myoblasts and osteoblasts (Engler et al., 2006).

In addition to lacking pluripotency, differentiated cells also have reduced proliferative capacity compared to stem cells. For example, mature, terminally differentiated neurons do not have the ability to self renew. When neurons are lost in the adult brain, they are replaced by cells from a small sub-population of multipotent neural stem cells in the sub-ventricular and sub-granular zones (Levitin & Kaczmarek, 2002), not by proliferation of neurons.

Induced pluripotent stem cells (iPS cells) are a further source of pluripotent cells. These are reprogrammed somatic cells (for example, fibroblasts), which are able to express various pluripotent stem cell markers in addition to forming cells from the three germ layers (Takahashi & Yamanaka, 2006). Fibroblasts can be induced into iPS cells using lentiviral or (Yu et al., 2007) adenoviral (Stadtfeld, 2008; Zhou et al, 2009) vectors containing genes associated with pluripotency. Induced pluripotent stem cells are not yet a completely viable alternative to embryonic stem cells as the long-term characterization of their stability in culture has yet to be established. However, recent work using cells derived from iPSC's have provided interesting results, including the formation of miniature brain organoids (Lancaster et al, 2013), beating mouse hearts (Lu et al, 2013) and vascularised livers (Takebe et al, 2013).

Mouse embryonic stem cells (mESCs) are frequently used for studying neuronal differentiation and development as their differentiation protocols are relatively well characterised. Mouse embryonic stem cells however are not completely analogous to human embryonic stem cells as they differ in the signalling pathways they use. For example, mouse embryonic stem cells signal through the leukaemia inhibitory factor pathway during pluripotency, whilst human embryonic stem cells do not. However, the overall self-renewal strategy is similar between human and mouse embryonic stem cells (Ginis et al., 2004).

1.2 Neuronal Differentiation

1.2.1 In Vertebrate Development

Overall vertebrate development from an embryo can be considered in four stages (Levitin & Kaczmarek, 2002). The first stage of development is the cleavage of the fertilized egg. The cleavage stage produces a number of identical cells each containing a copy of the genome. The cells of the inner cell mass (which are plated out to form embryonic stem cells) are isolated at this stage of development.

The next stage of development is the patterning, where the cells are allocated to the three germ layers (ectodermal, mesodermal and endodermal). This stage is analogous to the EB stage in ES cells. The cells that are destined to eventually become neuronal cells are found within the ectodermal germ layer. The third stage in development is morphogenesis, during which gastrulation occurs. Gastrulation involves extensive migration of the patterned cells in order to form the main body plan.

The fourth stage of development is differentiation. Differentiation is the process by which cells become structurally and functionally different from each other, forming into specialized tissues (Levitin and Kaczmarek, 2002). The stages involved in neuronal differentiation are outlined below. Within this report, the term ‘neural’ is used to denote any cells or tissue of the central nervous system including neurons, astrocytes and oligodendrocytes, whereas the term ‘neuronal’ specifically refers to neurons.

1.2.1.1 Neural Induction and Formation of the Neural Tube

The cells that undergo neural induction are found in the dorsal layer of the ectodermal tissue. The remaining ventral cells in the ectodermal tissue form the epidermis. The dorsal layer of ectodermal cells thickens to form a region known as the neural plate, from which the nervous system is derived.

The neural plate is formed by the induction of a small group of cells in the neuroepithelium. Induction involves many different types of signalling, including bone morphogenetic protein (BMP) signalling.

BMP is a type of transforming growth factor (TGF- β) protein, of which Nodal and Activin are also examples (Seuntjens et al., 2009). BMP influences differentiation by diverting cells away from the neuronal fate. Neurectodermal specification is encouraged by inhibition of BMP signalling by neural inducer molecules such as Noggin.

Only a small fraction of neural plate cells mature into functional neurons. Their partially differentiated neighbouring cells remain present as multipotent neural stem cells in the adult sub-ventricular (SVZ) and sub-granular (SGZ) zones. Thus neurogenesis is enabled to continue in the adult brain.

As gastrulation reaches its' conclusion, the neural plate is folded in order to form the neural tube. As this occurs, neural crest cells migrate away from the dorsal region of the neural tube. The cells that remain within the neural tube form the central nervous system and become patterned (in terms of identity and gene expression) along the dorso-ventral and antero-posterior axis of the neural tube.

1.2.1.2 Dorsal-Ventral Patterning

Neurons of the central nervous system become specified according to their position relative to the dorsal and ventral regions of the neural tube. This patterning is regulated by BMP and sonic hedgehog (Shh) signalling. These two growth factors act antagonistically to create a dorsal-ventral Shh gradient. The type of neurons formed depends upon Shh concentration. Retinoic acid (a component of the N2B27 medium used in this study, as outlined later) also has an effect on patterning and is secreted by the notochord, a mesodermal rod-like structure that runs along the ventral midline.

1.2.1.3 Antero-Posterior Patterning

FGF (fibroblast growth factor) signalling is the main regulator of neuronal fate along the antero-posterior axis. FGF is secreted by mesodermal tissue and its signalling is graded from a high posterior level to a low anterior levelling. This gradient of FGF signalling gives rise to antero-posterior patterning of Hox gene expression. The expression of Hox genes specifies the identity of the motor neurons.

Thus motor neurons are sub-divided into pools along the dorsal-ventral and antero-posterior axes. The motor neurons within each pool direct axonal growth towards specific target muscles.

1.2.1.4 Neuronal Migration

Neurons extend out processes from the central body called neurites. Neurites are further subdivided into dendrites and axons. Dendrites conduct electrical impulses towards the central cell body (the soma), whilst axons direct electrical impulses away from the soma. During neuronal growth, the region at the end of the axon is known as the neuronal growth cone. The neuronal growth cone directs axonal outgrowth during migration. Growth cones generate traction through retrograde actin flow (Franze & Guck, 2010), generated by myosin IIb activity (these processes are described in more detail later in this Chapter). Migration of the growth cone is based on attractive and repulsive cues. The stiffness of the extra-cellular matrix has a profound effect on growth cone migration (Koch et al, 2012; Flanagan et al, 2002). Growth cones tend to migrate towards more deformable substrates.

Once migration is complete, synapse formation and refinement occurs. During initial synapse formation, more connections are formed than are necessary for normal nerve function. During refinement, excess motor neurons die due to activation of apoptotic pathways (programmed cell death). The surviving neurons then mature to become fully functional adult neurons.

1.2.2 Neurogenesis in Adult Brain

As mentioned before, the creation of neurons continues in the adult brain to replace neurons that die during normal adult function. This process is known as neurogenesis. Neurogenesis occurs from the small populations of neural stem cells in the adult sub-ventricular (SVZ) and sub-granular zones (SGZ) mentioned earlier. These locations are niches for the neural stem cells. Niches are privileged settings for support of self-renewal (Conti et al., 2005) and thus, all stem cells exist within niches *in vivo*.

Cells within the adult sub-ventricular zone are more predisposed towards glial (specifically, astrocytic) differentiation than cells within the developing central nervous system. This may be due to higher expression of epidermal growth factor receptors (EGFR), which causes neural stem cells to become more susceptible to the astrocytic-inducing effects of leukaemia inhibitory factor (LIF). Within *in vitro* culture, mouse embryonic stem cells require the addition of LIF to the growth medium in order to remain undifferentiated. LIF acts through the JAK/STAT signalling pathway (Niwa et al, 1998).

A balance between proliferation and differentiation regulates neural stem cell numbers within the adult niches. In addition to this, programmed cell death (apoptosis) has an effect on balancing stem cell numbers.

1.2.3 Neuronal Development *in vitro*

Mouse embryonic stem cells are maintained undifferentiated in culture through the addition of LIF and serum to the growth medium. Removal of serum leads to spontaneous differentiation. Serum generally has a negative influence on neuronal differentiation due to the presence of BMP4, which inhibits the conversion of mouse embryonic stem cells to neural precursor cells (Finley et al, 1999; Zhang et al, 2010). LIF removal can also cause spontaneous differentiation, forming some populations of neuronal cells (Smukler et al, 2006). Mouse embryonic stem cells can be directed more

accurately towards the neuronal fate *in vitro* by addition of neurogenic growth factors and careful control over the microenvironment.

1.2.3.1 Neuronal Development in Adherent Monoculture

A protocol was developed by Ying et al (2003), based on earlier work by Pachernik et al (2002) that allowed for differentiation of mouse embryonic stem cells into neurons in adherent monoculture. The majority of other neuronal differentiation protocols for mESC's involve the use of EB's (Wichterle & Peljto, 2008; Okada et al, 2008; Lee et al, 2000) or neural EB's (Bouhon et al, 2005). Whilst these protocols do robustly produce populations of neural cells, the three-dimensional nature of EB's prevents some cells from coming into contact with the extracellular matrix. As this study was focused purely on the influence of the cell-matrix interactions, it was desirable to reduce the effects of cell-cell interactions as much as possible.

The Ying et al (2003) protocol involved the use of N2B27, a serum-free medium containing N2 and B27 supplements. The B27 supplement contains retinyl acetate, a naturally occurring form of vitamin A (Brewer et al, 1993). Vitamin A oxidises to form retinoic acid, which promotes neuronal differentiation. Both supplements also contain a variety of growth factors, such as apo-transferrin, which support serum-free growth.

Embryonic stem cells were plated onto gelatin-coated well plates at a cell density of $(0.5\text{-}1.5) \times 10^4$ cells/cm². The medium was then changed every 48 hours. Expression of Sox1 (**Figure 1.1**) increases over the first 4 days of culture in the medium before reaching a plateau, which is maintained until day 8. Sox1 expression then decreases after day 8 as neuronal and glial differentiation occurs (Sox1 is downregulated during neuronal and glial differentiation).

After 48 hours, Oct4 (a transcription factor involved in pluripotency in embryonic stem cells) began to decrease until day 4 of culture. During the same time, expression of nestin increases. Nestin is a type IV intermediate filament that is expressed in the

developing central nervous system by neural precursors (Mokry & Nemecek, 1998). At Day 4, attached neural precursor cells have a ‘rosette’-like morphology.

After Day 4, nestin begins to become downregulated as β III-tubulin expression increases from day 6 to day 8. β III-tubulin is a microtubule filament, which is expressed as neural precursors differentiate into immature neurons (Engler et al, 2006) and extend axonal processes. Beyond day 8, cells differentiate into a variety of cells including mature motor neurons, dopaminergic neurons, astrocytes and oligodendrocytes and express the associated markers for these cells (MAP2, tyrosine hydroxylase, GFAP and Olig2 respectively).

1.2.3.2 Effect of microenvironment upon neuronal differentiation

The examples described above mainly involve the use of media containing various growth factors that favour neuronal commitment. It is likely that other elements of the microenvironment, besides the soluble, also have an effect upon the proliferation and neuronal differentiation of embryonic stem cells. Work carried out by Mondragon et al. (2009) examined the relationship between the oxygen tension in which embryonic stem cells are maintained and the efficiency of neuronal differentiation. It was found that the percentage of cells expressing neuronal markers at the end of the Ying et al. (2003) protocol increased when the local oxygen tension was reduced to a near-physiological hypoxic oxygen tension of 2% from the ambient laboratory oxygen tension of 20%. The increase in yield of the neuronal differentiation process in near-physiological oxygen tensions suggests that control over the oxygen microenvironment may be a crucial factor in increasing purities and yields of the embryonic stem cell differentiation process.

Within current differentiation protocols, cell yield and enrichment are often low due to the mixed populations of undifferentiated and differentiated cells that result post-differentiation. As well as potentially reducing the efficacy of any therapy developed, this raises concerns in terms of cost efficiency, as the usage of resources such as medium and other consumables is high, in relation to the yield of target cells obtained.

The presence of undifferentiated stem cells in any cell therapy to be administered into a patient is also likely to raise safety and regulatory concerns with the Food and Drug Administration (FDA) regarding tumorigenicity (Knoepfler, 2009).

Marker	Early/Mid/Late	Expressed By
Sox1	Early	Early neuroectodermal marker in mouse embryo, neural stem cells
Nestin	Early/Mid	All dividing neuronal populations, neural precursors, neural stem cells
Pax6	Mid	Radial glia, neural stem cell
RC2	Mid	Neural precursor, radial glia, neural stem cells
Vimentin	Mid	Radial glia, neural stem cell
β III tubulin (TuJ1)	Mid/Late	Immature neurons, represent extent of neuronal maturation of neural stem cells (expression increases during their differentiation)
MAP2	Late	Mature neuronal marker
GABA	Late	GABAergic neuronal marker
Tyrosine hydroxylase (TH)	Late	Dopaminergic neuronal marker
GFAP	Late	Astrocyte marker
Olig2	Late	Oligodendrocyte marker

Figure 1.1: Figure outlining known mid, early and late neuronal markers commonly used in phenotype determination within in vitro culture

The Mondragon et al (2009) study suggests that other elements of the microenvironment aside from the soluble may be important in creating a more ideal niche for stem cell neuronal differentiation. Within this study, the influence of the mechanical component of the microenvironment will be investigated.

1.3 Mechanotransduction

It is apparent that mechanical forces have a considerable influence upon cell function and behaviour. The field of mechanobiology involves the study of the molecular responses of cells to mechanical forces (Merryman & Engler, 2009). Cells sense and react to mechanical forces by a process known as mechanotransduction. Cells respond to a variety of different mechanical stimuli, such as the stiffness of the substrate they grow upon, cyclic strain of local contraction and shear due to fluid flow. Individual cells

vary in the ranges and types of forces that they respond to (Tee et al, 2009). For example, the differentiation of stem cells into cardiac and vascular endothelial cells is found to be particularly sensitive to shear due to blood flow (Stolberg & McCloskey, 2009). Some cells, such as those of central nervous system are also more vulnerable to damage from mechanical forces than others. For this reason, the cells of the central nervous system are relatively well protected from injury (Laplaca & Prado, 2009).

A study by Chowdhury et al. (2009) found that soft, embryonic stem cells are more responsive (in terms of their spreading on surfaces) to local cyclic strain than harder, more differentiated cell types. Cell stretching of heart cells has been found to activate cell-signalling pathways that lead to release of Ca^{2+} ions (Prosser et al, 2011).

In this study, it is the mechanical properties of the underlying growth surface, which is of greatest interest. In the *in vivo* environment, adherent cells attach to the surrounding, or underlying extra-cellular matrix. The extra-cellular matrix is a three-dimensional scaffold consisting of various structural proteins, such as fibronectin, collagen, vitronectin and laminin. It has a variety of functions including anchoring cells, providing cell support and sequestering growth factors to control their diffusion (Discher et al., 2009). It also has a role in regulating the migration, growth and survival of cells. For example, fibronectin binding plays a role in the migration and organization of germ layer tissue during gastrulation (Ffrench-Constant et al, 1991).

Another very important characteristic of the extracellular matrix is its elasticity. The elasticity of the extracellular matrix has been found to influence cell shape (Pelham & Wang, 1997), protein expression (Collingsworth et al, 2002), gene expression (Chowdhury et al, 2010), migration speed (Peyton & Putnam, 2005; Lo et al, 2000) and organization (Engler et al., 2008). Different tissues subsequently have different elasticities (Figure 1.2).

Tissue stiffness varies during development (Murayama et al, 2006), ageing (Lee & Oh, 2010) and disease processes (Discher et al., 2009). For example, matrix stiffness is found to increase during glial scarring (Georges et al, 2006) and myocardial infarction

(Engler et al, 2008) whilst it is found to decrease between postnatal and adult brain development (Discher et al, 2009).

Tissue	Elasticity of Tissue (kPa)	Reference
Mouse blastocyst	~3.39	Murayama et al. (2006)
Endoderm	~0.1-0.3	Krieg et al. (2008)
Brain	~0.1-0.8	Keung et al. (2009)
Mesoderm	~0.5-1.0	Krieg et al. (2008)
Nerve	~0.5-1.0	Flanagan et al. (2002)
Smooth Muscle	~5.0-9.0	Engler et al. (2004)
Skeletal Muscle	~8.0-17.0	Engler et al. (2006)
Demineralised Bone	>30.0	Engler et al. (2006)

Figure 1.2: Elasticities of various mammalian tissues

The stiffness, or compliance of the extracellular matrix is usually considered in terms of Young's modulus. Young's modulus, as originally described by Young & Kelland (1845) is a measure of elasticity of a material, defined by the ratio between stress and strain. The unit of measurement is the pascal (Pa) or N/m². Stress is defined as the force exerted on an object divided by the area upon which the force is exerted. Strain expresses the amount of deformation an object experiences under stress. Therefore, elastic modulus describes the amount of force per unit area required to cause a given amount of non-permanent deformation (Keung et al., 2009). Young's modulus only applies as long as the relationship between stress and strain is linear. Before looking at the known effects of material properties on cell function, it is worth reviewing the internal structures that give shape to a cell. In addition to allowing mechanotransduction to occur in response to physical forces, these structures also give shape to cells and allow them to exert forces on materials.

1.3.1 Known Mechanotransduction Mechanisms and Associated Components

The complete mechanism for the sensing of stiffness by a cell is unknown. What is known is that various cell structures combine in order to detect forces or signals from the ECM and produce an appropriate response. (Tee et al., 2009). The known mechanisms and components involved are outlined below.

1.3.1.1 Integrins and Focal Adhesions

Integrins are multifunctional, integral cell surface proteins, which have generated much interest in mechanotransduction research as they play a central role within the mechanisms studied to date (Baker & Zaman, 2009). Integrins connect the extracellular matrix to the cytoskeleton. The intracellular domain of integrins attach to the cytoskeleton at specific sites. These specific attachment sites are known as focal adhesions and consist of a complex of various proteins including vinculin, paxillin, talin and α -actinin. The spatial distribution of focal adhesions is one of the most influential factors on the magnitude and efficiency of force transduction (Baker & Zaman, 2009). Integrins tend to contain more developed focal adhesions on surfaces with higher Young's moduli (Jacot et al., 2009).

The extracellular head of the integrin binds to extracellular matrix components, such as fibronectin, vitronectin, laminin and collagen at specific sequences known as RGD (arginine-glycine-aspartate) motifs (Baker & Zaman, 2009). Different types of integrins are involved in interactions with different extracellular matrix proteins. For example, integrin $\alpha 5\beta 1$ interact with fibronectin, integrins $\alpha v\beta 5$ interacts with vitronectin and integrin $\alpha 6\beta 1$ interacts with laminin. Various human embryonic stem cell lines express high levels of $\alpha 5$, $\alpha 6$, αv , $\beta 1$ and $\beta 5$ integrin sub-units. The integrins expressed by mesenchymal stem cells may become upregulated or downregulated during differentiation (Tan et al., 2012).

In a study by Katsumi et al. (2005) it was found that the mechanical stretching of NIH3T3 fibroblasts induced conformational activation of $\alpha v\beta 3$ integrin in these cells.

Binding of integrins to the ECM was found to mediate the activation of c-Jun NH₂-terminal kinase (JNK). Therefore, in addition to mechanically linking the actin cytoskeleton to the extracellular matrix and acting as an intracellular source of force transduction, integrins appear to also be able to convert mechanical signals such as stretch into chemical signalling pathways.

1.3.1.2 Actin Cytoskeleton

The actin cytoskeleton is a network of stress fibres, which extend throughout the cell. The stress fibres consist of polymerised F-actin. The cytoskeleton mechanically couples the ECM (through integrins and focal adhesions) to the transcriptional machinery of the nucleus, where it can influence the expression of certain genes. It acts as a conduit for force transduction throughout the cell. Despite a continuous remodelling process that occurs, it maintains an overall stable shape. This allows cells to resist forces exerted by the ECM. (Wang et al, 2009).

The overall isometric tension throughout the cytoskeleton is known as its prestress and is the primary means of maintaining cellular integrity. Furthermore, it is this prestress which allows for long range force transduction within the cell and allows for mechanical signals applied at the cell surface to be conveyed to the nucleus, where further mechanochemical reactions occur. As well as maintaining an overall prestress the cytoskeleton can be contracted in order to pull against the fibres of the extracellular matrix when sensing the mechanical microenvironment. This is the process, which regulates growth cone motility in neurons (Franze & Guck, 2010). Actin tensile strength varies between cells. These variations play a vital role in germ layer organisation during gastrulation (Krieg et al, 2008). In embryonic cells, myosin IIb and F-actin concentrate at the cell periphery (Skoglund et al, 2008), a phenomenon that is conserved in embryonic stem cells (Hemsley et al, 2011).

1.3.1.3 Non Muscle Myosin II

Nonmuscle myosin II (NMMII) is an isoform of the myosin protein responsible for contracting the actin cytoskeleton. Myosin contains six sub-units (two heavy chains and four light chains). Myosin proteins are able to slide against the actin filament before returning to their original positions. This process is known as the power stroke and is responsible for actin contractions (Nelson & Cox, 2005).

There are conflicting views on how myosin becomes activated. The widely held belief (Itoh et al., 1989) is that myosin becomes activated by phosphorylation of its light chain at MLC20 by the myosin light chain kinase (MLCK) enzyme. However, some studies (Gao et al., 2001; Nakamura et al., 2008) claim that this mechanism is not necessary and that contraction can occur without the phosphorylation of the myosin light chain. Studies on the effect of myosin on cell mechanobiology often inhibit NMM II using a molecule known as blebbistatin (Engler et al., 2006). Calcium ions, in addition to influencing the cellular response to stiffness through myosin activation, also have an influence on cellular response to stiffness through the RhoA/ROCK signalling pathway. Calcium signalling decreases with decreasing stiffness (Keung et al., 2009).

1.3.1.4 Rho/ROCK and ERK Regulation

Rho proteins are known to influence cytoskeletal tension by regulating myosin activity (Paszek et al., 2005). ERK is a protein that forms part of the MAPK/ERK regulatory pathway. This pathway is involved in the transcription of a number of genes, including genes involved pluripotency. Rho and ERK form a part of a signalling circuit that regulates the tensional homeostasis of the cell.

On stiffer substrates, integrin clustering causes ERK to become activated, depending on growth factor concentrations. ERK activation increases Rho-dependent myosin activity, thereby generating tension within the actin cytoskeleton.

1.3.1.5 Microtubules

Microtubules are a further structural component of the cytoskeleton. Unlike F-actin however, they do not have a dominant role in mechanotransduction. Instead they play an important role in maintaining cell internal organisation, shape and structure, as they are physically highly robust. They are constantly depolymerised and polymerised from α and β tubulin subunits, according to the structural requirements of the cells (Desai & Mitchison, 1997). In neurites, they form long, parallel bundles that allow for structural stability. Their stability in neurites is dependent on microtubule-associated proteins, such as MAP2 (Franze & Guck, 2010). In addition to their structural role, they have also been implicated in neurite extension (Georges et al, 2006).

1.3.1.6 Intermediate Filaments

Intermediate filaments are the third form of cytoskeletal fibre. Unlike actin stress fibres and microtubules, they do not play a key role in mechanotransduction or motility. Their main purpose is to provide stability and resist deformations in cells (Lodish et al, 2000). Although they do not play a key role in cell function, they can be highly abundant in cells. Within neurons in particular, they are by far the most abundant fibres found in neurites (Tyler et al, 2012). Subtypes of neural intermediate filaments are numerous, and include nestin, neurofilaments (NF's) and glial fibrillary acidic protein (GFAP).

1.3.1.6 Ezrin/Radixin/Moesin (ERM)

The Ezrin/Radixin/Moesin complex of proteins, more commonly known as ERM proteins regulates the interaction between the actin cytoskeleton and the plasma membrane by acting as a cross-linker between the two structures (Tsukita et al., 1997). ERM proteins become activated through phosphorylation of a threonine residue present in C-terminus domain (Parisiadou et al., 2009), to form pERM.

ERM proteins have also been implicated in the initial formation of integrin-based adherens junctions. They are however not involved in the maintenance of these junctions (Tsukita et al., 1997). Furthermore, modulation of ERM activity by leucine-rich repeat protein kinase 2 (LRRK2) was found to have had an effect upon neuronal development, in terms of neurite outgrowth and neuronal process maintenance (Parisiadou et al., 2009).

1.3.1.7 Cytoskeletal-Nuclear Interaction

The stiffness of the cell's nucleus varies depending on cell type and the presence of external forces. For example, nuclear stiffness increases in endothelial cells upon exposure to shear forces such as fluid flow. Conversely, nuclear stiffness is found to be lower in stem cells. The stiffness of the nucleus has an effect on various physical properties of the cell, such as structure and mechanical response to forces but can also have an effect in terms of gene expression in response to force (Dahl et al., 2009).

The nucleus is connected to and influenced by the extracellular mechanical microenvironment via the actin cytoskeleton. The actin cytoskeleton connects with the nucleoskeleton through a structure known as the LINC (linker to nucleoskeleton and cytoskeleton) complex. The LINC complex consists of various proteins including nesprins, SUN proteins and lamins (Wang et al., 2009). Similarly to the cytoskeleton, the nucleus also contains actin and myosin, in the form of a nucleoskeleton. This nucleoskeleton, like the cytoskeleton, has a defined prestress and thus allows for mechanotransduction within the nucleus.

The LINC complex of proteins and nuclear scaffolds can be arranged to focus forces from the actin cytoskeleton to specific DNA regulatory enzymes. In addition to this, different cells may have differential tethering between nuclear scaffold and genes. This may mean different responses to the same external stimuli. Stress and strain experienced by the nuclear scaffold may also lead to changes in chromatin organization, leading to changes in the accessibility of certain genes to certain

transcription factors (Wang et al., 2009). Mechanical forces applied at the cell surface can therefore influence gene expression within the nucleus.

1.4 Effect of surface material properties on cells

The structural and chemical properties of materials exert a number of key influences on cell function. The response to these properties varies greatly between cell and tissue types, as different cells will vary greatly in their internal structure. In the next section, examples of different cell responses to changes in material properties are outlined.

1.4.1 Effect of surface material properties on fibroblasts

In the earliest work involving substrate stiffness and cells, Pelham & Wang (1997) developed a mechanically tuneable growth substrate consisting of polyacrylamide (PA) cross-linked with varying concentrations of bis-acrylamide and functionalised with collagen-I. This substrate was used to investigate the effect of substrate stiffness upon morphology, motility and focal adhesion formation in 3T3 fibroblasts.

In that study it was found that on softer substrates, fibroblasts became more spindle-shaped and lost stress fibres, compared to stiffer substrates, where appeared well spread. Focal adhesions appeared to be more stable on stiffer substrates, where regular, wedge-shaped complexes formed compared to softer substrates, where complexes appeared to be irregular.

Yeung et al. (2005) investigated the effect of varying substrate stiffness upon morphology, adhesion, F-actin and α -5 integrin expression in 3T3 mouse fibroblasts. In this study, it was found that fibroblasts appeared to become larger and more spread on stiffer substrates compared to the softest substrates, consistent with the findings of Pelham & Wang (1997). In terms of cytoskeleton, F-actin and integrin expression

increased with substrate stiffness. Actin stress fibres disappeared below stiffnesses of 3.5 kPa.

Other effects have been reported in fibroblasts in response to changes in material properties. For example, fibroblast nuclei have been observed to flatten on stiff materials (400 kPa), compared to softer (400 Pa) materials where they appear round (Lovett et al, 2013). Furthermore, they have been observed to polarise on rigid materials, but not on soft materials (Khoutorsky et al, 2011). This process is dependent upon focal adhesion organisation and structure, which is regulated by the Shp2 protein (Lee et al, 2012) in this case.

1.4.2 Effect of surface material properties upon mesenchymal stem cells

Work by Engler et al. (2006) showed that induced differentiation of mesenchymal stem cells (MSC's) into neuronal, myogenic and osteogenic lineages was strongly influenced by matrix stiffness. RNA profiling showed a 5-fold increase in neuronal gene expression on soft gels (0.1-1.0 kPa), a 6-fold increase in myogenic gene expression on gels with stiffness near that of striated muscle (11 kPa) and a 4-fold increase in osteogenic gene expression on the stiffer of the gels (34 kPa). The 5-fold increase in neurogenic transcripts was taken as an average increase across a variety of neuronal cytoskeletal mRNA transcripts including nestin (expressed during early “commitment”), β -III tubulin (expressed in immature neurons), NFL (a mature neurofilament marker) and NCAM (an early/mid neural adhesion protein). MSC's also became more branched on softer materials.

The work furthermore suggested that the differentiation response to matrix stiffness is dependent upon non-muscle myosin II (NMM II). This was investigated using blebbistatin, an inhibitor of all isoforms of NMM II. Blebbistatin acts by inhibiting the activation of NMM II by actin without having an effect on myosin light chain kinase (MLCK). There was less cytoskeletal organisation on softer gels than on stiffer gels. Cytoskeleton organization increased with matrix stiffness.

This study clearly highlighted the effect of matrix elasticity upon differentiation into multiple lineages. There have been other studies, which have looked at the effect of matrix elasticity on specific MSC differentiation pathways. Soft materials (1-5 kPa) have been observed to increase chondrogenesis in MSC's (Bian et al, 2012), even in the absence of induction factors. Osteogenic expression has also been observed to increase as Young's modulus decreases (Hu et al, 2011), however for a range that is substantially higher than other studies (5 MPa-25 MPa). This reflects the higher Young's modulus of mineralised bone compared to other tissue. In induced neural differentiation medium, soft (1 kPa) materials favoured neuronal differentiation, whilst stiffer (10 kPa) materials favoured glial differentiation (Her et al, 2012).

In terms of other effects of Young's modulus on MSC behaviour, increasing Young's modulus from 200 Pa to 2 kPa has been observed to decrease spreading, migration and proliferation rate in normal culture conditions (Lei et al, 2010). In terms of non-stiffness effects, topography appeared to have an interesting effect on cell phenotype. Multipotency was retained in induced differentiation medium when MSC's were cultured in lattice-orientated nanopits (McMurray et al, 2011).

1.4.3 The effect of surface material properties upon cardiomyocytes

Another study by Engler et al. (2008) showed that embryonic cardiomyocytes contract best upon collagen I-coated polyacrylamide (PA) gels with stiffness close to that of striated muscle (approx. 10 kPa). Furthermore that study found that if matrix stiffness was close to that of a fibrotic scar (where $E = 35-70$ kPa), such as that found within a diseased, post-infarct heart, contractile capacity became limited.

The work carried out by Engler et al. (2008) suggests that in addition to efficiently differentiating stem cells towards certain lineages, the elasticity of the substrate may also have an effect on their *in vivo* function and efficacy (in this case the beating of cardiomyocytes). This may have important implication when administering cells into diseased areas, where the normal mechanical microenvironment may be severely

disrupted, undermining the *in vivo* efficacy of the transplanted cells. It may also have a bearing on the choice of material used for tissue engineering scaffolds.

Another study (Chopra et al, 2012) found that when cardiomyocytes were cultured on hyaluronic (HA) gels coated with fibronectin, gelatin or fibrinogen (as opposed to collagen-I), cells were able to assemble actin into organised networks on soft materials, contrasting with the findings with PA gels by Engler et al (2008). Thus, surface chemistry and choice of material clearly influences the effects on cells.

1.4.4 Effect of surface material properties upon myoblasts

The fusion of myoblasts into myotubes is the first step in skeletal muscle differentiation. A study conducted on PA gels by Engler et al. (2004b), there appeared to be an optimal range of substrate elasticity for striation of actin and myosin in myotubes (a physiological characteristic of skeletal muscle tissue).

The optimal range of substrate elasticities for skeletal muscle differentiation is narrow. This has an implication when cells are introduced into diseased areas (for example during infarctions or muscular dystrophy). Here, substrate stiffness may be significantly increased. Within this environment, cells may not fully differentiate into skeletal muscle and may differentiate into connective tissue instead.

The increase in cross-linking required for gel stiffening may have other effects on gels (depending on the choice of material). These include reduction in access to binding sites and changes in other mechanical properties of the material. These effects have been found to have a negative effect upon spreading and growth of myoblasts (Grover et al, 2012).

Another study found that as myoblasts differentiated in 3D fibrin gels (as opposed to 2D PA gels), they remodelled the surrounding gel (Chiron et al, 2012), increasing its thickness. Furthermore, micropatterning of soft gels also has an effect upon myoblast

differentiation (Zatti et al, 2012). Myoblasts cultured in wider channels fuse more readily (but proliferate less rapidly) than cells in narrower channels.

In a separate study using myoblasts, Engler et al. (2004a) found that substrate stiffness, and subsequently cytoskeletal organization had a dominant effect on spreading over ligand density.

1.4.5 Effects of surface material properties upon endothelial cells

Deroanne et al. (2001) discovered that when human umbilical vein endothelial cells (HUVEC) were cultured on softer substrates, morphology shifted from a monolayer pattern to that of tube-like structures characteristic of cells undergoing tubulogenesis. Decreasing the stiffness of the substrate also caused a reduction in actin and vinculin (a focal adhesion protein) expression. Soft substrates have subsequently been implicated in the remodelling of other focal adhesion proteins in Endothelial cells (Wei et al, 2008). Thus remodelling of the cytoskeleton and focal adhesions appeared to be a crucial prerequisite for angiogenesis. In addition to being implicated in tubulogenesis, focal adhesions also enable endothelial cells to mechanically sense blood flow, via “rafts” of lipids that are able to mobilise along the cell membrane surface (Fuentes & Butler, 2012).

In addition to modulus, biomaterials may influence endothelial cell differentiation and growth in other ways. As mentioned earlier, the ECM is able to sequester growth factors and release them as required by cells during development. Based upon this, Aguirre et al (2012) developed a “smart biomaterial” that was able to release VEGF and VEGFR as required by endothelial cells during angiogenesis.

1.4.7 Effect of surface material properties on bone

Bone tissue undergoes a constant process of remodelling, whereby bone is formed by osteoblasts and resorbed by osteoclasts (Bakker & Nullend, 2010). The balance between these two populations of cells is controlled by osteocytes. Osteocytes are

highly mechanosensitive to dynamic loading and compression of the growth material. In addition to being influenced by the matrix, they also have the ability to influence the Young's modulus of the growth material, a process that is dependent on Lrp5 and Wnt signalling (Zhao et al, 2013).

The adhesion of osteoblasts is influenced by nanotopography, in the form of engineered grooves and pits (Nikkah et al, 2012), as well as surface chemistry (Anselme & Bigerelle, 2012). Based upon these findings, a bioreactor was developed by Van Dyke et al (2012), which was able to simulate the fluid flow and mechanical loading of the growth material for bone cell growth. This is an interesting example of how the mechanical influence of the growth material can be designed into larger scale cell expansion processes.

1.4.8 Effect of surface material properties upon the malignant phenotype

The modulation of the tensional homeostasis within the cell during tumour formation was investigated in work conducted by Paszek et al. (2005). Unlike normal, non-malignant cells, malignant cells are able to stiffen on soft materials. This process is dependent on elevation in ERK and Rho signalling. Myosin IIb was able to contract the cytoskeleton independent of external ECM tension.

1.4.9 Effect of surface material properties on neural development and growth

In both the human and rat adult brain, Young's modulus has been found to vary substantially, from 0.1 kPa to 16 kPa (Tyler et al, 2012). However, the majority of the neuronal tissues isolated within the laboratory, including spinal cord and grey matter have very soft Young's moduli, usually within the 500 Pa-2 kPa modulus range (Flanagan et al, 2002; Christ et al, 2010). This is considerably less than the values (see Figure 1.2) for muscle (approximately 17 kPa) and bone (30 kPa and upwards).

Differences exist between neural stells too. Despite being implicated in fibrosis in the diseased state, glial cells actually have lower Young's modulus than neurons (Lu et al, 2006). There are also differences within the cells themselves. Neurites (axons and

dendrites) have lower moduli (Jiang et al, 2011) than the cell body of the neuron (the soma). The majority of studies on the effects of stiffness upon neuronal growth therefore focused on softer gels, within the ranges outlined above.

1.4.9.1 Effect of surface material properties on neural stem cells and neural precursor cells

The terms neural stem cell and neural precursor (or progenitor) are used fairly interchangeably within the literature. Broadly speaking, they describe populations of proliferating cells, which are able to differentiate into immature neuronal or glial cells. Neural stem cells tend to describe populations that exist in the adult brain, which replace damaged or dying tissue, whilst the term precursor describes a cell within the early development stages, such as embryogenesis.

In two studies involving neural stem cells (Saha et al, 2008; Banerjee et al, 2009) isolated from the adult rat hippocampus, proliferation in expansion medium peaked at lower moduli (between 1-4 kPa). When cells were allowed to differentiate into immature neurons (positive for β -III tubulin) in neuronal differentiation medium, expression was maximised on soft materials (200 Pa in the Banerjee study, 500 Pa to 1 kPa in the Saha study). In mixed glial/neuronal medium, the percentage of cells existing as astrocytes increased from 10 kPa onwards in the Saha study (2008). Thus neural stem cells tended to prefer soft materials for both neuronal differentiation and proliferation.

A study conducted by Liepzig & Schoichet (2009) showed that proliferation of NSPCs or neural stem/progenitor cells was maximized on a substrate stiffness of 3.5 kPa, whilst neuronal differentiation and migration was maximized on a substrate with stiffness less than 1 kPa.

When neural precursors isolated from spinal cord cultures were plated on various Young's moduli (300 Pa, 6 kPa, 27 kPa and 47 kPa) by Previtera et al (2013), early differentiation into mature MAP2-positive neurons was maximised on 6 kPa and 27

kPa gels whilst late differentiation was maximised on 6 kPa gels. The lack of consensus on precise Young's moduli effects across different stages neuronal differentiation process (for neural stem cells, neuronal progenitors or primary neurons) has been directly addressed within this study.

Other aspects of surface structure and chemistry have also been shown to impact precursor cells. For example, the presence of laminin on the growth surface has been observed to enhance the migration, expansion and differentiation of neural stem/precursor cells (Flanagan et al, 2006). Nanotopographic cues, in the form of PDMS nanopillars have been shown to increase the "yield" of early neurons from ES cell-derived neuronal precursors, when compared to flat PDMS surfaces (Migliorini et al, 2011). Ma et al (2004) created a three-dimensional collagen-based polymer scaffold for cell growth, in which neural stem/precursor cells were able to form functional synapses and neural networks. If a similar scaffold could be created with the appropriate mechanical properties, it could be a means of efficiently creating biomaterials for tissue engineering purposes for expanding and differentiating neural precursors.

1.4.9.2 The effect of surface material properties on primary neuronal cultures

The next group of studies used primary immature or mature, terminally differentiated neuronal cell cultures. These cells were usually defined as β -III tubulin-positive and would usually mature into MAP2-positive functional neurons.

In a study conducted by Flanagan et al. (2002), it was found that primary embryonic spinal cord neurons exhibit more neurite (dendritic and axonal) branching on softer rather than stiffer substrates. The range of stiffnesses that neurons responded to was much narrower than that of fibroblasts.

A study conducted by Georges et al (2006) found that in mixed cortical cultures, neurons grow independently of astrocytes on softer substrates whilst they appear to only grow over glial cells on stiffer substrates, due to the soft nature of glial cells. This

may have an impact on cell transplantation into injured areas of the spinal cord, where a lesion area is likely to be surrounded by a stiff, fibrotic scar.

Jiang et al (2007) looked at the effect of substrate elasticity upon adhesion of primary cultures of embryonic rat spinal cord. When neurons were separated from the mixed population, adhesion increased with stiffness. Previtera et al (2010) cultured mixed hippocampal cultures on a variety of materials. Here, the cell concentration (cells/cm^2) of neuronal cells at 24h and 48h increased as Young's modulus was increased from 500 Pa to 2 kPa. Concentrations then appeared to remain constant as moduli increased to 18 kPa.

Another property of the ECM that will likely affect neuronal cell growth is surface chemistry. Lam et al (2011) found that when the growth factors bFGF and EGF were immobilised onto nanofibers, axonal growth improved in human ES-derived neural cells. Using these findings, Kunze et al (2011) devised a micropatterned, microfluidic device containing a three-dimensional layered hydrogel able to culture cortical neuron cultures. Microfluidic devices allow for testing on cells using much smaller volumes of reagents, and thus significantly reducing consumable costs. The mechanical properties of microfluidic devices could be further optimised (through coating with gels) to improve their differentiation.

1.4.9.3 Effect of surface material properties on glial cells

In the Jiang et al (2007) study mentioned earlier, glial cells were also isolated from the mixed embryonic spinal cord culture and seeded onto variable gel moduli. In this case, cell concentration of GFAP-positive mature astrocytes increased on stiff ($>100 \text{ kPa}$) materials. Similarly, Moshayedi et al (2010) found that astrocytes formed complex morphologies and spread more on stiffer materials (10 kPa), compared to softer materials (100 Pa), where they tended to become rounded. When oligodendrocyte progenitor cells were cultured on varying Young's moduli, survival, proliferation and maturity into mature oligodendrocytes was maximised at 1 kPa gels (Jagielska et al, 2012). As with neuronal cells, glial cells also respond to other mechanical properties of the biomaterials other than elasticity. Minev et al (2013), for example showed that glia

proliferate less and become unable to form stress fibers when cultured on tall, 5 µm micropillars, compared to flat substrates.

1.4.9.4 Effect of extracellular matrix stiffness upon neuroblastoma differentiation

Lam et al (2010) conducted a study to investigate the relationship between the stiffness of the extracellular matrix and differentiation of neuroblastomas (both spontaneously and in the presence of retinoic acid). It was found that an increase in stiffness caused an increase in average neurite length. Increased neurite length is an indicator for differentiation of neuroblastomas.

1.4.10 Effect of surface material properties on pluripotent stem cells

In terms of their physiological niche, cells of the day-eight blastocyst have a Young's modulus of approximately 3.4 kPa (Murayama et al, 2006), similar to that of neuronal tissue. When Pillarisetti et al (2011) carried out measurements of live mESC's, cell Young's modulus was found to be 265 Pa. It would therefore be expected that the majority of work with ES cells would involve softer materials.

Chowdhury et al (2010) carried out an experiment looking at the effect of soft materials on mouse embryonic stem cell self-renewal. It was found that self-renewal could be maintained for five days on soft materials in the absence of LIF. However, the effects of biomaterial mechanical properties on pluripotent stem cell differentiation are relatively poorly characterised. In the current study, mESC neuronal differentiation has been characterised in far greater detail on a stage-by-stage basis.

An earlier study by Evans et al (2009) looked at the effect of PDMS Young's modulus on the early differentiation of mESC into bone. The range of Young's modulus (40 kPa to 2.3 MPa) was higher than the physiological range given above. Cell attachment, measured as the number of cells attached after 24 hours of culture was unaffected by Young's modulus in normal culture medium. Proliferation on the other hand, increased with Young's modulus. When cells were induced to differentiate, osteogenic marker

expression and bone mineralisation increased with Young's modulus. The stiffest material had a Young's modulus closest to mineralised bone.

In another study (Eroshenko et al, 2013) using PDMS substrates, attachment of human embryonic stem cells (hESC's) at 12h in spontaneous (undirected) differentiation medium did not vary with Young's modulus. Again the modulus range used in that investigation was 80 kPa to 1 MPa, similar to the Evans et al (2009) study. Jaramillo et al (2012) found that early endoderm gene expression was increased on softer (30 Pa) materials when compared to mesoderm, ectoderm and pluripotent gene expression.

Two recent studies have attempted to look at the effect of substrate stiffness on neuronal differentiation. Keung et al (2012) found that softer polyacrylamide materials increased the number of cells positive for β -III tubulin, Pax6 and Sox1 following early hESC and iPSC neuronal differentiation. Soft materials also increased the percentage of cells positive for TH during later neuronal differentiation. The moduli used in that study covered a broad range (100 Pa, 700 Pa, 75 kPa and TCP). Kothapalli et al (2013) carried out a similar study with mESC-derived EB's in three-dimensional culture. Both neurite length and percentage of cells differentiating towards the neuronal lineage increased with Young's modulus from 20 Pa to 1 kPa. The percentage of cells differentiating into astrocytes showed the opposite trend. Taken together, this suggests that materials with modulus in the range of 100 Pa to 1 kPa favour neuronal differentiation over softer or stiffer materials.

In a study that did not involve material stiffness, Ma et al (2008) showed that hESC-derived EB's undergoing neuronal differentiation generate more neural progenitors and greater neurite outgrowth on laminin-coated biomaterials, compared to fibronectin, collagen I and poly-d-lysine. Interestingly, laminin is the earliest ECM protein to appear in blastocysts, appearing as early as day eight (Ingber, 2006). Clearly, other material properties also affect ES cell differentiation.

Furthermore, Lakins et al (2012) found that, unlike with fibroblasts and mesenchymal stem cells, hESC's tended to have more organised F-actin structures on soft materials

(400 Pa) compared to stiffer material (60 kPa). Poh et al (2010) showed that ES cells did not stiffen on rigid materials. Thus, ES cells are mechanically different to the majority of adult cells.

1.4.11 Materials Used in Studies

The majority of studies were conducted using mechanically tuneable polyacrylamide gels, functionalised for attachment with collagen I. This material was originally described in the Pelham & Wang (1997) study. The synthesis procedure involves a number of steps involving a variety of chemicals (Figure 1.4). Modulus was modified in these gels by changing the concentration of bis-acrylamide in acrylamide.

In the Saha et al. (2008) study, a mechanically tuneable substrate named vMIPN was developed to investigate the optimal elasticity for the proliferation and differentiation of adult neural stem cells (aNSC). The material consisted of layers of various polymers including polyacrylamide, bisacrylamide and polyethylene glycol (PEG). Elasticity was varied by changing the polyacrylamide and bisacrylamide concentrations. The substrate was functionalised with an RGD peptide.

1.4.12 GXG

GXG was the material used within this study. GXG is a substrate consisting of gelatin (in phosphate buffer saline, PBS or deionised water) cross-linked with glutaraldehyde in order to form a mechanically tuneable growth surface for mouse embryonic stem cells. Changing the concentration of gelatin in PBS or water varies the Young's modulus. The Young's modulus can be varied from 2 kPa (where the concentration of GXG is 3% in PBS) to 35 kPa (where the concentration of GXG is 6% within water). The lowest value within the range is relatively high compared to the substrate created by Saha et al. (2008) whilst the highest value in the range are approximately equal to that achieved using polyacrylamide substrate in the Engler et al. studies (2006 & 2008).

In all of the studies mentioned, a large variety of different reagents (see Figure 1.4) are utilised, including many chemical reagents not commonly used within cell culture. The GXG method, in comparison uses gelatin (already widely used as a substrate in mouse embryonic stem cell culture and differentiation), glutaraldehyde and sodium borohydride in the GXG method. Furthermore, the number of steps required for each protocol favours the GXG method (Figure 1.4). Finally, the materials used in the other studies appear to be functionalised by the manual addition of either a custom made RGD peptide (Saha et al., 2008) or collagen I (Pelham & Wang, 1997). In comparison the gelatin (which is simply heat treated porcine collagen) in GXG is naturally functionalised for cell attachment and growth.

Substrate	Number of reagents used	Number of steps	Functionalisation Group	Elasticity Range in study (kPa)
vmIPN (Saha et al., 2008)	~15 (including acrylamide, polyethylene glycol, bisacrylamide)	~20-25 steps (2 overnight)	Custom made RGD peptide	~0.01-10
Polyacrylamide with collagen I (Pelham & Wang, 1997)	~7 (including acrylamide, bis-acrylamide, glutaraldehyde)	~15 steps (1 overnight)	Collagen I	~0.1-35
GXG	3 (gelatin, glutaraldehyde, sodium borohydride)	~10 steps (2 overnight)	Naturally occurring collagen in gelatin	~2-35

Figure 1.3: A comparison of the preparation and function of the substrates used in the Saha et al. (2008) and Engler (2006 & 2008) studies compared to GXG

An elastically tuneable, physiologically relevant growth surface could provide a means of dynamically controlling the mechanical environment during embryonic stem cell differentiation. Optimizing the Young's modulus of the substrate at specific stages of neuronal differentiation may provide a means of increasing yields and purities

associated with the process, which is currently a significant limiting step in the development of stem cell bioprocessing (Mondragon et al., 2009).

1.5 Aims and Objectives of Investigation

The aim of this study is to investigate the effect of changes in Young's modulus of GXG on the monoculture neuronal differentiation of mouse embryonic stem cells. Other investigations, such as the Kothapalli & Kamm (2013) study have tended to focus on the entire differentiation process, starting from ES cells and ending with the formation of neurons, without looking at the stages in between. The aim of this study was to define the effect of Young's modulus of differentiation, stage-by-stage in order to assess whether the effects remain constant across the entire process or whether they are dynamic and thus vary with maturity. Within this study, the mESC monoculture neuronal differentiation (Ying et al, 2003) process was split into three stages.

The first stage involved the formation of neural precursors from mouse embryonic stem cells. Neural precursor cells were defined as being nestin-positive (Lendahl et al, 1990; Engler et al, 2006; Ying et al, 2003; Migliorini et al, 2011; Previtera et al, 2013). The second stage involved the formation of immature neurons from the neural precursors. Immature neurons were defined as positive for β -III tubulin (Sullivan & Cleveland, 1986; Engler et al, 2006; Ying et al, 2003; Migliorini et al, 2011). The final stage was the maturation of immature neurons into mature neurons, positive for MAP2 (Bernhardt & Matus, 1984; Jiang et al, 2007; Previtera et al, 2013).

The first part of this study involved development of GXG and the neuronal differentiation process. Protocols and conditions were optimised in the initial work. This was followed by characterisation of the starting population, and the time frames during which neuronal markers began to appear. The latter work allowed for selection of time points during differentiation for harvesting of cells for seeding onto materials for analysis. The next stage investigated modulus effects on two non-mESC cell lines, in order to provide a basis for comparison with the ES work. The final part of the first chapter involved seeding mESC's in normal growth medium as well as spontaneous

differentiation medium, in order to assess whether any effects were medium dependent.

The next two chapters looked at the effects on cells of Young's modulus over three time frames of differentiation. There were three cell effects that we investigated. The first was cell attachment at 24h (the time point used in the Evans et al, 2009 study). The second was expansion of colonies to the 72h (post-seeding) time point. The third effect was enrichment. This involved looking at presence of key markers and expression of genes associated with both pluripotency and the neural lineages.

The second chapter looked at the impact of Young's modulus on the differentiation of mESC's into neural precursors, in terms of the three effects listed above. Image analysis, immunocytochemistry, flow cytometry and qPCR were used to investigate the effects. This was then related to polymerisation of actin and tubulin using two small molecule inhibitors.

The final chapter looked at the impact of Young's modulus on the differentiation of neural precursors into immature neurons, and finally immature neurons into mature neurons. This was carried out by partially differentiating mESC's on TCP to the relevant stages of neuronal differentiation (four days for neural precursors or six days for immature neurons) prior to seeding.

The central hypothesis behind the study was that physiologically soft materials favour the formation of neurons from mouse embryonic stem cells in neuronal differentiation medium.

2 Materials and Methods

2.1 Cell Culture

2.1.1 Mouse Embryonic Stem Cells (MESC's)

Passage 80-100 E14Tg2A mouse embryonic stem cells (Stem Cell Sciences, Cambridge, UK) were cultured on cell culture treated T-25 flasks (Thermo Scientific NUNC, Langenselbold, Germany). The medium recipe used for normal culture is outlined below:

Medium Component	Manufacturer	Volume (mL)
Glasgow Minimum Eagles Medium	Invitrogen (Paisley, UK)	112.5
Foetal Bovine Serum	SeraLab (Batch:102004, Haywards Heath, UK)	12.5
Non-Essential Amino Acids	Invitrogen (Paisley, UK)	1.25
Glutamax	Invitrogen (Paisley, UK)	1.25
Antibiotic-Antimycotic	Invitrogen (Paisley, UK)	1.00
Leukemia Inhibitory Factor (LIF)	Millipore (Watford, UK)	0.125
β -Mercaptoethanol	Invitrogen (Paisley, UK)	0.25

Figure 2.1: Media components for normal pluripotent cell culture. Volumes given are for 125 mL of medium.

- Fresh T-25 flasks were coated with 0.5 mL of 0.1% v/v gelatin (Sigma-Aldrich, Gillingham, UK) for 30 minutes prior to passaging.
- In order to passage cells, spent medium was firstly aspirated before being washed once with 6 mL of 0.1% v/v phosphate buffer saline (PBS; Sigma-Aldrich, Gillingham, UK).
- Following this, 0.5 mL of 0.25% bovine trypsin-EDTA was added to the flasks. Cells were incubated with the trypsin at 37°C for three minutes.

- The trypsin was then quenched by dispensing 2.5 mL of normal culture medium into the flasks. The quenched suspension was aspirated and dispensed 3-4 times in order to create a single cell suspension and eliminate aggregates.
- The quenched cell suspension was then aspirated and dispensed into a 25 mL centrifuge tube and centrifuged at 300 x g for three minutes.
- Whilst the cell suspension was centrifuged, the gelatin was aspirated from the fresh flasks.
- Following centrifugation, the supernatant containing the trypsin and quench medium was carefully removed from above the cell pellet. The cells were then resuspended in normal culture medium (recipe above), whose volume dependent on the passage split ratio (3 mL for 1:6 or 4 mL for 1:8). Cells were split at a ratio between 1:6 and 1:8. 5 mL of normal culture medium was dispensed into the flasks. 0.5 mL cell suspension was then carefully added to each culture flask.

2.1.2 Mouse Embryonic Fibroblasts

Fibroblasts were passaged as above, using the same consumables, apart from the media. The medium used for culturing fibroblasts was Dulbecco's Medium Eagles Medium (Invitrogen, Paisley, UK)), supplemented with 15% v/v fetal bovine serum (SeraLab, Haywards Heath, UK), 1% v/v Glutamax (Invitrogen, Paisley, UK), 1% v/v non-essential amino acids (Invitrogen, Paisley, UK). For GXG experiments, the seeding density and rationale was identical to that for mESC's, albeit in normal culture medium.

2.1.3 Human EB Retinal Differentiation

Human embryoid bodies (EB's) were derived from induced pluripotent stem cells (iPSC's), and were kindly provided by Vishal Sharma from the Department of Biochemical Engineering at UCL. Briefly, undifferentiated iPSC's were formed in suspension over three days in 30 mm non-adherent culture dishes (Sterilin, Caerphilly,

UK) in 3 mL retinal induction medium. Retinal induction medium consisted of DMEM/F12 (Invitrogen, Paisley, UK), 10% v/v Knockout Serum Replacement (Invitrogen, Paisley, UK), 1 ng/mL human recombinant Dkk-1, 1 ng/mL human recombinant Noggin and 5 ng/mL human recombinant IGF-1 (all R&D Systems, Minneapolis, USA) and 1% v/v N2 Supplement (PAA Laboratories, Yeovil, UK).

Roughly 30 EB's were then selected from the dish per well in a 6-well plate. The EB's were centrifuged at 300 x g and resuspended in retinal differentiation medium before being seeded onto the GXG materials. The retinal differentiation medium consisted of DMEM/F12 (Invitrogen, Paisley, UK), 10 ng/mL human recombinant Dkk-1, 10 ng/mL human recombinant Noggin, 10 ng/mL human recombinant IGF-1, 5 ng/mL basic fibroblast growth factor (all R&D Systems, Minneapolis, USA), 1% v/v N2 Supplement and 2% v/v B27 Supplement (PAA Laboratories, Yeovil, USA).

2.2 GXG Preparation

Gelatin stock solutions were made up according to earlier atomic force microscopy measurements (using the same deionised water) made by Dr Andrew Pelling (The Pelling Lab, Ottawa, Canada), which related concentration to Young's modulus (see Figure 2.2 below). Gelatin powder (Sigma-Aldrich, Gillingham, UK) was dissolved in the relevant solution according the concentrations below (% w/v corresponds to grams of gelatin in 100 mL solution) and autoclaved. Following autoclaving, gelatin stock solutions were stored at 4°C.

Concentration (% w/v)	Solution	Young's modulus
3	Phosphate buffer saline	2 kPa
4	Water	18 kPa
6	Water	35 kPa

Figure 2.2: The relationship between concentration of gelatin (where percentage related to grams/100mL of solution) and Young's modulus, as measured by atomic force microscopy. Modulus was dependent both on concentration and the solution used.

- Prior to coating of the culture surface, gelatin stock solutions were warmed in a water bath (37°C) for 10-15 minutes until the solution was melted completely.
- The stock solution was then added to glutaraldehyde in a 15 mL tube at a concentration of 5 µL glutaraldehyde per mL of gelatin stock solution (3 mL of gelatin added to 15 µL glutaraldehyde for a triplicate wells in a 6-well plate).
- The GXG mixture was immediately mixed by vortexing before being added to the culture surface. 0.7 mL was added to each well in the 6-well plates, whilst 5.25 mL was added to the T75 flasks (70 µL per cm² surface area). The GXG-coated flasks or wells were left overnight at 4°C in a humidity chamber.
- The next morning, the plates were washed three times with PBS (2 mL per well in 6-well plates). On the third addition, PBS was left on GXG in order to prevent the biomaterial from drying out whilst sodium borohydride was prepared.
- Sodium borohydride (NaBH₄) was used as a reducing agent to react with excess, unreacted glutaraldehyde. The powdered form of NaBH₄ (VWR, Lutterworth, UK) was dissolved in ice cold PBS at a concentration of 1 mg NaBH₄ per mL of PBS solution (usually 15-20 mL borohydride solution made up for a 25 mL centrifuge tube). After very brief mixing, the solution was immediately added to the GXG culture surface (0.25 mL per cm² of culture surface).
- The well plates or T-flasks were kept on ice for one hour to allow the reduction step to proceed.
- Following the reduction step, the reacted NaBH₄ solution was aspirated. The culture surfaces were then washed twice with PBS. The second PBS wash was left on the GXG overnight at 4°C.
- The next morning (on the third day of the protocol), the PBS from the second wash stage was removed and a third and final PBS wash stage performed. Normal GMEM culture medium, without LIF, was then added to the culture surface (0.2 mL per cm² culture surface).

- The GXG plates with –LIF medium were incubated at 37°C for four hours prior to seeding to allow for pH equilibration.
- Finally, the equilibration medium was removed and cells seeded onto GXG for experiments.

2.3 Neuronal Differentiation

2.3.1 MESC

The medium used for neuronal differentiation was N2B27, as described by Ying et al (2003). The formulation is shown in the Figure 2.3 below.

- The culture plates used as the tissue culture polystyrene (TCP) control were first gelatinized for 30 minutes. 1 mL of gelatin was dispensed into each well in 6-well plates, whilst 6 mL of gelatin was dispensed into the T-75 flasks.
- Spent medium was then aspirated from each flask of undifferentiated mESC's.
- Cells were washed once with 6 mL of 0.1% v/v PBS.
- 0.5 mL of 0.25% bovine trypsin-EDTA solution was then dispensed into the flasks. Cells were incubated in trypsin for three minutes at 37°C.

Component	Manufacturer	Volume (mL)
DMEM:F12 with Glutamax	Invitrogen (Paisley, UK)	99
N2 (100x diluted)	PAA (Yeovil, UK)	1
Neurobasal Medium	Invitrogen (Paisley, UK)	98
B27 Neuromix (50x diluted)	PAA (Yeovil, UK)	2
β-Mercaptoethanol	Invitrogen (Paisley, UK)	0.4
Foetal Bovine Serum (Not added for partially-differentiated cells)	SeraLab (Batch:102004; Haywards Heath, UK)	2

Figure 2.3: Medium components used to formulate 200 mL of N2B27 neuronal differentiation medium.

- The trypsin was then quenched by dispensing 2.5 mL of normal GMEM medium without LIF into the flasks. The cell suspension was aspirated and dispensed 3 times in order to create a single cell suspension and eliminate aggregates.
- The quenched cell suspension was aspirated from the flasks and dispensed into a 25 mL centrifuge tube and centrifuged at 300 x g for three minutes.
- Following centrifugation, the quenched trypsin supernatant was removed from above the cell pellet. The cell pellet was then resuspended in 10 mL of N2B27 medium with 1% v/v serum.
- Cell counts were then made in order to calculate the volume of N2B27 cell suspension required to achieve the desired seeding density of 1×10^4 cells/cm² (as characterized in Chapter 3, Figure 3.3). In order to make cell counts, 10 µL of suspension was aspirated from the cell suspension in N2B27 and dispensed underneath a coverslip mounted on a hemocytometer.
- The hemocytometer grid was then viewed using phase contrast microscopy (with a 10x objective). Any cells contained within the grid were counted (including cells lying on the top and left borders of the grid, but not the bottom and right borders).
- The output of these counts was the cell concentration in the suspension ($\times 10^4$ cells/mL). This method was also used to calculate total cell concentration at the end of four days of differentiation.

The volume of cell suspension required to achieve a seeding density of 1×10^4 cells/cm² was calculated using the below formula:

$$V_1 = (V_2 \cdot C_2) / C_1$$

Where: V_1 = Volume needed from cell suspension (mL)

V_2 = Total seeding volume (mL) = 0.2 mL for each cm² culture area

C_1 = Hemocytometer Cell Count ($\times 10^4$ cells/mL)

C_2 = Cell concentration required to achieve seeding density of 1×10^4 cells/cm² in the total seeding volume, $V_2 = 5 \times 10^4$ cells/mL

- The volume V_1 was then removed from the cell suspension and diluted with N2B27 medium to a volume of V_2 .
- The gelatin (in the case of the TCP control) or equilibration medium (in the case of GXG) was then aspirated from the plates or wells.
- The cell suspension was immediately dispensed (2 mL per well in a 6-well plate or 15 mL per T75 flask) onto the culture surface in order to ensure that GXG did not dry out. The plates or well plates were swirled several times and placed in an incubator at 37°C (5% v/v CO₂).
- Cells were fed with fresh medium every two days. This involved aspirating half the spent medium from each well (1 mL) or plate (7.5 mL) and replacing with the same volume of fresh medium. Serum was not added to fresh medium past day four.

2.3.2 Partially-Differentiated Cells

MESC's were partially-differentiated in tissue culture treated T75 flasks (Thermo Scientific NUNC, Langenselbold, Germany) for four or six days in N2B27 medium as outlined above.

- On the day of seeding, 6-well plates (for attachment, expansion and immunocytochemistry studies) or T75 flasks (for flow cytometry and qPCR) were gelatinized.
- Cells were then harvested as outlined above ([2.3.1: MESC Neuronal Differentiation](#)) with scaled up volumes at each step (15 mL of PBS, 1 mL of trypsin per T75 flask and 5 mL of quench medium) before being resuspended in 10 mL N2B27 medium (without serum).
- Cell counts were again made using a hemocytometer at this stage. For attachment and expansion studies, the same 1×10^4 cells/cm² seeding density was used in order to directly compare findings against the mESC results. However, this seeding density did not produce sufficient cells at day four in

T75's for flow cytometry or qPCR analysis. Therefore, for these experiments, partially-differentiated cells were directly replated onto GXG or TCP. To standardize the starting density, three mESC neuronal differentiations were carried out in T75's and the lowest value chosen as the starting seeding density (3.5×10^5 cells/mL for four day partially-differentiated cells – data not shown).

Cells were then seeded as with mESC's onto GXG or TCP, in N2B27 medium.

2.4 Attachment and Expansion Studies

2.4.1 Phase Contrast Microscopy

Attachment and expansion were quantified for cells using confluency measurements at 24h and 72h, respectively. All increase in cell number over the first 24h (0-24h) post-seeding was considered as attachment. Any increase in cell number from 24h to 72h was considered expansion. Cells were first washed three times with PBS prior to measurements. Addition and removal of PBS for the wash step was standardised using an S1 pipet filler (Thermo Scientific, Hudson, USA), where aspiration and dispension speeds could be controlled to be consistent from run-to-run.

Phase contrast images were then obtained at 24h and 72h for confluency analysis. Images were obtained using an Eclipse TE2000-U microscope (Nikon, Kingston-Upon-Thames, UK) with a 4x objective, which was provided with the microscope. Five images were obtained from each well. Images were obtained randomly at roughly defined points (at the top-left, top-right, bottom-right, bottom-left and centre of each well). This was performed in three wells (to make up a technical triplicate) for each modulus condition. Three technical triplicates made up one biological replicate. This was repeated over three independent cell passage numbers (experiments performed on different days) to make up a biological triplicate.

2.4.2 Image Analysis

Confluency was measured from the phase contrast images using ImageJ software (rsbweb.nih.gov; NIH, Bethesda, USA). Images were first turned into an 8-Bit Binary grayscale. An intensity threshold value was then selected in order to remove any non-cellular artefacts from the image. Threshold values remained within $\pm 10\%$ of each other across the technical replicates. The “fill holes” function was used to remove any white gaps in cells. The result was a white image with cells marked as black objects. ImageJ then automatically measured percentage confluency by dividing the area of black objects by the area of the white space.

The mean of these confluency measurements was calculated for each technical replicate (from the five images for each well). Mean and standard deviation was then calculated from the three technical replicates to make up a biological replicate for the condition ($N=1,2,3$). The final mean and standard deviation was then calculated from three biological replicates. All one-way ANOVA and t-test statistical analysis was then performed from the three biological replicates.

Cell enumeration was performed on the confluency values to give values for cell concentration. A standard curve was created to calculate cell areas at various time-points during differentiation (0h, 24h, 48h, 96h). The % confluency (from above) was then multiplied by the area of the image in cm^2 to give the total area occupied by cells. This value was matched to the given value of cell area at the given time-point (24h or 72h) to obtain a cell number for that field of view. This was divided by the area of the image to give rise to a cell concentration value in cells/cm^2 .

2.5 Immunocytochemistry Analysis

2.5.1 Preparation – Fixation, Permeabilisation and Blocking

- Well plates were removed from the incubator and washed twice with PBS.

- 0.5 mL of 3.5% v/v paraformaldehyde (Sigma-Aldrich, Gillingham, UK) in PBS with 2% v/v sucrose (Sigma-Aldrich, Gillingham, UK) was dispensed into each well. Plates were incubated with the paraformaldehyde for ten minutes at 37°C.
- Following fixation, cells were again washed three times with PBS. 0.5 mL of 0.25% v/v Triton X-100 (Sigma-Aldrich, Gillingham, UK) was then dispensed into each well in order to permeabilise the cell membranes for intracellular antibodies. Cells were incubated with Triton at 37°C for three minutes, before being washed three times with PBS.
- The final preparation stage was a blocking step, which was performed in order to discourage non-specific binding of antibody cells. 0.5 mL of 2% v/v goat serum in PBS was dispensed into each well. Cells were incubated at room temperature for 20 minutes. The blocking agent was then removed using two PBS wash steps.

2.5.2 Antibody Staining

- 0.5 mL of primary antibody solution at a dilution of 1:400 in 2% goat serum (1:200 was used for nestin as it was not easily visible at higher ratios) was dispensed into each well. Cells were incubated overnight at 4°C with the primary antibodies. In the case of phalloidin, cells were incubated, covered in foil for one hour at room temperature at a dilution of 1:100. As phalloidin is a conjugated dye, secondary antibody incubation was not required. Thus these cells went immediately to the DAPI stage.
- Following incubation overnight, plates were washed three times with PBS. 0.5 mL of secondary antibodies (Invitrogen, Paisley, UK) were then dispensed into each well at a dilution of 1:400 in 2% v/v goat serum. Plates were incubated with the secondary antibodies, covered in foil at room temperature for one hour.
- The last stage was to stain cell nuclei, using 4',6'-diamidino-2-phenylindole (DAPI). Following a further three wash stages in PBS, 0.5 mL of DAPI

(Invitrogen, Paisley, UK) was dispensed into each well at a dilution of 1:500 in PBS. Cells were incubated at room temperature for two minutes before the DAPI was aspirated and the final three wash stages in PBS were performed. The final PBS wash was left in the wells to prevent cells drying out. All immunocytochemistry imaging was carried out using an Eclipse TE2000-U microscope (Nikon, Kingston-Upon-Thames, UK) with the supplied objective lenses.

The primary antibodies used are given below, along with the manufacturer and dilution:

1° Antibody	Manufacturer	Dilution
REX1	Millipore (Billerica, USA)	1:400
UTF1	Millipore (Billerica, USA)	1:400
OCT4	Santa Cruz Biotechnology (Dallas, USA)	1:400
Ki67	Millipore (Billerica, USA)	1:400
Nestin	Millipore (Billerica, USA)	1:200
A2B5	Millipore (Billerica, USA)	1:400
β-III Tubulin	Sigma-Aldrich (Gillingham, UK)	1:400
RC2	Millipore (Billerica, USA)	1:400
Phalloidin	Invitrogen (Paisley, UK)	1:100
α-Tubulin	Abcam (Cambridge, UK)	1:400
MAP2	Sigma-Aldrich (Gillingham, UK)	1:400

Figure 2.4: Primary antibodies used for immunocytochemistry analysis, along with manufacturer and dilution in 2% v/v goat serum.

2.6 Flow Cytometry

2.6.1 Preparation

The flow cytometry preparation protocol was similar to that above for immunocytochemistry analysis, except that cells were prepared in suspension rather than in-situ on well plates.

- Cells were firstly harvested from T75 flasks by trypsinisation, as outlined previously.
- Following centrifugation, the quenched medium supernatant was removed before cells were resuspended in PBS (with 2-3 aspirations and dispensions in order to create a single cell suspension).
- Hemocytometer counts (from a 10 µL cell suspension sample) were then used, similarly to before, in order to dilute cells to a concentration of 1×10^6 cells/mL, the recommended concentration for the flow cytometer. Cells were diluted to the appropriate concentration in PBS. All subsequent stages were performed in 2 mL vials (Eppendorf, Hamburg, Germany) on ice.
- As cells were analysed live using a cell surface marker, no fixation or permeabilisation stage was required. One vial was created for each sample (2 kPa, 18 kPa, 35 kPa, TCP and undifferentiated E14). In addition two additional vials were created. One was used for the isotype control (to isolate out background and non-specific fluorescence), whilst the other as an unstained control (in order to isolate target populations of cells for analysis using forward scatter/side scatter).
- Vials containing cells suspended in PBS were centrifuged in order to prepare for blocking. All centrifugations were performed at 2500 rpm for five minutes at 4°C, unless otherwise stated. Following centrifugation, the supernatant PBS was aspirated carefully and cells were resuspended in 600 µL 2% v/v goat serum blocking solution. This was followed by brief vortexing to ensure the

formation of a single cell suspension, cells were incubated for 20 minutes on ice.

- Following blocking, vials were again centrifuged to prepare cells for primary antibody addition. The supernatant was then aspirated carefully and 1 µL PSA-NCAM antibody (Abcam, Cambridge, UK) was added to the sample cell pellets. 1 µL IgM isotype control (Sigma-Aldrich, Gillingham, UK) antibody was added to the isotype control samples. These were then both diluted by aspirating 400 µL of 2% goat serum into the vials. Following vortexing, the cells were incubated with the primary or isotype control antibodies for one hour on ice. Unstained controls were simply resuspended in PBS, vortexed and kept on ice until they were analysed in the flow cytometer.
- Following primary antibody incubation, vials were centrifuged to prepare for secondary antibody addition. An additional PBS wash stage was performed before vials were centrifuged again (in order to reduce the risk of non-specific binding of secondary antibodies on excess PSA-NCAM primary antibodies in solution). 1 µL of goat anti-mouse IgM 488 secondary antibody (Invitrogen, Paisley, UK) was then added to each sample and isotype control. This was diluted with 400 µL of goat serum as before. Following vortexing, cells were incubated for one hour on ice with the secondary antibody.
- Following this, vials were centrifuged to prepare for the final PBS wash and flow cytometry analysis. Cells were washed once more with PBS, and centrifuged for a final time. Cells were resuspended in 1 mL PBS, vortexed and taken over (on ice) immediately for flow cytometry analysis.

2.6.2 Flow Cytometry Analysis

Flow cytometry analysis was performed using the CyAn ADP flow cytometer (Beckman Coulter, High Wycombe, UK).

- Following initialization of the device (including a self-cleaning cycle of the flow tubes), a run was performed using the unstained control. This was done in

order to set device conditions (voltage and event rate, for example) as well as to gate out viable cells from the overall population using forward scatter and side scatter. 1 mL of the unstained control was dispensed into the flow tubes supplied for the machine.

- Once viable cells were gated out, a histogram was set up with an event limit of 10,000. An isotype control run was then performed using these conditions. 1 mL of the isotype control was dispensed into the flow tubes supplied for the machine. From the resulting histogram, the lower 99.0% of the peak was gated out as a negative control. Any fluorescence in the subsequent samples above this gated value was counted as positive.
- The PSA-NCAM stained samples were then run using the gated histogram from the isotype control. 1 mL of each sample was dispensed into the flow tubes supplied for the machine. Summit software (Beckman Coulter, High Wycombe, UK) was used for all analysis.

2.7 qPCR

- Following differentiation, cells were harvested from the T75's by trypsinisation.
- After the quenched trypsin was removed, PBS was aspirated onto the cell pellet. The cells were pelleted once again by centrifugation and the supernatant aspirated carefully using a pipette (Gilson, Middleton, WI, USA).
- The dry cell pellets were stored at -20°C. All subsequent steps were performed on ice.

2.7.1 RNA Extraction

- RNA was extracted from the cell pellets using the RNeasy Micro Kit (Qiagen, Sussex, UK). The cell pellets were thawed briefly at room temperature and flicked by hand to displace from the bottom of the centrifugation tube.
- 75 µL of Buffer RLT was dispensed into the pellet. The lysed suspension was aspirated and dispensed a number of times in order for the reaction to proceed fully. The lysed suspension was then pipetted into QIAshredder spin column

(Qiagen, Sussex, USA). The spin column was placed in a 2 mL collection tube (Qiagen, Sussex, USA) and centrifuged at full speed for two minutes. 75 µL of 70% ethanol was then dispensed into the lysate solution in the 2 mL collection tube. The solution was aspirated and dispensed multiple times until it became clear. The solution was then aspirated from the collection tube and dispensed into an RNeasy MiniElute spin column (Qiagen, Sussex, UK), placed inside a fresh 2 mL collection tube. The lid of the spin column was gently closed and the tube centrifuged at 8,000 x g for 15 seconds. The spin column was removed to allow the flow through liquid within the collection tube to be poured out. The spin column was then placed back inside it.

- 350 µL of Buffer RW1 was dispensed into the spin column. The lid was again gently closed and the tube centrifuged at 8,000 x g for 15 seconds. The flow through within the collection tube was again poured out as waste before the spin column was replaced.
- 70 µL of Buffer RDD was dispensed into a separate 0.5 mL vial (Eppendorf, Hamburg, Germany). To this, 10 µL of DNase I stock solution was added. The vial was gently inverted twice to mix. 10 µL of DNase I mixture was then dispensed onto each spin column filter. The tubes were then allowed to incubate at room temperature for 15 minutes. Following the incubation step, 350 µL of Buffer RW1 was added to each spin column. The lid was closed gently and the tube centrifuged at 8,000 x g for 15 seconds. After centrifugation, the 2 mL collection tube was discarded, with the follow through liquid. The spin column was then placed in a fresh 2 mL collection tube.
- 500 µL of Buffer RPE was then dispensed into the spin column. The lid was gently closed and the tube centrifuged at 8,000 x g for 15 seconds. Following removal of the spin column, the follow through liquid in the collection tube was poured out as waste. 500 µL of 80% ethanol was then dispensed into the spin column. The lid was gently closed and tube centrifuged at 8,000 x g for two minutes. The collection tube (along with the flow through liquid) was

discarded. The spin column was then placed in a fresh 2 mL collection tube. The lid was opened and the tube centrifuged at full speed for five minutes. The collection tube was then discarded again along with the follow through liquid.

- The spin column was then placed in a 1.5 mL collection tube (Qiagen, Sussex, UK) for the elution stage. To elute, 14 µL of RNase free water was dispensed into the centre of the spin column filter membrane. The lid was closed gently and finally the tube was centrifuged at full speed for a minute to elute the template RNA into the 1.5 mL collection tube.
- The concentration of RNA in elute was measured using a Nanodrop spectrophotometer (Thermo Scientific, Delaware, USA). The spectrophotometer measured RNA concentration using absorbance at wavelengths of 260 nm and 280 nm. 1 mL of distilled water sample was dispensed onto the reader and a blank measurement made before each sample reading. Following the reading, the vials were kept at -80°C for storage.

2.7.2 cDNA Synthesis

1 mg of RNA (calculated from the spectrophotometer reading) was then used to synthesise first strand cDNA using the RETROscript First Strand Synthesis Kit (Qiagen, Sussex, UK), again as per the manufacturer's instructions, using random decamers to prime the first strand reaction. A Mastercycler EP Realplex (Eppendorf) thermocycler was used to carry out the synthesis reaction. The steps are outlined below:

- The template RNA vials were defrosted on ice. The Reverse Transcriptase (Qiagen, Sussex, UK), RT Buffer (Qiagen, Sussex, UK), RNase-free water (Qiagen, Sussex, UK) and gDNA wipeout buffer (Qiagen, Sussex, UK) were also thawed, albeit at room temperature.
- The genomic DNA elimination reaction was then set up on ice. To increase the accuracy of volume measurements, large stock quantities were made and aliquoted for each gene and sample studied. For example for six genes across the four samples (2 kPa, 18 kPa, 35 kPa and TCP), samples were made for 24

reaction wells. An extra 10% volume was added to factor in pipetting error. One 0.5 mL vial (Eppendorf, Hamburg, Germany) was used for each reaction well. For each reaction well, 14 μ L was made up containing 2 mL gDNA wipeout buffer, x mL template RNA (where x is the mL of RNA elute containing 1 mg of RNA) and (12-x) mL of RNase free water. 14 μ L of elimination reaction mixture was dispensed into each 0.5 mL vial. The vials were briefly spun (10,000 rpm for five seconds) in order to mix. The vials were then placed inside the thermocycler and incubated at 42°C for two minutes.

- The reverse transcription master mix was then set up on ice. 6 μ L was created for each reaction well, containing 1 μ L Reverse Transcriptase, 4 μ L RT Buffer and 1 μ L RT Primer Mix. Primer sequences are proprietary but details can be found at www.qiagen.com/GeneGlobe/. Primer assays are detailed in Figure 2.5. Once again, a large volume master mix was made up for the total number of reactions plus an additional 10% for pipetting error. 6 μ L of reverse transcription master mix was dispensed into each vial containing 14 μ L of gDNA elimination reaction mixture. The vials were briefly spun (10,000 rpm for five seconds) in order to mix.
- The vials were then placed in the thermocycler. A second protocol was run, where the vials were first incubated for 15 minutes at 42 before being incubated at 95 for three minutes. The cDNA samples were stored long term at -20°C.

2.7.3 PCR Plate Setup

For gene expression analysis, 1 μ L of the cDNA was used in a SYBRGreen real time PCR reaction using the Eurogentec (Southampton, UK) SYBR Green PCR Kit and the pre-validated QuantiTect Primer Assays (Qiagen, Sussex, UK) under the manufacturer's protocols.

- The components of the qPCR master mix were thawed on ice. These included the MESA Blue MasterMix (Eurogentec, Southampton, UK), QuantiText Primer Assay (Qiagen, Sussex, UK) and RNase-free water (Qiagen, Sussex, UK).
- The larger volume qPCR master mix was made up in a 1.5 mL tube (Eppendorf, Hamburg, Germany) to be aliquoted into cDNA samples. Per 20 µL sample, 10 µL of MESA Blue MasterMix, 2 µL of Primer Assay and 8 µL of RNase-free water was used. In total, three (technical triplicate) samples were made per condition studied (2 kPa, 18 kPa, 35 kPa and TCP), in addition to two additional control samples (NTC – no template control and NRT – no reverse transcription control). An additional sample was made up to account for pipetting error, bringing the total up to 15 samples for four conditions. After pipetting, the tube was centrifuged briefly (10s) at 10,000 rpm to mix.
- The MasterMix was then aliquoted into 0.5 vials to prepare for plate setup. Four vials were used per gene (one for each condition; 2 kPa, 18 kPa, 35 kPa and TCP). 60 µL was aliquoted into each vial. 3 µL of cDNA (from the previous stage) was pipetted into each vial containing MasterMix. They were mixed by aspirating and dispensing several times using the pipette before being centrifuged for 10s at 10,000 rpm.
- 20 µL of the gene sample for study was then pipetted from the vials into each well of the qPCR plate (BioRad, Hemel Hempstead, UK).
- 20 µL of MasterMix alone (without cDNA) was dispensed into the penultimate row (row G) of the PCR plate as the NTC control. Additionally, 20 µL of MasterMix with 1.0 mg RNA (from earlier) but without cDNA was added to the last row (row H) of the PCR plate as the NRT control.
- The lid was then covered by a supplied plastic cover (BioRad, Hemel Hempstead, UK). A straight edged object was then used to force out air bubbles between the plate and cover.
- Finally the PCR plate was kept on ice to prepare for immediate analysis.

2.7.4 PCR Analysis

After being centrifuged at $300 \times g$ for three minutes, the PCR plates were placed in a CFX Connect Real-Time PCR Detection System (Qiagen, Sussex, UK). The “Quickplate SYBR Assay (Clear Wells)” protocol (Eurogentec, Southampton, UK) was then selected. The lid of the machine was opened and the plate placed into the holder. The lid was closed and the protocol was run.

For relative quantification, the $\Delta\Delta C_t$ method (Pfaffl, 2001) was used. Briefly, C_t refers to the threshold cycle, the number of PCR cycles required for the threshold (set by the machine) value of fluorescence signal to be overcome by the sample. $\Delta\Delta C_t$ is equal to the difference between $\Delta C_{t\text{ treated}}$ (the difference in C_t between each sample and the equivalent housekeeping genes for that condition) and $\Delta C_{t\text{ control}}$ (the difference in C_t between each TCP control and the housekeeping genes for the control). RNA levels were normalised against the housekeeping genes GAPDH and TBP, as selected in Chapter 3. All calculations were performed using the BioRad CFX Manager software (BioRad, Hemel Hempstead, UK).

Primer	Product Code	Role (Chapter)
β-Actin	QT00095242	Housekeeping (3)
Gapdh	QT01658692	Housekeeping (3,4,5)
PGK1	QT00306558	Housekeeping (3)
RN18	QT02448075	Housekeeping (3)
TBP	QT00198443	Housekeeping (3,4,5)
OCT4 (Pou5f1)	QT00109186	Pluripotency (4)
UTF1	QT00252112	Pluripotency (4)
FGF5	QT00108906	Early differentiation (4)
T-Brachyury	QT00094430	Mesoderm (4)
Sox17	QT00160720	Endoderm (4)
Nestin	QT00316799	Neural precursor (4)
β-III Tubulin	QT00124733	Neuronal (4,5)
GFAP	QT00101143	Astrocyte (4)
TH	QT00101962	Late Neuronal (4)
GAD2	QT00101416	Late Neuronal (4)

Figure 2.5: Primer assays used for qPCR analysis. Primer, Qiagen code and role of gene shown (with Chapter number in which gene was used).

2.8 Blebbistatin and Nocodazole Inhibition

2.8.1 Blebbistatin

Powdered blebbistatin was dissolved into DMSO to form a stock solution. This solution was then aliquoted into vials and stored at -20°C for further use. For experiments, these aliquots were diluted in 10 mL of normal culture medium without LIF to a final concentration of 50 µM. This concentration was chosen on the basis of previous studies using blebbistatin (Engler et al, 2006; Chowdhury et al, 2009).

Prior to treatment, spent medium was removed from the T25's (E14) and T75's (Partially-differentiated cells). The medium containing blebbistatin was then added to the flasks, which were allowed to incubate for 30 minutes. Following this pre-treatment, the blebbistatin was removed and the cells were prepared for differentiation as outlined earlier.

2.8.2 Nocodazole

Nocodazole was aliquoted and stored in a similar fashion in DMSO to blebbistatin (see above). These aliquots were diluted to a final concentration of 50 µm in 35 mL of N2B27 medium. This medium was then added to the cell suspension before seeding (Spedden et al, 2012).

2.9 Rate of Spreading

In order to analyse rate of spreading, partially-differentiated cells were pre-treated with CellTracker (Invitrogen, Paisley, UK) using a similar method to that for blebbistatin. CellTracker highlights the cell perimeter under fluorescence in such a way that it becomes easy to accurately measure cell surface projection area using image analysis software. Cell tracker was diluted in 10 mL of medium (at a dilution ratio of 1:200) before being added directly to the adhered partially-differentiated cells within

the T75 flasks. The cells were then harvested and seeded for differentiation experiments as outlined earlier.

Images were obtained 2 hours, 4 hours and 6 hours following seeding using the fluorescence bulb on the Eclipse TE2000U (Nikon, Kingston-Upon-Thames, UK). Five cells were selected at random from each well (from one field of view). A total of 15 cells were thus selected for each condition. The images were analysed in the same way as with attachment, where ImageJ was used to create binary images of cells (black) on the surfaces (white). The “analyze particles” function was used to measure the projection areas of individual cells.

The mean projection areas of cells were compared across the four conditions at the time points mentioned above. The projection areas at t=4h and t=6h were also normalized to the initial projection area (the projection area at t=2h) in order to measure rate of spreading.

2.10 Statistics

All statistical analyses were carried out using SPSS software (v.21; IBM). One-way ANOVA analysis was used to calculate statistical significance amongst trends across the four materials. Tukey’s test for multiple comparisons was then used to identify where the statistical differences lay. For the blebbistatin and nocodazole experiments, as the comparisons were being made between the treated and untreated conditions, rather than across the population as a whole, independent-samples t-test was used for each condition.

In all cases, a p-value less than 0.05 was considered statistically significant (95% confidence interval).

3 GXG and Protocol Development

In this chapter, a number of initial challenges were addressed before the effect of Young's modulus on mouse embryonic stem cell (mESC) neuronal differentiation was investigated. The neuronal differentiation conditions outlined in Ying et al (2003) produce large colonies of nestin-positive neural precursors (Engler et al, 2006) and β -III tubulin positive immature neurons (Engler et al, 2006). However, the commercially available RHB-A (Stem Cells Inc, Cambridge, UK) medium caused a number of variability issues in terms of cell attachment and expansion. As attachment and expansion were key to the central hypothesis of this study, this was a problem that immediately required addressing.

3.1 Aims

With this in consideration, the first experiments were aimed at characterizing the starting conditions used for the experiments. Factors such as medium formulation (commercially produced vs. 'in-house' preparation), serum concentration and seeding density were all decided upon at this stage. Optimizing these conditions, allowed for maximal neuronal precursor formation for Young's modulus study,

In order to compare differentiation across different Young's modulus conditions, it was necessary to develop assays, which could robustly compare differentiation across conditions. It was also important to establish the time-points during differentiation where key markers for cell identity (for neural precursors, immature neurons and glial cells) would be expressed.

To achieve this, the pluripotency of the starting cell populations were validated along with the time-lapse emergence of key phenotype markers during differentiation. The two key quantitative assays used in testing the main hypotheses of this study were then validated, namely real-time, quantitative polymerase chain reaction (qPCR) and flow cytometry.

Prior to commencing Young's modulus work in mESC's, two non-mESC cell lines (fibroblasts and human embryoid bodies) were plated on GXG in order to provide a basis for comparison for the mESC cell work.

The final work in this chapter involved seeding mESC's in other, non-neuronal differentiation conditions, in order to assess whether the effect of Young's modulus on mESC attachment and expansion was influenced by the growth medium.

3.2 How does medium composition affect attachment of mESC's in neuronal differentiation medium?

Attachment of mESC's was key to the central hypothesis tested in this study. It was therefore, imperative to maximise the initial attachment of mESC's in neuronal differentiation medium. The most commonly used monolayer neuronal differentiation medium for mESC's is N2B27, as formulated in the study by Ying et al (2003). MESC's seeded on gelatin-coated tissue culture polystyrene (TCP) in N2B27 medium expand in adherent monolayer culture, to form colonies with rosette-like morphologies, positive for neural precursor and later immature neuronal markers such as nestin and β -III tubulin respectively. Further differentiation leads to development of mature neuronal subtypes such as GABAergic and tyrosine hydroxylase-positive neurons.

The commercially available version of N2B27, termed RHB-A (Stem Cells Inc, Cambridge, UK) is a modified, proprietary formulation. Initial attempts at seeding in RHB-A medium resulted in negligible colony formation at day four, typified by the morphologies observed on the top line of figures in Figure 3.1.

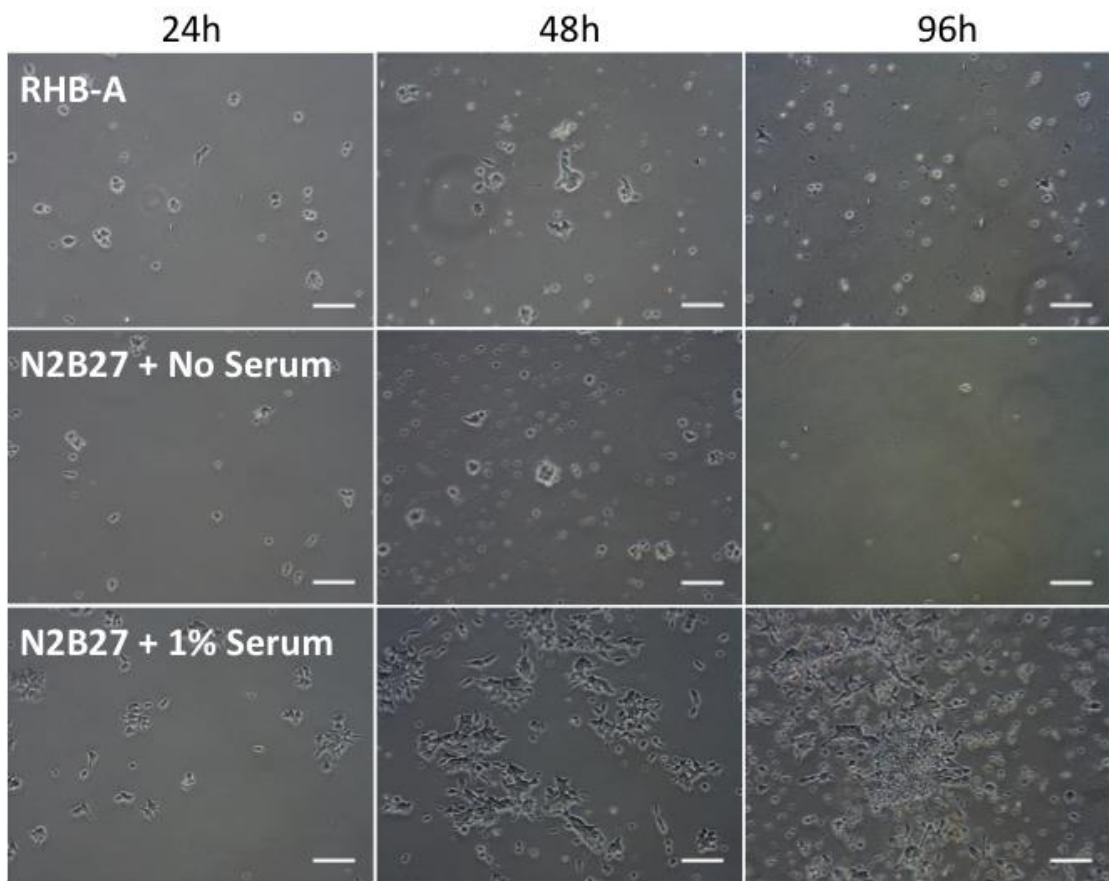


Figure 3.1: Comparison of cell attachment and growth over 96h in 3 different neuronal differentiation media. Top: RHB-A, a commercially available, pre-prepared medium. Middle: N2B27 with no serum, prepared in the laboratory according to the medium recipe given by Ying et al (2003). Bottom: N2B27, the same medium, with 1% v/v serum added. Scale Bars = 100 μ m.

Attachment did occur over the first 48h, but following this there was a significant amount of cell detachment and death. There were some rare occasions where cells did remain attached (results not shown) following attachment, but the run-to-run reproducibility of this effect was not satisfactory for attachment studies.

Neuronal differentiation in N2B27 is typified by significant amount of cell detachment and death, as the medium selects against cells that do not differentiate towards a neuronal lineage, but the amounts of detachment and lack of expansion at 96h in RHB-A was excessive in comparison to the images seen in the Ying et al (2003) study.

Based on this, the decision was made to formulate the N2B27 medium ‘in house,’ using the defined components given in the Ying et al (2003) paper. When cells were seeded in this more chemically defined medium (Figure 3.1, middle row), a similar profile emerged in expansion following attachment. Forming neuronal precursors at the 96h time-point was as difficult as with RHB-A.

The persistence of these initial problems led to the conclusion that serum may have been the key to promoting cell spreading and expansion. Fetal bovine serum (FBS) is commonly used as a medium component in order to promote attachment in many adherent cells, including mESC’s owing to its vitronectin and to a lesser extent, fibronectin content (Hayman et al, 1985). However, serum is undesirable for early neuronal differentiation as it contains the bone morphogenetic protein BMP-4 (Finley et al, 1999). BMP-4 antagonises Shh and noggin, two growth factors that play a key role in early neurogenesis (see Introduction). Thus N2B27 medium is formulated for serum free growth.

It was hoped, that by using a small amount of serum (1% v/v in N2B27) during seeding, cells would remain adhered during expansion. The bottom row of Figure 3.1 highlights the improvement that was observed with serum use during attachment. Cells attached with similar numbers at 24h, whilst forming a markedly more spread out morphology than that of the RHB-A and zero-serum N2B27 medium. Following attachment, despite there being a continued detachment effect, considerably more cells appeared to form

colonies than in the other media. This effect was reproducible across numerous passages. Cells appeared to maintain a homogeneous morphology during differentiation, implying that differentiation was occurring efficiently. On the basis of these findings, the effects of serum were investigated further.

Three different serum conditions were used to complete optimization of the medium; 0%, 1% and 5% v/v serum. The highest condition was used in order to ascertain whether attachment could be improved further and whether morphologies would remain homogeneous during expansion.

As before, adding 1% v/v serum to N2B27 during seeding caused cells to become more spread at 24h when compared to the serum-free N2B27. Increasing the serum concentration to 5% v/v also lead to cells having a spread morphology at 24h following seeding (Figure 3.2A). However, the cell morphologies did not appear to be as homogeneous as that observed in the 1% v/v serum condition, implying that non-neuronal differentiation is taking place.

Most cells detached in the 0% serum condition between the 24h and 72h time-points. Those cells that remained attached appeared to be rounded and did not form large colonies at 72h. In N2B27 medium with 1% v/v serum, cells expanded to form dense, rosette-like colonies. These colonies contained cells that were more spread out than the few cells that remained attached on the zero serum condition. 5% v/v serum also resulted in cells proliferating and forming colonies but cellular morphologies were again not as homogeneous as that of the 1% v/v serum condition. Ying et al (2003) reported that serum use does produce some non-neuronal epithelial-like cells.

Confluence was quantified at 24h from phase contrast images in order to assess whether 5% serum significantly increases attachment compared to the 1% and 0% conditions. Serum concentration had no significant ($p=0.393$) effect upon attachment of cells at 24h (Figure 3.2B).

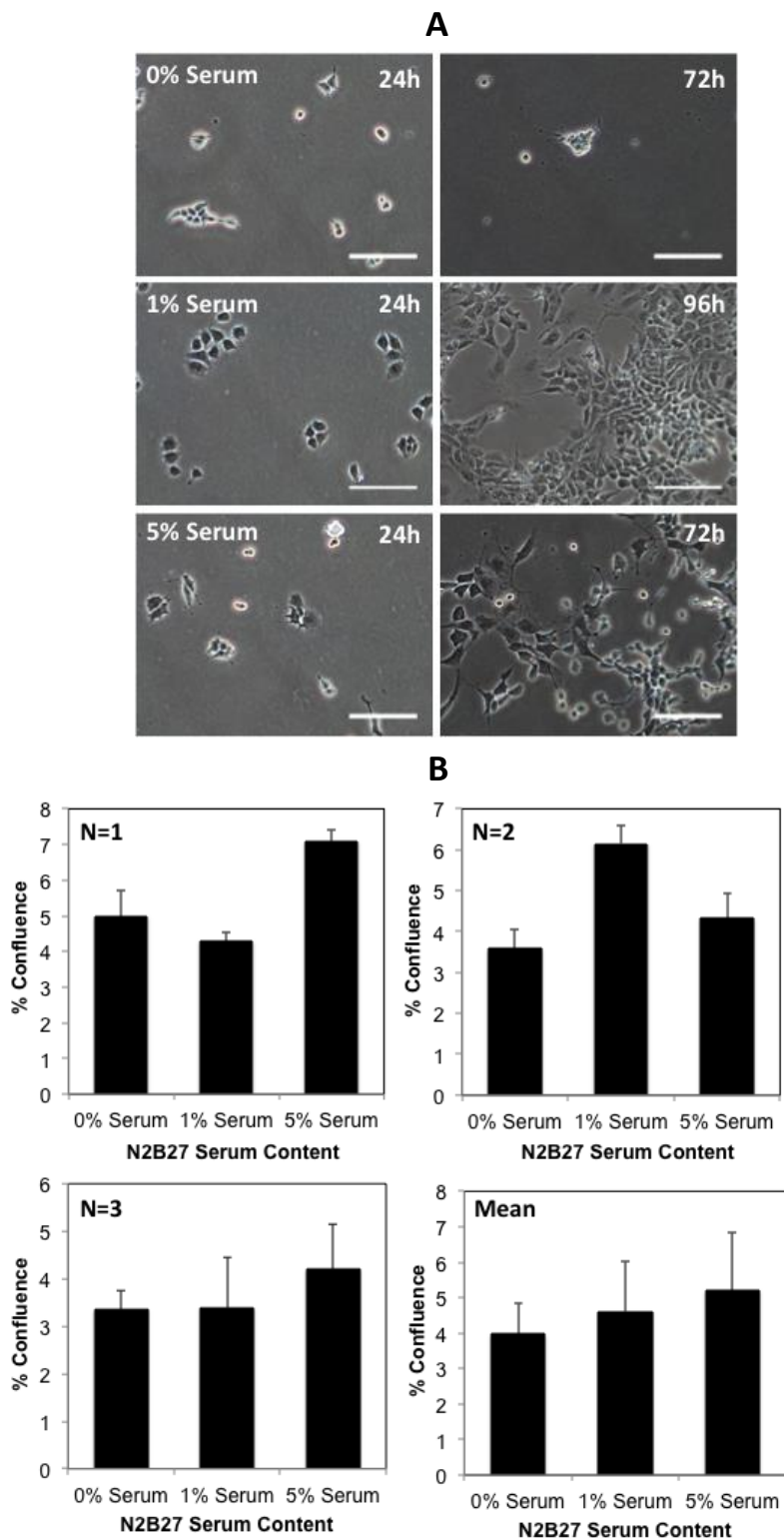


Figure 3.2: The effect of serum on attachment and expansion. (A) Representative phase contrast images at 24h and 72h (96h for 1% v/v serum) of mESCs seeded onto TCP in N2B27 containing 0%, 1% and 5% v/v serum. All scale bars = 100 μ m. (B) Confluency measurements at 24h for mESCs seeded on TCP in N2B27 with increasing concentrations of serum (0%, 1%, 5%). All three biological replicates shown as well as the mean. Error bars represent standard deviation from the mean.

Based on these findings, the homemade N2B27 medium containing 1% v/v serum was chosen as the medium for seeding and expanding cells for attachment studies. Serum free medium did not allow for colony expansion following seeding, whilst 5% serum did not provide any benefits in attachment to compensate for the more heterogeneous morphologies observed at 24h and 72h.

3.3 How does seeding density affect attachment of mESC's in neuronal differentiation medium?

A seeding density range of $0.5\text{--}1.5 \times 10^4$ cells/cm² was recommended for N2B27 medium (Ying et al, 2003). In order to maximise colony formation at day four so that sufficient quantities of cells were available for analysis, it was of interest to investigate the effect of seeding density on cell concentrations following differentiation.

Two seeding densities were chosen for study; 1×10^4 cells/cm² and 2×10^4 cells/cm². The higher value was outside of the recommended range (Ying et al, 2003). MESC's were seeded at these two densities onto gelatin-coated T-75 flasks (made of TCP) in N2B27 neuronal differentiation medium (with 1% v/v serum). Cells were then allowed to expand for four days before harvesting. This was ample time for large colony formation (Figure 3.1 – see N2B27 + 1% serum condition at 96h).

Prior to harvest at day four, the spent medium from the flasks was aspirated. A cell count was then performed on this medium to measure detached cell concentration. This would indicate whether there was a critical value for seeding density, above which increases in attached cell concentration would not be supported. Trypan blue staining revealed that cells were non-viable in the spent medium, as expected (data not shown). Differentiated cells were harvested by trypsinisation and counted using a hemocytometer in order to compare differences in attached cell concentration with seeding density.

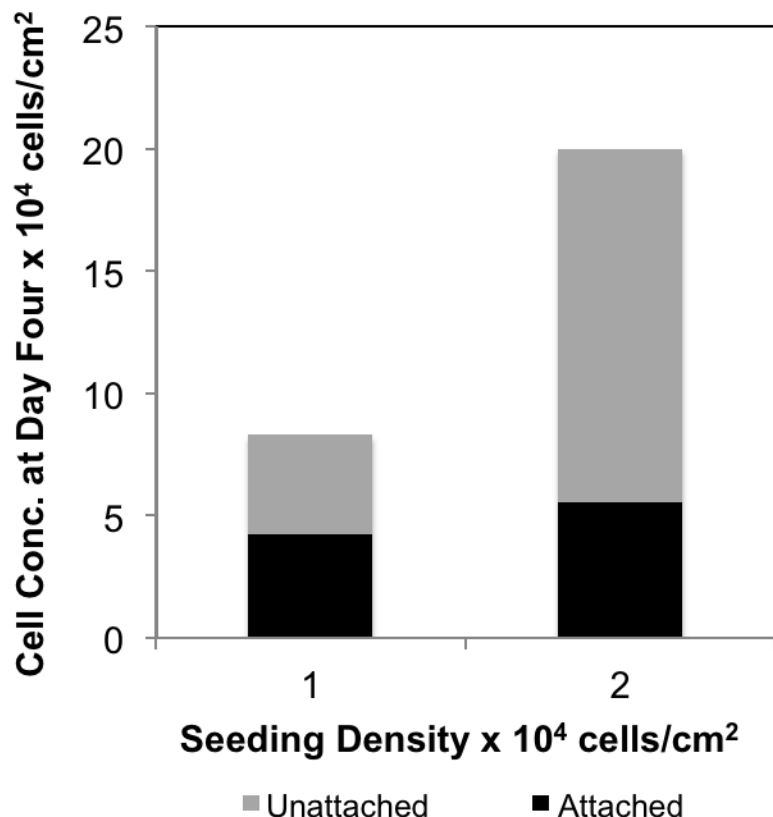


Figure 3.3: Comparison of cell concentration at day four of neuronal differentiation on TCP at two seeding densities: 10,000 cells/cm² and 20,000 cells/cm². Cell concentration of the harvest was measured as attached and cell concentration in the spent medium measured as unattached cells.

Attached cell concentration at day four was 24% higher with a 100% increase in seeding density from 1 to 2×10^4 cells/cm² (Figure 3.3). The seeding density increase was accompanied by a 72% increase in unattached cell concentration. The large increase in detached cell concentration with the increase in seeding density negated the slight increase in attached cell concentration. The lower, 1×10^4 cells/cm² seeding density was chosen as a result.

3.4 Validation of starting cell populations and neuronal differentiation marker expression

Before the mESC's underwent neuronal differentiation, their identity was validated in order to ensure that they were true pluripotent cells. Immunocytochemistry analysis was performed for four pluripotent markers; Rex1, Oct4, UTF1 and Ki67. The first three are characteristic transcription factors present in the nuclei of pluripotent stem cells (Ben-Shushan et al, 1998; Nichols et al, 1998; Okuda et al, 1998). Ki67 is actually a marker for proliferative cells (Yu et al, 1992), but as unlimited self-renewal is one of the key characteristics of pluripotent stem cells, it can act as a useful negative control for differentiation.

When immunocytochemistry analysis was performed for these four factors (Figure 3.4), UTF1 and Oct4 were revealed to be present in the nuclei (staining corresponded closely to that of nuclear stain DAPI) of the mESC's. Ki67 was also present in the nucleus and cytoplasm of all cells (it is not a transcription factor). This was evidence that cells were proliferative. Morphology alone is not a very effective indication of phenotype, but the cells did exhibit typical mESC morphologies. They were rounded, and densely packed into compact colonies. Interestingly, Rex1 was not revealed in cell nuclei during immunocytochemistry analysis. Rex1 is not as fundamental a marker for pluripotency or stemness as Oct4 and is in fact regulated by Oct4 (Ben-Shushan et al, 1998). In that study, high levels of Oct4 activity were found to repress Rex1 expression in certain conditions. It is likely that this phenomenon has occurred in the mESC's used for this investigation, explaining the abundance of Oct4 and the absence of Rex1.

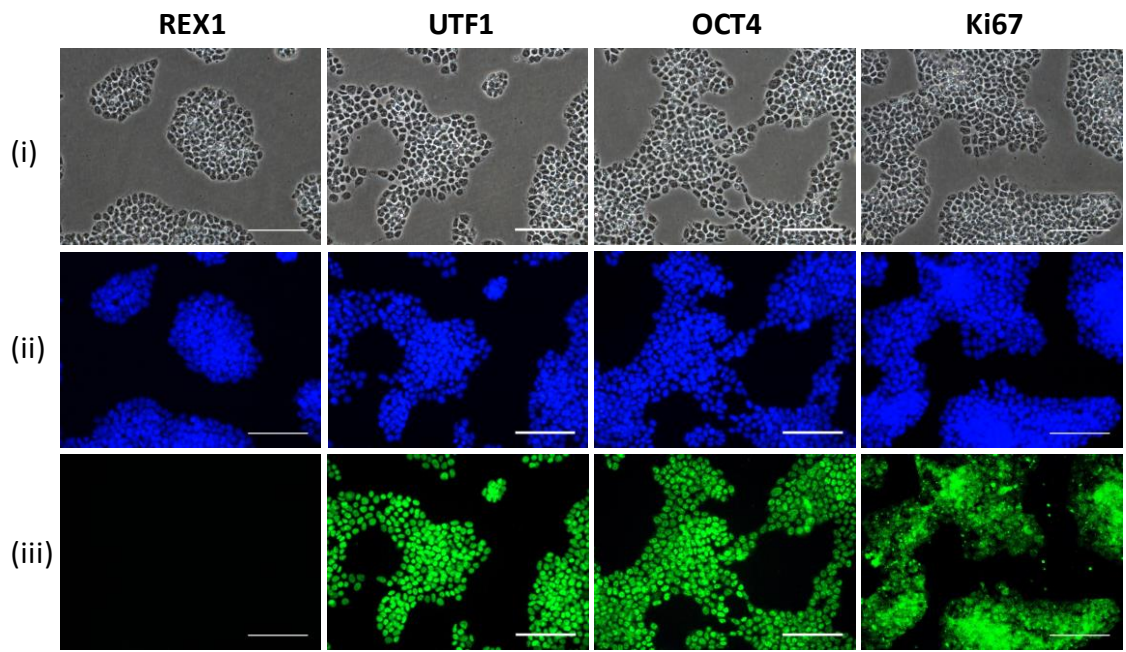
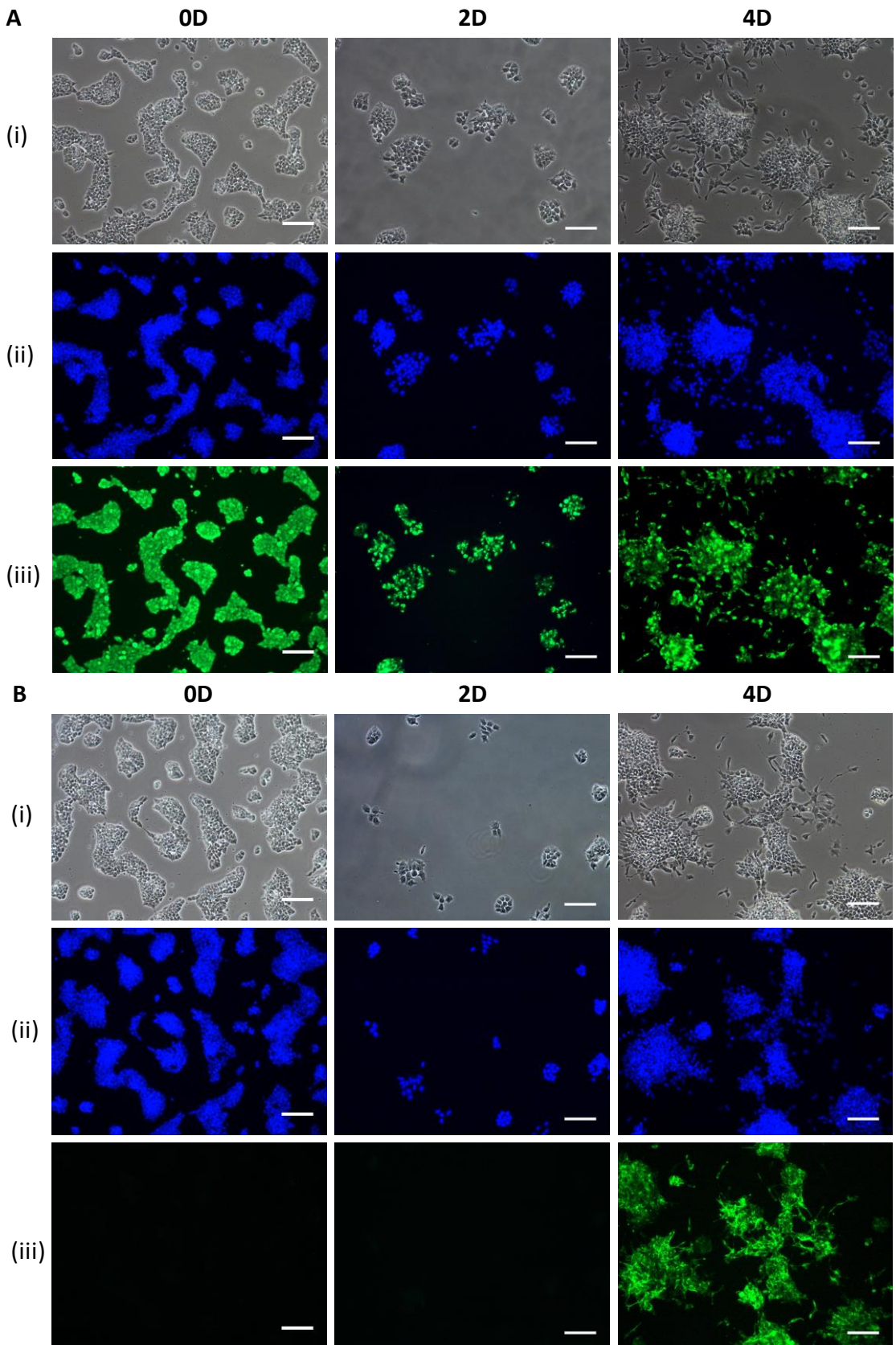


Figure 3.4: Immunocytochemistry (ICC) validation of starting populations of mouse embryonic stem cells prior to differentiation. (i) Phase contrast. (ii) DAPI, a nuclear stain. (iii) ICC. From left to right: Rex1, UTF1, Oct4 and Ki67. All scale bars = 100 μ m.

In order to compare neuronal differentiation on varying Young's moduli, it was important to understand at what time-points key markers for differentiation would begin to be observed in colonies. Four markers were chosen for characterization of mESC neuronal differentiation in N2B27 medium; nestin, β -III tubulin, A2B5 and RC2. Nestin is a marker for neural precursors (Engler et al, 2006). It is found in rosette-like colonies early on during differentiation (Ying et al, 2003), forming filamentous structures within the cytoplasms of progenitor cells. Some of these nestin-positive cells in colonies then go on to differentiate further into cells positive for β -III tubulin (Ying et al, 2003). These immature, post-mitotic cells are the earliest indicators of neuronal specification. These immature neurons then undergo maturation to form a variety of specialized neuronal subtypes, including dopaminergic neurons and GABAergic neurons.

RC2 is a marker for radial glial cells in the mouse cortex (Park et al, 2009), also used to identify mouse neural stem cells (Conti et al, 2005). There is some evidence (Park et al, 2009) that its expression is controlled by nestin activity, which would explain why it is often co-expressed with that marker in progenitor cells. A2B5 is a cell surface marker for O2-A oligodendrocyte progenitor (Baracskay et al, 2007) and type-II astrocyte cells (Scolding et al, 1999) in mice, and so is an earlier indicator for the presence for non-neuronal glial cells. Glial cells play a supportive role for neurons, both during normal growth (astrocytes) as well as during repair of damaged tissue (oligodendrocytes). Neural stem cells that do not differentiate towards the neuronal lineage would be expected to form into glial cells.

MESC's were seeded in N2B27 medium with 1% v/v serum at a seeding density of 1×10^4 cells/cm² for six days. Cells were fixed and immunocytochemistry analysis was performed at day zero (undifferentiated mESC's), day two, day four and day six. Cells were not differentiated further if a marker was expressed before day six. As seen in Figure 3.5A, A2B5 was observed in mESC's and continued to be present in cells throughout differentiation to four days. It was concluded that A2B5 was not an effective marker for neuronal differentiation.



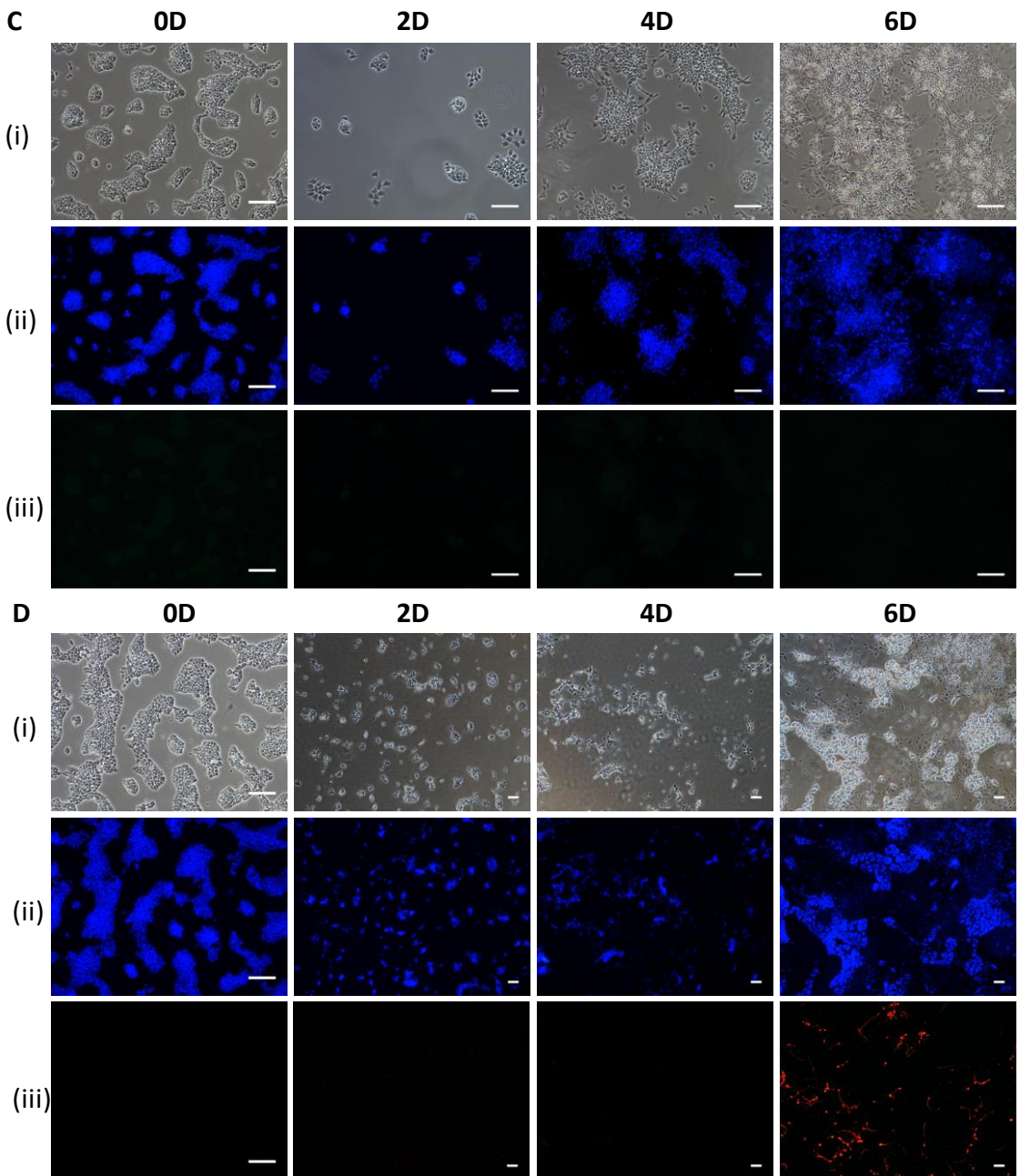


Figure 3.5: Time-lapse immunocytochemistry (ICC) analysis for validation of neuronal differentiation. MESC's were seeded on TCP in N2B27 medium and allowed to differentiate for four (A and B) or six days (C and D). Four neuronal markers were tested: (A) A2B5 (B) Nestin (C) RC2 (D) β -III Tubulin. (i) Phase contrast. (ii) DAPI, a nuclear stain. (iii) ICC. All scale bars = 100 μ m.

Nestin (Figure 3.5B) was a more robust indicator of neuronal differentiation. It was not observed on any of the mESC's at day zero. Similarly, no nestin-positive cells were observed at day two of differentiation. At day four, however, as colonies began to expand to form rosette-like morphologies, nestin appeared abundantly in cells. Nestin formed filamentous internal structures. These filaments were particularly rich in parts of the cell undergoing extension into neurites.

The nestin-positive neural precursors were similar in morphology and internal nestin structures to the progenitors (Ying et al, 2003), neural stem cells (Conti et al, 2005; Saha et al, 2008) and primary neuronal cultures (Previtera et al, 2013) seen in previous studies. The wide range of cells that appear to contain nestin in literature reflects its persistence during neuronal differentiation. Nestin begins to disappear in cultures fairly late on during differentiation (Ying et al, 2003), making it an effective neural precursor or immature neuronal marker.

In contrast to A2B5, the other glial marker, RC2 was not found on any of the colonies (Figure 3.5C) after six days of differentiation. As with A2B5, a decision was made not to use this marker as an indicator for mESC neuronal differentiation.

The final marker characterised was β -III tubulin, which was used to isolate the time-point at which immature neurons were formed from the neural precursors. As observed in Figure 3.5D, β -III tubulin did not appear in cells until later on in differentiation. It appeared in cells at day six, as cells extend and branch out their neurites within and between colonies of precursors. It appeared evenly within the immature neuron bodies as well as their neurites. Cells positive for the marker appeared to form networks between colonies. Whilst a large portion of mESC's became nestin-positive neural precursors at day four, a noticeably smaller fraction of neural precursors form into β -III tubulin positive neuronal cells at day six.

3.5 Assay validation for flow cytometry and qPCR

3.5.1 PSA-NCAM negative control

Flow cytometry and quantitative polymerase chain reaction (qPCR) are two techniques, which together provide a detailed understanding of the changes in cell phenotype that occur during differentiation. Flow cytometry allows for quantification of immunocytochemistry, by measuring the percentage of cells in a population positive for a particular marker. Measurement of neural precursor marker expression in mESC's provided a negative control for differentiation studies as well as further characterizing the starting population.

If the marker used for flow cytometry is a cell surface antigen marker, cells can be analysed viable without fixation. Viable cells can be prepared for analysis with minimal processing and wash stages. This allows for less cell losses during preparation and for a more accurate representation of cell identity in culture than cells that are fixed in paraformaldehyde for an extended period of time.

Most markers for neural precursors and neurons, such as β -III tubulin and nestin, are present within the cytoplasm and so require fixation (making them non-viable) and permeabilisation in order to bind to their targets. However, PSA-NCAM (polysialic acid neural cell adhesion molecule) is a neural adhesion marker expressed at the cell surface, where it plays a role in neurogenesis and progenitor migration (Gago et al, 2003). Being expressed at the cell surface, fixation and permeabilisation are not required and thus cells can be analysed whilst viable.

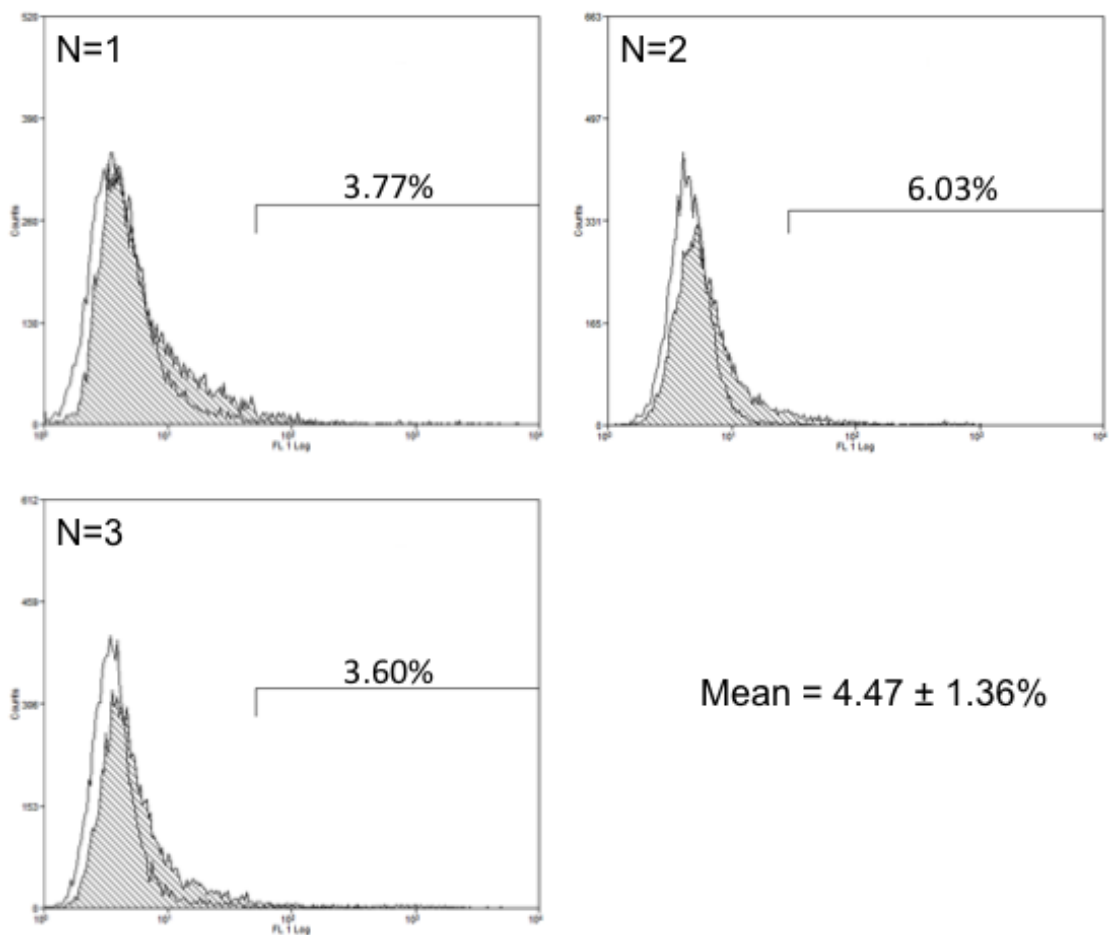


Figure 3.6: Flow cytometry analysis for neural cell adhesion marker PSA-NCAM in undifferentiated E14 mouse embryonic stem cells. All three biological replicates (independent passages) shown, as well as mean \pm standard Deviation. N=3.

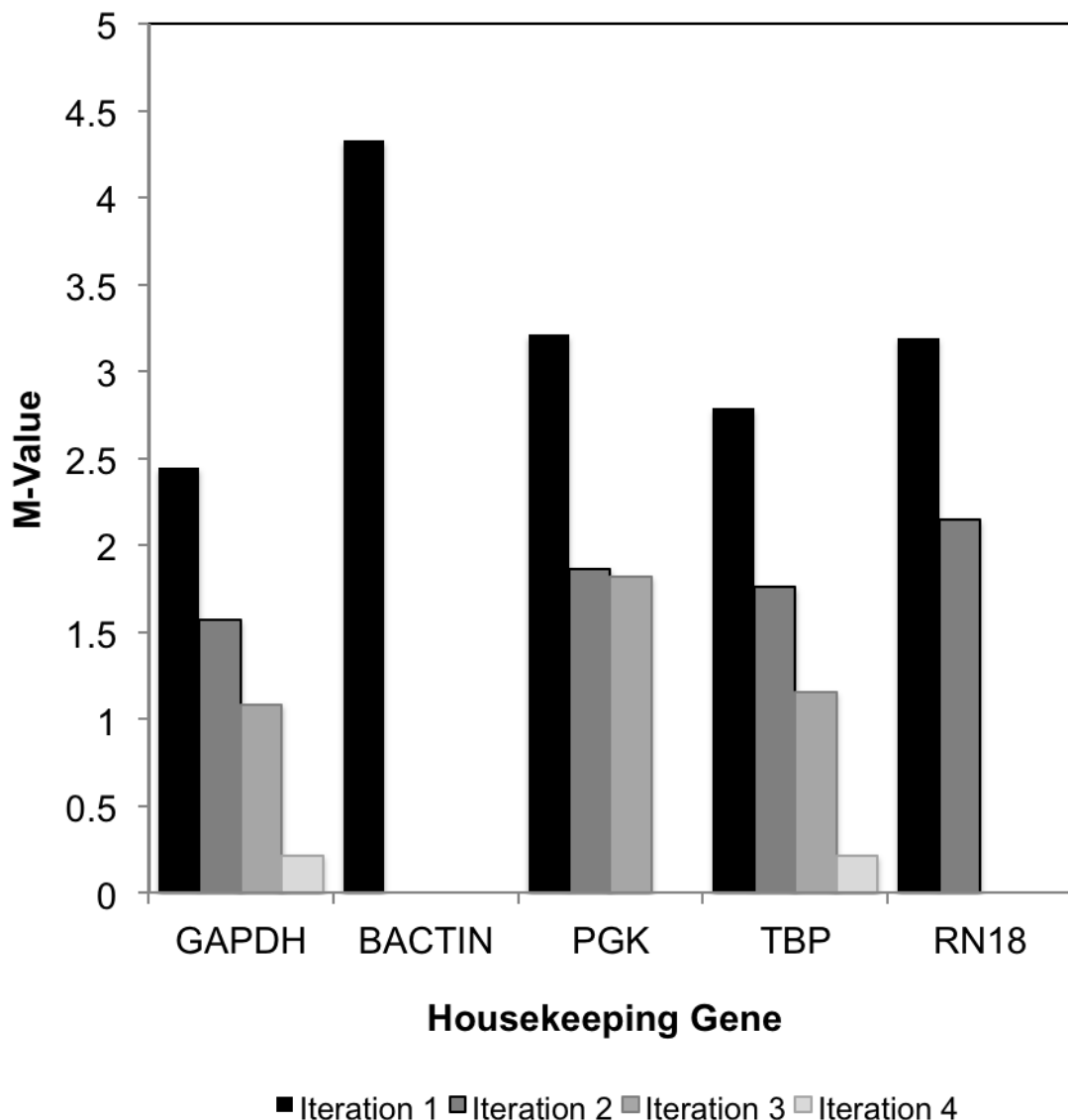
When flow cytometry was carried out on mESC's (Figure 3.6), 4.47% of cells were positive for PSA-NCAM. The vast majority (>95%) of cells were negative for the marker. When considered along with the previous immunocytochemistry data, this confirmed that the majority of cells within the starting population were undifferentiated mESC's. Any increase in the percentage of cells positive for PSA-NCAM above this value indicated that neuronal differentiation is occurring. As with nestin, PSA-NCAM is present extensively in both developing progenitors as well as more mature types (it is found in the brain subventricular zone), and so is a useful marker for neuronal populations across numerous identities and subtypes.

3.5.2 qPCR Internal Control Gene Selection

Quantitative PCR (qPCR) allows for real time quantification of gene expression in cells. Expression of genes can be compared across a number of conditions to observe phenotype changes at a cellular level. In order to compare expression across conditions, expression has to be normalized to the cellular DNA content as well as an internal control gene, whose expression will not vary significantly with a change in phenotype.

The choice of internal control gene(s) varies between cell lines and conditions used. A popular method used for deciding suitable internal control gene candidates was devised by Vandesompele et al (2002). This method utilised the M-value, which is a measure of stability for internal control genes. Higher M-values correspond to lower degrees of stability. The M-value was measured for a host of candidate genes over three samples of E14 mESC's. What followed was an iterative process starting with the removal of the internal control gene with the highest M-value. The M-values were then re-measured and again the gene with the highest value was removed. This was continued until the M-values of the remaining genes were under 0.7, which is the value that appeared to eliminate the most variable and outlying genes in the data set in the Vandesompele et al (2002) study.

A



B

	n=1	n=2	n=3	Mean	SD
GAPDH and TBP	0.496	0.565	0.431	0.497	0.067

Figure 3.7: Internal control gene stability study tests. (A) Iterative elimination of unstable internal control genes in E14 mESC's. At each iteration, the gene with the highest M-value was eliminated until the most stable pair emerged. (B) Validation of internal control gene stability in mESC's seeded on 3 GXG materials (2 kPa, 18 kPa, 35 kPa) and TCP. All three biological replicates, mean and standard deviation shown.

Five genes were chosen as internal control candidates for this study, based on extensive previous use for mESC studies in this laboratory; GAPDH (glyceraldehyde 3-phosphate dehydrogenase), β -actin, PGK1 (phosphoglycerokinase), TBP (TATA box binding protein) and RN18 (18S ribosomal RNA). Three consecutive passages of mESC's were used in order to assess internal control stability.

Following qPCR analysis, four iterations of removal were required before the M-value was below 0.7 (Figure 3.7A). The genes were ranked in order of increasing stability as follows: β -actin, RN18, PGK1, TBP and GAPDH. GAPDH and TBP were the two most stable internal control genes, both having M-values within the target range. Once these two genes were established as the two most stable, their stability was validated on cells harvested after four days of neuronal differentiation on GXG and TCP (over three, independent biological replicates). As Figure 3.7B shows, the M-value for GAPDH and TBP remained below 0.7 across the three replicates. The mean and standard deviation confirm that these internal control genes were suitable for experimentation on GXG.

3.6 The effect of GXG Young's modulus on attachment of mouse fibroblasts

Before investigating how mESC's would behave in response to changes in Young's modulus, it was important to establish how Young's modulus would affect a previously investigated mature cell type. This was done in order to compare the behaviour of cells on GXG to cells other elasticity tuneable materials. It also provided a basis for comparison for the effects on undifferentiated cells.

Mouse embryonic fibroblasts (MEF's) were seeded in DMEM culture medium with 15% v/v serum on three GXG materials (2 kPa, 18 kPa and 35 kPa) corresponding to three different body tissues (brain, muscle and bone respectively) as measured previously (Engler et al, 2006). TCP was used as a control. As with Figure 3.2B, confluence was measured from phase contrast images, in this case at 6h following seeding, in order to quantify cell attachment with Young's modulus. 6h was chosen due to the rapid nature of fibroblast spreading.

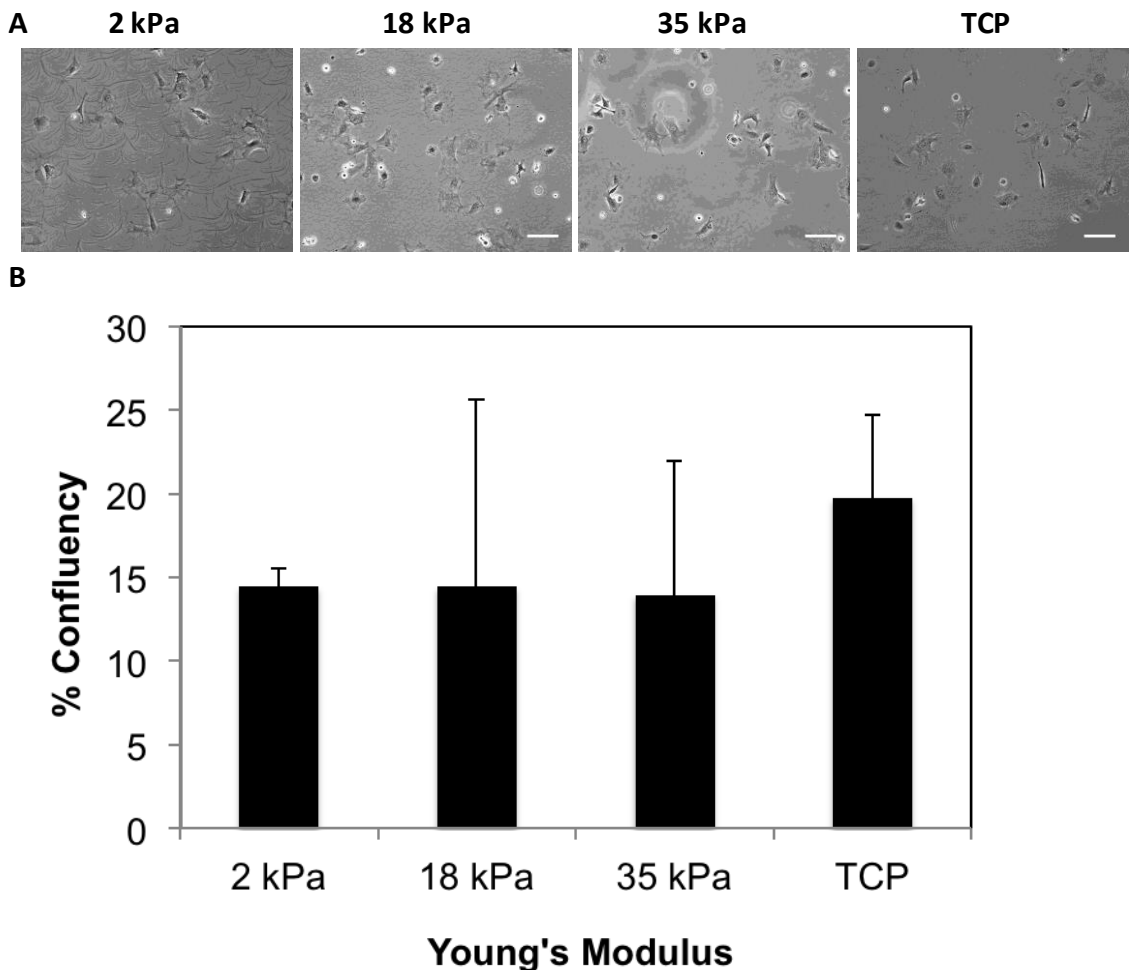


Figure 3.8: (A) Phase contrast images of fibroblasts seeded for 6h on three GXG materials (2 kPa, 18 kPa and 35 kPa) and TCP. Scale bars = 100 μ m. (B) Confluency measurement made from phase contrast images taken at 6h post seeding of fibroblasts seeded on three GXG materials and TCP. Fibroblasts were seeded in normal culture medium. Error bars shown represent standard deviation (measured from three technical replicates). Confluency measurement represent mean of three technical replicates (three separate wells from a six-well plate).

Phase contrast images at 6h (Figure 3.8A) revealed little difference in numbers of cells attached across all four materials. Morphological differences were minor, but it did appear that cells were more homogeneously spindle-shaped on the softest 2 kPa material. On the stiffer 18 kPa, 35 kPa and TCP material, whilst some cells were similarly spindle-shaped, others had a larger projected area, with the cell periphery extended out in every direction. The physiological elasticity of smooth muscle associated with fibroblasts has previously been measured to be 8-17 kPa, closest to the intermediate stiffness GXG material.

Confluency analysis of the phase contrast images supported the initial observation that mean attachment did not vary with Young's modulus (Figure 3.8B). The higher confluence of cells here compared to that of mESC's at 24h (Figure 3.2B) reflects the larger projection area of fibroblasts compared to mESC's. Young's modulus has no overall effect on attachment of mouse embryonic fibroblasts.

Earlier studies on fibroblasts (Pelham & Wang, 1997; Yeung et al, 2005), using polyacrylamide gels, found that cells become more spread on stiffer materials as in this study. This was as a result of fibroblasts forming more polymerized stress fibers on stiffer materials compared to soft. Stress fibers are formed on the 2 kPa materials (Yeung et al, 2005), but not with the same abundance as on the stiffer materials. Another earlier study (Wang et al, 2000) did find increase growth on stiffer materials, but this was using BrdU staining at 24h, rather than confluency analysis at 6h.

3.7 Effect of Young's modulus on attachment and enrichment of human embryoid bodies in neuronal differentiation medium

After attachment was characterized in fibroblasts, an experiment was conducted using human embryoid bodies (EB's) in retinal differentiation medium. The effects of Young's modulus on human EB's have been previously investigated and so provide another basis of comparison for mESC's.

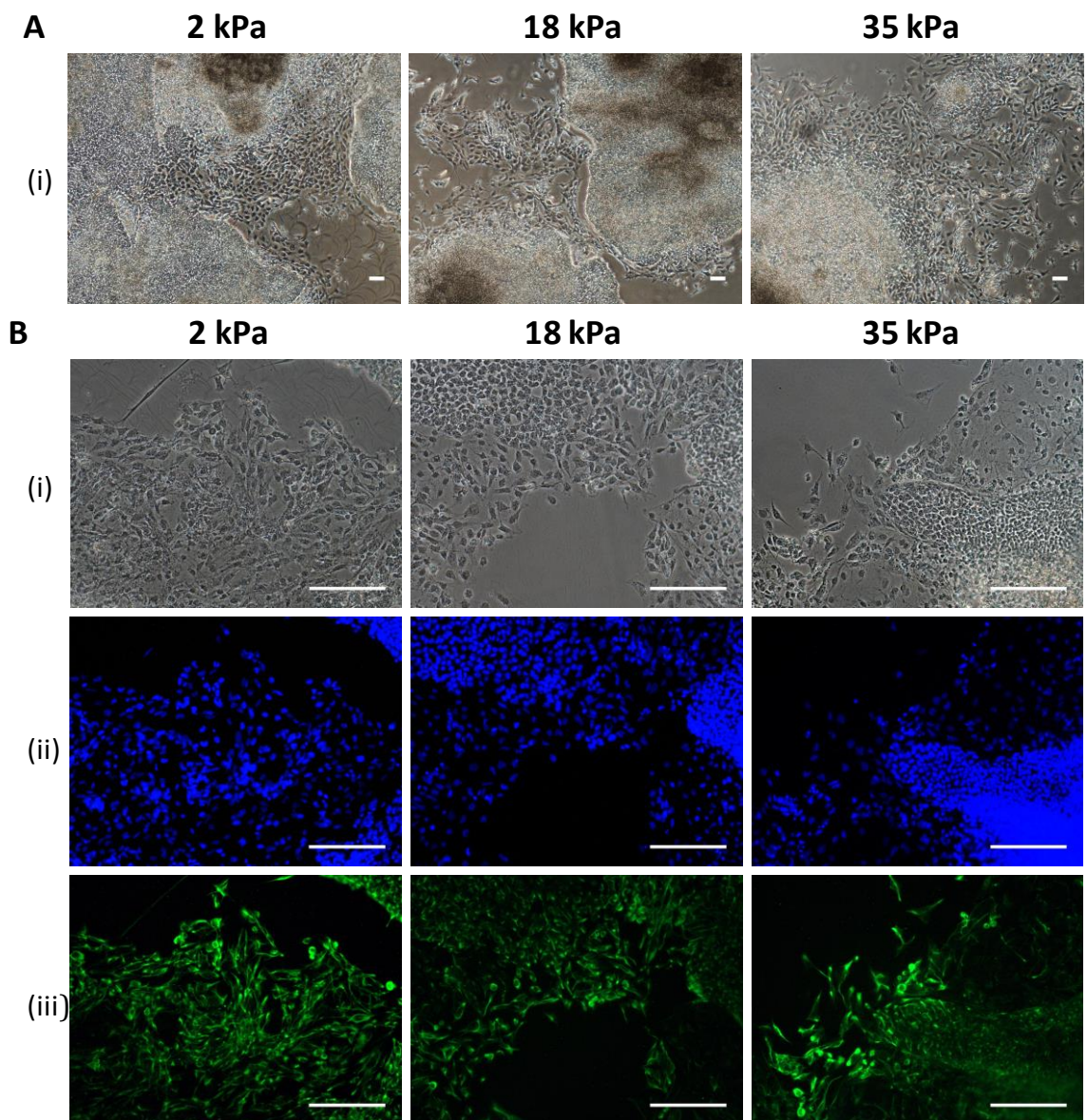


Figure 3.9: Human embryoid bodies (EB's) seeded on three different GXG materials (2 kPa, 18 kPa and 35 kPa) for five days. (A) Phase contrast image showing cell morphologies formed at day five of differentiation (4x objective). (B) Immunocytochemistry (ICC) analysis (20x objective) for nestin, a neural precursor marker. (i) Phase contrast. (ii) DAPI, a nuclear stain. (iii) ICC for nestin. All scale bars = 100 μ m.

Human EB's were plated in medium promoting retinal differentiation (Bae,D. et al, 2012). Like the differentiating mESC's, these cells become nestin-positive roughly four or five days into differentiation. The human EB's were plated onto the 3 GXG materials (2 kPa, 18 kPa and 35 kPa) and allowed to differentiate for five days. Phase contrast images were obtained at this time-point (Figure 3.9A). Cells were then fixed and immunocytochemistry analysis was performed for nestin (Figure 9B).

Cells rapidly expanded to form very dense aggregates covering much of the surface of the plates at day five (Figure 3.9A). The final confluence was considerably higher on the 2 kPa and 18 kPa materials (almost fully confluent) when compared to the 35 kPa material, where these dense aggregates were smaller. At the periphery of these aggregates, cells extended out to form rosette-like morphologies. Whilst the dense, aggregates were smaller on the 35 kPa material compared to the 2 kPa and 18 kPa materials, there were similar numbers of cells within the less dense, rosette-like colonies.

When immunocytochemistry was performed, these rosette-like colonies were abundant in nestin when compared to the denser aggregates, as expected (Figure 3.9B). However, as there are less dense aggregates compared to nestin-positive precursors on the stiff material the conclusion was made that a higher proportion of cells were nestin-positive on the stiffer material compared to softer materials. This is despite there being similar numbers of nestin-positive cells overall on all materials.

This is consistent with previous work using mouse EB's undergoing neuronal differentiation in three-dimensional culture (Kothapalli et al, 2013), where the percentage of cells undergoing neuronal differentiation increased with Young's modulus. However, separating the effects of Young's modulus from cell-to-cell interactions becomes difficult at the levels of cell density observed in EB studies.

3.8: Effect of Young's modulus on mESC attachment and expansion in normal pluripotent growth medium and undirected differentiation medium

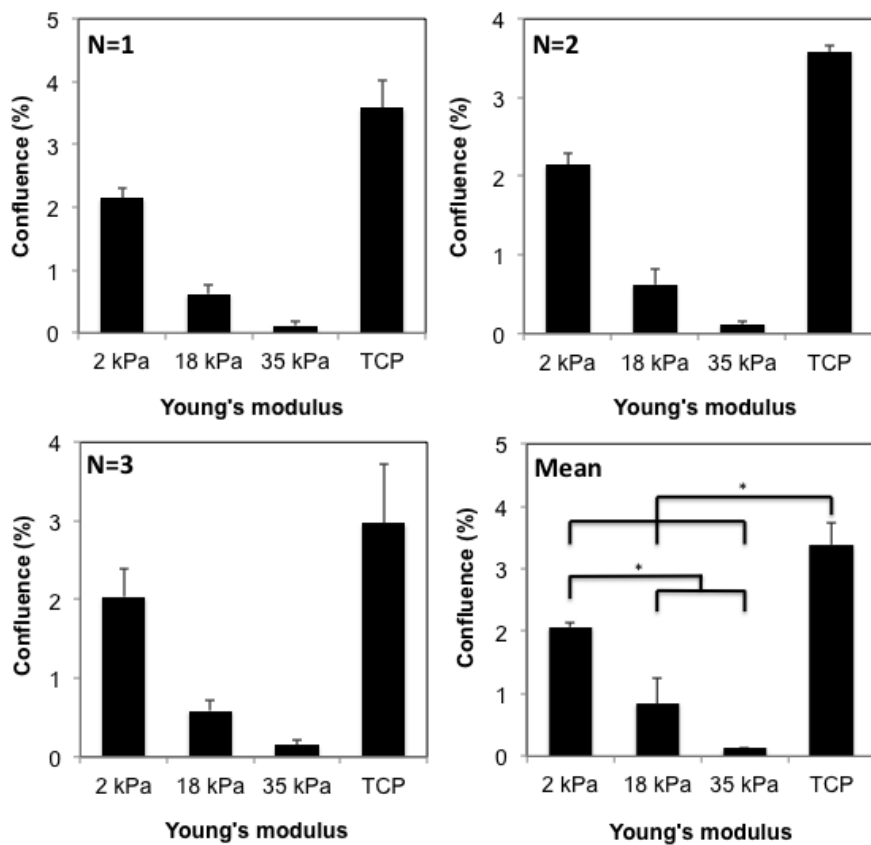
Before investigating the effects of Young's modulus on mESC attachment in N2B27 medium, it was important to isolate the cooperative effects from the soluble microenvironment. MESC's were seeded in two media; GMEM with LIF, which is normal maintenance medium (containing 10% v/v serum) containing the pluripotency promoting agent LIF; and GMEM without LIF, which is maintenance medium that does not contain LIF. The former medium was used to maintain cells in a pluripotent state *in vitro*. The latter medium was used to allow cells to spontaneously differentiate.

3.8.1 Effect of Young's modulus on mESC attachment and expansion in normal pluripotent growth medium

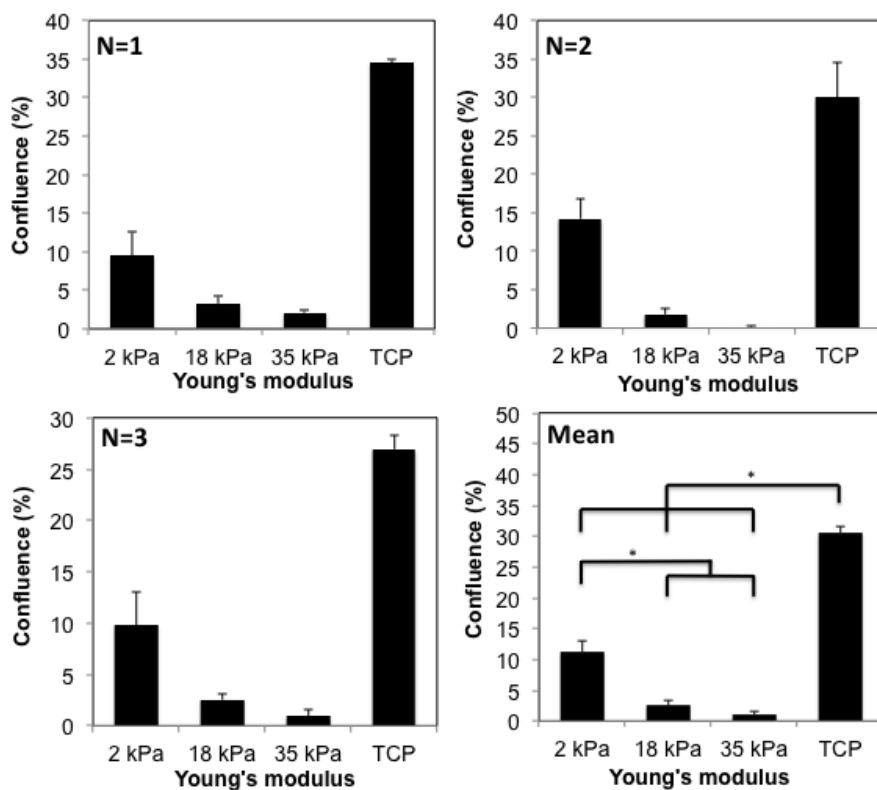
MESC's were harvested and seeded in GMEM with LIF at a seeding density of 1×10^4 cells/cm² in order to directly compare attachment and expansion with N2B27 neuronal differentiation medium. Cells were seeded onto three GXG materials (2 kPa, 18 kPa and 35 kPa) and TCP. Confluency was then measured from phase contrast images obtained at 24h and 72h following seeding. The 24h time-point was used to quantify cell attachment, whilst the 72h time-point was used to quantify differences in expansion of cells with Young's modulus.

At 24h, attachment was maximized on the softest, 2 kPa GXG material (Figure 3.10A). Attachment decreased significantly ($p<0.005$) by 59% on the 18 kPa material and 94% ($p<0.001$) on the 35 kPa material. Attachment was however 39% lower ($p<0.005$) on the 2 kPa material compared to the TCP.

A



B



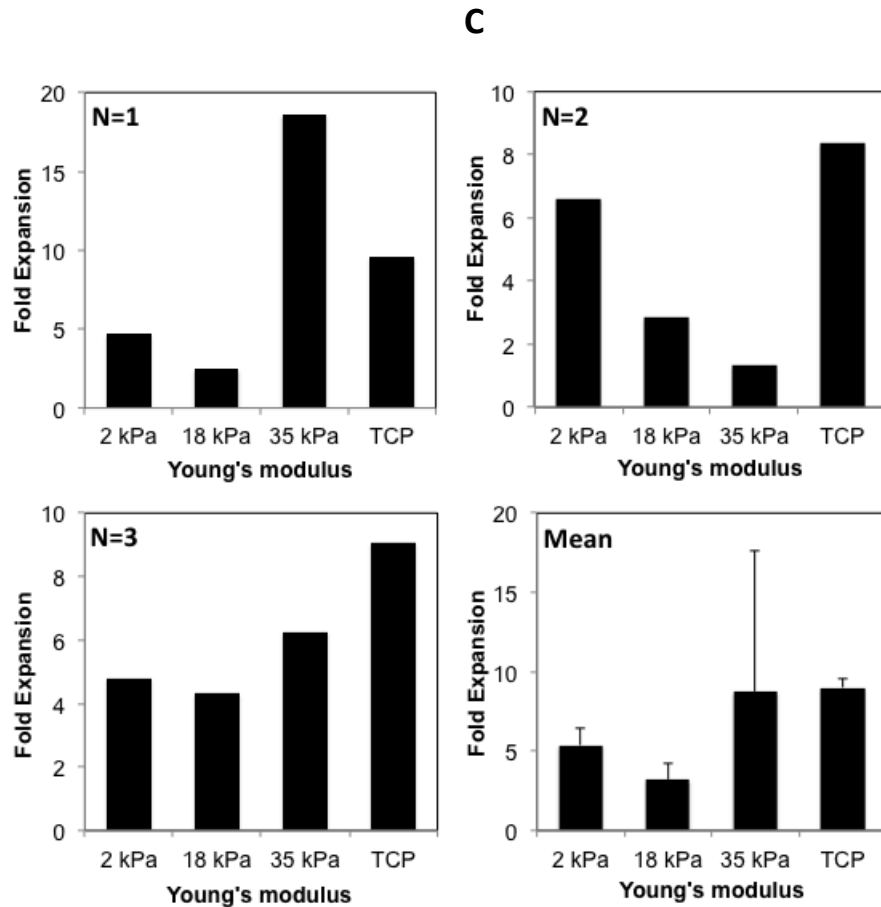


Figure 3.10: Confluency measurements from image analysis of mESC's seeded in GMEM with LIF, a growth factor that supports pluripotency. (A) Confluency measurements at 24h. (B) Confluency measurements at 72h. (C) Fold expansion of mESC colony size (confluency at 72h divided by confluency at 24h). All three biological replicates and mean shown. Error bars represent standard deviation from the mean. N=3.

Of the three GXG materials, the softest 2 kPa GXG material yielded the highest confluence at 72h (Figure 3.10B), reducing 77% on the 18 kPa material ($p=0.01$) and 91% on the 35 kPa material ($p<0.005$). Confluence on the 2 kPa material was 63% ($p<0.001$) lower than the TCP material, a greater difference than that at 24h. It should be noted that TCP is biased for attachment by physical and biochemical (NUNCLON Delta) treatment, and so cannot be directly compared to GXG. Rather than being a direct control (which would be a 1 GPa GXG) it is an example of ‘current laboratory practice.’ The corona plasma treatment that TCP undergoes has been previously found to have a detrimental effect on biomaterial surface chemistry, in terms of elasticity and topography (Yang et al, 2013).

Values of confluence at 72h were divided by confluence measurements at 24h in order to measure fold expansion, normalized to the original attached value. Fold expansion did not significantly vary ($p=0.389$) between the four materials (Figure 3.10C). Therefore, Young’s modulus had no effect upon expansion in maintenance medium.

Work by Evans et al (2009) using mESC’s in normal culture medium seeded on PDMS substrates, found that Young’s modulus did not have an effect on attachment at 24h, contrary to the findings of this study. That study also showed no difference in expansion over four days, which is in agreement with our findings. It should be noted that the Evans et al (2009) study used a considerably higher range of moduli (41 kPa upwards) than that of this study. The lack of significant difference ($p=0.053$) in attachment between 18 kPa and 35 kPa in Figure 3.10A implies that the trend observed by Evans et al (2009) would be observed at higher moduli in this study. The soft material in this study show closer agreement with the 3.4 kPa modulus measurements for the early mouse blastocyst (Murayama, 2006) in comparison to the Evans et al (2009) study.

3.8.2 Effect of Young's modulus on attachment and expansion of mESC's in spontaneous differentiation medium

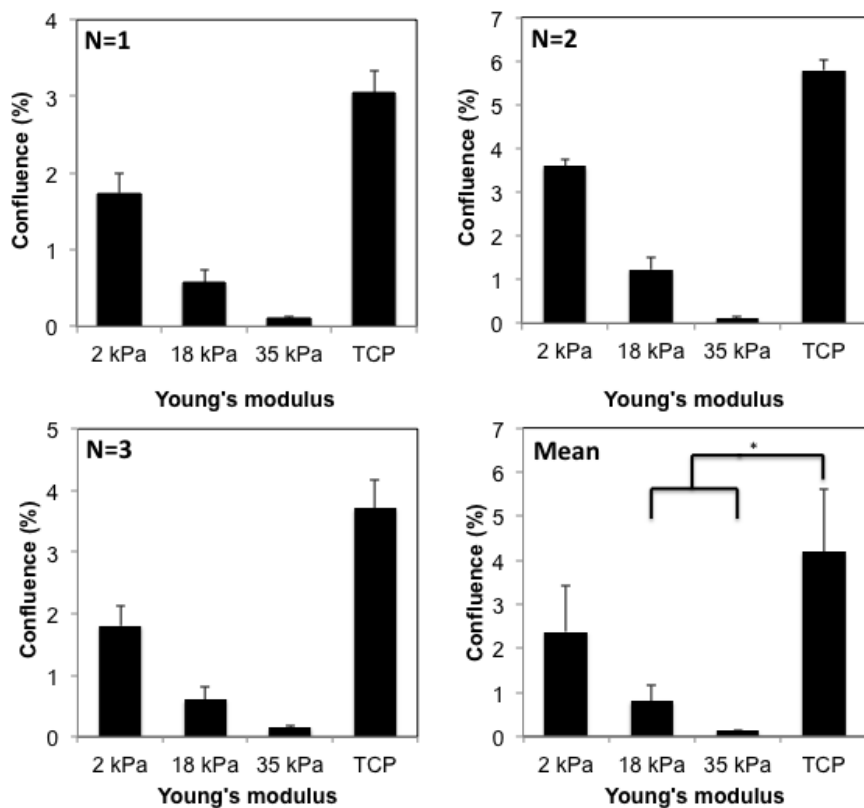
The final set of experiments in this chapter investigated the relationship between Young's modulus, attachment (24h) and expansion (24h to 72h) in GMEM without LIF, which is a medium used for spontaneous differentiation. It served as an interesting basis of comparison with the N2B27 medium, which is comparatively very efficient in driving cells towards the neural lineage.

MESC's were seeded at the same seeding density as before (1×10^4 cells/cm²) on the three GXG materials and TCP. Contrary to the findings in maintenance medium, there was no significant difference ($p>0.05$) in confluence at 24h (Figure 11A) between 2 kPa and any of the materials. The only significant differences in attachment were between the TCP and the stiffer (18 kPa and 35 kPa) GXG materials ($p<0.01$).

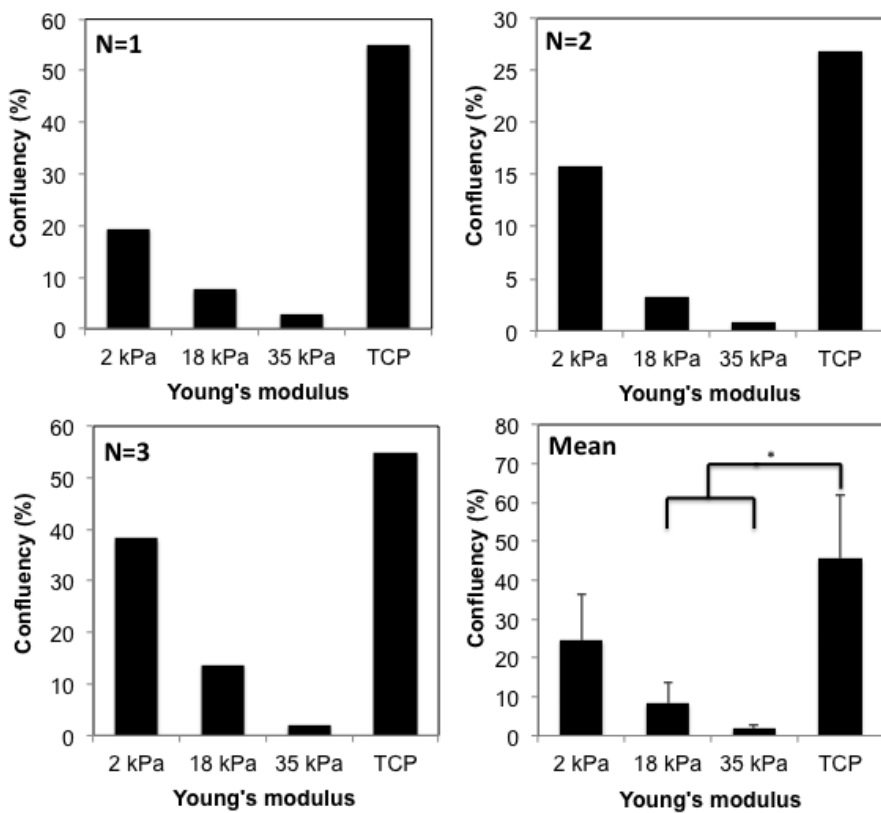
Interestingly, the mean attachment values at 24h were similar to that in GMEM with LIF. This implies that the influence of Young's modulus on attachment is independent of medium composition and so was specific to mESC's. However, the attachment effect was less reproducible in the medium without LIF, as evidenced by the larger error bars and the lack of significance when statistical analysis was carried out. The larger variations in attachment without LIF compared to when LIF is present reflect the differences in heterogeneity as cells begin to commit to other lineages in the spontaneous differentiation medium. Comparing the mESC data to the findings in fibroblasts (Figure 3.8), it is clear that the effects of Young's modulus are lineage dependent and so a more heterogeneous mixture of cells is likely to produce a heterogeneous response to modulus.

The higher attachment on 2 kPa compared to stiffer GXG materials reflects the fact that 2 kPa represents the Young's modulus closest to that of mESC's (Pillarisetti et al, 2011) themselves as well as the early blastocyst (Murayama et al, 2006). It's likely that a stiffness-matching effect is occurring, where mESC's are preferentially attaching to materials that resemble both their own Young's modulus of elasticity as well as the

A



B



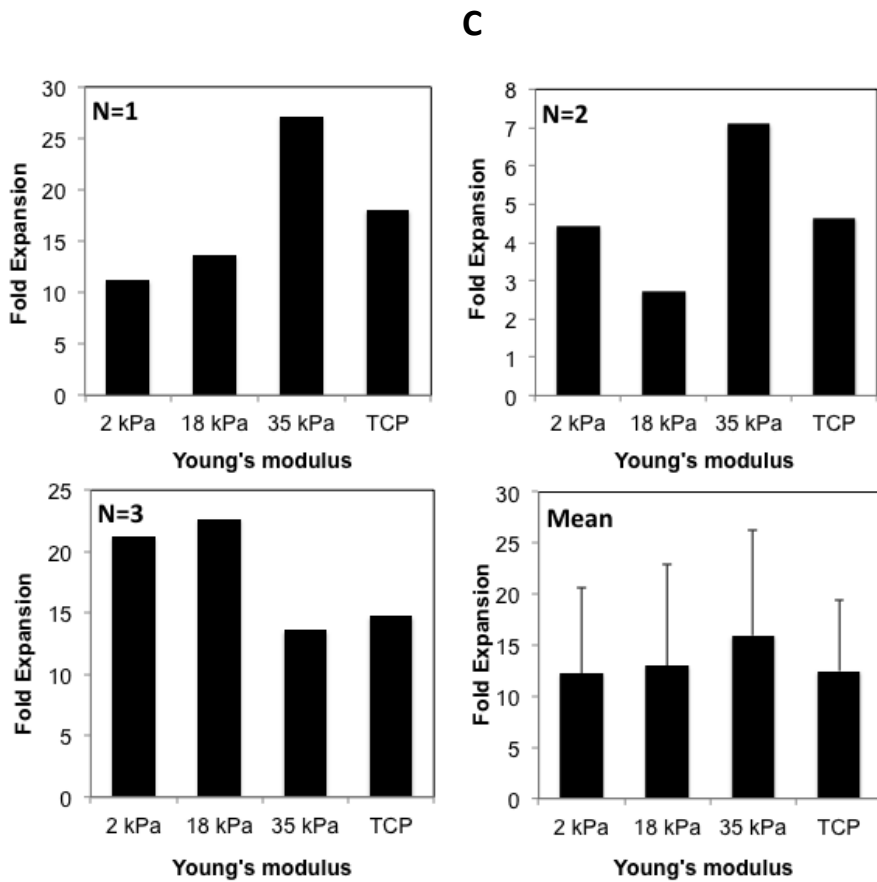


Figure 3.11: Confluency measurements from phase contrast measurements of mESC's seeded in GMEM without LIF, a medium used for spontaneous differentiation. (A) Confluency measurements at 24h. (B) Confluency measurements at 72h. (C) Fold expansion (confluency at 72h divided by confluency at 24h). All three biological replicates and mean shown. Error bars represent standard deviation from the mean.

N=3.

elasticity of their equivalent native tissue. It should be noted that ES cells only exist in *in vitro* culture, and so some degree of adaptation to these conditions must occur.

The same pattern emerged at 72h as at 24h (Figure 11B). There was no significant ($p>0.05$) difference in attachment between the softest 2 kPa material and any of the other materials. The fold expansion did not vary significantly ($p>0.05$) with Young's modulus either (Figure 11C). The larger error bars in comparison to the maintenance medium again likely reflect heterogeneity in cell commitment brought about by the spontaneous differentiation medium.

3.9 Summary of Findings

In order to investigate the effect of Young's modulus on neuronal differentiation of mESC's, a number of set conditions would be required. These conditions were validated by the results shown in this chapter. MESC's would be seeded in N2B27 formulated in-house, containing 1% v/v serum at a seeding density of 1×10^4 cells/cm².

To compare the formation of neural precursors and neurons on different materials, nestin, PSA-NCAM and β -III tubulin were chosen as markers for neuronal differentiation. For qPCR, GAPDH and TBP were chosen as internal control genes due to their sustainably low M-values.

Attachment of mESC's in medium containing LIF (ideal for self-renewal) decreased with increasing GXG Young's modulus. When other cell types were seeded on varying Young's moduli, it was found that material elasticity did not impact the attachment of fibroblasts and human EB's. When mESC's were seeded in medium without LIF (where spontaneous differentiation is likely to occur), there was no impact of Young's modulus on differentiation.

4 Does Young's modulus affect attachment and enrichment of mouse embryonic stem cells undergoing neuronal differentiation?

4.1 Aims

After protocols were established for differentiating mouse embryonic stem cells (mESC's) robustly on GXG, the next stage was to investigate how the neuronal differentiation of mESC's was affected by Young's modulus. In Chapter 3, when mESC's were seeded in normal culture medium, there was a dramatic increase in attachment on soft materials compared to stiffer materials. This was however not accompanied by a change in self-renewal with modulus.

Earlier studies using primary neural precursors (Georges et al, 2006; Jiang et al, 2007; Previtera et al, 2010) have shown that there is no change in attachment with modulus in mature cells. This was also demonstrated in Chapter 3.8 of this study, where mouse embryonic fibroblasts were seeded in normal culture medium (with a similar serum content to the culture medium used for mESC's) on varying GXG Young's moduli. This implies that the effect of Young's modulus on attachment changes as cells mature. Furthermore, it has also been previously demonstrated that soft materials favour the neuronal differentiation of mesenchymal stem cells (Engler et al, 2006) as well as neural stem cells (Saha et al, 2008). Therefore, the hypothesis under study in this chapter was that increased neural precursor formation from mESC's on soft materials in neuronal differentiation medium is due to favourable attachment.

The first test for this hypothesis was to look at how elasticity affected the initial attachment and expansion of cells. This was followed by an analysis of cell morphology and phenotype at day four of differentiation. By finding out whether Young's modulus directly impacts the phenotype of cells formed, it could be understood whether any increase in neural precursor formation was due to favourable initial attachment, or due to a direct promotion of the neuronal fate. The final set of experiments in this chapter investigated whether the effect of Young's modulus on initial attachment was

dependent on stress fibre stabilization and/or microtubule formation, in order to derive an underlying mechanism for any effect on attachment.

4.2 Does Young's modulus influence attachment and early expansion of mESC'S?

4.2.1 Does Young's modulus influence attachment of mESC's in neuronal differentiation medium?

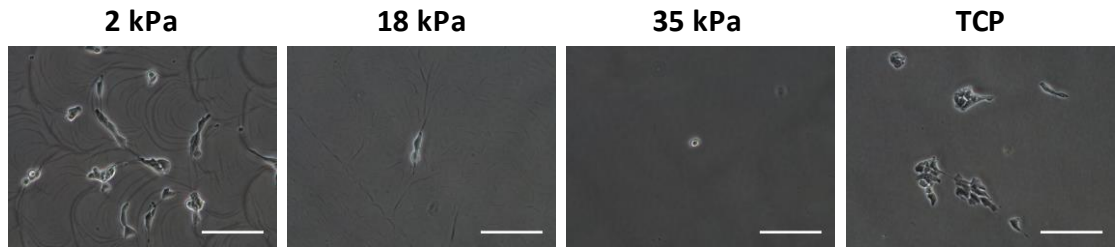
It was established in the previous chapter that soft materials promoted initial attachment of mESC's in normal maintenance medium. This effect was not reproducible in spontaneous differentiation medium. In order to assess the effect of Young's modulus on attachment in neuronal differentiation conditions, mESC's were seeded onto three different GXG Young's moduli, corresponding with the brain (2 kPa), muscle (18 kPa) and bone (35 kPa) as well as gelatin-coated tissue culture polystyrene (TCP), in N2B27 medium with 1% v/v serum (as characterised in Chapter 3). When confluence was measured at 24h, it was found that amongst the GXG materials, attachment was maximized on the softest 2 kPa substrate (Figure 4.1A), whose Young's modulus corresponded with that of mESC's (Pillarisetti et al, 2011), brain (Engler et al, 2006) and early mouse blastocysts (Murayama et al, 2006). Compared to the 2 kPa material, confluency decreased 76% ($p=0.056$) on the 18 kPa material and 95% on the 35 kPa material (Figure 4.1B).

This favorability of attachment on physiological Young's moduli is consistent with the findings of other studies using mature cell types, such as fibroblasts (Pelham & Wang, 1997; Yeung et al, 2005) and osteoblasts (Gonzalez et al, 2012) where adhesion tends to increase on physiologically elastic materials. It does however contrast with previous findings using mouse (Evans et al, 2009) and hESC's (Eroshenko et al, 2013), where attachment did not vary with Young's modulus. It should be noted that these studies were carried out in expansion medium on material elasticities varying from 40 kPa to 3 MPa, significantly higher than this study. On GXG, attachment did not significantly ($p=0.854$) vary with an increase in Young's modulus from 18 kPa to 35 kPa (Figure 4.1B), suggesting that similar outcomes would result in this study.

These results suggest that cells are more likely to attach to materials that match the elasticity of their native tissue. The stiffness of the substrate may thus be a very influential cue in recruiting and engrafting cells to target areas for cell therapy. Furthermore, the mechanical condition of tissues may change within the diseased state. During spinal cord injury for example, significant stiffening of the lesion site has been previously observed due to glial hypertrophy and fibrotic scarring. This has also been shown to prevent cell engraftment, as well as restrict neuronal access to growth factors (Georges et al, 2005).

Another key factor to consider is the differentiation medium. Whilst all cells must initially settle on the material due to gravitational settling, a detachment process must occur over the first 24 hours in order to produce the effect observed in Figure 4.1A. The significant amounts of cell detachment and subsequent death point towards a selection process against non-neuronal cell lineages during differentiation, where only neuronal lineages are allowed to survive. The N2B27 differentiation medium already has some capacity to select against non-neuronal lineages (see Chapter 3). Thus it is likely that there was some coordination between the effects of attachment and the effects of the soluble environment. Whilst it is unclear what the exact mechanism behind the selection process is, the effect is clearly exacerbated at higher, non-physiological Young's moduli. This is another indicator that substrate Young's modulus is a key microenvironmental cue for neuronal differentiation.

A



B

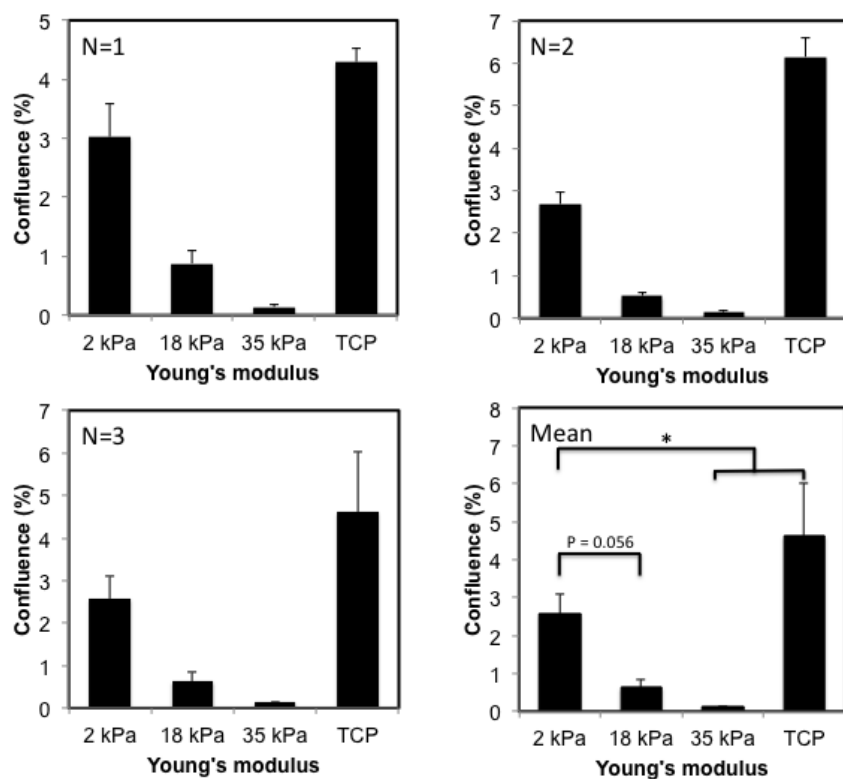


Figure 4.1(A): Phase contrast images of mESCs seeded for 24h on GXG and TCP in N2B27 neuronal differentiation medium. Scale bars = 100 μ m. Figure 4.1(B): Analysis of cell confluency from phase contrast images of mouse embryonic stem cells attached for 24h onto 3 different GXG materials and TCP. Cell confluence at 24h increased with GXG Young's modulus. All three biological replicates shown as well as the mean. Error bars present standard deviation from the mean. * represents a p-value less than 0.05 following one-way ANOVA analysis with Tukey post-hoc correction for multiple comparisons.

D

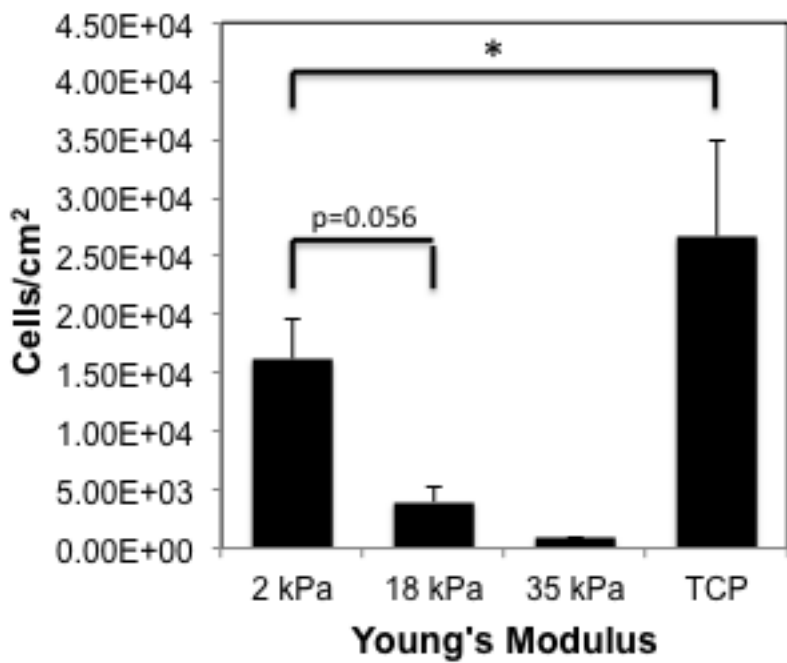


Figure 4.1(D) Analysis of cell concentration from phase contrast images of mouse embryonic stem cells attached for 24h onto 3 different GXG materials and TCP. Cell concentration at 24h decreased with GXG Young's modulus. Values shows are mean from three cell counts. Error bars present standard deviation from the mean. *represents a p-value less than 0.05 following one-way ANOVA analysis with Tukey post-hoc correction for multiple comparisons.

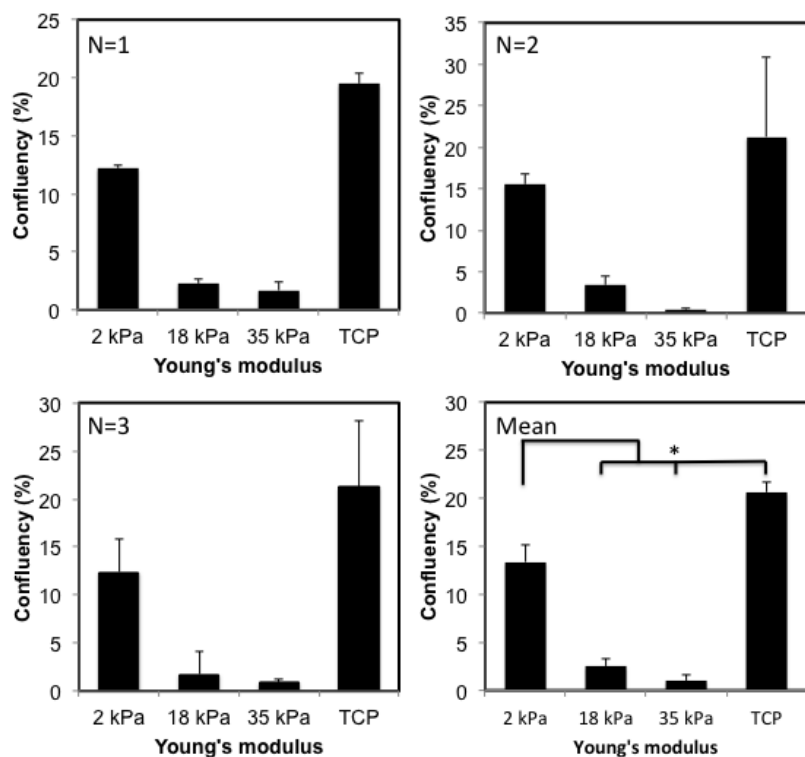
4.2.2 Does Young's modulus influence expansion of mESC's in neuronal differentiation medium?

Confluency was measured at 72h (post-seeding) to assess whether, following the initial attachment at 24h, there was any effect of Young's modulus on expansion of neuronal precursor colonies. As seen in Figure 4.2A, the confluence pattern observed at 24h was conserved at 72h. In this case, confluence decreased 81% on the 18 kPa material and 93% on the 35 kPa material, when compared to the 2 kPa GXG material.

Confluence was highest on the softest substrate, whose modulus corresponds to that of embryonic stem cells, brain and early mouse blastocysts. When 72h confluence was compared to that of 24h confluence, the resulting 'fold expansion' did not vary with Young's modulus (Figure 4.2B). This is consistent with other studies, using both mESC's and human ES cells. Candiello et al (2013) showed that proliferation of mESC's (measured by Alamar Blue assay) did not vary with alginate gel stiffness. A study using human ES cells (Keung et al, 2010) also failed to find any difference in proliferation between varying elasticities of polyacrylamide gels. In a recent study by Eroshenko et al (2013), initial proliferation did not vary on any of the materials studied, including variable elasticity PDMS substrates, feeder cells or fibronectin-coated tissue culture polystyrene. It should be noted that the other studies all used normal expansion medium (typically minimum eagles medium with upwards of 10% serum) as opposed to neuronal differentiation medium, which is not specifically designed for proliferation.

It was concluded that Young's modulus had no effect upon proliferation or expansion of mESC colonies in neuronal differentiation medium. The increase in confluence after three days of differentiation was exclusively due to increased initial attachment over the first 24h on the physiologically soft GXG material (Figure 4.1).

A



B

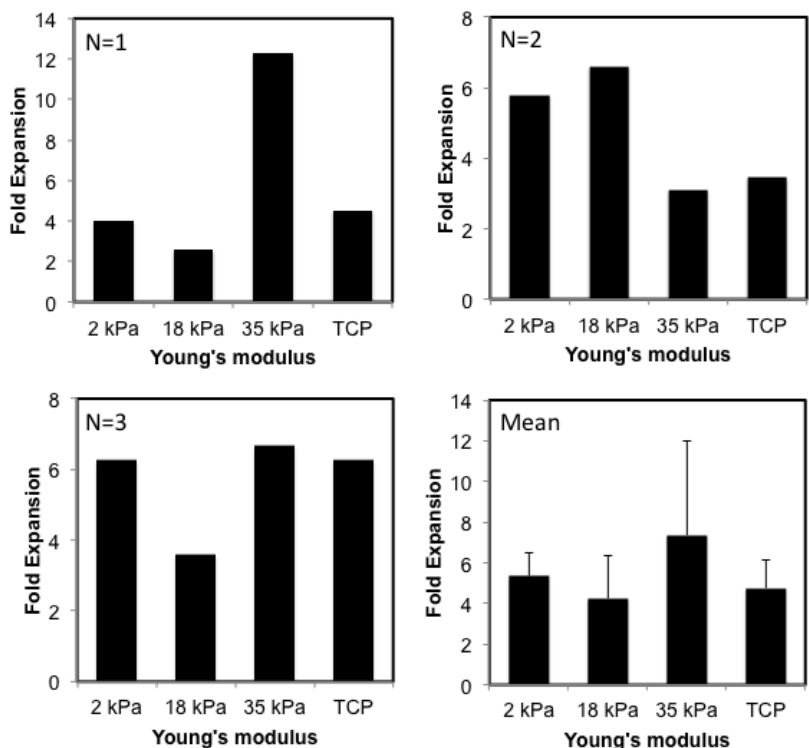


*Figure 4.2 (A): Analysis of cell confluence from phase contrast images of mouse embryonic stem cells attached for 72h onto GXG and TCP in N2B27 neuronal differentiation medium. * represents a p-value less than 0.005. (B): Fold expansion in colony size between 24h and 72h (72h confluence divided by 24h confluence).*

4.3 Does Young's modulus affect the morphology or phenotype of cells formed after four days of mouse embryonic stem cell differentiation in N2B27 medium?

After establishing the effects of Young's modulus on initial attachment and subsequent expansion, the next step was to investigate the effects of Young's modulus on the identity of cells formed following differentiation.

4.3.1 Does Young's modulus affect the morphology of cells formed after four days of mESC differentiation in N2B27 medium?

The first step was to look at morphologies following differentiation, in order to understand whether cellular shape was affected by Young's modulus.

Immunocytochemistry analysis was then performed to relate these morphologies to specific phenotypes of cells formed following differentiation. Cells were differentiated for four days, as this was the time-point where nestin, a marker for neural precursors (Ying et al, 2003) began to appear, as seen in Chapter 3.

MESC's were seeded onto three GXG materials and TCP and differentiated for four days in neuronal differentiation medium. Phase contrast microscopy was first used to observe the morphology of cells formed at day four. As seen in Figure 3, three distinct cellular morphologies were seen to appear on all four materials at day four of differentiation. They have been termed **A**, **B** and **C**. Morphology A consisted of dense colonies of rounded cells. This was the predominant cell morphology observed on the stiffest material (35 kPa). When immunocytochemistry was carried out (Figure 4A), some nestin was found within the centre of the dense colonies, but the majority of the more typically characteristic filamentous nestin was found on the periphery. This suggests that neuronal differentiation originates from the periphery of the colonies before proceeding inwards towards the centre. Sox17 (a marker for primitive endoderm) was found abundantly in cells within these colonies (Figure 4B). Cells positive for early mesodermal marker T-brachyury (Wilkinson, 1990) were found more sporadically (Figure 4C).

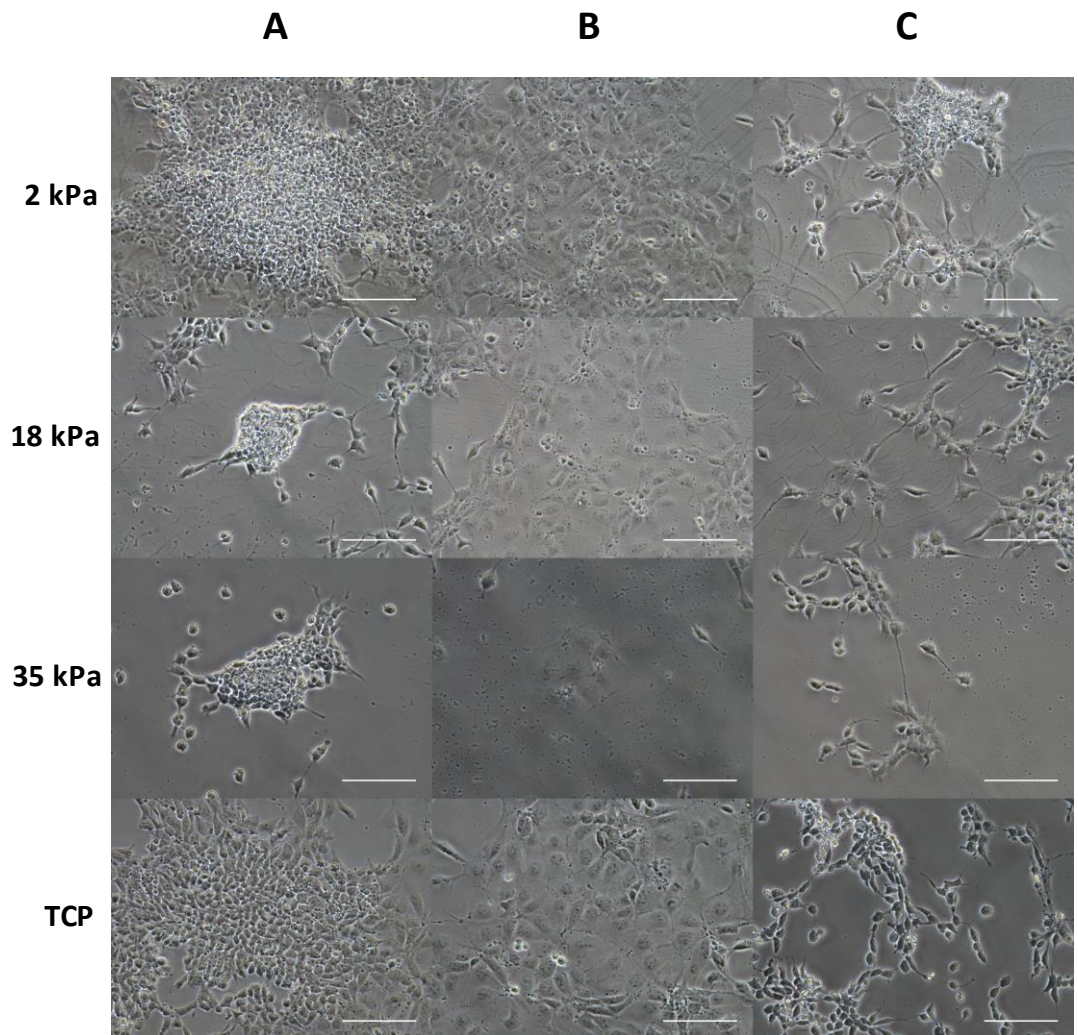
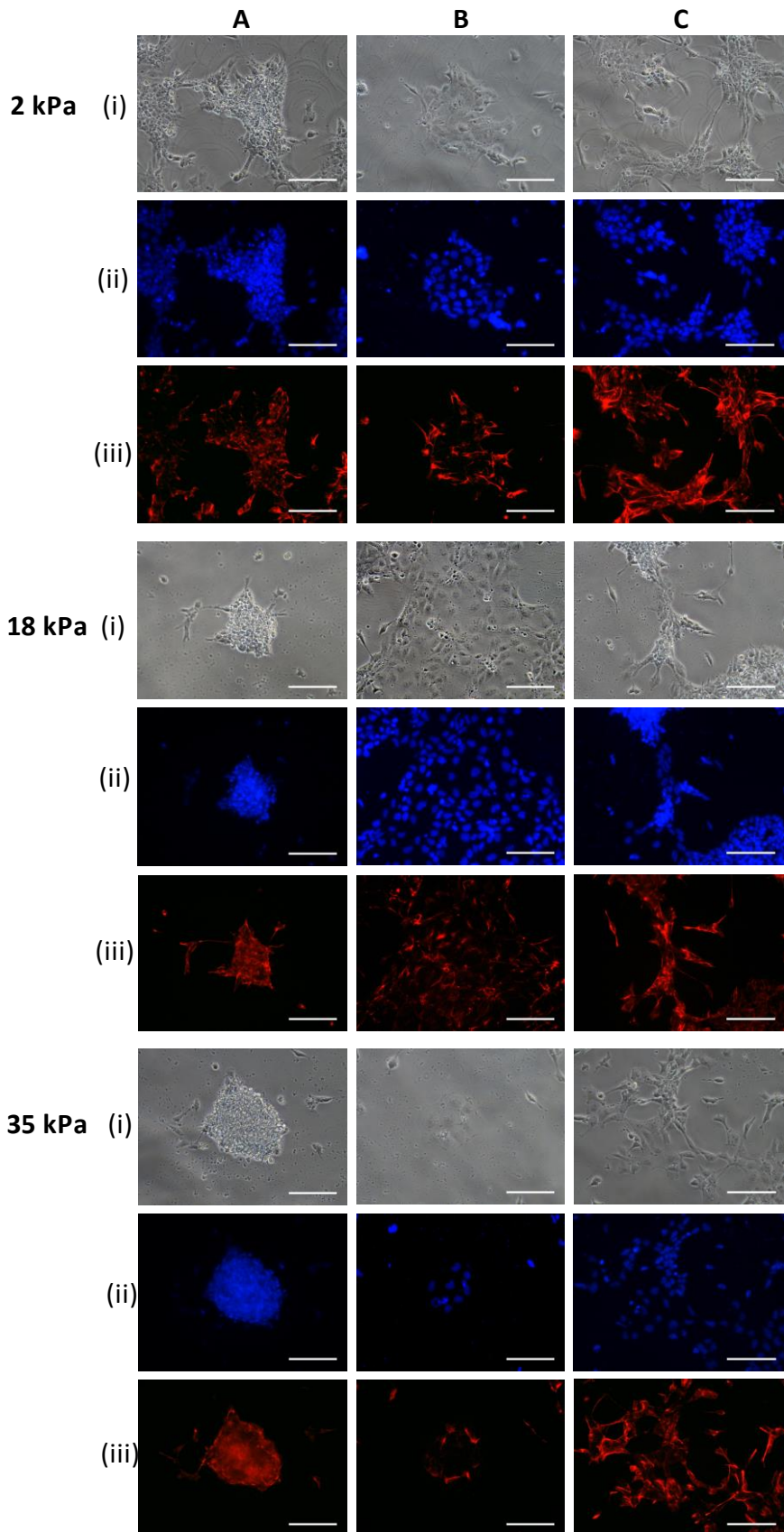


Figure 4.3: Phase contrast images showing morphologies of cells formed after four days of mouse embryonic stem cell differentiation in N2B27 neuronal differentiation medium on the three GXG materials (2 kPa, 18 kPa and 35 kPa) and TCP. (A) Rounded, dense colonies. (B) Large, flattened colonies. (C) Colonies of branched, spindle-like, spread cells. All scale bars = 100 μ m.



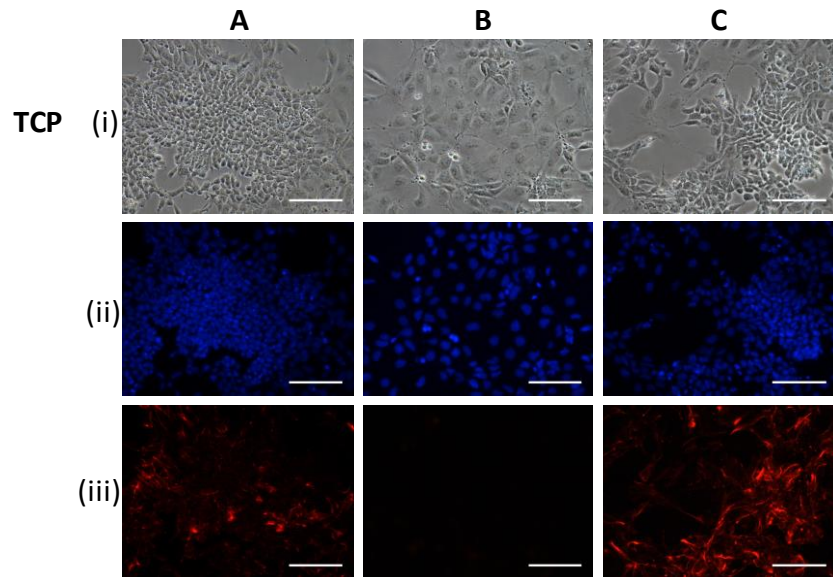


Figure 4.4A: Relating the three different morphologies (A = Dense, B = Flat, C = Spread) formed on the three GXG materials (2 kPa, 18 kPa and 35 kPa) and TCP to presence of nestin-positive cells. For each Young's modulus condition and morphology type shown, three images given. (i) Phase contrast images. (ii) DAPI, a nuclear stain. (iii) Immunocytochemistry (ICC) analysis for nestin, a neural precursor marker. All scale bars = 100 μ m.

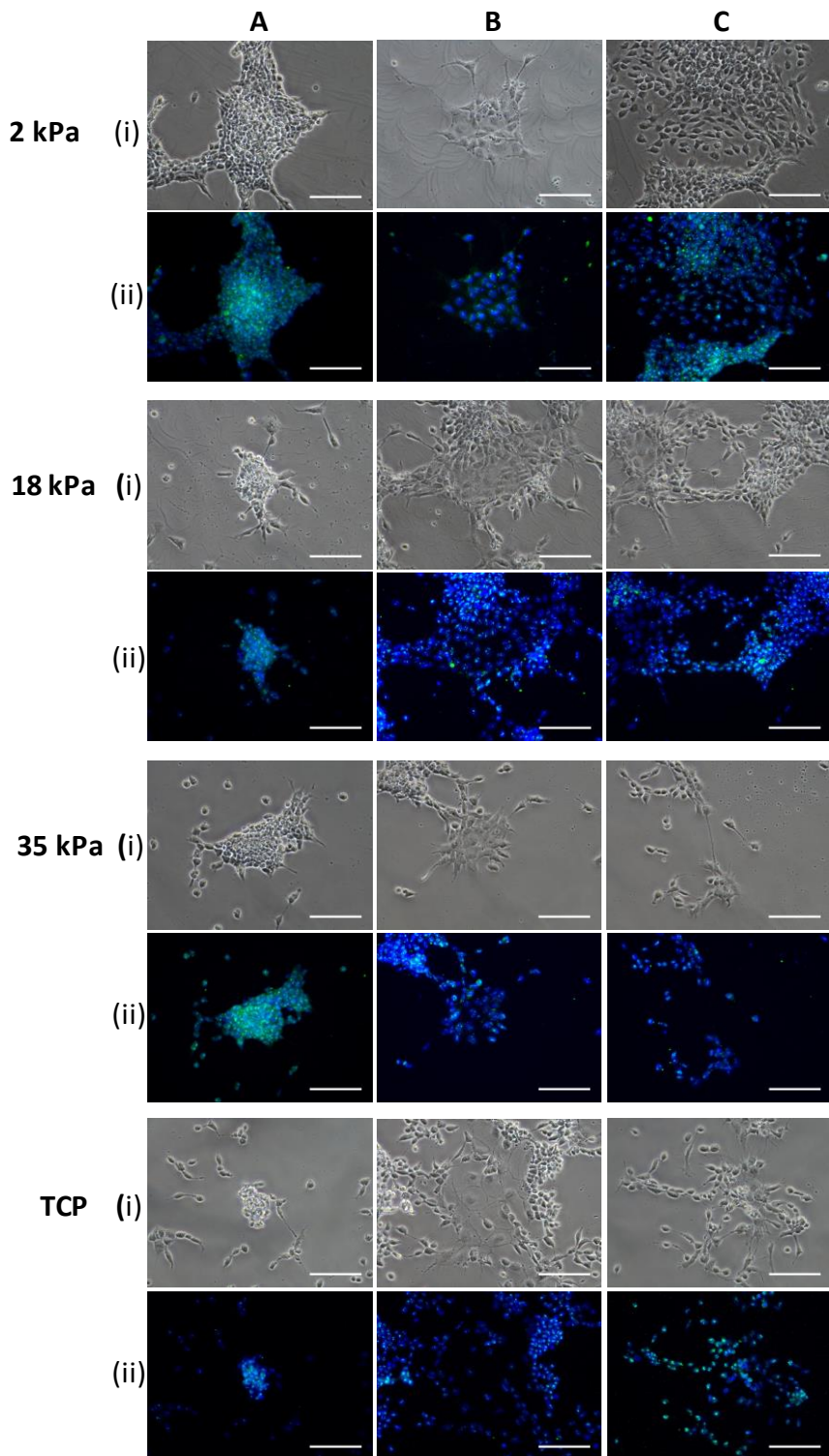


Figure 4.4B: Relating the three different morphologies (A = Dense, B = Flat, C = Spread) formed on the three GXG materials (2 kPa, 18 kPa and 35 kPa) and TCP to presence of Sox17-positive cells. For each Young's modulus condition and morphology type shown, three images given. (i) Phase contrast images. (ii) DAPI, a nuclear stain. (iii) ICC analysis for Sox17, a marker for endoderm. All scale bars = 100 μ m.

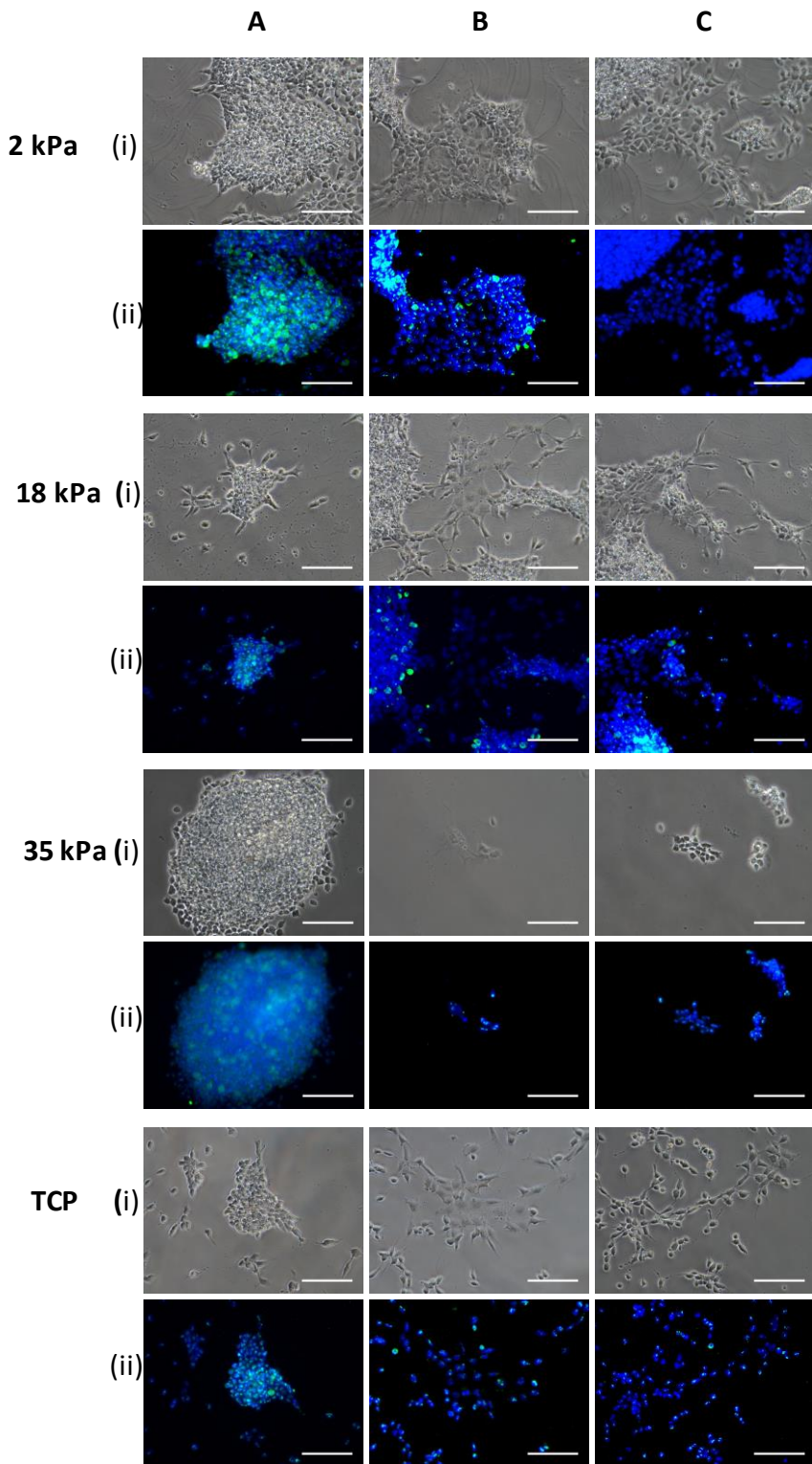


Figure 4.4C: Relating the three different morphologies (A = Dense, B = Flat, C = Spread) formed on the three GXG materials (2 kPa, 18 kPa and 35 kPa) and TCP to presence of T-Brachyury-positive cells. For each Young's modulus condition and morphology type shown, three images given. (i) Phase contrast images. (ii) DAPI, a nuclear stain. (iii) ICC analysis for T-Brachyury, a marker for mesoderm. All scale bars = 100 μ m.

Cells with morphology B were larger bodied and flattened in shape, giving rise to cobblestone-like colonies. These cells closely resembled neuroepithelial cells. This type of cell has previously been reported (Ying et al, 2003) to be an artifact of the N2B27 protocol when serum is present. However, this morphology was not commonly present on any of the materials. These cells were not found to be positive for nestin (Figure 4.4A), Sox-17 (Figure 4.4B) or T-brachyury (Figure 4.4C). These may be more mature cells of a non-neuronal lineage.

Cells with the third morphology, C, were spindle-shaped and spread in nature. The cells extended out to form neurite-like branches. These cells contained the characteristic filamentous nestin associated with neural precursor cells (Figure 4.4A). These were the cells that differentiated out from the periphery of the dense colonies (morphology A) in order to form characteristic neural precursor rosettes and eventually immature neurons. These cells were also found to be positive for Sox17 (Figure 4.4B) and T-brachyury (Figure 4.4C), suggesting that they are at a very early stage of differentiation.

4.3.2 Does Young's modulus affect neural precursor or immature neuron formation from mESC's in neuronal differentiation medium?

The aim of the next set of experiments was to better understand how Young's modulus influenced the changes in cell identity during differentiation. By comparing the proportion of neural precursor cells across materials, it was hoped that any effect that soft materials have in directly promoting neuronal differentiation could be isolated from the favourability in attachment seen in Figure 4.1.

In order to compare changes in phenotype with time across the various materials, a time-course immunocytochemistry study for four markers (two pluripotent, two neuronal) was performed. Of the pluripotent markers, OCT4 (Figure 4.5A) and UTF1 (Figure 4.5B) were investigated. As observed in the pluripotent characterization in Chapter 3, the first two markers are transcriptional factors expressed in the nuclei of ESC's. Analysis for Ki67 was also carried out.

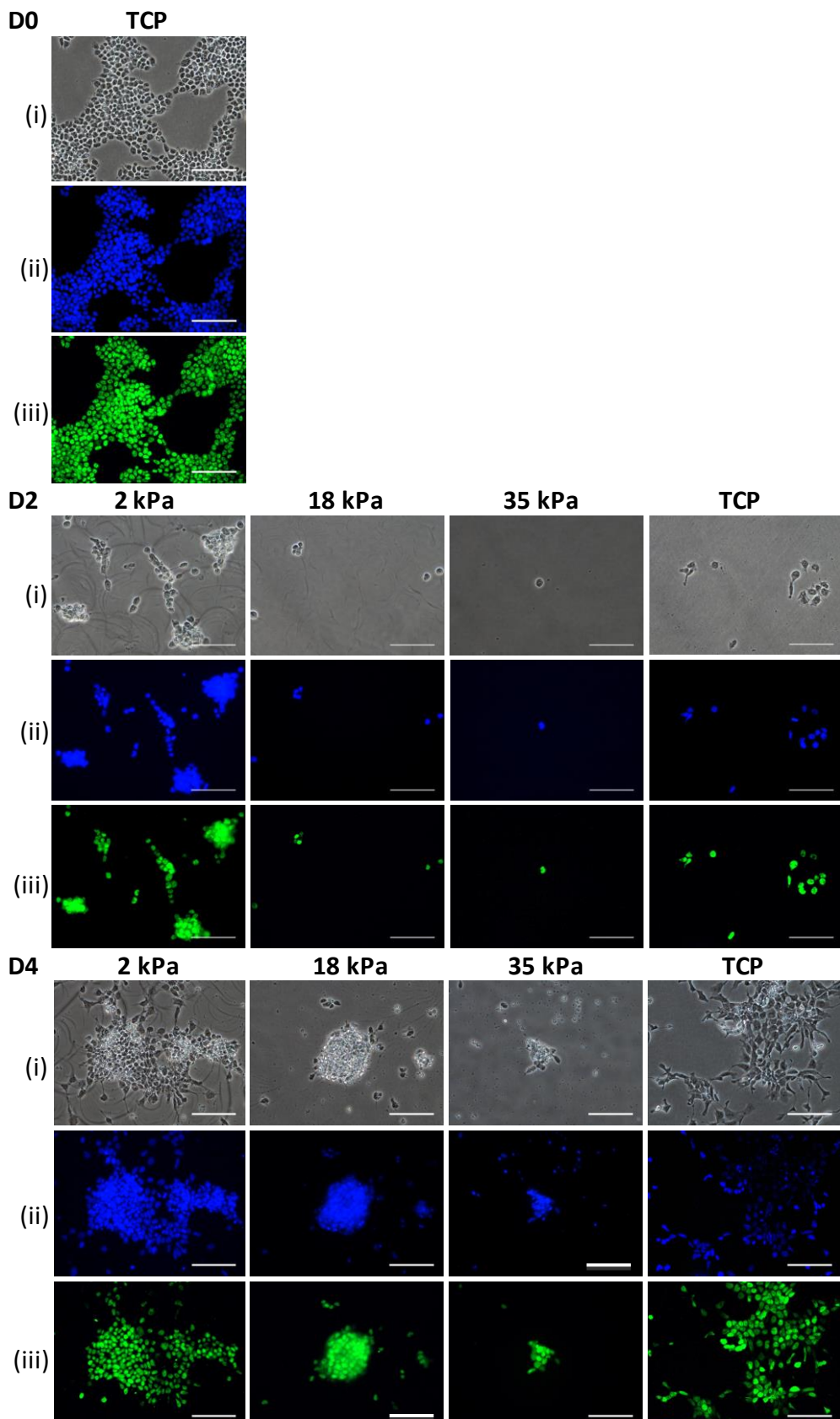


Figure 4.5A: Four-day (D0,D2,D4) time course analysis for OCT4, a marker for pluripotency in MESCs seeded on three GXG materials (2 kPa, 18 kPa and 35 kPa) and TCP in N2B27 medium. (i) Phase contrast. (ii) DAPI, a nuclear stain. (iii) ICC for OCT4.. Scale Bars = 100 μ m.

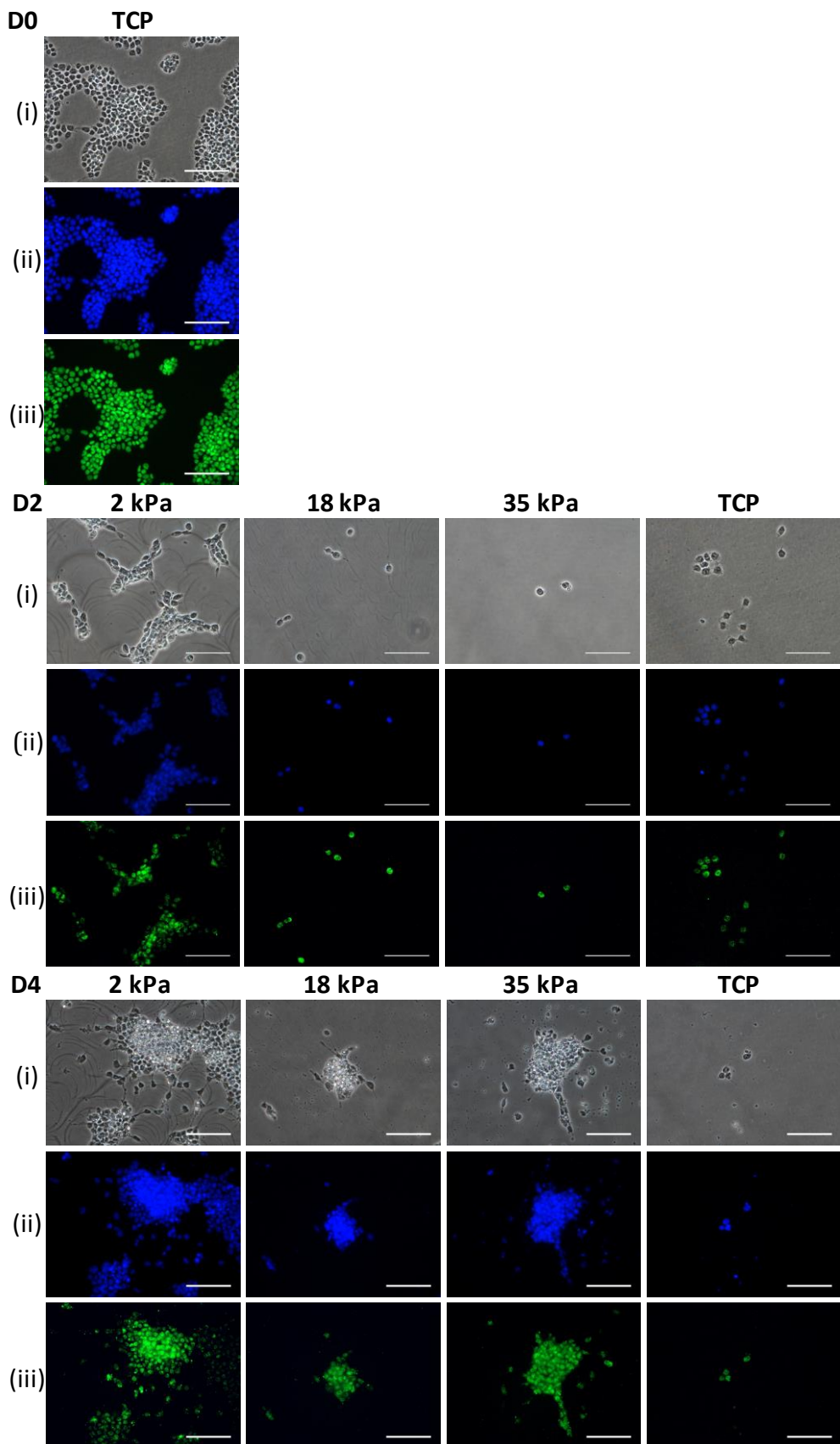


Figure 4.5B: Four-day (D0,D2,D4) time course analysis for UTF1, a marker for pluripotency in MESC's seeded on three GXG materials (2 kPa, 18 kPa and 35 kPa) and TCP in N2B27 medium. (i) Phase contrast. (ii) DAPI, a nuclear stain. (iii) ICC for UTF1. Scale Bars = 100 μ m.

As proliferative capacity decreases during neuronal differentiation, it was expected that this marker would not be found in neural precursors.

Figure 4.5 showed that over the course of neuronal differentiation, OCT4 and UTF1 remained present in cells at day two and day four. OCT4 has previously been shown to remain expressed during differentiation, despite the appearance of mature cell type-specific markers (Lee et al, 2010). Chowdhury et al (2010) showed that soft materials could maintain OCT4 expression in normal culture medium even without the presence of LIF. However, the continued expression of OCT4 at day four in our investigation was independent of Young's modulus, contradicting that finding. As seen in Chapter 3, the effects of Young's modulus on mESC's do vary in spontaneous differentiation medium. Kothapalli & Kamm (2013) also recently demonstrated that OCT4 remains on at day four during neuronal differentiation of mESC-derived EB's on three-dimensional hydrogels, in broad agreement with our findings. UTF1 has not been as extensively studied, but it suggests along with the OCT4 results, that cells maintain some pluripotent identity during early neuronal differentiation. This effect was however independent of Young's modulus.

As seen in Chapter 3, Ki67 (Figure 4.6) is a marker for proliferative cells commonly found in the nuclei of undifferentiated ESC's. This marker was less prevalent in differentiated cells compared to undifferentiated cells. It was not present in cells on the softest GXG material after four days of differentiation. It was found in some cells on the stiffer material in the denser colonies of cells, but not abundantly. This implies that cells with morphology A are more proliferative than morphology B or C. We concluded that these cells are closer to the undifferentiated state than the flattened (B) or spread (C) cells. Other studies have proposed that proliferation decreases with an increase in Young's modulus in neuroblastoma (Lam et al, 2010) and neural stem/progenitor cells (Liepzig & Shoichet, 2009), but these are very different cell types to mESC's. Previtera et al (2013) showed a contrary finding, demonstrating that proliferation (also based on Ki67 immunocytochemistry analysis) was increased on stiffer materials for purified neural precursors, consistent with the GXG results albeit with a primary spinal cord cell source.

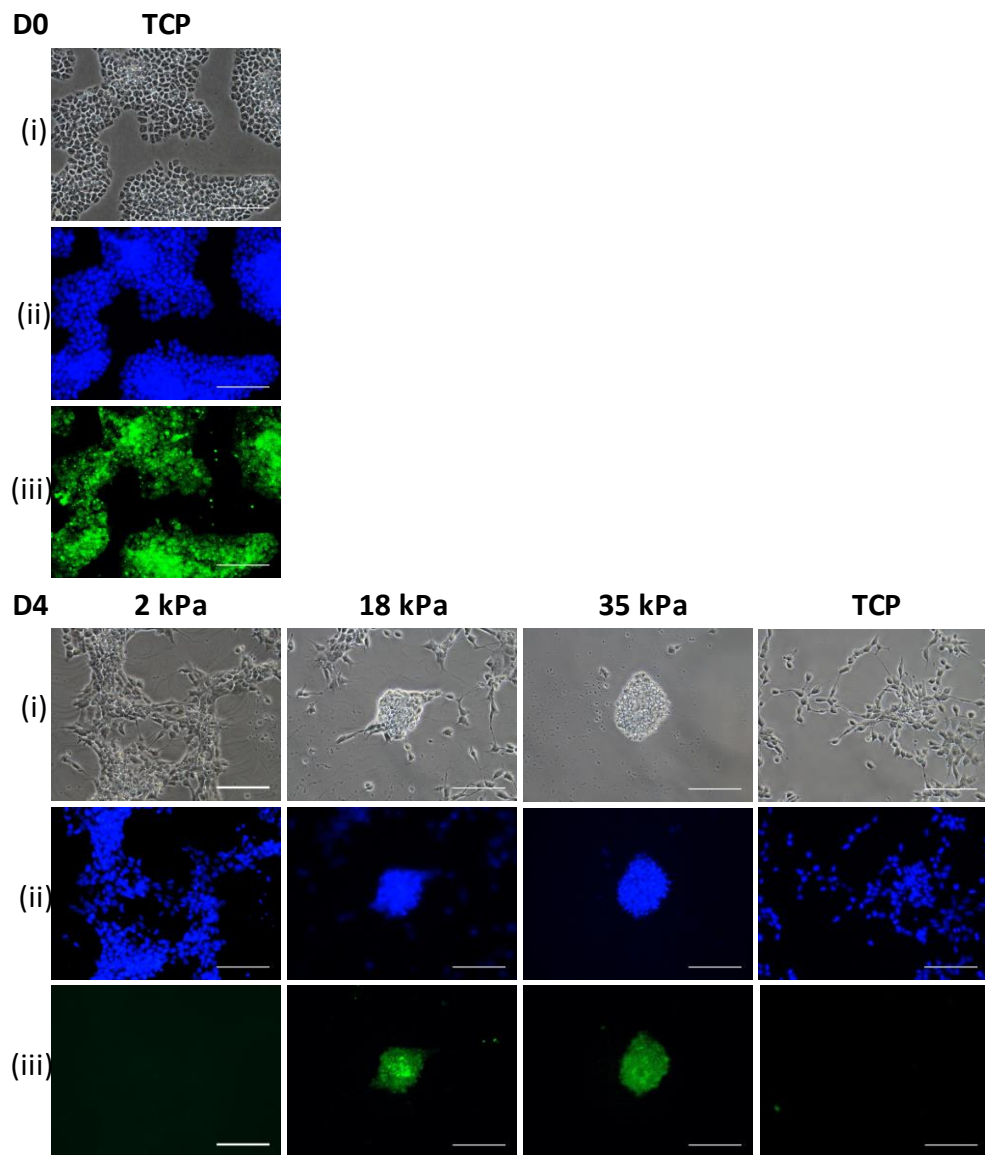


Figure 4.6: ICC analysis for Ki67, a marker for proliferative cells in MESCs seeded on three GXG materials (2 kPa, 18 kPa and 35 kPa) and TCP in N2B27 medium.(i) Phase contrast. (ii) DAPI, a nuclear stain. (iii) Ki67. Images obtained at day zero and day four post-seeding. Scale Bars = 100 μ m.

Proliferation in the Previtera et al (2013) study did decrease over time on all materials, despite growth being in expansion and not differentiation medium.

Following on from the analysis of pluripotent markers, the next stage was to investigate the effect of Young's modulus on formation of neural precursors and immature neurons from mESC's in N2B27. From the earlier neuronal characterization work (Chapter 3), nestin and β -III tubulin were identified as the two most suitable markers for neuronal differentiation. Nestin was used as a marker for neural precursor cells (Ying et al, 2003), whilst β -III tubulin was used as a marker for immature neurons.

Time-course immunocytochemistry analysis for nestin (Figure 4.7A) over the first four days of neuronal differentiation revealed that nestin began to be observed after two days on all four materials, which was earlier than expected. At day four, nestin was observed across all four materials.

Longer-term differentiation (seven days) of neural stem cells (Banerjee et al, 2009) revealed a similar result, where nestin-positive neural precursor formation did not vary with Young's modulus. In the same study by Previtera et al (2013), there were more nestin-positive cells on stiffer materials at day five of neural precursor growth in expansion medium than on soft. Conversely, Engler et al (2006) found higher expression of nestin on soft materials when mesenchymal stem cells were differentiated in neuronal differentiation medium. Variations in conditions and cell types between studies led to different responses to Young's modulus.

Staining for β -III tubulin started at day four as it was not previously found in cells at this stage of neuronal differentiation (Chapter 3). At day six, β -III tubulin was again found in colonies on all four materials (Figure 4.7B). However, on stiffer GXG materials the extension of β -III tubulin positive neurites was restricted within colonies. On the softest material (2 kPa) and TCP, neurites rich in β -III tubulin branched and extended between colonies.

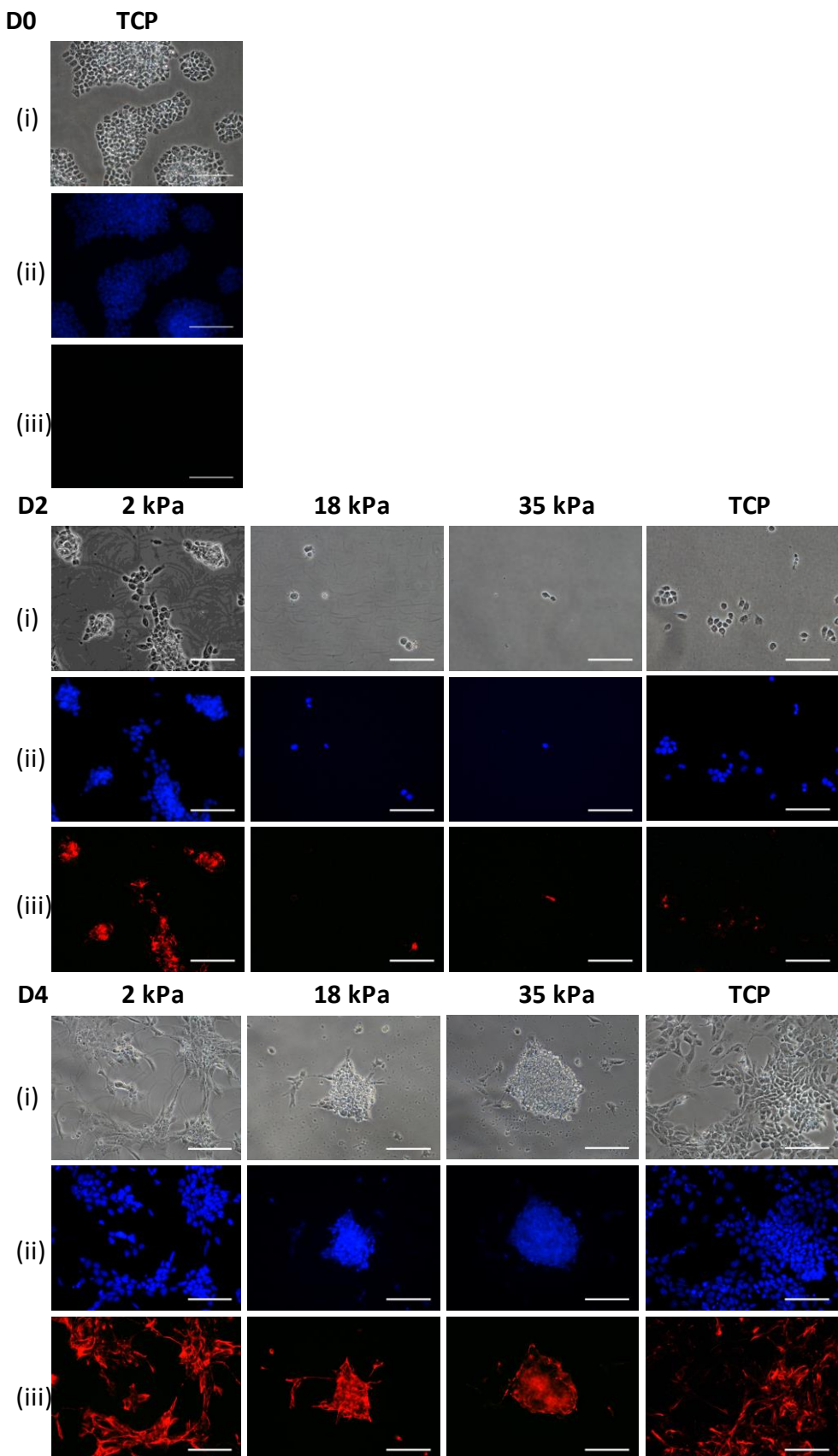


Figure 4.7A: Four-day time course analysis for nestin, a marker for neural precursor cells in MESC's seeded on three GXG materials (2 kPa, 18 kPa and 35 kPa) and TCP in N2B27 medium. (i) Phase contrast. (ii) DAPI, a nuclear stain. (iii) ICC for nestin.. Scale Bars = 100 μ m.

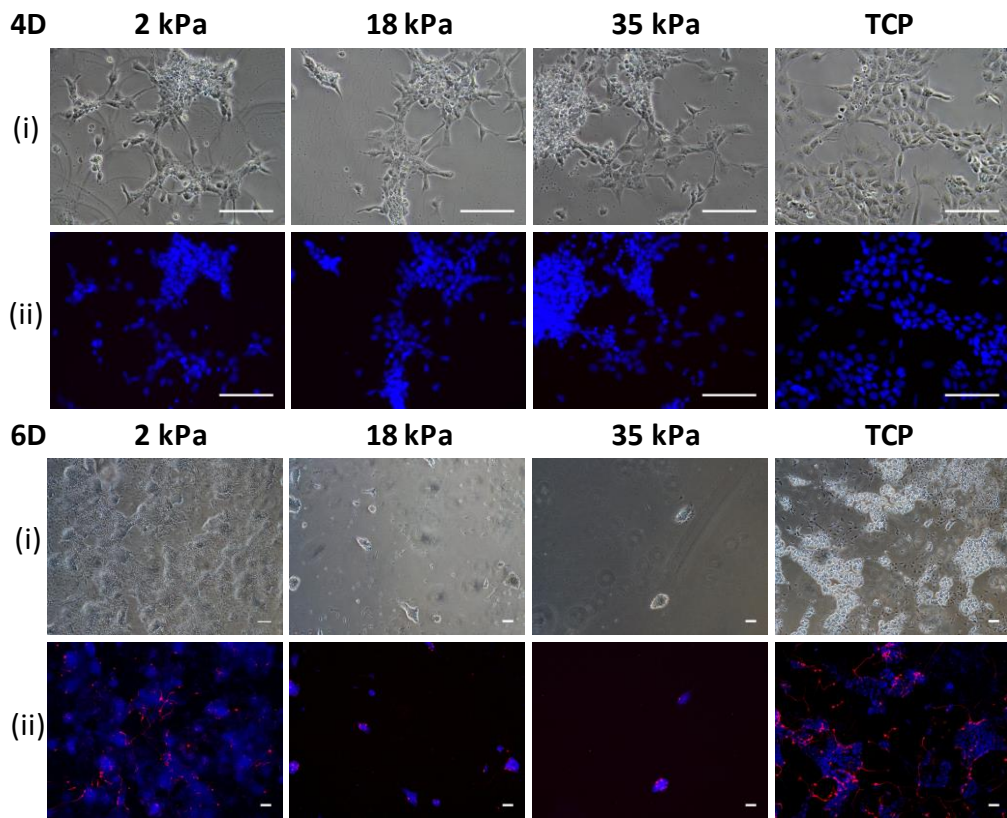


Figure 4.7B: Immunocytochemistry analysis for β -III tubulin, a marker for immature neurons in MESCs seeded on three GXG materials (2 kPa, 18 kPa and 35 kPa) and TCP in N2B27 medium. (i) Phase contrast. (ii) DAPI, a nuclear stain. (iii) ICC for β -III tubulin. ICC performed at day four and day six post-seeding. Scale Bars = 100 μ m.

Immunocytochemistry analysis by Kothapalli & Kamm (2013) in a recent study demonstrated that both neurite length and formation of β -III tubulin-positive cells from mESC-derived EB's were maximized at a similar Young's modulus to our own study. Both neurite length and β -III tubulin-positive cell formation decreased as Young's modulus decreased to the 100's of Pa. Keung et al (2012) showed agreement with this data using similar techniques for induced pluripotent stem cells, which were differentiated for nine days towards a neuronal lineage. The proportion of cells positive for β -III tubulin significantly decreased at higher Young's moduli (75 kPa). However, when the same techniques were used for hESC's, the findings showed similarity to the GXG results. The proportion of cells that were β -III tubulin positive did not significantly decrease within a similar Young's modulus range. Earlier work by Flanagan et al (2002) also showed agreement with our data, as primary spinal cord neurites became more branched with a decrease in Young's modulus (albeit over a lower Young's modulus range).

When considered along with the nestin findings, this suggests that more neural precursors and immature neurons form on the softest GXG material, but this effect was due to increased initial attachment on the soft material rather than a direct promotion of neuronal differentiation. The increased branching and extension of β -III tubulin-rich neurites on soft materials was likely due to increased paracrine signalling between colonies. An increase in the density of colonies resulted in considerably less distance for signalling to occur between them.

4.3.3 Does Young's modulus enrich populations of neural precursors during mESC differentiation in N2B27 medium?

In order to further confirm the hypothesis that the increase in numbers of neural precursors on soft materials was due to favourable initial attachment, flow cytometry for neural cell surface marker PSA-NCAM (see Chapter 3) was carried out. By comparing the percentage of cells positive for the marker across the four materials, it could be ascertained whether soft materials were directly promoting neuronal

differentiation by increasing the proportion of neural precursors in the total population. Comparison between the harvest cell counts (which were expected to correspond with the confluence measurements at 72h) and this value allowed for confirmation that neural precursor yield increased due to favorable initial attachment and not due to a neuronal promotion effect. Neuronal precursor yield was defined as the product of the total harvested cell concentration (cells/cm^2) and percentage of cells positive for PSA-NCAM.

As seen in Figure 4.8, total cell concentration showed a significant ($p<0.005$) decrease on the 18 kPa (57%) and 35 kPa (80%) when compared to the soft, 2 kPa GXG material. These findings were consistent with the earlier 72h expansion results shown in Figure 4.2A.

Flow cytometry analysis did not show any variation in percentage of cells positive for PSA-NCAM with Young's modulus. This implies that soft materials do not select for the formation of neural precursors over other cell lineages. The increase in percentage of cells positive for the marker (30-40% of cells were positive on all four materials) compared to that for undifferentiated cells (4.79% from Chapter 1) confirmed that differentiation towards the neuronal lineage was taking place on all four materials.

Cell yield of PSA-NCAM positive neural precursors thus exhibited a similar pattern to that of total harvested cell yield. It was concluded that that soft materials increase the yield of neural precursors from mESC's in N2B27, without enriching them.

The balance between these two properties – yield and enrichment is a crucial consideration when designing bioprocesses effectively. Regenerative medicine is no exception in this regard. For safety reasons, high cell enrichment is highly desirable in the end cell therapy product. Elimination of non-target cells (undifferentiated as well as other lineages) in stem cell-derived products is a key FDA requirement in reducing the risk of tumorigenicity (Knoepfler, 2009).

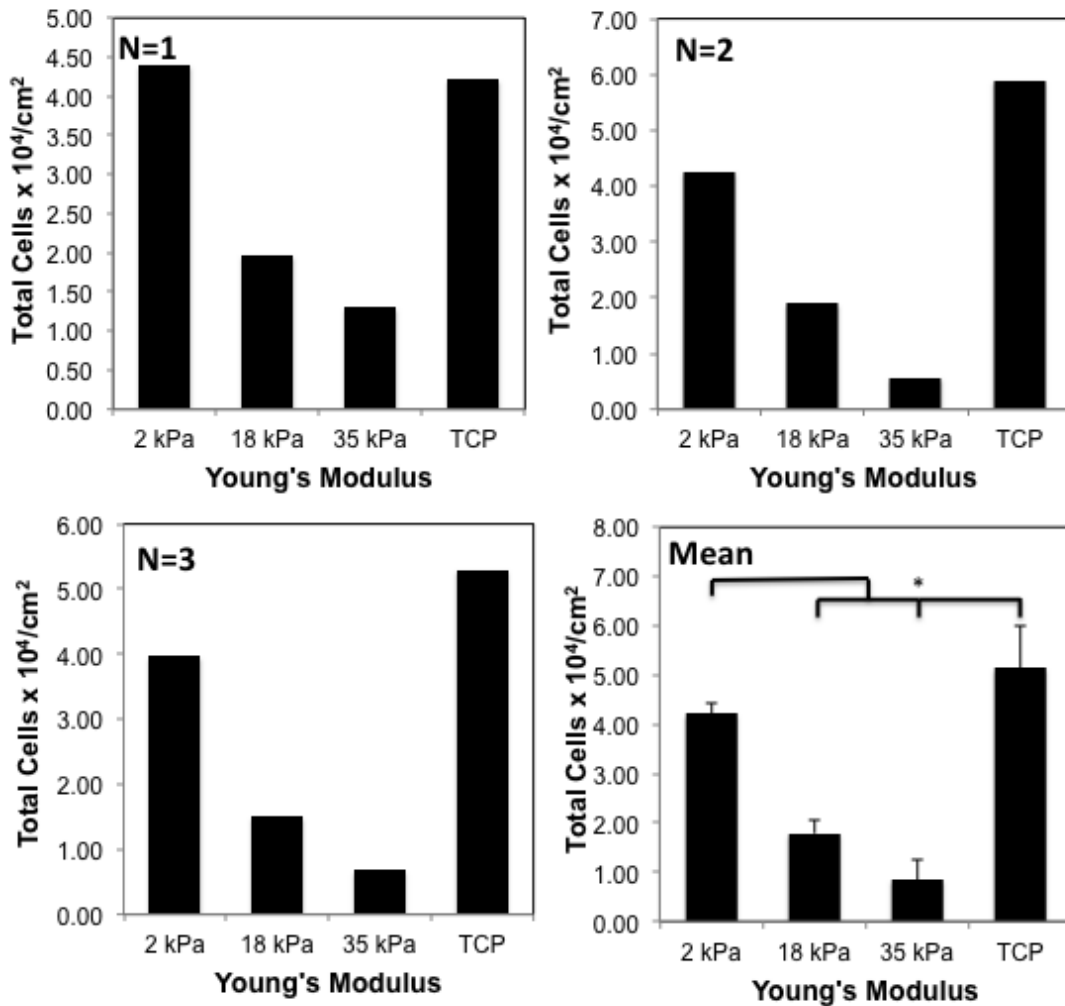


*Figure 4.8: Total cell concentration at day 4 of neuronal differentiation on three GXG materials (2 kPa, 18 kPa and 35 kPa) and TCP. Three biological replicates and mean shown. Error bars represent standard deviation from the mean. * represents a p-value less than 0.005 as measured by one-way ANOVA (followed by Tukey post-hoc correction).*

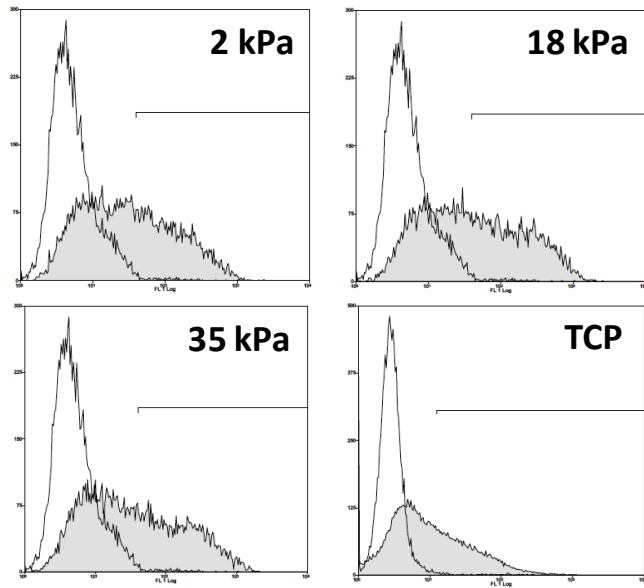
It is likely that the 30-40% neural precursor (characterized by the PSA-NCAM marker) enrichment achieved here would be too low for a cell therapy product and would require significant further processing before being considered as being appropriately pure for use.

4.3.4 Does Young's modulus affect gene expression during mESC differentiation in N2B27 medium?

Whilst immunocytochemistry and flow cytometry are useful in understanding how many cells within a population are of a particular phenotype, it does not allow us to understand behaviour at a genetic level. Real-time qPCR (quantitative polymerase chain reaction) allows for cells to be characterized in such a way. Ten genes were chosen for investigation, including three pluripotent genes (OCT4, Nanog and UTF1), four neuronal-associated genes (Nestin, β -III tubulin, Sox1 and PSA-NCAM), one mesodermal gene (T-brachyury), one endodermal gene (Sox17) and one gene expressed very early on during differentiation, at the epiblast stage (FGF5).

The results for the pluripotent and neuronal markers confirmed the previous conclusions. There was no significant variation ($p > 0.05$) in gene expression with Young's modulus for any of the neuronal genes (Figure 4.10). The lack of variation in Sox17 and T-brachyury expression suggested that variations in Young's modulus did not encourage differentiation into other lineages. Returning to the enrichment versus yield discussion, this means that whilst neuronal lineages are not being affected, other non-target (undesirable from a bioprocessing and safety perspective) genes were not being enriched in place.

A



Young's Modulus	% PSA-NCAM
2 kPa	35.90 ± 5.58
18 kPa	40.53 ± 9.64
35 kPa	38.30 ± 11.91
TCP	32.16 ± 14.77

B

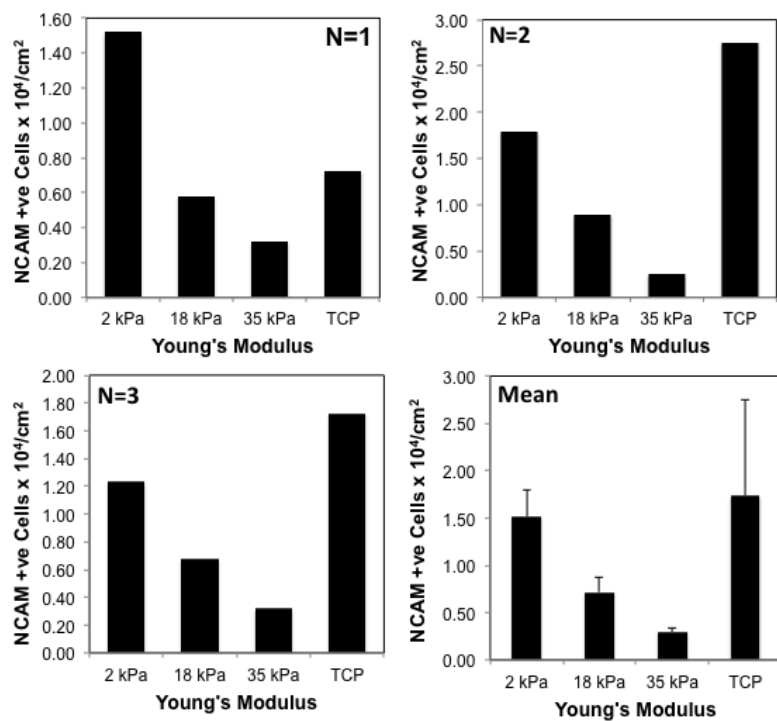
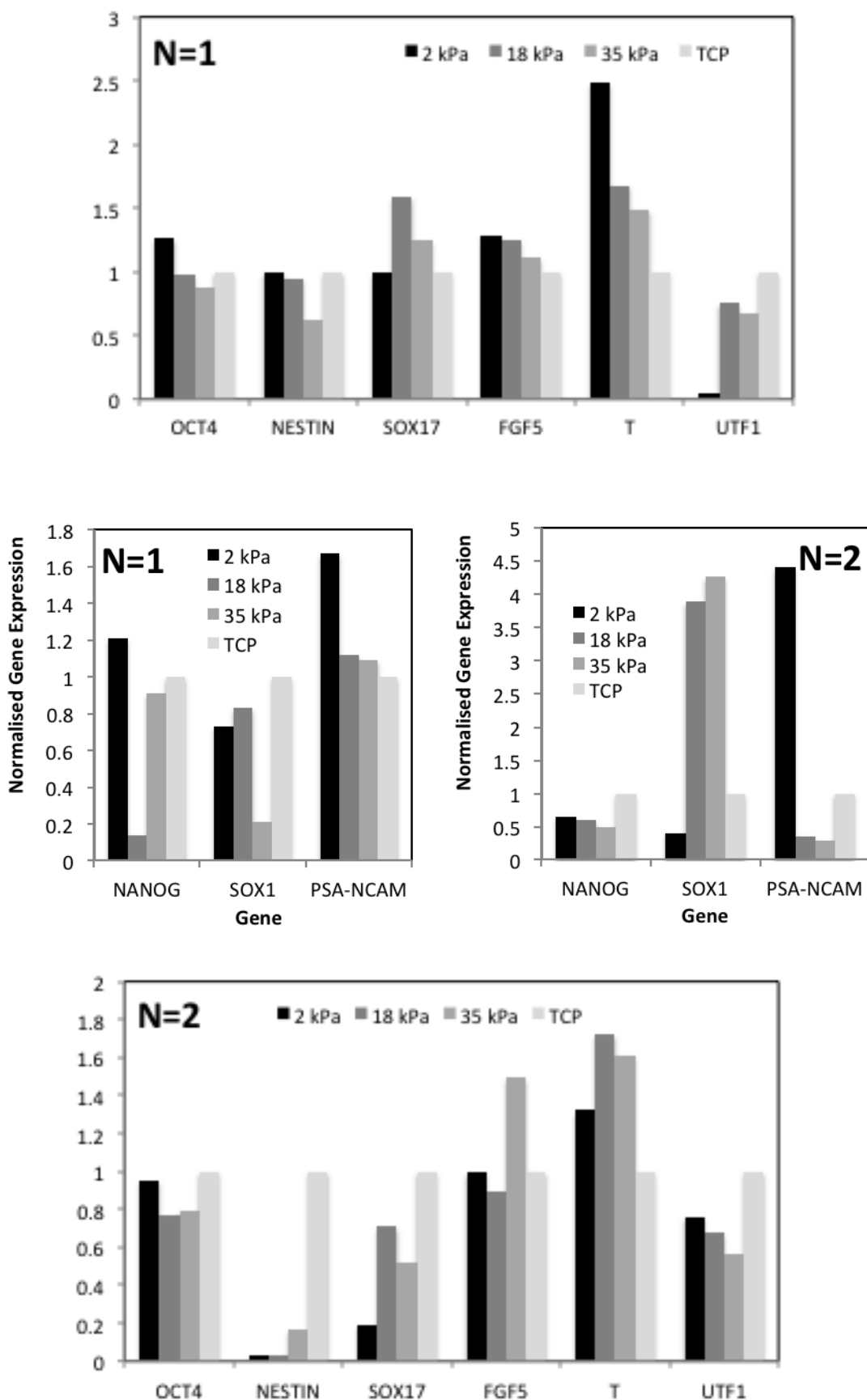


Figure 4.9(A): Flow cytometry results for PSA-NCAM, a neural precursor marker in mESC's differentiated for four days in N2B27 medium. The histogram shown is representative of a biological replicate. The white area represents the isotype control, whilst the shaded area represents the stained sample. The values given in the table are the means \pm standard deviations derived from biological triplicates. Figure 4.9(B): Yield of PSA-NCAM positive neural precursors following four days of differentiation from three GXG materials and TCP. All three biological replicates shown as well as the mean.

Similar work in mesenchymal stem cells (Engler et al, 2006) contradicted these findings by demonstrating that neuronal gene expression (PSA-NCAM, nestin and β -III tubulin) increases on soft materials. Other studies using other lineages for mesenchymal stem cells have also shown changes in gene expression with Young's modulus. Two recent studies have shown upregulation in target phenotype gene expression during osteogenic (Wang et al, 2012) and cardiac (Li et al, 2012) differentiation with Young's modulus. Conversely, downregulation in target gene expression was observed during chondrogenic differentiation (Kwon, 2013). It should be noted that mesenchymal stem cells are more mature than embryonic stem cells and so are not directly comparable.

In terms of ESC's, different differentiation lineages have shown different effects with changes in Young's modulus. However, the ranges of moduli used in the studies vary greatly with each other. In one such study by Evans et al (2009) where mouse embryonic stem cells were differentiated towards the osteogenic lineage, osteogenic markers Runx2 and Spp1 were upregulated with an increase in Young's modulus from 41 kPa to 2.3 MPa. This was however across two orders of magnitude in PDMS substrate Young's modulus, a much larger range than the GXG used in our study. Conversely, during induced endoderm differentiation in mESC's (Jaramillo et al, 2012), endoderm genes were downregulated as Young's modulus increased (from 4 Pa to 250 Pa). Recent studies looking at spontaneous differentiation of mESC's (Candiello et al, 2013) and hESC's (Eroshenko et al, 2013) have agreed with our findings that gene expression (in particular, ectoderm) is unaffected by Young's modulus.

These findings led us to conclude, along with the attachment, immunocytochemistry and flow cytometry data, that soft materials favour the promotion of neural precursor cells from mESC's through increased initial attachment without directly promoting neuronal specification. This confirms the central hypothesis of this chapter.



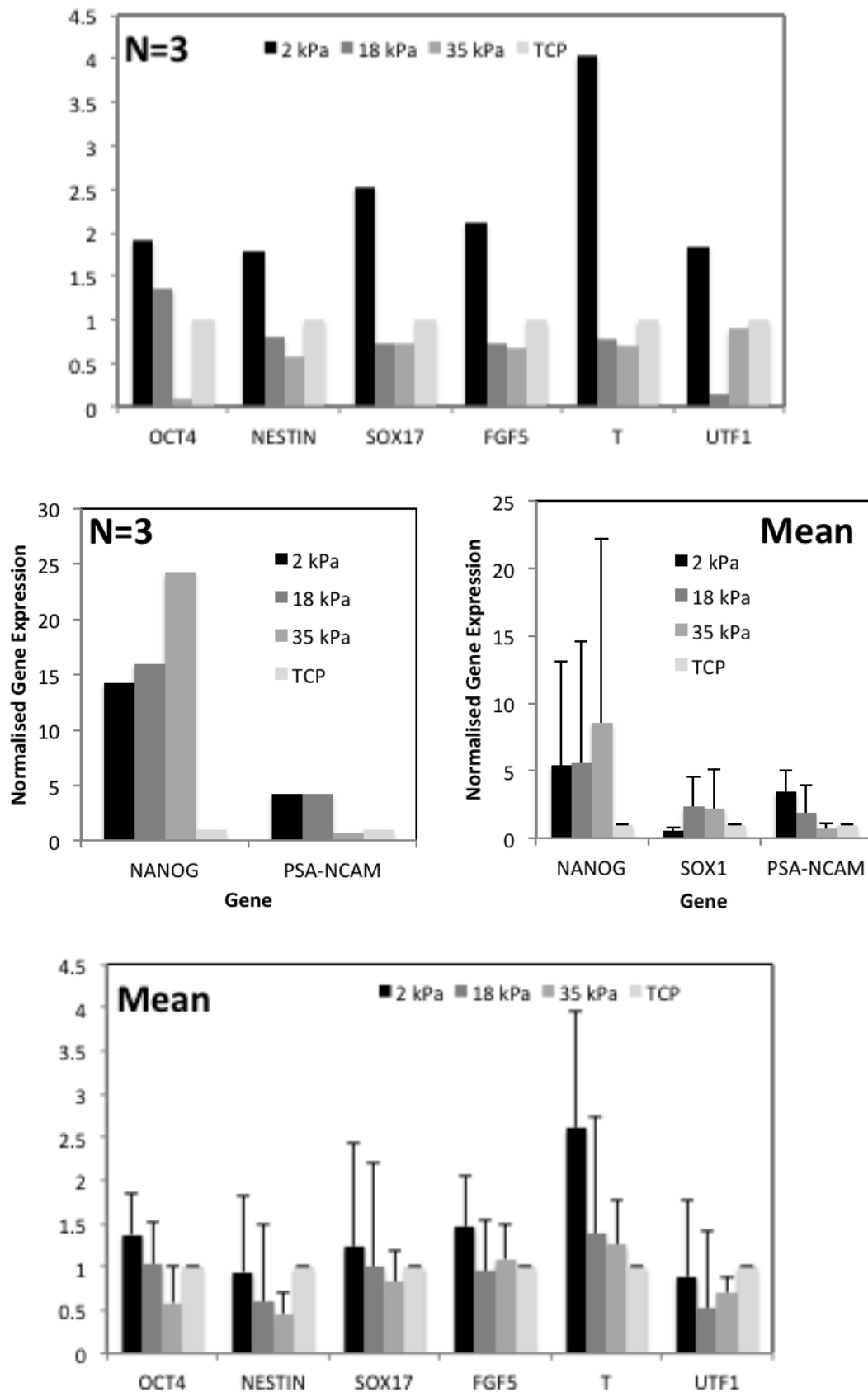


Figure 4.10: Changes in early gene expression with modulus, as measured using real time qPCR. All biological replicates shown as well as the mean (the error bars represent standard deviation values).

4.4 Is the favourable attachment of mESC's on soft materials dependent on stress fiber stabilization or microtubule formation?

After it was established that the increase in neural precursor cell yield on soft materials was due to favourable attachment and not direct promotion of the neuronal fate by the material, an attempt was made to elucidate the mechanism behind this attachment effect. Two inhibitors were used to investigate this mechanism. One was blebbistatin, which inhibits stress fiber contraction (via non-muscle myosin II or NMMII). The other was nocodazole, which inhibits microtubule formation. Stress fibers and microtubules are the two most influential components of the cytoskeleton, and so they are instrumental in allowing cells to adhere and spread on materials (Wang et al, 2009).

As shown in Figure 4.11, attachment was unaffected by blebbistatin inhibition, both when cells were pre-treated with it as well as when cells were seeded with it. Blebbistatin is a reversible inhibitor, and so it is likely that pre-treated cells will eventually reform a similar actin structure as they exhibited prior to inhibition.

Cells were then stained with phalloidin, a dye that specifically binds to F-actin in cells. When ES cells were stained with phalloidin, F-actin appeared diffuse and concentrated mainly within the periphery of cells (Figure 4.12). This was in contrast to cells such as fibroblasts (Pelham & Wang, 1997) and mesenchymal stem cells (Engler et al, 2006), which form organised stress fibers within the cytoplasm. This is also likely to be one of the reasons why ES cells are more three-dimensional in nature than fibroblasts, which tend to be flattened, spread and two-dimensional (Chapter 3). As mentioned earlier, actin also concentrates at the cortical regions in cells during the gastrulation stage of embryogenesis (Krieg et al, 2008; Skoglund et al, 2008).

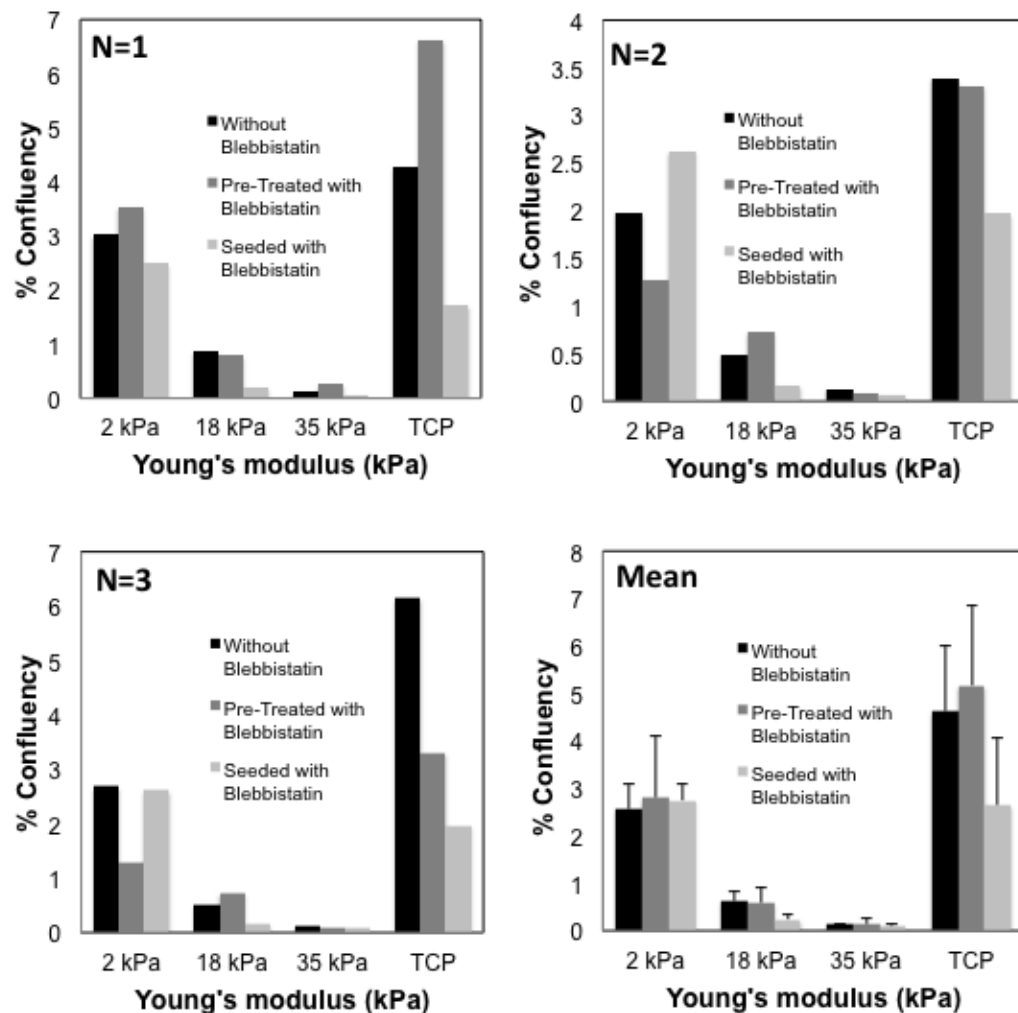


Figure 4.11: The effect of blebbistatin, an inhibitor of myosin IIb-dependent actin stress fiber formation, on mESC attachment at 24h. Cells were either seeded without blebbistatin, pre-treated for 30 mins prior to seeding or seeded in medium containing blebbistatin. Each of the replicates are shown as well as the mean and standard deviation (N=3).

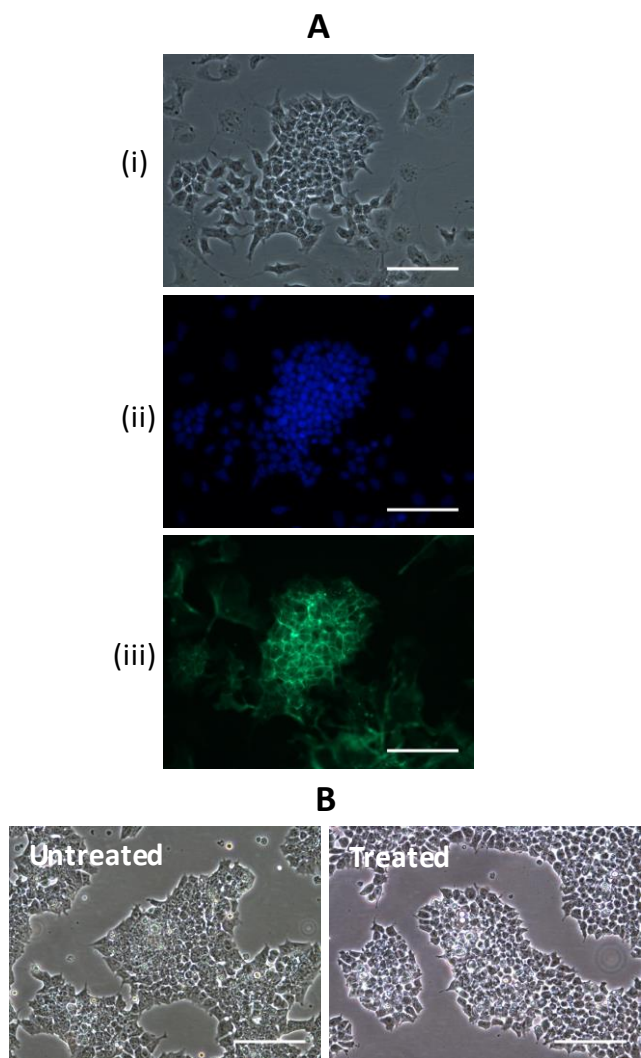


Figure 4.12 (A): Immunocytochemistry analysis in undifferentiated mESCs using phalloidin, a dye used to reveal F-actin within the cytoplasm. (i) Phase contrast. (ii) DAPI, a nuclear stain. (C) ICC for phalloidin. Figure 4.12 (B) MESC morphology before and after blebbistatin treatment (cells treated for 30 mins). All scale bars = 100 μm .

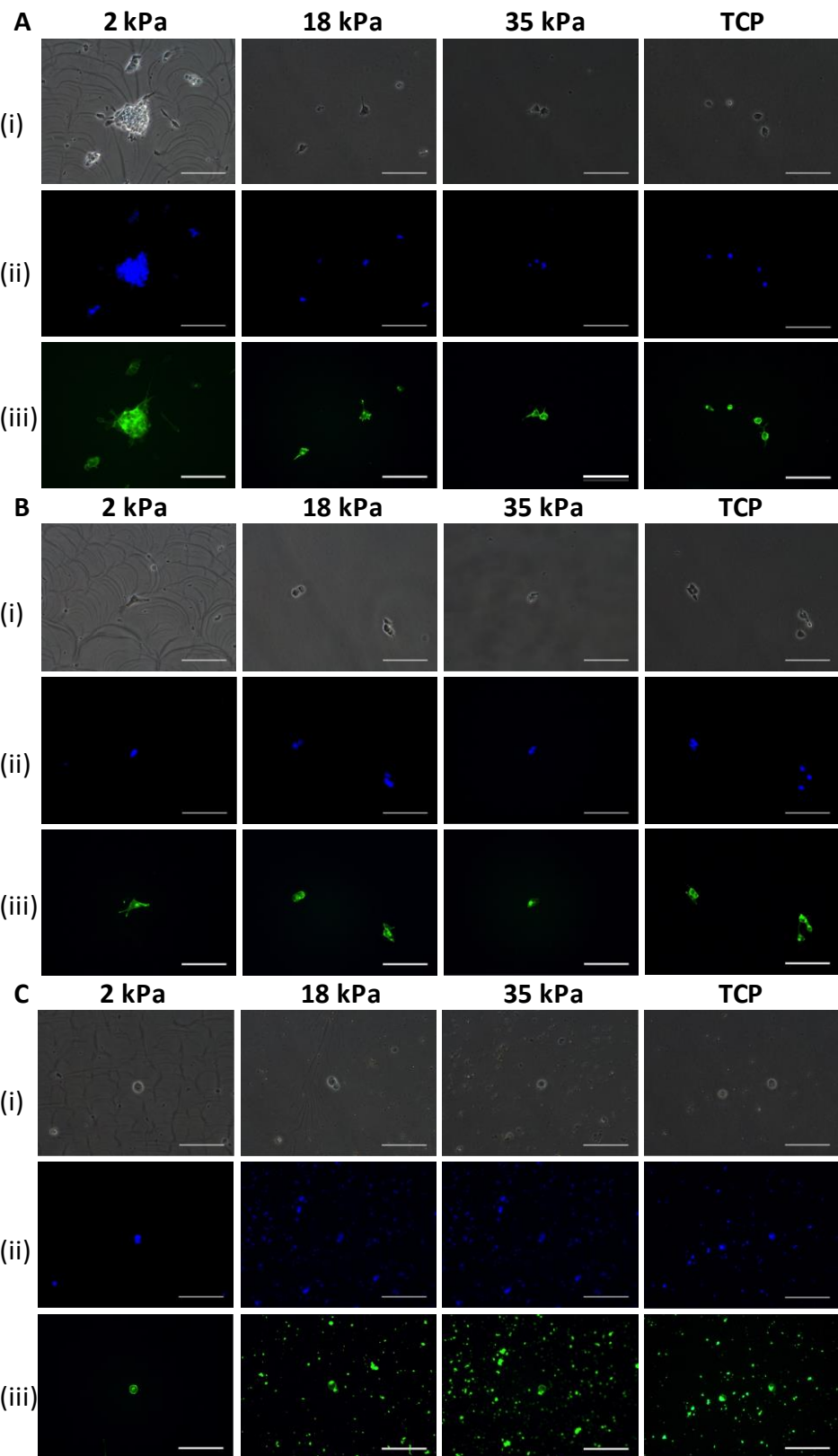


Figure 4.13: F-actin in mESCs seeded for 24h on three GXG materials (2 kPa, 18 kPa and 35 kPa) and TCP in Neuronal Differentiation medium: (A) without blebbistatin, (B) pre-treated with blebbistatin for 30 mins, (C) seeded with blebbistatin. From top to bottom: (i) Phase contrast. (ii) DAPI, a nuclear stain. (iii) ICC for phalloidin. All scale bars = 100 μ m.

When phalloidin staining was performed on cells seeded for 24h on GXG and TCP (Figure 4.13) without blebbistatin, stress fibres were not formed on any of the materials. F-actin appeared diffuse, mainly concentrated at the cell cortex.

As expected, when cells were pre-treated with blebbistatin or seeded with blebbistatin, the same F-actin structure was observed in treated cells as in untreated cells, as no organised F-actin stress fibres were present in the untreated condition. The lack of stress fibres in mESC's prevented blebbistatin from having any effect on initial attachment. Thus mESC's do not require actin stress fibre stabilization in order to attach to any material.

The actin cytoskeleton is the main conduit for the transduction of mechanical signals to the nucleus. The nucleoskeleton, which also contains polymerized F-actin is connected to both the cytoskeleton as well as the transcriptional machinery of the cell (Wang et al, 2009). For this reason, actin stress fibre contraction, dependent on myosin IIb (the protein inhibited by blebbistatin) is implicated in gene expression (Engler et al, 2006) responses to changes in stiffness. However, as the mouse ES cells have no organised stress fibers, there is no conduit for mechanotransduction of mechanical signals from the ECM to the nucleus. This may explain why Young's modulus changes do not provoke gene expression responses in mESC's during early differentiation (Figure 4.10).

Microtubules are another key structural component of cells. Unlike F-actin, microtubules have not been previously found to be implicated in gene expression responses to changes in Young's modulus. However, as the effect of Young's modulus on neural precursor formation is based on attachment and not gene expression, it is possible that the effect of Young's modulus on mESC's may be dependent on another structural component other than the actin cytoskeleton. Thus, this chapter's final pair of experiments aimed to investigate whether attachment was dependent on the formation of microtubules from α -tubulin. This was achieved by inhibiting microtubule formation using another small molecule, nocodazole.

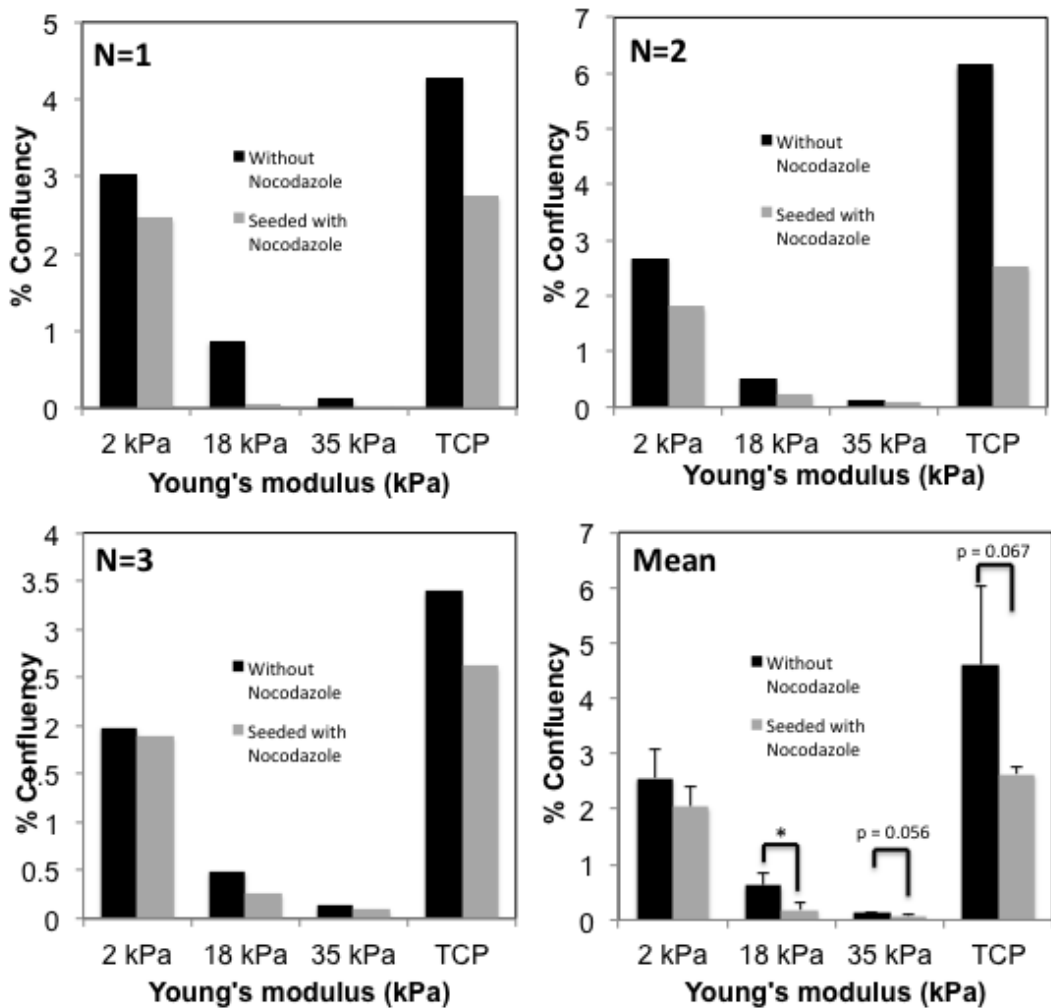


*Figure 4.14: The effect of nocodazole, an inhibitor of microtuble formation, on mESC attachment at 24h on 3 GXG materials (2 kPa, 18 kPa, 35 kPa) and TCP. Cells were either seeded without nocodazole or seeded in medium containing nocodazole. Each of the replicates are shown as well as the mean and standard deviation (N=3). * represents a p-value less than 0.05 as measured by one-way ANOVA (followed by Tukey post-hoc correction).*

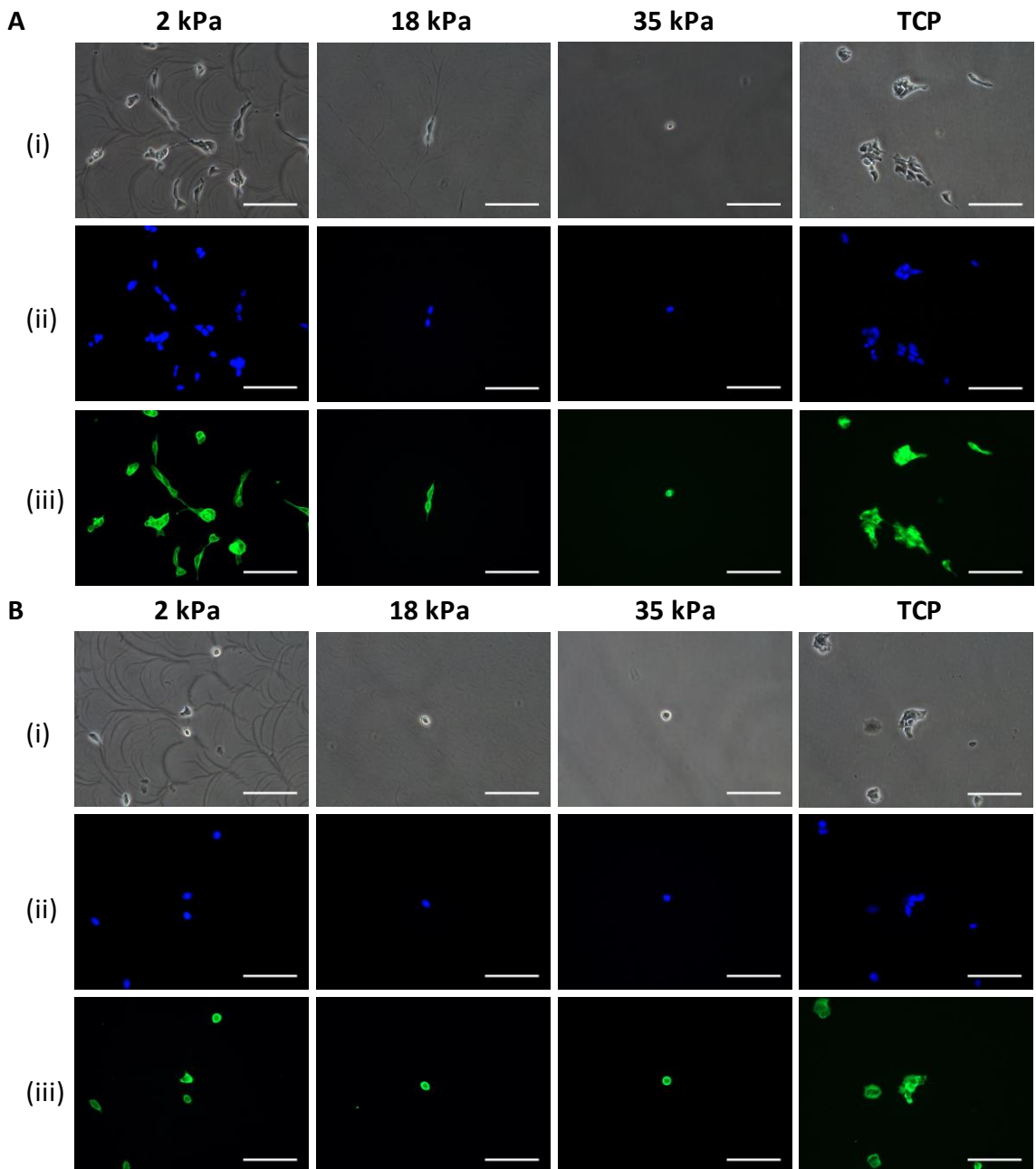


Figure 4.15: Immunocytochemistry analysis for α -tubulin, a protein which polymerizes to form microtubules, a key structural component of the cytoskeleton. MESC's were seeded for 24h on three GXG materials (2 kPa, 18 kPa and 35 kPa) and TCP in Neuronal Differentiation medium: A) cells seeded without nocodazole (untreated) B) cells seeded with nocodazole, an inhibitor of microtubule formation. (i) Phase contrast. (ii) DAPI, a nuclear stain. (C) ICC for α -tubulin. All scale bars = 100 μ m.

As with blebbistatin, seeding with nocodazole had no significant ($p=0.322$) effect upon attachment on the soft 2 kPa GXG material. However, on stiffer GXG materials attachment decreased with nocodazole seeding compared to the untreated condition. This result was only significant ($p<0.05$) on the 18 kPa GXG materials, where attachment decreased by 71%. However the p -value was 0.056 on the 35 kPa material (confluence decreased 44%), implying that a trend did exist.

Interestingly, cells that do attach on stiffer materials cannot remain attached (or cannot initially attach) if microtubule formation is inhibited. Cells on the softest material remain attached regardless of microtubule formation. Microtubule concentration has been previously been implicated in the stiffening of neuronal cells (Spedden et al, 2012). This may also be the case in ES cells, as they do not have the actin stress fibres required for stiffening. Cells have been previously shown to undergo 'stiffness matching' (Tee et al, 2009). This is where cells stiffen on stiff materials and remain soft on soft materials. In a soluble microenvironment that promotes neuronal differentiation, the stiffening of cells on stiff materials is unlikely to occur without microtubule formation. Therefore, cells on stiffer materials (cells which have undergone stiffening themselves) are more susceptible to the effects of nocodazole than cells on softer materials.

4.5 Summary of Findings

It was concluded that soft materials favour the formation of neural precursors from mESC's in neuronal differentiation medium. This effect is dependent upon increased attachment of mESC's on soft materials, rather than a direct promotion of neuronal differentiation. This was demonstrated using a number of assays for cell identity. The assays revealed no differences in gene expression, or marker presence with Young's modulus. When compared to the increased confluence at 24h on soft materials, this confirmed the central hypothesis. It was furthermore found that this effect is neither dependent on stress fibre stabilisation. Interestingly, mESC's did not attach on stiffer materials if microtubule polymerisation was inhibited.

5 Does Young's modulus affect attachment and enrichment of partially-differentiated mouse embryonic stem cells differentiated in N2B27 medium?

Once it was understood how Young's modulus influenced the formation of neural precursor from mESC's, the next stage was to investigate how modulus affected later stages of mESC neuronal differentiation. In Chapter 4, it was found that when mESC's were seeded on GXG in neuronal differentiation medium, attachment was maximized on the softest GXG material, whose elasticity was most similar to that of the early mouse blastocyst. This favourable attachment led to increased neural precursor formation at day four. Despite this, soft materials had no direct effect promoting neuronal differentiation.

5.1 Aims

The aim of Chapter 5 was to investigate whether Young's modulus had an effect on the attachment of partially-differentiated cells. This involved differentiating mESC's for a defined period of time on TCP (partial differentiation), before differentiating them further on GXG. Previous studies using stem cells at a more advanced stage of differentiation such as mesenchymal stem cells (Engler et al, 2006) and neural stem cells (Banerjee et al, 2009; Saha et al, 2008; Leipzig & Schoichet, 2009) have shown that, unlike with mESC's, soft substrates directly favour neuronal differentiation, independent of initial attachment.

Similar results were found in more mature neuronal cell types such as neural precursors (Georges et al, 2006; Jiang et al, 2007; Previtera et al, 2010) and primary cortical neurons (Flanagan et al, 2006). In these cases, neuronal growth and maturation was optimized on soft materials. Taking this into account with the results of Chapter 4, this suggests that the effect of Young's modulus on neuronal differentiation changes as cells mature. During early differentiation of mESC's, Young's modulus favours attachment without directly promoting the neuronal fate. This effect

reverses in mature neuronal cell types (although this has only been characterized using primary cultures of neurons), where Young's modulus directly promotes neuronal differentiation independent of attachment. The combined work of these chapters will hopefully allow for a complete characterization and optimisation, stage-by-stage, of the effect of Young's modulus on neuronal differentiation of mESC's into mature neuronal cell types.

As with the previous chapter, the first experiments focused on the effect of Young's modulus on attachment of partially-differentiated cells. Partially-differentiated cells were defined as mESC's differentiated for four days in neuronal differentiation. This was then followed by a study of the influence of Young modulus on expansion and enrichment of partially-differentiated cells in neuronal differentiation medium. The impact of Young's modulus on attachment was then related to stress fibre or microtubule polymerization in order to deduce an underlying mechanism. The effect of modulus on the rate of cell spreading was also examined. The final experiments in this Chapter looked at the effect of Young's modulus on maturation of partially-differentiated neurons, which were mESC's partially-differentiated for six days in N2B27 medium (forming immature neurons) prior to seeding onto the materials.

5.2 Does Young's modulus influence attachment and early expansion of partially-differentiated cells?

The aim of the first set of experiments was to investigate how Young's modulus influenced the initial attachment and subsequent expansion of mESC's partially-differentiated for four days in N2B27 medium (on TCP). This length of time (as characterized earlier in Chapter 3) was sufficient for colonies of nestin-positive neural precursors to begin to form in culture. The cells formed at this stage were termed the "partially-differentiated cells".

5.2.1 Does Young's modulus affect attachment of partially-differentiated cells in N2B27 medium?

Partially-differentiated cells were seeded onto the same three different GXG Young's moduli as before (2 kPa, 18 kPa and 35 kPa), as well as gelatin-coated tissue culture polystyrene (TCP). When attachment was measured at 24h, confluence was highest on the softest GXG material (Figure 5.1A), whose Young's modulus was closest to that of the brain and central nervous system (Engler et al, 2006; Flanagan et al, 2002).

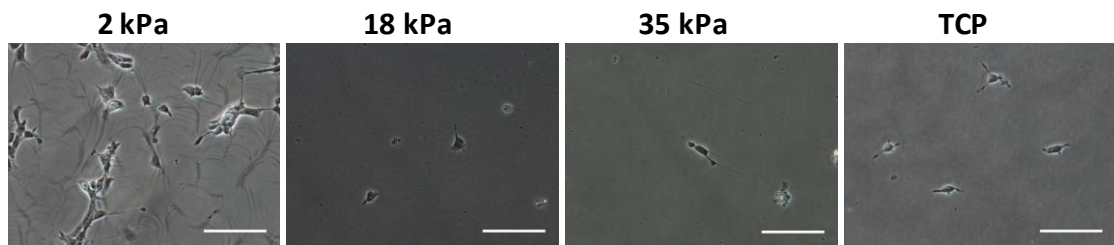
Attachment decreased 66% on the 18 kPa material and 83% on the 35 kPa material (Figure 5.1B). Attachment also decreased on TCP (by 69%).

Attachment has not been previously observed to vary with Young's modulus in neural precursors (Georges et al, 2006; Jiang et al, 2007; Previtera et al, 2010) or neural stem cells (Banerjee et al, 2009; Saha et al, 2008). Astrocyte attachment however, has been found to increase with Young's modulus (Georges et al, 2006; Jiang et al, 2007).

Attachment of oligodendrocyte progenitor cells decreased on softer materials (1 kPa), when compared to glass (Jagielska et al, 2012). However, there was no trend across other moduli in that study.

It should be noted that the source material used in other work varied significantly when compared to this study. Here, the starting population was likely to consist of a mixture of undifferentiated cells as well as cells at various stages of neuronal differentiation (perhaps a small number of cells from other lineages too). The cells used in the other studies were either primary cultures or their direct derivatives. Whilst the level of heterogeneity may have been similar, the type of cells and level of maturity was likely to vary from study-to-study.

A



B

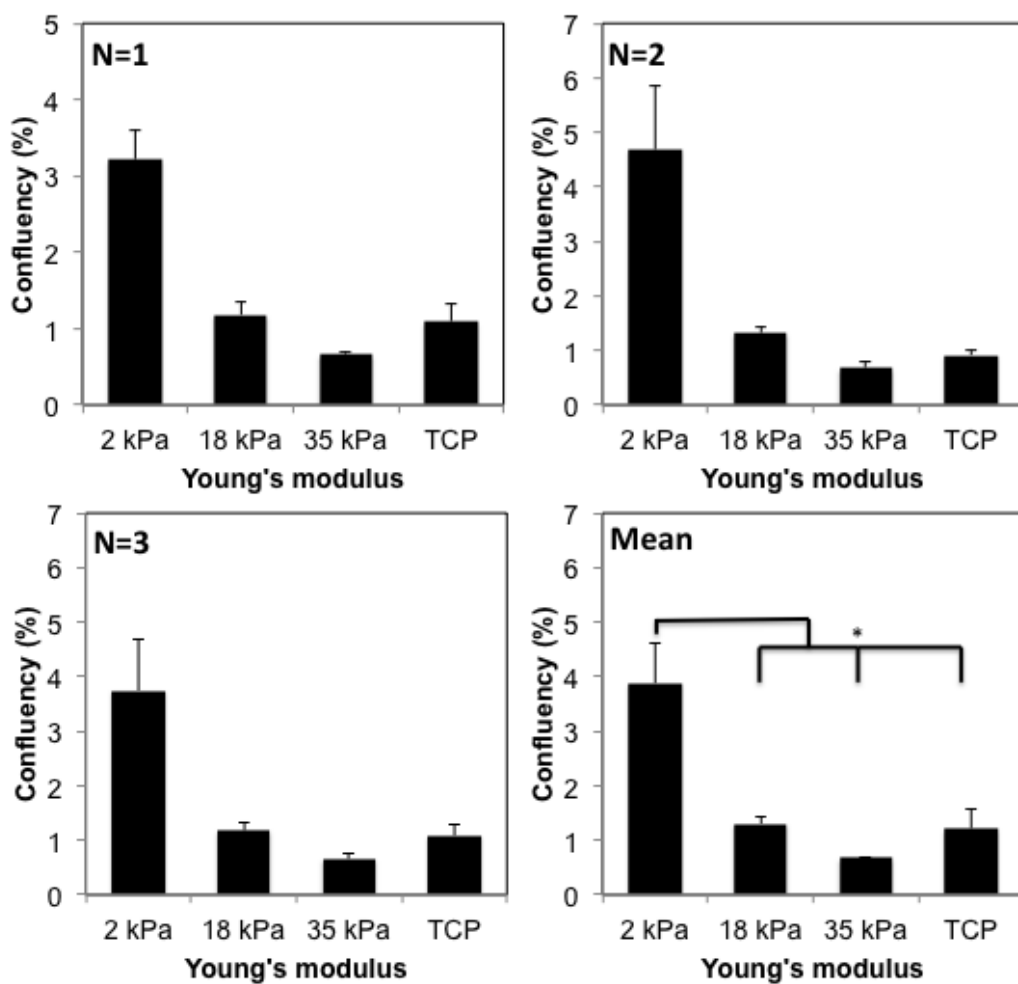


*Figure 5.1 (A): Phase contrast images of four-day partially-differentiated cells seeded for 24h on GXG (2 kPa, 18 kPa and 35 kPa) and TCP in N2B27 medium. Scale bars = 100 μ m. Figure 5.1 (B): Analysis of confluency for partially-differentiated cells attached for 24h onto three different GXG materials and TCP in N2B27 medium. Confluency measurements were made from phase contrast images. All three biological replicates shown as well as the mean and standard deviation. * represents a p-value less than 0.005, measured by one-way ANOVA with Tukey post-hoc correction.*

D

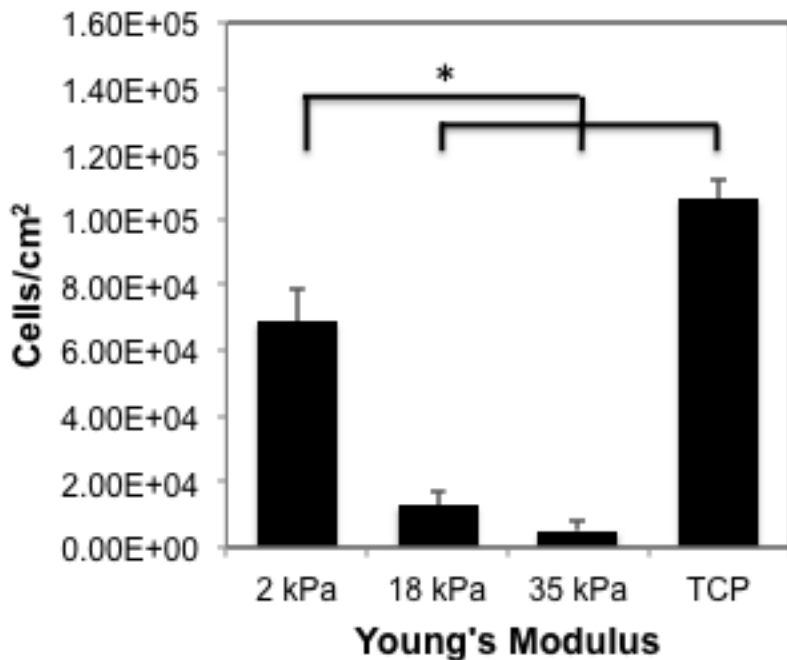


Figure 5.1(D) Analysis of cell concentration from phase contrast images of mouse embryonic stem cells attached for 24h onto 3 different GXG materials and TCP. Cell concentration at 24h decreased with GXG Young's modulus. Values shows are mean from three cell counts. Error bars present standard deviation from the mean. * represents a p-value less than 0.05 following one-way ANOVA analysis with Tukey post-hoc correction for multiple comparisons.

5.2.2 Does Young's modulus affect expansion of partially-differentiated cells in N2B27 medium?

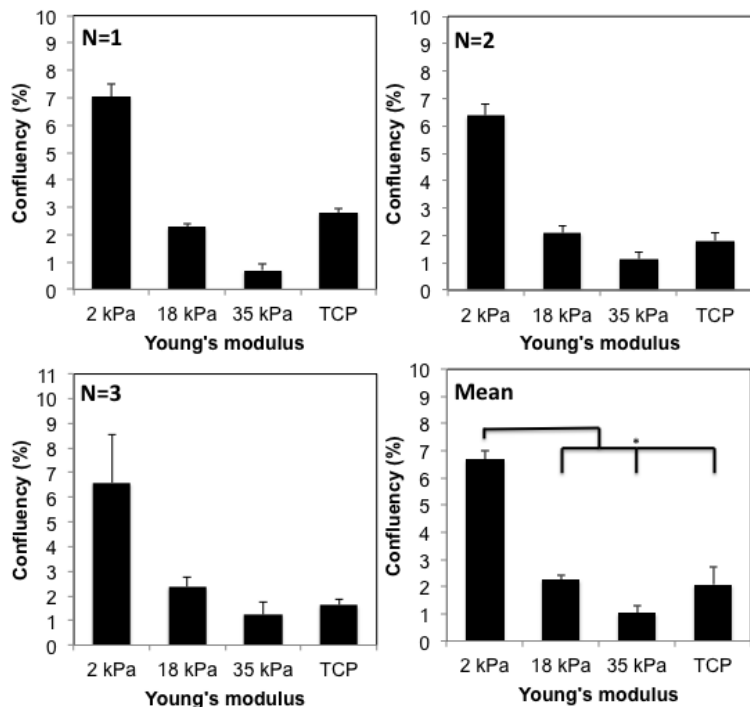
When partially-differentiated cells were allowed to expand after attaching, an identical trend emerged at the 72h time-point post-seeding (Figure 5.2A). Confluence decreased 66% on the 18 kPa material and 85% on the 35 kPa material. However, fold expansion did not vary significantly ($p=0.874$) between any of the four materials (Figure 5.2B).

A variety of effects have been previously recorded in response to changes in Young's modulus. Saha et al (2008) showed, similarly to this study, that there was no variation in adult rat hippocampal neural stem cell proliferation with Young's modulus for all moduli above 1 kPa. In another study using adult rat hippocampal neural stem cells (Banerjee et al, 2009), proliferation increased on softer materials (2 kPa) compared to stiffer materials (20 kPa).

In the Banerjee study, cells were cultured encapsulated within alginate hydrogels in maintenance medium. Another study using adult neural stem cells (Leipzig & Shoichet, 2009) showed a similar finding, where proliferation increased on 3 kPa materials compared to 7 kPa. Interestingly, proliferation then proceeded to decrease below 1 kPa, indicating that a narrow range of modulus is required for optimal proliferation of neural stem cells. When purer cultures of neuronal precursor cells, derived from primary embryonic rat spinal cord (Previtera et al, 2013) were plated onto polyacrylamide gels, proliferation (measured three days after seeding) decreased as Young's modulus increased from 6 kPa to 27 kPa. Proliferation did however remain unchanged within that range of elasticity at day five and day ten.

It was concluded that Young's modulus had no effect on expansion of partially-differentiated cells in this study. The higher confluence on soft materials at the 72h time-point was due to favourable initial attachment, not due to increased proliferation. Fold expansion was lower here than in the first chapter, where mESC's were used. This was likely due to the decreased proliferative capacity of the more differentiated cells used in this chapter.

A



B

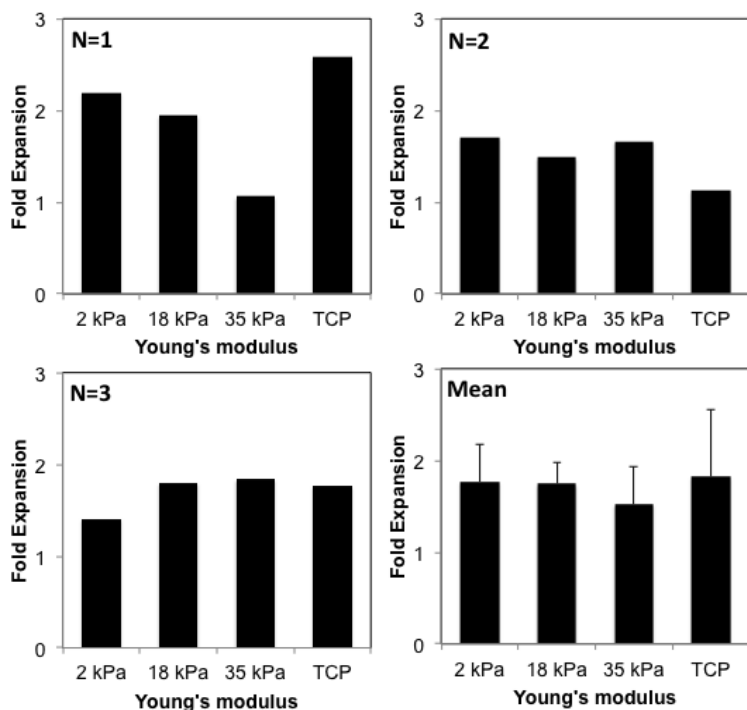


*Figure 5.2(A): Analysis of cell confluency from phase contrast images of partially-differentiated cells attached for 72h onto three GXG materials (2 kPa, 18 kPa and 35 kPa) and TCP. * represents a p-value less than 0.005 using ANOVA. Figure 5.2(B): Fold expansion in colony size between 24h and 72h (72h confluency divided by 24h confluency).*

5.3 Does Young's modulus affect the initial rate of spreading of partially-differentiated cells?

Rate of spreading measurement allowed for identification of whether the higher confluence on soft materials was exclusively dependent on initial attachment of partially-differentiated cells. To investigate rate of spreading, partially-differentiated cells were seeded onto three GXG materials and TCP after being incubated for 30 minutes in CellTracker, a membrane-specific dye that allowed for easy identification of the cell perimeter. Measurements of projected cell surface area were made at two, four and six hours after seeding.

As Figure 5.3 shows, there was no difference in rate of spreading (increase in projection area) amongst the GXG materials. There was a 36.5% increase in projected area on TCP, but overall mean cell surface area was the same across all materials at the 6h time-point. Soft materials did not increase rate of spreading.

In an earlier study (Georges et al, 2006), mixtures of cortical neurons were plated onto varying Young's moduli. In that study, cellular projected area at 24 hours was significantly higher on stiff materials (9 kPa) compared to the soft materials (100 Pa). This contradicted our findings at 6 hours, where projection area did not vary with modulus. The mean projected areas of cells in this study (500 to $700 \mu\text{m}^2$) were lower on every GXG material compared to the $2000 \mu\text{m}^2$ measured in that study (Georges et al, 2005) for a similar Young's modulus range. This likely reflects the differences in source material. Cortical neurons are considerably more mature and larger in surface area (when taking into account their long, branched neurites) than the day four neuronal precursors in this study.

In other studies using other cell types such as fibroblasts (Pelham & Wang, 1995); C2C12 skeletal myoblasts; FC7 fibroblasts (Engler et al, 2004b); and endothelial cells (Yeung et al, 2005), projected areas (defined as spreading) were also higher on stiffer materials.

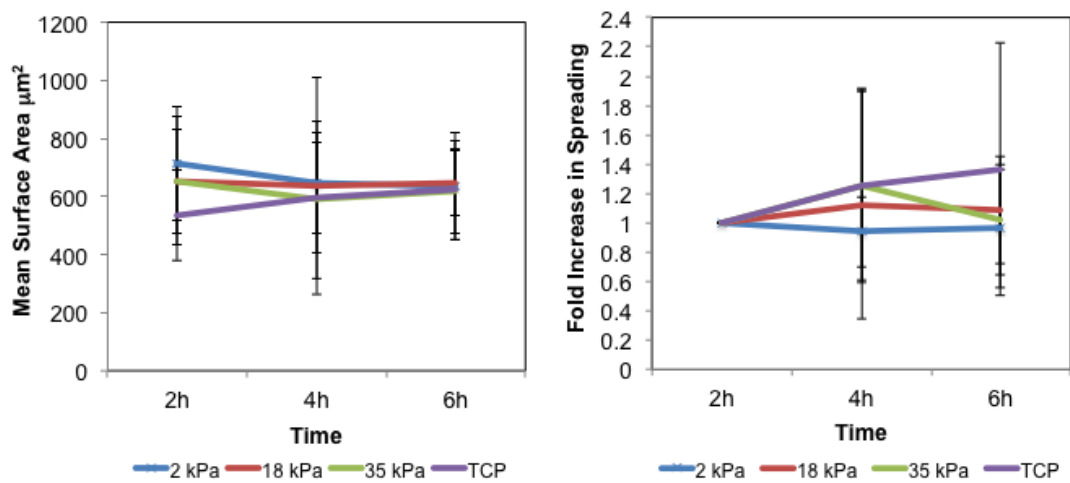


Figure 5.3: Rate of spreading for partially-differentiated cells over the first six hours of attachment on three GXG materials (2 kPa, 18 kPa and 35 kPa) and TCP in neuronal differentiation medium. The figure on the left shows the mean surface area of cells. The figure on the right shows cell surface area normalized against the initial value at $t=2\text{h}$. Error bars represent standard deviation from the mean, based upon three technical triplicates (from three independent GXG wells for each condition based). $N=15$ randomly selected cells.

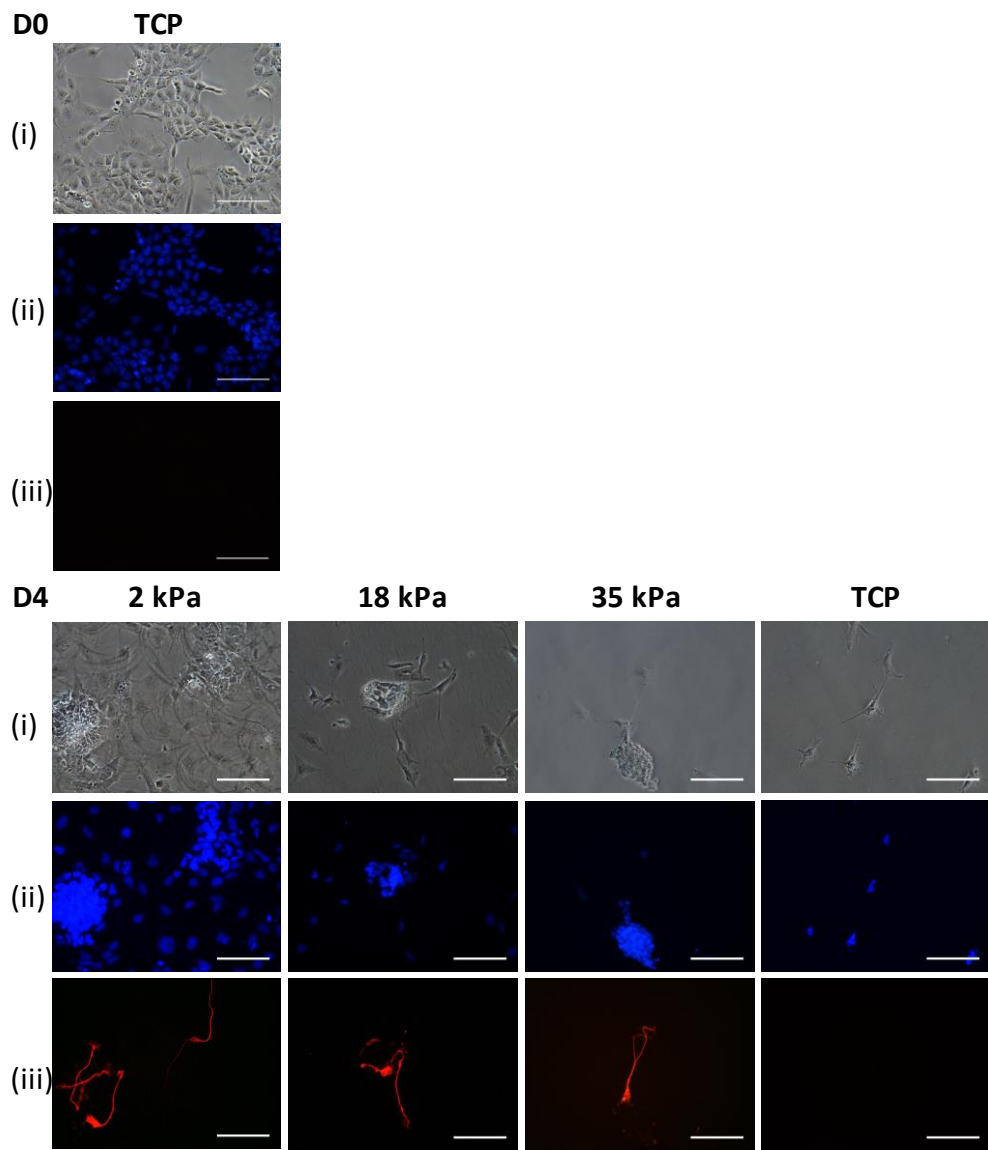


Figure 5.4: Immunocytochemistry (ICC) analysis for immature neuronal marker β -III tubulin for partially-differentiated cells differentiated for four days in N2B27 medium on three GXG materials (2 kPa, 18 kPa and 35 kPa) and TCP. D0 represents cells on TCP at day four of mESC neuronal differentiation (partially-differentiated cells). These cells were then differentiated for four days before being stained to reveal the presence of neurons. (i) Phase contrast. (ii) DAPI, a nuclear stain. (iii) ICC for β -III tubulin. All scale bars = 100 μ m.

5.4 Does Young's modulus affect the phenotype of cells formed after four days of neuronal precursor differentiation in N2B27 medium?

5.4.1 Does Young's modulus affect the formation of immature neurons from partially-differentiated cells in N2B27 medium?

Partially-differentiated cells were allowed to further differentiate for four days on GXG and TCP in neuronal differentiation medium. At this stage, immunocytochemistry was performed for β -III tubulin, a marker for immature neurons (Ying et al, 2003).

This marker was used, as it is typically the earliest neuronal subtype to appear during differentiation (Chapter 3). At day four, β -III tubulin appeared in colonies on all three GXG materials (Figure 5.4). Furthermore, unlike in Chapter 4, cells containing β -III tubulin extended neurites out from the colonies on all four materials. In Chapter 4, neurites only extended out from colonies on the 2 kPa material. Young's modulus therefore has no effect on the formation of immature neurons from partially-differentiated cells.

This trend was consistent with the findings of other studies (with a similar Young's modulus ranges) that used β -III tubulin immunocytochemistry analysis on neural stem cells in neuronal differentiation medium (Saha et al, 2008; Banerjee et al, 2009). A similar result was also shown in another study using MAP2, a more mature neuronal marker (Previtera et al, 2010). There were other studies, which provided contradictory findings both to this study as well as when compared to each other. For example, more β -III tubulin positive cells were shown to be present on lower moduli (Georges et al, 2006) in an earlier study, whilst more have been found on higher moduli (Previtera et al, 2013; Kothapalli & Kamm, 2013) in two recent studies. These discrepancies reflect variations in source material (embryonic, adult, spinal cord or brain) as well as differentiation length and conditions. There is a limited basis for comparison between biomaterials and TCP. The study by Saha et al (2008) did find that the proportion of

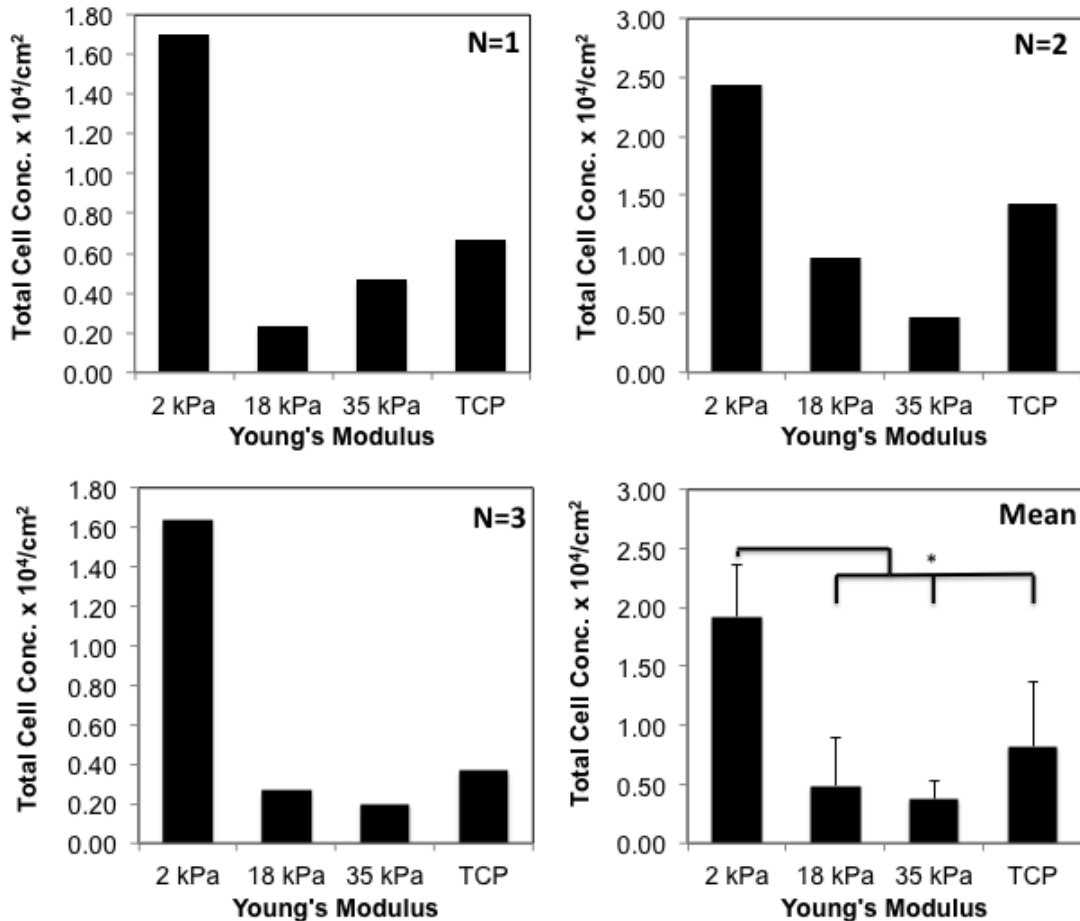


Figure 5.5: Total cell concentration after partially-differentiated cells were differentiated for a further four days in N2B27 neuronal differentiation medium on three GXG materials and TCP. All three biological replicates shown, as well as the mean. Error bars represent standard deviation from the mean. N=3. * represents a p-value less than 0.05 using one-way ANOVA with Tukey post-hoc correction.

total cells that were β -III tubulin positive was significantly higher on biomaterials compared to TCP, which was consistent with our findings.

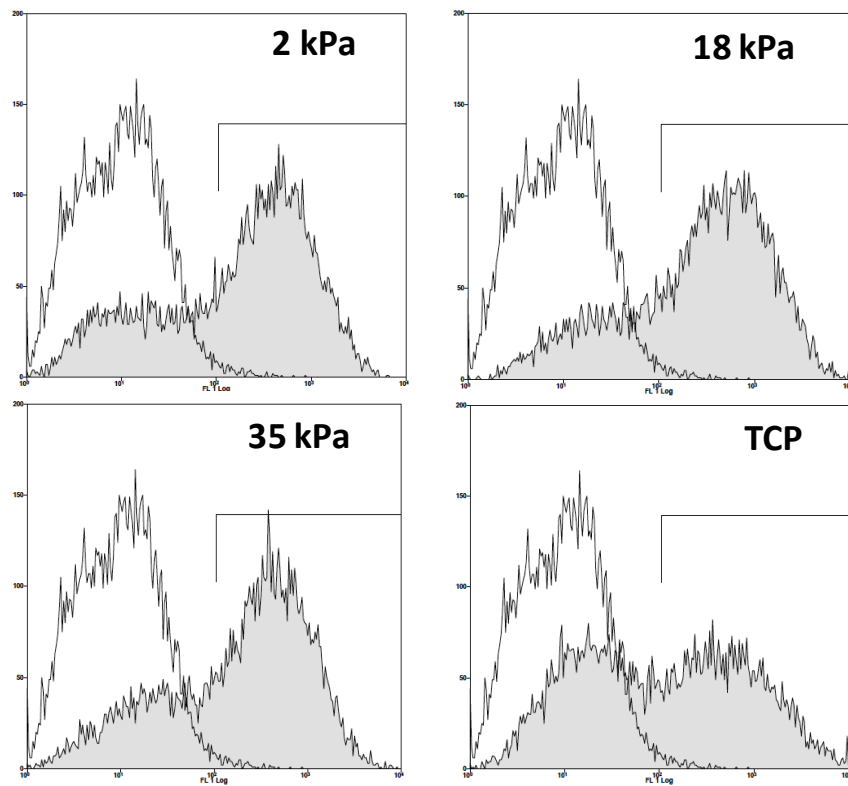
5.4.2 Does Young's modulus affect yield of PSA-NCAM positive cells following differentiation in N2B27 medium?

A similar trend was emerging in partially-differentiated cells as with the mESC's in Chapter 4, where neuronal differentiation was not being directly promoted on soft materials. In order to test this hypothesis further, flow cytometry was again performed for PSA-NCAM. In order to isolate whether any increases in neuronal yield from partially-differentiated cells on soft materials were solely due to the favourable initial attachment and not due to a direct promotion of the neuronal fate, the flow cytometry findings were compared to the total cell concentration at harvest.

To achieve this, cell counts (Figure 5.5) were performed at day four in order to assess the total cell concentration (normalized against culture surface area) on each GXG material and TCP. Total cell concentration was maximized on the softest material, reducing by 75-80% on the stiffer GXG materials and almost 60% on the tissue culture polystyrene. This finding was in agreement with the results of Figure 5.1 and 5.2, where confluence analysis at 24h and 72h revealed the same patterns.

As with the mESC's in Chapter 4, there was no significant ($p=0.583$) variation in percentage of cells positive for PSA-NCAM (Figure 5.6A). The percentage varied from 60-75% across all four materials. In the case of all three GXG materials, the percentage of cells positive for PSA-NCAM was significantly higher ($p<0.05$) than the value at day four of mESC differentiation on TCP (32%). The value for partially-differentiated cells on TCP after four days was also higher, but not significantly so ($p=0.056$). This is evidence that neuronal differentiation was occurring on all materials.

A



Young's Modulus	% PSA-NCAM
2 kPa	69.73 ± 7.56
18 kPa	70.53 ± 7.13
35 kPa	73.15 ± 7.73
TCP	62.75 ± 13.23

B

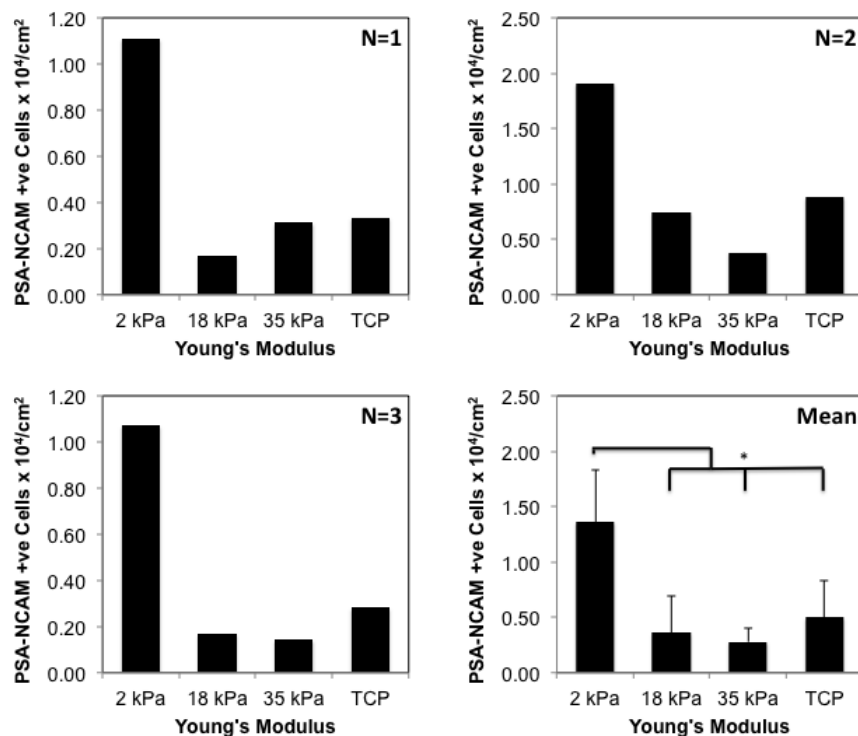


*Figure 5.6 (A): Flow cytometry analysis showing percentage of cells positive for PSA-NCAM in Partially-differentiated cells were differentiated for a further four days in N2B27 medium on GXG and TCP. White area = isotype control. Shaded area = Stained sample. The values given in the table are the means ± standard deviations derived from biological triplicates. (B) Yield of PSA-NCAM positive cells at day four. Values are the product of total cell concentration at day four (Figure 5) and percentage of cells positive for PSA-NCAM at day four. All three biological replicates shown as well as the mean. Error bars represent standard deviation from the mean based on the three replicates (N=3). * represents a p-value less than 0.05 based on one-way ANOVA analysis followed by Tukey post-hoc correction.*

Interestingly, the rate of change in percentage of cells positive for PSA-NCAM was higher for partially-differentiated cells differentiating for four days on GXG than for mESC's differentiating for four days on TCP. The rates of change were similar for both cell types on GXG. The rate of increase did not vary on the TCP throughout the eight days of differentiation. This suggests the GXG increases the rate of neuron formation compared to TCP without directly promoting the neuronal fate.

When the product of the total cell concentration and the percentage of cells positive for PSA-NCAM was calculated, the resulting yield of PSA-NCAM positive cells following differentiation varied with Young's modulus according to a similar pattern to that observed in Figure 5 (Figure 5.6B). PSA-NCAM positive yield was maximized upon the softest GXG material (2 kPa). The percentage decreased significantly ($p<0.05$) upon the other materials, falling by 74% on the 18 kPa material, 80% on the 35 kPa material and 63% on the TCP.

Despite the yield of neural precursors being maximized on the soft material, the percentage of cells positive for the marker did not vary. Therefore, this effect is due to favourable initial attachment over the first 24 hours and not due to a direct promotion of the neuronal fate.

5.4.3 Does Young's modulus influence mature neuronal gene expression in partially-differentiated cells after four days of differentiation in N2B27 medium?

The final test for the hypothesis that soft substrates do not directly promote the neuronal fate involved looking at the effect of Young's modulus on gene expression in cells following differentiation. Changes in phenotype, as measured by changes in cell surface antigen presence do not tell the complete story. Real time qPCR allowed for quantification of changes in key neuronal marker expression at a cellular level. In addition to β -III tubulin, three mature genes were investigated: 1) GFAP (glial fibrillary acidic protein), a gene expressed in astrocytes, which are non-neuronal glial cells that play a number of supportive roles to neuronal growth; 2) TH (tyrosine hydroxylase), a gene expressed in dopaminergic neurons, a neuronal subtype whose

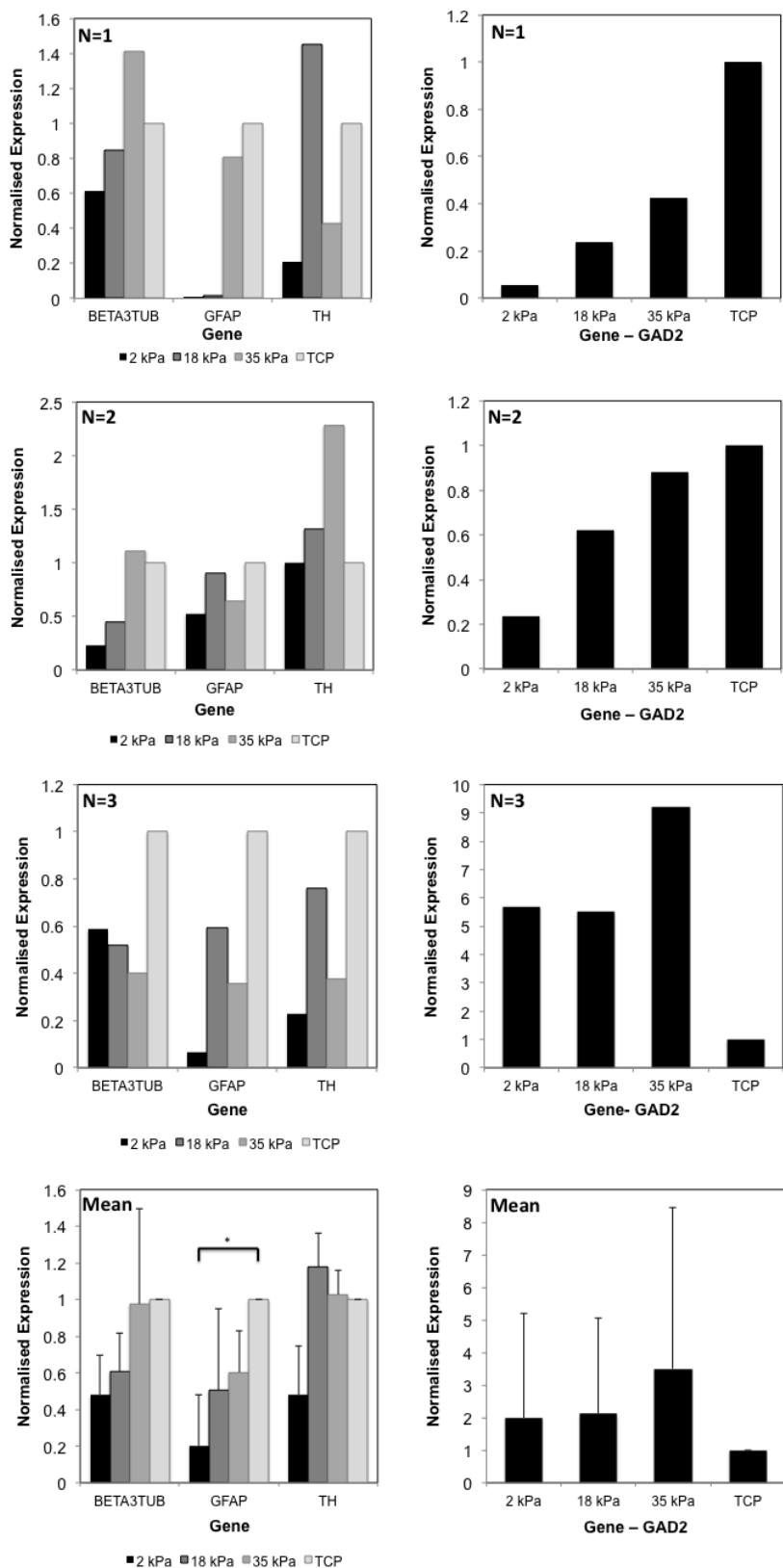


*Figure 5.7: Expression of three mature neuronal genes and one astrocytic gene (GFAP) with varying Young's modulus for cells differentiated for a total of eight days (4 days on TCP, 4 days on GXG and TCP). All three biological replicates shown as well as the mean. Error bars represent standard deviation from the mean. * represents a p-value less than 0.05 for one-way ANOVA analysis with Tukey correction.*

death is associated with the development of Parkinson's disease; and 3) GAD2 (glutamate decarboxylase 2), a gene expressed by GABAergic neurons, a subtype responsible for production of the neurotransmitter GABA (γ -aminobutyric acid).

As shown in Figure 5.7, gene expression did not vary significantly ($p>0.05$ in all cases) with Young's modulus for any of the mature neuronal genes. Previous investigations into seeding neuronal cultures onto varying substrate moduli have yielded varying results for gene expression measurements. Neuronal differentiation has mostly been characterised by expression of β -III tubulin, which is one of the genes used in this study as well. In most cases, β -III tubulin expression has been observed to decrease with Young's modulus. Georges et al (2006), for example, found that β -III tubulin expression in mixed cortical neuronal cultures was significantly higher on soft (100 Pa) materials compared to stiffer (9 kPa) materials, on both polyacrylamide gels as well as fibrin-based gels. The cortical neurons were cultured in similar medium components to our study (DMEM:F12 and neurobasal medium), however without the direct neuronal promoting agents (N2 and B27) as they were investigating growth rather than differentiation.

Saha et al (2008) exhibited a similar result when adult neural stem cells were seeded onto vMIPN's (a synthetic hydrogel). In that study, β -III tubulin expression peaked at 500 Pa to 1 kPa before decreasing on 10 kPa materials. However, expression reduced from 500 Pa to 100 Pa, contrary to the earlier finding by Georges et al (2006). Mixed cortical neurons and neural stem cells, consisting of either primary cultures or their immediate derivatives, are not directly comparable as starting materials for differentiation and growth as they may vary in neuronal subtype and levels of maturity.

Although the partially-differentiated cells of this study are also likely to be heterogeneous, with a mixture of embryonic stem cells, neuronal precursors as well as small amounts of other lineages (see Morphology B in Chapter 4), they are not derived from primary cultures. Furthermore, they have been previously adapted to culture (for

up to 90 passages) on tissue culture polystyrene before the experiments have begun. A study by Banerjee et al (2009) using neural stem cells did, however, show agreement with our study. In that study β -III tubulin expression did not vary between 2 kPa and 20 kPa. This was contrary to the findings of Saha et al (2008), which also used neural stem cells.

When hESC's and iPSC's were differentiated in three-dimensional cultures for nine days (Keung et al, 2012), β -III tubulin expression also, similarly to Georges et al (2006), increased at 100 Pa compared to 700 Pa, 75 kPa and TCP. Further differentiation (19 days) into mature cell types revealed the same trend using image analysis (not directly comparable with gene expression) for tyrosine hydroxylase (TH). However, the percentage of TH-positive cells compared to total neurons did not vary with modulus, which is in broad agreement with the findings of this study using qPCR.

Interestingly, astrocytic gene expression (measured by GFAP expression) did show a trend towards reduced expression as Young's modulus decreased ($p=0.054$). Whilst overall there was no significant difference in expression, Tukey post-hoc correction did reveal a significant ($p=0.035$) decrease in GFAP expression on the soft, 2 kPa GXG material, when compared to TCP. There is evidence from previous work that supports this finding. Saha et al (2008) found that when adult neural stem cells were differentiated in mixed neuronal-glial medium (not directly comparable to the N2B27 medium used in our study), the percentage of total cells existing as astrocytes (positive for the GFAP marker when image analysis was performed), increased with Young's modulus from 1 kPa to TCP. Similarly to our own study, this percentage did not vary from 1 kPa to 10 kPa.

When primary rat spinal cord cells were plated (Jiang et al, 2007) onto varying moduli (in Neurobasal:B27 differentiation medium, similar to this study), whilst numbers of mature, MAP2-positive neurons did not vary with modulus, the percentage of cells that were mature astrocytes (GFAP positive) increased with Young's modulus. Taking this evidence into consideration, it appears that whilst soft materials did not enrich specific neuronal subtypes (GABAergic or dopaminergic, for example) over

others, the stiffest materials increased enrichment of non-neuronal astrocyte cells. So the increased neuronal yield on softer materials is accompanied by antagonism of the astrocytic fate. The reason for this may lie in the dynamics of the internal cell structure. Georges et al (2006) found that astrocytes are only able to polymerise actin stress fibers on stiffer materials. Astrocytes cannot form stress fibers on softer materials, and thus cannot adhere. This is the reason why following spinal cord injury, stiffening due to fibrosis leads to astrocyte hypertrophy and glial scarring at the expense of neuronal outgrowth, which becomes severely limited (partially due to reduced growth factor and nutrient access). Astrocyte adhesion was observed to increase with modulus increase in the Georges et al (2006) study. Neurons were able to polymerise F-actin on both soft and stiff materials. Following attachment on GXG, cells that specified into neurons were able to remain adhered and grow on both soft and stiff materials. Astrocytes, unable to form stress fibers on soft materials, were not able to form on these substrates in that study.

A study of the effect of 3D hydrogel Young's modulus on mouse EB neuronal differentiation (Kothapalli & Kamm, 2013) in Matrigel, collagen and hyaluronic acid found that neuronal differentiation was maximized on "stiffer" gels (900 Pa to 1 kPa), whilst astrocyte differentiation was favoured softer gels (5-20 Pa). The modulus ranges were significantly different from that used within this study (and the majority of other studies). It was also unclear as to how stable the 5-20 Pa gels were in terms of degradation. Furthermore, whilst this trend was conserved on all three materials there seemed to be some discrepancy in these results between materials. For example, the 90 Pa hyaluronic acid substrate had a higher percentage of cells differentiating towards a neuronal fate and a considerably lower percentage towards the astrocytic fate when compared to the 320 Pa collagen-I substrate.

Although expression of GFAP was reduced on soft GXG materials in this study, there was overall no increase in neuronal gene expression on soft materials. Therefore the increased neuronal yield on the 2 kPa GXG material was due to increased initial attachment on the physiologically soft Young's modulus, not due to a direct promotion of the neuronal fate. Once it was established that attachment was the cause of the

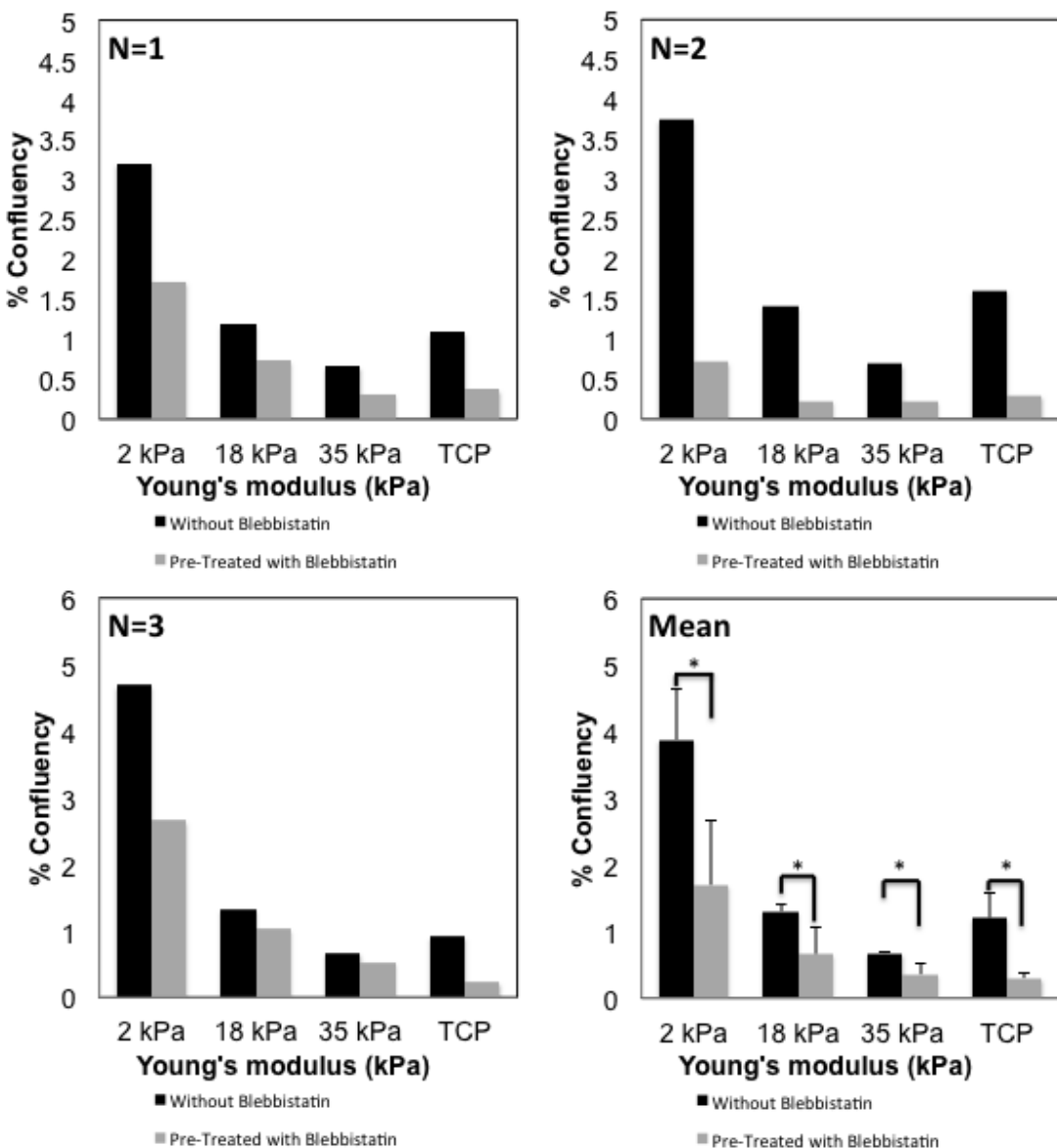
increased neural precursor formation at day four, an attempt was made to establish a mechanism for this effect.

5.5 Is the attachment of partially-differentiated cells influenced by inhibition of stress fiber stabilization or microtubule formation?

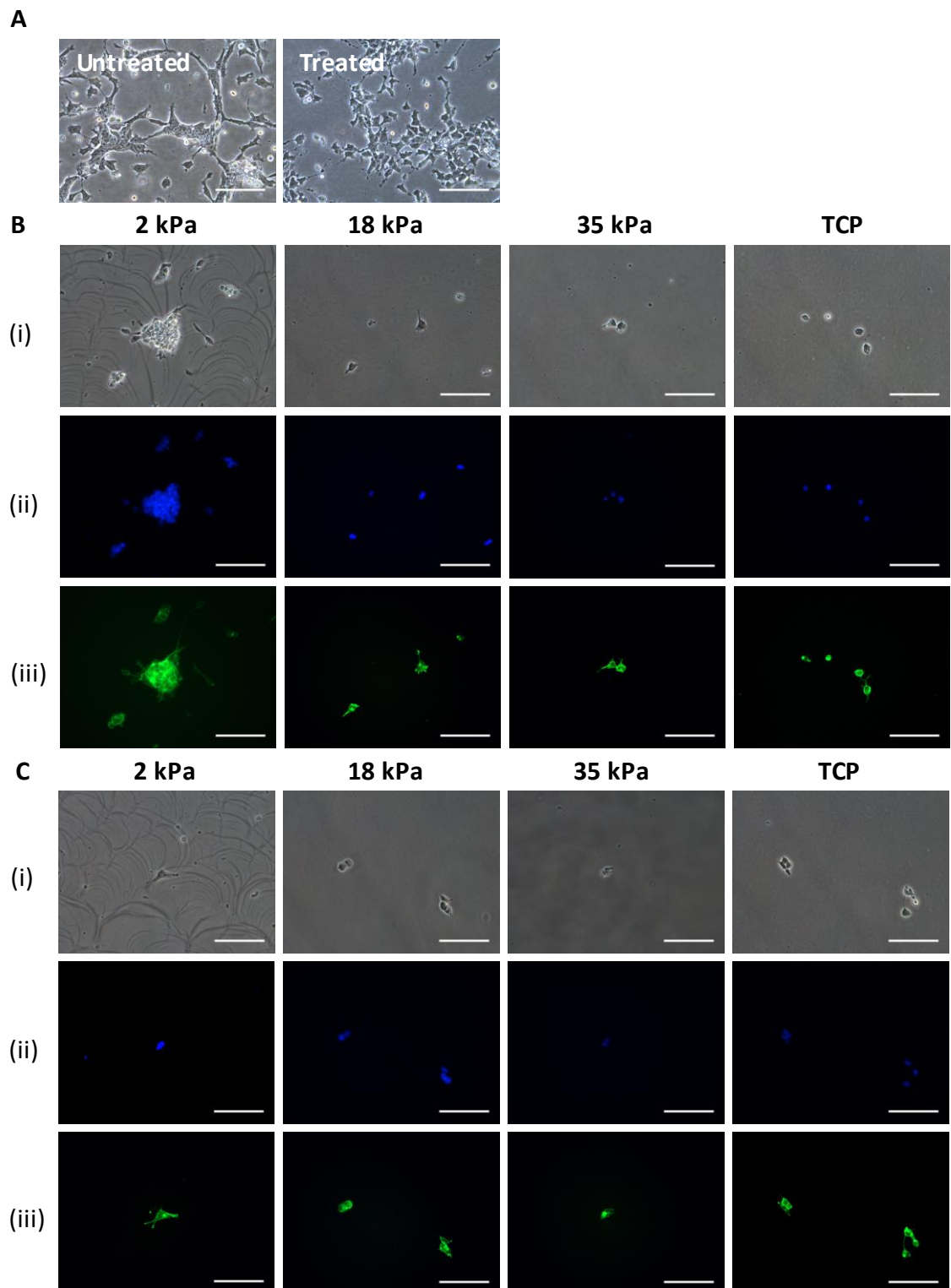
5.5.1 Is the improved attachment of partially-differentiated cells on soft materials related to F-actin stress fiber polymerization?

In order to understand whether the attachment on GXG was influenced by stress fiber polymerization or microtubule formation, the effects of each had to be isolated using small molecule inhibitors. As with Chapter 4, two inhibitors (Blebbistatin and Nocodazole) were used in order to establish a mechanism for the effect of Young's modulus upon partially-differentiated cell attachment. F-actin and α -tubulin were identified as the two most influential internal protein components of the cellular cytoskeleton, responsible for exerting forces on the extracellular matrix. By inhibiting these two proteins from polymerizing, it was possible to isolate which of the two, if any, would prevent Young's modulus from influencing attachment.

Blebbistatin inhibits the action of myosin IIb, a protein involved in F-actin polymerisation and cytoskeleton contraction. Partially-differentiated cells were treated for 30 minutes with the small molecule before harvesting and seeding onto GXG and TCP. Figure 5.9A shows that following blebbistatin pre treatment, cells became more compact and less spindle-shaped (extended) in their morphology. When attachment was studied at 24h, confluency decreased significantly ($p<0.05$) with blebbistatin pretreatment on all four materials, when compared to the untreated condition (Figure 5.8).



*Figure 5.8: Effect of blebbistatin pre-treatment on attachment of partially-differentiated cells on three GXG materials (2 kPa, 18 kPa, 35 kPa) and TCP in N2B27 medium. Confluency measurements were made at 24h for both untreated cells (see Figure 1B) and treated cells in neuronal differentiation medium. All three biological replicates and mean shown. Error bars represent standard deviation from the mean. * represents a p-value less than 0.05 using an independent t-test analysis between the untreated and the treated condition.*



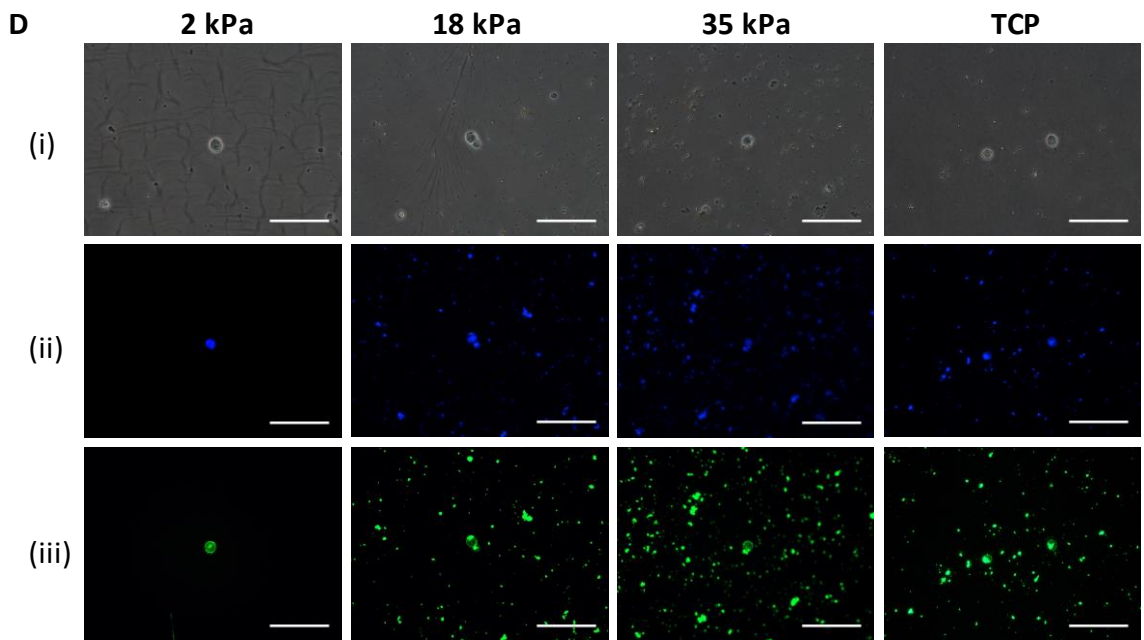


Figure 5.9: (A) Morphological changes (Post-blebbistatin represents 30 mins of treatment) accompanied by blebbistatin inhibition of stress fiber stabilization in mESC's partially-differentiated for four days.

Figure (B-D) Immunocytochemistry analysis using phalloidin, a dye which highlights F-actin. MESC's were partially-differentiated for four days before being seeded for 24h on three GXG materials and TCP in N2B27 medium. (B) Cells untreated with blebbistatin; C) Cells pre-treated for 30 mins with blebbistatin; D) Cells containing blebbistatin post-seeding. (i) Phase contrast. (ii) DAPI, a nuclear stain. (iii) ICC for F-actin. All scale bars = 100 μ m.

This implies that F-actin polymerisation influences the attachment of partially-differentiated cells on every material. Attachment decreases on all materials, as F-actin polymerises on both soft and stiff materials (Georges et al, 2006) in neuronal cells. However, there is no significant difference in attachment with Young's modulus with blebbistatin treatment. For this reason, the conclusion was made that stress fiber depolymerisation reduced the influence of Young's modulus on attachment.

To identify whether polymerised stress fibers existed within partially-differentiated cells on GXG and how they were influenced by blebbistatin, immunocytochemistry was performed using phalloidin, a fluorescent dye that specifically stains F-actin. As with undifferentiated cells, phalloidin appeared to mainly concentrate and polymerise at the periphery of the cells (Figure 9B), particularly in regions of the cell body that appeared to be spreading outwards to form neurite growth cones. This phenomenon was consistent with the findings of Georges et al (2006). In that study, it was also found that F-actin can polymerise on both soft and stiff materials. As seen in Figure 9, the appearance of actin in this study is comparably diffuse. Actin doesn't tend to form stress fibers in neurons (rather it tends to aggregate at points of extension), but the images in Georges et al (2006) do suggest a level of organization not observed in partially-differentiated cells. However, the partially-differentiated cells are not as mature as the cortical neurons used within that study, and thus may have cytoskeletal structures akin to that of mESC's rather than mature neurons.

Overall, these cytoskeletal structures were unaffected by blebbistatin pre-treatment. (Figure 9C). Actin remained concentrated at the periphery, driving the outwards spreading of the cells. However, continued blebbistatin treatment overnight (Figure 9D) did not allow for cells to spread. Instead, cells formed rounded structures with no actin accumulation in the cytoplasm. A significant amount of actin-rich cell debris was observed on stiffer materials, as the extended periods of blebbistatin inhibition likely caused substantial cell death.

5.4.2 Is the improved attachment of partially-differentiated cells on soft materials related to microtubule formation?

Nocodazole is an inhibitor of α -tubulin polymerization into microtubules. Following harvest, partially-differentiated cells were seeded on three GXG materials and TCP in neuronal differentiation medium containing nocodazole. As before, attachment was measured at 24h and compared to the untreated condition.

As shown in Figure 10, attachment did not vary significantly ($p>0.05$) with nocodazole treatment on any material. This was in contrast to our findings in Chapter 2 with mESC's, where attachment decreased on stiffer materials with nocodazole treatment. The formation of microtubules from α -tubulin had no effect upon the attachment of partially-differentiated cells upon any material, and by extension no effect upon the effect of Young's modulus upon attachment of partially-differentiated cells.

As with before, immunocytochemistry analysis was performed to look at whether α -tubulin formed polymerized microtubule structures in partially-differentiated cells, and how this was affected by nocodazole treatment. An antibody against α -tubulin was used in order to investigate the internal structural changes.

Partially-differentiated cells appeared to develop polymerized microtubule filaments from α -tubulin, on every material (most noticeably on the 2 kPa and 18 kPa GXG materials). α -tubulin was distributed fairly evenly throughout the cytoskeleton on all the materials, and did not accumulate significantly at the cell periphery as F-actin did in the same cells.

In response to nocodazole treatment, cells remained attached and were able to spread on all materials. Noticeably, the microtubule filaments did not form from α -tubulin, as

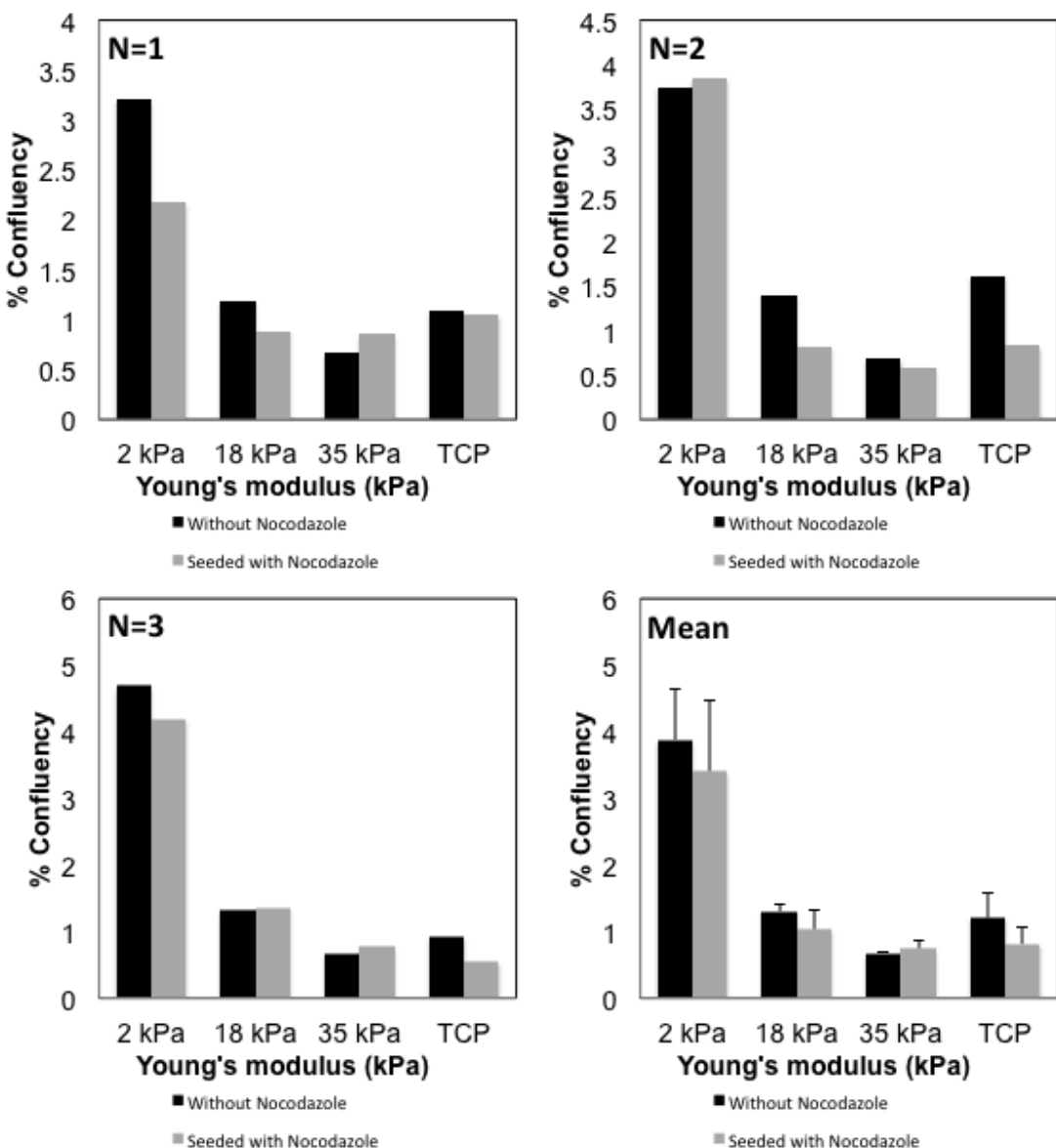


Figure 5.10: Effect of nocodazole on attachment of partially-differentiated cells at 24h on three GXG materials and TCP in neuronal differentiation medium. All three biological replicates and mean shown.

Error bars represent standard deviation from the mean.

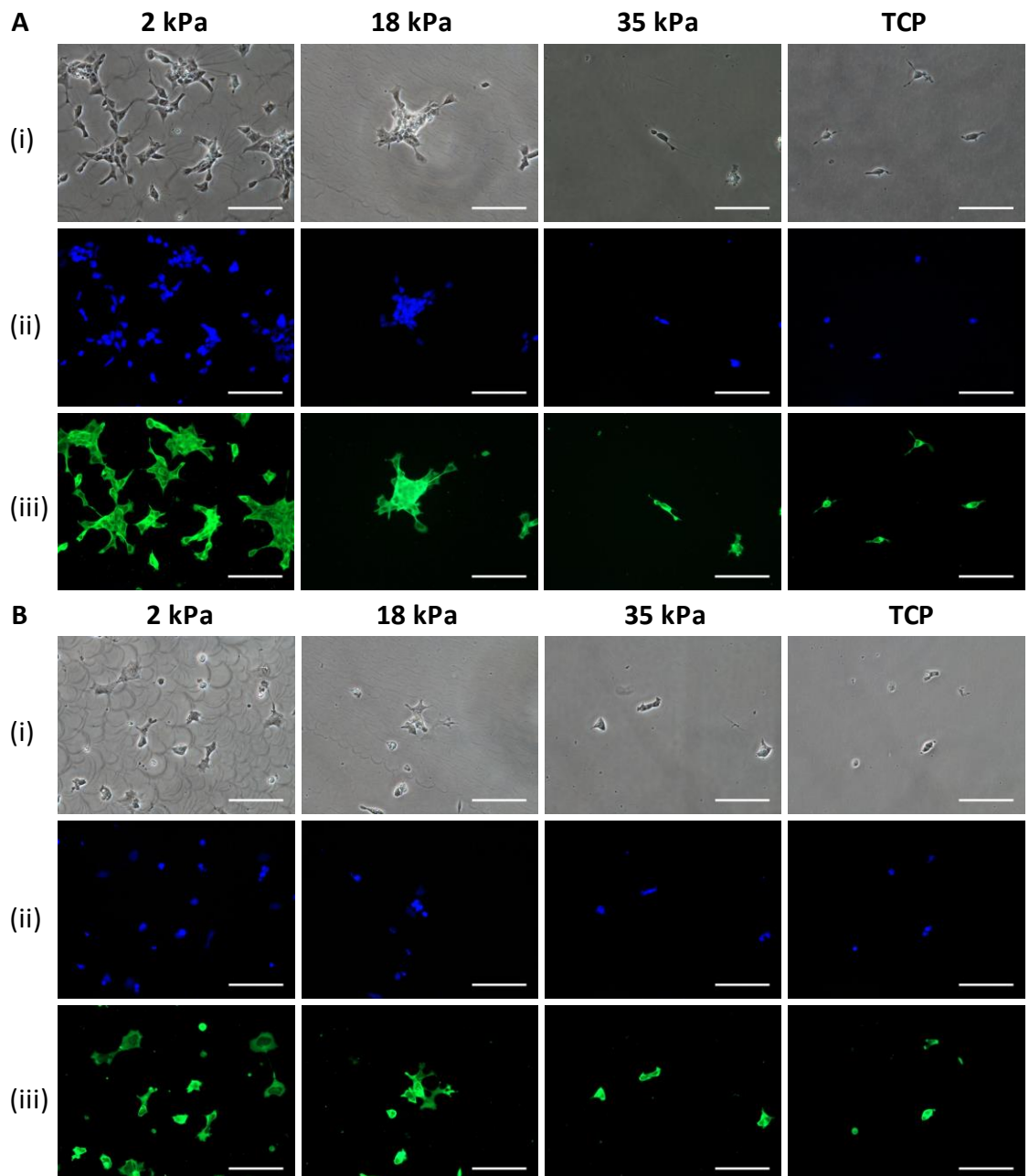


Figure 5.11: Immunocytochemistry analysis for α -tubulin in Partially-differentiated cells were seeded for 24h on three GXG materials and TCP in neuronal differentiation medium: A) without nocodazole, an inhibitor of microtubule formation; and B) containing nocodazole. (i) Phase contrast. (ii) DAPI, a nuclear stain. (c) ICC for α -tubulin. All scale bars = 100 μ m.

expected. This implies that partially-differentiated cell spreading following attachment is dependent on actin and not upon microtubule polymerisation in the cytoskeleton.

Tubulin is mostly associated with neuronal cells in the form of the β isoform (β -III in particular). However, the α subtype has been demonstrated to play an important role in a variety of mechanical processes in neuronal cells. Whilst microtubules do not directly influence gene expression, as they are not directly linked to the cell nuclear machinery (as the actin cytoskeleton is), they do respond to changes in Young's modulus in other ways. Spedden et al (2012)'s elasticity mapping of neuronal cells revealed that localized stiffening in neurons is dependent on microtubule formation (an effect which can be inhibited by nocodazole), and not on stress fiber polymerization.

When considered along with the data in Figure 10, this implies that neuronal cells do not have to stiffen in order to attach to stiffer GXG materials, unlike with undifferentiated cells (Chapter 2). Microtubules are also implicated in neurite extension, and are even able to take over in order to drive extension when actin polymerisation is inhibited (Georges et al, 2006).

Taken together, the data suggests that actin polymerisation plays the most important role in driving attachment of partially-differentiated cells on all GXG materials. Actin and α -tubulin then cooperate to drive neurite extension as the neuronal cells form their characteristic branched networks.

5.5 Does Young's modulus affect the attachment and expansion of partially-differentiated neurons maturing in N2B27 medium?

The final set of experiments looked at mESC's partially-differentiated further, to six days instead of four. Day six is where β -III tubulin, the immature neuronal marker begins to appear in colonies of nestin-positive differentiating cells (Chapter 1). The previous work looked at the effect of Young's modulus on mESC's differentiating into neural precursors (Chapter 4) and partially-differentiated neural precursors into

immature neurons (Chapter 5.2-5.4). The final stage was to investigate how Young's modulus affected the maturation of partially-differentiated neurons (days six to twelve of mESC neuronal differentiation in N2B27).

5.5.1 Does Young's modulus affect the attachment of partially-differentiated neurons maturing in N2B27 medium?

As with the mESC's and partially-differentiated cells, the effect of Young's modulus on attachment was isolated from the effect on expansion and phenotype changes. In order to investigate the effect of Young's modulus on attachment, mESC's were partially-differentiated for six days on TCP in N2B27 neuronal differentiation medium. These cells were then harvested and seeded onto three GXG materials (2 kPa, 18 kPa and 35 kPa) as well as TCP in N2B27 medium. Two seeding densities were chosen to investigate attachment and expansion. One was the same seeding density as for the mESC's (1×10^4 cells/cm 2) and the other was a direct replate of all cells from TCP. These low seeding density was chosen so that any effect of Young's modulus on attachment could be related to the findings in mESC's and four day partially-differentiated cells. The higher seeding density was chosen so that the Young's modulus effects could be overcome by using higher starting cell concentrations. Confluency was measured from phase contrast images of cells seeded for 24h in N2B27 medium .

As seen in Figure 5.12, the results for partially-differentiated neurons contrasted substantially with the results for mESC's and partially-differentiated cells. There was no significant difference in attachment between any of the materials, whether cells were replated (Figure 5.12B, p=0.511) or seeded at a lower density (Figure 5.12C, p=0.481). The pattern in attachment with Young's modulus was conserved, and thus this effect is independent of seeding density. There was some decrease in attachment on the 35 kPa compared to 2 kPa and 18 kPa, but this was not significant overall (p>0.05 in all cases). Young's modulus therefore had no effect upon attachment of partially-differentiated neurons.

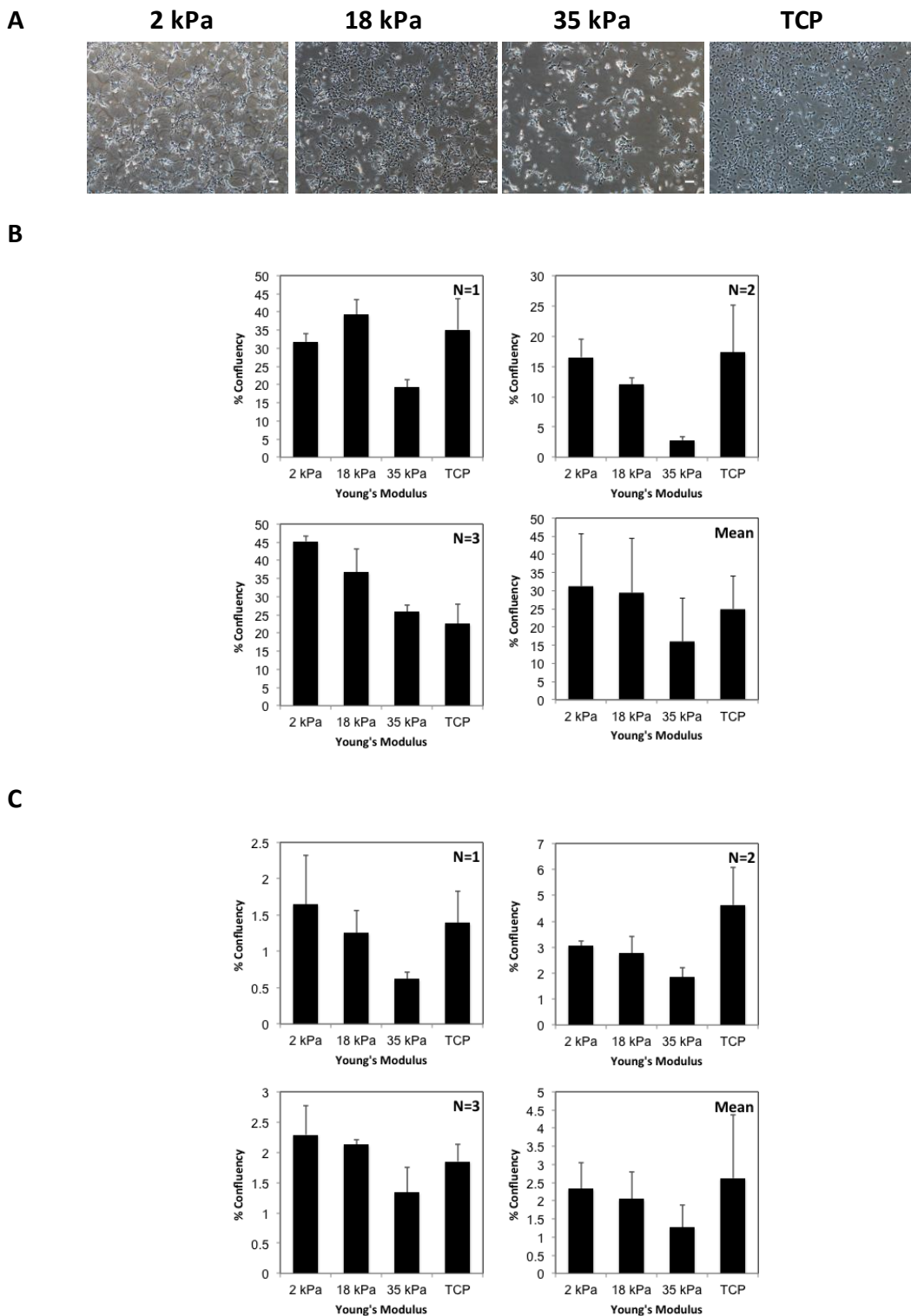


Figure 5.12: (A) Phase contrast images of partially-differentiated neurons directly replated onto 3 GXG materials (2, 18 and 35 kPa) and TCP. Images taken 24h after seeding. Scale bars = 100 μm . B-C) 24h for partially-differentiated neurons either (B) replated or (C) seeded at a density of 1×10^4 cells/cm 2 on three GXG materials and TCP. All three replicates and mean shown. Error bars represent standard deviation from the mean (from technical triplicates in N=1,2,3 and from biological replicates for the mean).

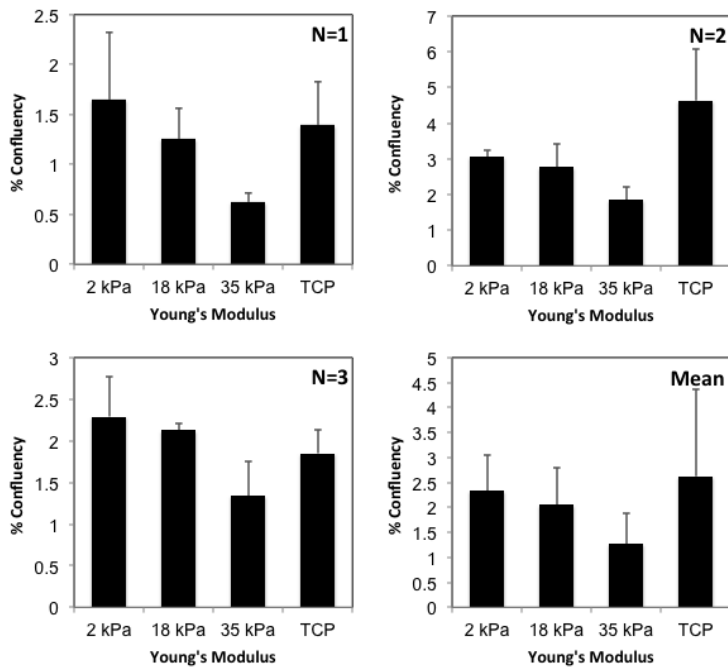
Morphology (Figure 5.12A) did not drastically vary on any of the GXG materials. The majority of cells on the GXG materials were morphology C (Chapter 4), the spread, spindle-like cells. This was expected, as cells are at a more advanced stage of maturity than in the previous chapter. The cells on the TCP material, however, were a mixture of cells of morphology C, and morphology B; the flattened, neuroepithelial-like cells observed in considerably smaller numbers at day four in Chapter 4. This suggests that, unlike the softer materials, TCP allowed for considerable numbers of morphology B cells (negative for nestin, amongst other neuronal markers) to attach, survive and grow.

Whilst this trend contrasts with the earlier work shown in Chapter 3,4 and this Chapter, it is consistent with the majority of earlier work involving neural precursors (Georges et al, 2006; Jiang et al, 2007; Previtera et al, 2010) and neural stem cells (Banerjee et al, 2009; Saha et al, 2008). This suggests that the starting cultures of neural precursors and neural stem cells in the other studies are more comparable to the six day matured partially-differentiated neurons than the nestin-positive partially-differentiated cells at day four. It was concluded that favourable attachment of cells on soft materials is maturity dependent, and that the effect reduces as cells reach more advanced stages of specification.

5.4.2: Does Young's modulus influence the expansion of partially-differentiated neurons undergoing maturing in N2B27 medium?

In order to investigate the effect of Young's modulus on expansion, the partially-differentiated neurons seeded at the lower density were allowed to expand to a time-point of 72h. We did not investigate the replated cells as they had already reached a high confluence at 24h. Confluency did not vary significantly ($p=0.541$) between any of the materials at 72h (Figure 5.13). As with the earlier findings in mESC's and partially-differentiated cells, fold-expansion did not vary significantly with Young's modulus ($p=0.808$). Based upon this evidence, it was concluded that maturity has no influence on the expansion of cells on any substrate modulus.

A



B

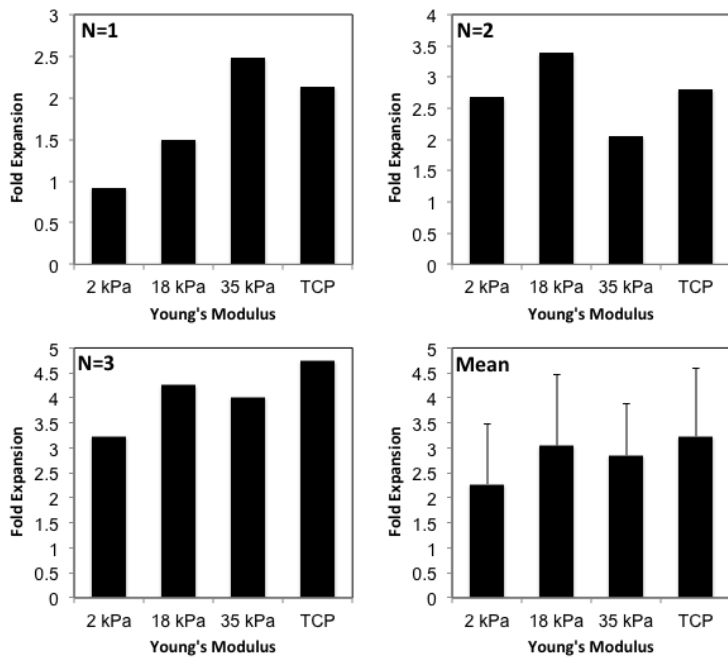


Figure 5.13: (A) 72h attachment of partially-differentiated neurons plated at a seeding density of 1x104 cells/cm² on three GXG materials (2, 18 and 35 kPa) and TCP. Figure 5.13(B) Fold expansion in colony size for partially-differentiated neurons in N2B27 medium (Confluence at 72h divided by confluence at 24h). All three replicates and mean shown. Error bars represent standard deviation from the mean.

5.5 Does Young's modulus affect the maturation of partially-differentiated neurons in N2B27 medium?

To test whether Young's modulus had an effect upon neuronal maturation, mESC's partially-differentiated for six days on TCP were directly replated onto GXG and TCP. These cells were then allowed to mature in N2B27 neuronal differentiation medium for six days. Immunocytochemistry was performed for β -III tubulin and microtubule-associated protein-2 (MAP2), a marker for mature neuronal cells.

β -III tubulin was found in cells on all three GXG materials on day six of maturation (Figure 5.14A). β -III tubulin-rich neurites were found most abundantly on the softest two GXG materials (2 kPa and 18 kPa) and not on the stiffest material (35 kPa). However, this was likely due to the increased cell concentration on these materials, as seen at 24h and 72h in Figures 5.12 and 5.13. Although confluency did not vary significantly across the replicates, within each replicate there was a trend towards decreased confluency on the stiffest, 35 kPa GXG material. This effect translated to a lower cell density at day six of maturation, which is likely to have affected the density of β -III tubulin positive cells in colonies. This is consistent with the findings in Chapter 4, where mESC's were differentiated for six days on GXG and TCP.

MAP2 was not found abundantly on any of the materials. The 2 kPa GXG material contained the most MAP2-positive cells. The 18 kPa GXG material contained less MAP2-positive cells, whilst the 35 kPa GXG material and TCP did not contain any of these cells (Figure 5.14B). The difference in MAP2-positive cells at day six between 2 kPa and 18 kPa existed despite there being no significant difference in confluency on these materials (Figure 5.12 and 5.13). This suggests that physiologically soft materials, with modulus closest to that of the brain and spinal cord (Engler et al, 2006; Flanagan et al, 2002) promote the formation of MAP2-positive neurons over stiffer materials.

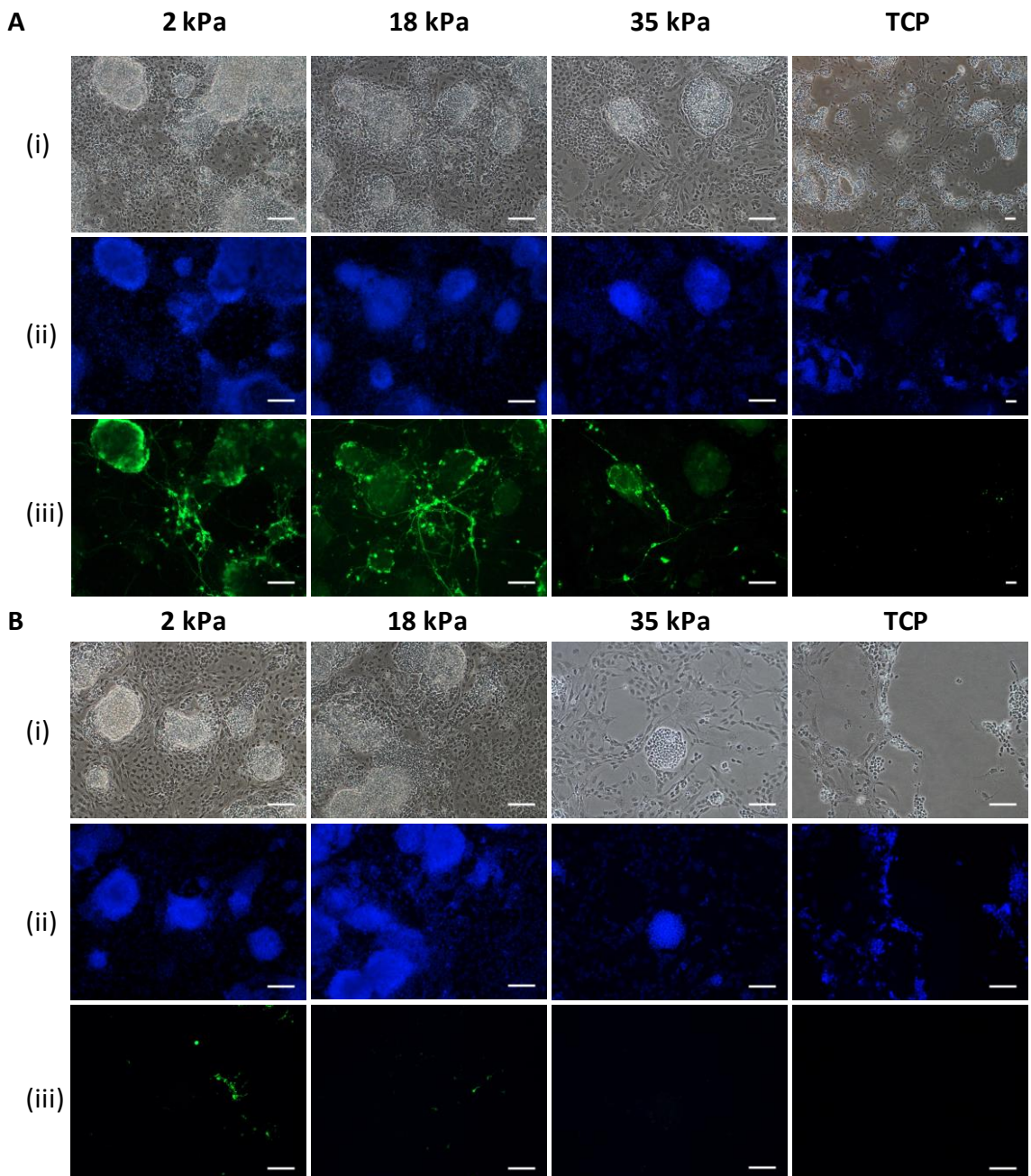
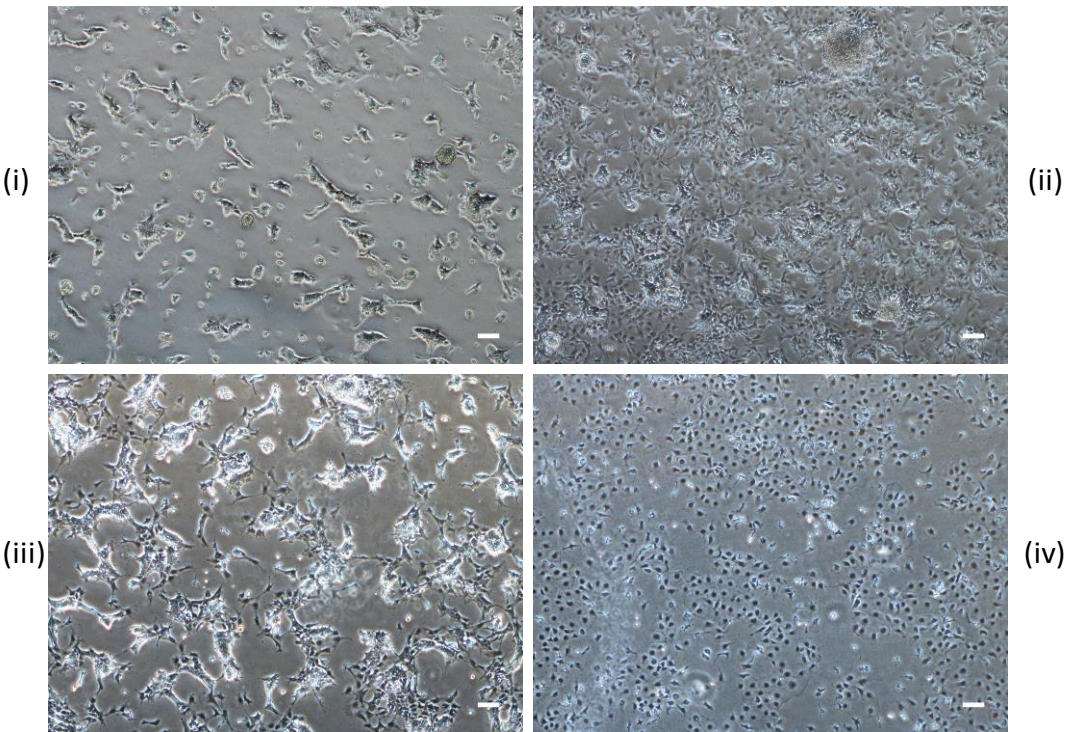


Figure 5.14: Immunocytochemistry analysis for: A) β -III tubulin and B) MAP2, a mature neuronal marker in Partially-differentiated neurons, seeded onto three GXG materials (2, 18 and 35 kPa) and TCP and allowed to mature for six days. (i) Phase contrast. (ii) DAPI, a nuclear stain. (iii) ICC for (A) β -III tubulin and (B) MAP2. All scale bars = 100 μ m.



(Optional) Figure 5.15: Phase contrast images revealing morphologies of cells partially-differentiated for six days on three GXG materials and TCP before being replated onto the corresponding GXG materials and TCP (for example six days on 2 kPa, harvested and plated onto 2 kPa for a further six days). (i) 2 kPa. (ii) 18 kPa. (iii) 35 kPa. (iv) TCP. Scale bars = 100 μm .

This result, whilst contrasting with the previous results (Figures 4.9A, 4.10, 5.6A and 5.7, where Young's modulus did not promote neuronal differentiation), is consistent with earlier work by Previtera et al (2013) using pure cultures of neural precursor cells where the percentage of cells which were MAP2 positive increased as modulus decreased from 27 kPa to 6 kPa. The soft modulus range is consistent with the measured ranges of Young's modulus for the brain and spinal cord (Flanagan et al, 2002).

There were negligible amounts of both β -III tubulin and MAP2 positive cells on TCP, (Figure 5.14). This result suggests, along with the comparison of morphology that TCP supports the attachment, survival and expansion of non-neuronal cell types.

It was concluded that, interestingly, the effect of Young's modulus on phenotype of cells formed following differentiation is dependent on cell maturity.

The final experiment performed was to assess whether the differences in morphologies of cells formed on the materials was due an adaptation or priming process that is undertaken on TCP. To test this, mESC's were differentiated for six days on three GXG materials and TCP, before harvesting them and seeding them onto their equivalent modulus material. As before, TCP resulted in a predominantly non-neuronal appearing morphology (the flat morphology B). 2 kPa resulted in a predominantly dense, rounded morphology of cells (the dense morphology A), whilst 18 kPa resulted in an even mixture of morphology B and the spread, spindle-like morphology C.

There is clearly a difference based upon adaptation that arises when cells are cultured for extended periods of time on varying Young's modulus. However, an explanation for why certain materials result in certain morphologies of cells forming is unclear, when considered against the literature. It would be expected, from the literature and from our own previous findings that cells of morphology C (spread) would be most abundantly found on the physiologically, soft material. This is a topic for potential future study.

6 Conclusions and Future Work

6.1 Conclusions

In Chapter 3, the optimal conditions for differentiation were determined. The decision was made to formulate the N2B27 medium with 1% v/v serum ‘in house’, instead of buying in the commercially available RHB-A. This was due to issues with variability in expansion and formation of neural precursors with the latter medium. Using 1% v/v serum was sufficiently enough serum to promote attachment, spreading and formation of neuronal precursor colonies, whilst not directly affecting the homogeneity of cells formed during differentiation.

The mESC’s were characterised as being pluripotent using immunocytochemistry analysis for key pluripotent markers as well as flow cytometry for PSA-NCAM, a neuronal adhesion markers (used as a negative control). MESC’s were found to be positive for OCT4, UTF1 and Ki67, whilst being negative for REX1 (which is a pluripotency marker, but downregulated when OCT4 is highly expressed). When flow cytometry was performed for PSA-NCAM, only 4.67% of cells were found to be positive for the neural precursor marker.

Neuronal differentiation was validated with a time-lapse study using a number of neuronal and astroglial markers. Based on immunocytochemistry analysis, nestin was chosen to identify formation of neural precursors (at day four) and β -III tubulin was chosen to identify formation of immature neurons (at day six).

For later qPCR studies, GADPH and TBP1 were chosen as the internal control genes due to their stability in mESC’s as well as differentiated cells across all four GXG materials, over three independent passage numbers.

When mouse fibroblasts were seeded on GXG, there was no significant difference in initial attachment with Young’s modulus. Human EB’s, when seeded on GXG in retinal

differentiation conditions, formed larger colonies on the 2 kPa and 18 kPa. However, presence of nestin-positive neural precursors was equal across all three materials, suggesting that the proportion of cells that were neural precursors was highest on the stiffest material.

MESC's were seeded on three GXG materials and TCP in pluripotent medium (GMEM+LIF) as well as spontaneous differentiation medium (GMEM-LIF). In pluripotent medium, attachment decreased significantly ($p<0.05$) with an increase in GXG Young's modulus. In spontaneous differentiation medium, attachment did not significantly vary with GXG Young's modulus ($p>0.05$), implying that the increased attachment on soft materials is dependent on seeding medium. Expansion did not vary with Young's modulus in either media.

When compared together, this shows that whilst mESC attachment increases with on soft materials, attachment in mature cells does not vary with Young's modulus. This implies that the effect of Young's modulus on attachment varies as cells differentiate and mature.

The main hypothesis of this study was that soft materials favour the formation of neurons from mESC's over stiff materials in neuronal differentiation medium. Based on the findings in Chapter 3, the effect of Young's modulus on attachment of mESC's forming into neural precursors (early differentiation) was investigated in Chapter 4. Chapter 5 then looked at the effect of Young's modulus on attachment and maturation of partially-differentiated cells and neurons (late differentiation). The end result was a stage-by-stage, dynamic characterization of the effect of Young's modulus on attachment and neuronal differentiation of mESC's.

In Chapter 4, it was found that attachment of mESC's in N2B27 medium was maximized on the softest GXG material, when compared to stiffer GXG materials. Despite this difference in initial attachment, subsequent expansion was unaffected by Young's modulus.

When immunocytochemistry analysis was carried out, it was found that neural precursor formation was maximized on the soft materials. However, flow cytometry analysis revealed that the proportion of the total cells that were neural precursors did not vary across the materials. A similar result was found when gene expression was measured by qPCR. Expression of pluripotent, neuronal and non-neuronal (other lineages) genes did not vary with Young's modulus. Taken together, these results suggest that soft materials increase the yield of neural precursors from mESC's without directly promoting neuronal differentiation. Instead, soft materials favour attachment of mESC's in N2B27 medium. This effect was found to not be dependent on F-actin or microtubule polymerization. Inhibition of these two processes had no effect on the maximization of attachment on soft materials.

The next stages of mESC differentiation into neurons were characterized in the same way in Chapter 5. First, mESC's were partially-differentiated for four days in N2B27 medium into nestin-positive neural precursors. These four-day partially-differentiated cells were seeded onto three GXG materials and TCP as before. Attachment of these partially-differentiated cells was again maximized on soft materials in N2B27 medium. The mean cellular projected area did not vary across materials and so did not contribute to the increased confluency on soft materials. Expansion and formation of β -III tubulin positive neurons was unaffected by GXG Young's modulus (although neurons did not form on the TCP control).

Flow cytometry and qPCR gene expression (for mature neurons) analysis revealed a similar result to before where an increase in neuronal yield on soft materials was not accompanied by an increase in proportion of total cells that were neuronal. Therefore, it was concluded that the increase in neuronal yield from partially-differentiated cells was due to favourable initial attachment of partially-differentiated cells and not a direct promotion of the neuronal fate. This effect was not dependent on stress fibre or microtubule polymerization.

Interestingly, qPCR analysis revealed that expression of non-neuronal astrocyte genes reduced on soft materials, compared to the TCP control. This implies that soft materials antagonize the astrocytic fate.

In the final experiments, mESC's were partially-differentiated further (for six days) into immature neurons to form partially-differentiated neurons. These partially-differentiated neurons were then allowed to attach and mature on the three GXG materials and TCP. Young's modulus had no significant ($p>0.05$) effect upon attachment of partially-differentiated neurons, in contrast to the previous findings. Expansion and formation of β -III tubulin again did not vary with Young's modulus. However, formation of mature, MAP2 positive cells was maximized on the soft materials despite no difference in attachment and expansion. The conclusion was made that soft materials directly promote the maturation of neurons, without promoting attachment. This was in contrast to the findings for early mESC neuronal differentiation.

Overall, the effect of Young's modulus on attachment and promotion of the neuronal fate are dependent upon cell maturity. The effect of modulus on attachment disappears as cells mature, whilst modulus begins to directly affect neuronal cell formation in more mature cells during neuronal differentiation. This will be a key consideration when designing future cell bioprocesses, as the entire differentiation stage cannot be considered as one process. Instead each stage of differentiation requires careful optimisation to maximise either attachment and by extension yield, or enrichment. This will also impact the design of biomaterials for neuronal tissue engineering, where materials will have to be carefully optimised for both attachment as well as differentiation, depending on the maturity levels of the cells.

6.2 Future Work

- The next immediate experiment to perform would be to drive mESC differentiation further towards clinically relevant populations of neurons, such as dopaminergic subtypes for treatment of Parkinson's. This would allow for the full characterization of the effect of Young's modulus on mESC neuronal differentiation into clinically relevant neuronal populations.
- One issue that was briefly touched upon earlier in Chapter 5 was the effect of Young's modulus upon the expression of GFAP, an astrocyte gene. Once further differentiation of neurons is characterized, this is where the impact of Young's modulus on promotion or antagonism of the astrocytic fate could be explored in further detail. These cells may be clinically relevant in their own right but will act as a contaminant in neuronal populations, particularly if they start undergoing glial scarring, which would significantly increase the Young's modulus of the material.
- Whilst actin stress fibers and microtubule networks are a very crucial element of the cell internal structure, they did not contribute to the cell response to Young's modulus. There are other structural components of the cell that do not play as key a role as the aforementioned molecules but may still prove vital in unlocking the reason why Young's modulus influences attachment as it does. Focal adhesion proteins, including integrins could be included in this study.
- Neuronal differentiation was chosen for study as it is perhaps the most well defined and intensely studied lineage for mouse embryonic stem cells, particularly in adherent monoculture, thanks to the Ying et al (2003) protocol. However, it would be very interesting to analyse the effects of Young's modulus on other lineages, which are associated with different ranges of Young's modulus to this study. It would be expected that whilst initial attachment of mESC's would show a similar result (as soft substrates are most

similar to that of the early mouse blastocyst), the effect of Young's modulus would change with maturation, particularly if cell function depends on certain mechanical characteristics. For example, cardiomyocytes are unable to contract and beat on materials, which are too soft or too stiff (Engler et al, 2008).

- Once the overall effect of Young's modulus on attachment is better understood, it would be interesting to investigate changes at the level of individual cells. Changes in softness could be measured by atomic force microscopy, for example. Optical tweezers could be used to investigate how cell stretching changes the effect of Young's modulus on attachment.
- GXG was used in this study as it is easier, faster and cheaper to produce than the majority of other biomaterials used for modulus studies. However, as seen in Kothapalli & Kramm's (2013) earlier work, different materials may produce different responses in cells.
- Although the biomaterials did support robust cell growth, individual steps in the synthesis protocols could be further optimized in order to improve their function further. An economic evaluation of the protocol could be performed in order to isolate the stages most suitable for optimization. A possible modification to the material could be to coat the materials with ECM component proteins.
- Once these effects are fully characterized in mouse, further characterization of the effect of Young's modulus on human embryonic stem cell or induced pluripotent stem cell differentiation into clinically relevant neuronal populations could be carried out.
- One of the benefits of using GXG is that it is easily scalable within the static culture format. It could be used to coat cell factories, for example. However in order to produce cells at a significantly larger scale, the bioreactor format may

be of greater use. In order to use bioreactors, cells may have to be cultured on microcarriers. Either the elasticity of the microcarriers themselves could be tuned using novel materials, or GXG could be used to coat microcarriers.

- Beyond the cell culturing stage, other processing stages may be impacted by the GXG coating of culture materials. Whilst robust processes for large scale harvesting and purification of target cells have yet to be developed, these steps are likely to be impacted by decisions made at the cell culture stage. If cells are harvested mechanically, it is possible that GXG may be removed along with the cells. Clumps of GXG or gelatin may interfere with further processing steps. This may necessitate appropriate design of further processing steps or a separate stage in order to remove GXG from the harvest material. The impact of GXG on downstream processing, as well as potential removal operations would require further investigation.
- As well as studying attachment, detachment on all Young's moduli could be studied in more detailed. One approach would be to use dilute solutions of trypsin in order to slowly enzymatically detach cells from GXG.
- In addition to the Young's modulus of elasticity, surface topography will have an important role in determining cell fate and attachment. Further study of the effect of topography using specially engineered biomaterials could be used for this study.
- Finally, coating the GXG material with key extracellular matrix proteins may aid in further improving cell attachment and differentiation. Laminin, for example, has been shown to play a key role in germ layer organization during gastrulation (Ingber, 2000).

7 References

1. Aguirre, A., Gonzalez, A., Navarro, M., Castano, O., Planell, J.A., Engel, E. (2012). "Control of microenvironmental cues with a smart biomaterials composite promotes endothelial progenitor cell angiogenesis." *European Cells and Materials* 24: 90-106
2. Anselme, K., Bigerelle, M. (2012). "On the Relation Between Surface Roughness of Metallic Substrates and Adhesion of Human Primary Bone Cells." *Scanning* 00:1-10
3. Baker, E., Zaman, M.H. (2009). "The Biomechanical Integrin." *Journal of Biomechanics* 43: 38-44
4. Baracskay, K.L., Kidd, G.J., Miller, R.H., Trapp, B.D. (2007). "NG2-positive cells generate A2B5-positive oligodendrocyte precursor cells." *Glia* 55(10): 1001-1010
5. Bakker, A.D., Klein-Nulend, J. (2010). "Mechanisms of Osteocyte Mechanotransduction." *Clinical Reviews in Bone and Mineral Metabolism* 8: 163-169
6. Banerjee, A., Arha, M., Choudhary, S., Ashton, R.S., Bhatia, S.R., Schaffer, D.V., Kane, R.S. (2009). "The influence of hydrogel modulus on the proliferation and differentiation of encapsulated neural stem cells." *Biomaterials* 30: 4695-4699
7. Ben-Shushan, E., Thompson, J.R., Gudas, L.J., Bergman, Y. (1998). "Rex-1, a gene encoding a transcription factor expressed in the early embryo, is regulated via Oct-3/4 and Oct-6 binding to an octamer site and a novel protein, Rox-1, binding to an adjacent site." *Molecular and Cellular Biology* 18(4): 1866-1878
8. Bernhardt, R., Matus, A.I. (1984). "Light and electron microscopy studies of the distribution of microtubule-associated protein 2 in rat brain: A difference between the dendritic and axonal cytoskeletons." *J Comp Neurol* 226: 203-219
9. Bian, L., Hou, C., Tous, E., Rai, R., Mauck, R.L., Burdick, J.A. (2013) "The influence of hyaluronic acid hydrogel crosslinking density and macromolecular diffusivity on human MSC chondrogenesis and hypertrophy." *Biomaterials* 34: 413-421
10. Chiron, S., Tomczak, C., Duperray, A., Laine, J., Bonne, G., Eder, A., Hansen, A., Eschenhagen, T., Verdier, C., Coirault, C. (2012). "Complex Interactions between Human Myoblasts and the Surrounding 3D Fibrin-Based Matrix." *PLoS One* 7(4): e36173

11. Chopra, A., Lin, V., McCollough, A., Atzet, S., Prestwich, G.D., Wechsler, A.S., Murray, M.E., Oake, S.A., Kresh, J.Y., Janmey, P.A. (2012). "Reprogramming cardiomyocyte mechanosensing by crosstalk between integrins and hyaluronic acid receptors." *Journal of Biomechanics* 45: 824-831
12. Chowdhury, F., Na, S., Li, D., Poh, Y., Tanaka, T.S., Wang, F., Wang, N. (2009). "Material properties of the cell dictate stress-induced spreading and differentiation in embryonic stem cells." *Nature Materials* 9: 82-88
13. Chowdhury, F., Li, Y., Poh, Y.C., Yokohama-Tamaki, T., Wang, N., Tanaka, T.S. (2010). "Soft substrates promote homogeneous self-renewal of embryonic stem cells via downregulating cell-matrix tractions." *PLoS One* 15(12):e15655
14. Christ, A.F., Franze, K., Gautier, H., Moshayedi, P., Fawcett, J., Franklin, R.J.M., Karadottir, R.T., Guck, J. (2010). "Mechanical difference between white and gray matter in the rat cerebellum measured by scanning force microscopy." *Journal of Biomechanics* 43: 2986-2992
15. Collingsworth, A.M., Zhang, S., Kraus, W.E., Truskey, G.A. (2002). "Apparent elastic modulus and hysteresis of skeletal muscle cells throughout differentiation." *American Physiological Society* 283: 1219-1227
16. Conti, L., Pollard, S.M., Gorba, T., Reitano, E., Toselli, M., Biella, G., Sun, Y., Sanzone, S., Ying, Q-L., Cattaneo, E., Smith, A. (2005). "Niche-Independent Symmetrical Self-Renewal of a Mammalian Tissue Stem Cell." *PLoS Biology* 3: 1594-1606
17. Bae, D., Mondragon-Teran, P., Hernandez, D., Ruban, L., Mason, C., Bhattacharya, S.S., Veraitch, F.S. (2012). "Hypoxia Enhances the Generation of Retinal Progenitor Cells from Human Induced Pluripotent and Embryonic Stem Cells." *Stem Cells and Development* 21(8): 1344-1355
18. Dahl, K.N., Booth-Gauthier, E.A., Ladoux, B. (2009). "In the middle of it all: Mutual mechanical regulation between the nucleus and the cytoskeleton." *Journal of Biomechanics* 43: 2-8
19. Davidson, L.A., Oster, G.F., Keller, R.E., Koehl, M.A. (1999) "Measurements of mechanical properties of blastula wall reveal which hypothesized mechanisms of primary invagination are physically plausible in the sea urchin *Strongylocentrotus purpuratus*." *Developmental Biology* 209: 221-238
20. Deroanne, C.F., Lapierre, C.M., Nusgens, B.V. (2001). "In vitro tubulogenesis of endothelial cells by relaxation of the coupling extracellular matrix-cytoskeleton." *Cardiovascular Research* 49: 647-658
21. Desai, A., Mitchison, T.J. (1997). "Microtubule polymerization dynamics." *Annual Review of Cell and Developmental Biology* 13: 83-117

22. Discher, D.E. (2009). "Growth Factors, Matrices, and Forces Combine and Control Stem Cells." *Science* 324: 1673-1677
23. Engler, A.J., Bacakova, L., Newman, C., Hategan, A., Griffin, M., Discher, D. (2004a). "Substrate Compliance versus Ligand Density in Cell on Gel Responses." *Biophysical Journal* 86: 617-628
24. Engler, A.J., Griffin, M.A., Sen, S., Bönnemann, C.G., Sweeney, H.L., Discher, D.E. (2004b). "Myotubes differentiate optimally on substrates with tissue-like stiffness: pathological implications for soft or stiff microenvironments." *The Journal of Cell Biology* 166(6): 877-887
25. Engler, A.J., Richert, L., Wong, J.Y., Picart, C., Discher, D.E. (2004c). "Surface probe measurements of the elasticity of sectioned tissue, thin gels and polyelectrolyte multilayer films: correlations between substrate stiffness and cell adhesion." *Surface Science* 570: 142-154
26. Engler, A.J., Sen, S., Sweeney, H.L., Discher, D.E. (2006). "Matrix Elasticity Directs Stem Cell Lineage Specification." *Cell* 126: 677-689
27. Engler, A.J., Carag-Krieger, C., Johnson, C.P., Raab, M., Tang, H., Speicher, D.W., Sanger, J.W., Sanger, J.M., Discher, D.E. (2008). "Embryonic Cardiomyocytes beat best on a matrix with heart-like elasticity: scar-like rigidity inhibits beating." *Journal of Cell Science* 121: 3794-3802
28. Eroshenko, N., Ramachandran, R., Yadavalli, V.K., Rao, R.R. (2013) "Effect of substrate stiffness on early human embryonic stem cell differentiation." *Journal of Biological Engineering* 7(1): 7
29. Evans, M.J., Kaufman, M.H. (1981) "Establishment in culture of pluripotent cells from mouse embryos." *Nature* 292: 154-156
30. Evans, N.D., Minelli, C., Gentleman, E., LaPointe, V., Patankar, S.N., Kallivretaki, M., Chen, X., Roberts, C.J., Stevens, M.M. (2009). "Substrate stiffness affects early differentiation events in embryonic stem cells." *European Cells and Materials* 18: 1-14
31. Ffrench-Constant, C., Hollingsworth, A., Heasman, J., Wylie, C.C. (1991). "Response to fibronectin of mouse primordial germ cells before and after migration." *Development* 113: 1365-1373
32. Finley, M.F.A., Devata, S., Huettner, J.E. (1999) "BMP-4 Inhibits Neural Differentiation of Murine Embryonic Stem Cells." *Journal of Neurobiology* 40(3): 271-287

33. Flanagan, L.A., Ju, Y.E., Marg, B., Osterfeld, M., Jamney, P.A. (2002). "Neurite branching on deformable substrates." *Neuroreport* 13: 2411-2415
34. Flanagan, L.A., Rebaza, L.M., Derzic, S., Schwartz, P.H., Monuki, E.S. (2006). "Regulation of Human Neural Precursor Cells by Laminin and Integrins." *Journal of Neuroscience Research* 83: 845-856
35. Fox, N., Damjanov, I., Martinez-Hernandez, A., Knowles, B.B., Solter, D. (1981). "Immunohistochemical localization of the early embryonic antigen (SSEA-1) in postimplantation mouse embryos and fetal and adult tissues." *Developmental Biology* 83(2): 391-398
36. Franze, K., Guck, J. (2010). "The biophysics of neuronal growth." *Reports on Progress in Physics* 73: 094601
37. Frilling, S., Andersson, E., Thompson, L.H., Jönsson, M.E., Hebsgaard, J.B., Nanou, E., Alekseenko, Z., Marklund, U., Kjellander, S., Volakakis, N., Hovatta, O., El Manira, A., Björklund, A., Perlmann, T., Ericson, J. (2009). "Efficient production of mesencephalic neurons by Lmx1a expression in embryonic stem cells." *Proceedings of the National Academy of Sciences USA*. 106(18): 7613-7618
38. Fuentes, D.E., Butler, P.J. (2012). "Coordinated Mechanosensitivity of Membrane Rafts and Focal Adhesions." *Cell Molecular Bioengineering* 5(2): 143-154
39. Gago, N., Avellana-Adalid, V., Baron-Van Evercooren, A., Schumacher, M. (2003). "Control of cell survival and proliferation of postnatal PSA-NCAM(+) progenitors." *Molecular and Cellular Neurosciences* 22(2): 162-178
40. Gao, Y., Ye, L., Kishi, H., Okagaki, T., Samizo, K., Nakamura, A., Kohama, K. (2001). "Myosin Light Chain Kinase as a Multifunctional Regulatory Protein of Smooth Muscle Contraction." *Life* 51: 337-344
41. Georges, P.C., Miller, W.J., Meaney, D.F., Sawyer, E.S., Janmey, P.A. (2006). "Matrices with Compliance Comparable to that of Brain Tissue Select Neuronal over Glial Growth in Mixed Cortical Cultures." *Biophysical Journal* 90:3012-3018
42. Ginis, I., Luo, Y., Miura, T., Thies, S., Brandenberger, R., Gerecht-Nir, S., Amit, M., Hoke, A., Carpenter, M.K., Itskovitz-Eldor, J., Rao, M.S. (2004). "Differences between human and mouse embryonic stem cells." *Developmental Biology* 269: 360-380
43. Grover, C.N., Gwynne, J.H., Pugh, N., Hamaia, S., Farndale, R.W., Best, S.M., Cameron, R.E. (2012). "Crosslinking and composition influence the surface properties, mechanical stiffness and cell reactivity of collagen-based films." *Acta Biomaterialia* 8: 3080-3090

44. Gunsilius, E., Gastl, G., Petzer, A.L. (2001). "Haematopoietic stem cells." *Biomedicine and Pharmacotherapy* 55(4): 186-194
45. Her, G.J., Wu, H.C., Chen, M.H., Chen, M.Y., Chang, S.C., Wang, T.W. (2013). "Control of three-dimensional substrate stiffness to manipulate mesenchymal stem cell fate toward neuronal or glial lineages." *Acta Biomaterialia* 9: 5170-5180
46. Hu, X., Park, S.H., Gil, E.S., Xia, X.X., Weiss, A.S., Kaplan, D.L. (2011) "The influence of elasticity and surface roughness on myogenic and osteogenic differentiation of cells on silk-elastin biomaterials." *Biomaterials* 32: 8979-8989
47. Ingber, D.E. (2006). "Mechanical control of tissue morphogenesis during embryological development." *The International Journal of Developmental Biology* 50: 255-266
48. Itoh, T., Ikebe, M., Kargacin, G.J., Hartshorne, D.J., Kemp, B.E., Fay, F.S. (1989). "Effect of modulators of myosin light-chain kinase activity in single smooth muscle cells." *Letters to Nature* 338: 164-167
49. Itskovitz-Eldor, J., Schuldiner, M., Karsenti, D., Eden, A., Yanuka, O., Amit, M., Soreq, H., Benvenisty, N. (2000). "Differentiation of human embryonic stem cells into embryoid bodies compromising the three embryonic germ layers." *Molecular Medicine* 6(2): 88-95
50. Jagielska, A., Norman, A.L., Whyte, G., Van Vliet, K.J., Guck, J., Franklin, R.J.M. (2012). "Mechanical Environment Modulates Biological Properties of Oligodendrocyte Progenitor Cells." *Stem Cells and Development* 21(16): 2905-2914
51. Jaramillo, M., Singh, S.S., Velankar, S., Kumta, P.N., Banerjee, I. (2012). "Inducing endoderm differentiation of modulating mechanical properties of soft substrates." *Journal of Tissue Engineering and Regenerative Medicine* 2012:10:1002
52. Jiang, F.X., Lin, D.C., Horkay, F., Langrana, N.A. (2011). "Probing Mechanical Adaptation of Neurite Outgrowth on a Hydrogel Material Using Atomic Force Microscopy." *Annals of Biomedical Engineering* 39(2): 706-713
53. Katsumi, A., Naoe, T., Matsushita, T., Kaibuchi, K., Schwartz, M.A. (2005). "Integrin Activation and Matrix Binding Mediate Cellular Responses to Mechanical Stretch." *The Journal of Biological Chemistry* 17: 16546-16549
54. Kehat, I., Kenyagin-Karsenti, D., Snir, M., Segev, H., Amit, M., Gepstein, A., Livne, E., Binah, O., Itskovitz-Eldor, J., Gepstein, L. (2001). "Human embryonic stem cells can differentiate into myocytes with structural and functional

- properties of cardiomyocytes.” *The Journal of Clinical Investigation* 108(3): 407-414
55. Kehat, I., Khimovich, L., Caspi, O., Gepstein, A., Shofti, R., Arbel, G., Huber, I., Satin, J., Itskovitz-Eldor, J., Gepstein, L. (2004) “Electromechanical integration of cardiomyocytes derived from human embryonic stem cells.” *Nature Biotechnology* 22: 1282-1289
 56. Keller, G. (2005). “Embryonic stem cell differentiation: emergence of a new era in biology and medicine.” *Genes and Development* 19: 1129-1155
 57. Keung, A.J., Healy, K.E., Kumar, S., Schaffer, D.V. (2009). “Biophysics and dynamics of natural and engineered stem cell microenvironments.” *Wiley Interdisciplinary Reviews: Systems Biology and Medicine* 2: 49-64
 58. Keung, A.J., Asuri, P., Kumar, S., Schaffer, D.V. (2012). “Soft microenvironments promote the early neurogenic differentiation but not self-renewal of human pluripotent stem cells.” *Integrative Biology* 4: 1049-1058
 59. Knoepfler, P.S. (2009). “Deconstructing Stem Cell Tumorigenicity: A Roadmap to Safe Regenerative Medicine.” *Stem Cells* 27(5): 1050-1056
 60. Kothapalli, C.R., Kamm, R.D. (2013). “3D matrix microenvironment for targeted differentiation of embryonic stem cells into neural and glial lineages.” *Biomaterials* 34: 5995-6007
 61. Krieg, M., Arboleda-Estudillo, Y., Puech, P.H., Kafer, J., Graner, F., Muller, D.J., Heisenberg, C.P. (2008). “Tensile forces govern germ-layer organization in zebrafish.” *Nature Cell Biology* 10: 429-436
 62. Kunze, A., Giugliano, M., Valero, A., Renaud, P. (2011). “Micropatterning neural cell cultures in 3D with a multi-layered scaffold.” *Biomaterials* 32: 2088-2098
 63. Lakins, J.N., Chin, A.R., Weaver, V.M. (2012). “Exploring the Link Between Human Embryonic Stem Cell Organization and Fate Using Tension-Calibrated Extracellular Matrix Functionalized Polyacrylamide Gels.” *Methods in molecular biology* 916: 317-350
 64. Lam, H.J., Patel, S., Wang, A., Chu, J., Li, S. (2010). “*In Vitro* Regulation of Neural Differentiation and Axon Growth by Growth Factors and Bioactive Nanofibers.” *Tissue Engineering: Part A* 16(8): 2641-2648
 65. Lam, W.A., Cao, L., Umesh, V., Keung, A.J., Sen, S., Kumar, S. (2010). “Extracellular matrix rigidity modulates neuroblastoma cell differentiation and N-myc expression.” *Molecular Cancer* 9: 35

66. Lancaster, M.A., Renner, M., Martin, C., Wenzel D., Bicknell, L.S., Hurles, M.E., Homfray, T., Penninger, J.M., Jackson, A.P., Knoblich, J.A. (2013). "Cerebral organoids model human brain development and microcephaly." *Nature*. Published online August 28th 2013.
67. LaPlaca, M.C., Prado, G.R. (2009). "Neural Mechanobiology and Neuronal Vulnerability to Traumatic Loading." *Journal of Biomechanics* 43: 71-78
68. Lee, H.H., Lee, H.C., Chou, C.C., Hur, S.S., Osterday, K., del Alamo, J.C., Lasheras, J.C., Chien, S. (2012). "Shp2 plays a crucial role in cell structural orientation and force polarity in response to matrix rigidity." *Proceedings of the National Academy of Sciences of the United States of America* 110(8): 2840-2845
69. Lee, H.Y., Oh, B.H. (2010). "Ageing and arterial stiffness." *Circulation Journal* 74(11): 2257-2262
70. Lee, S.H., Lumelsky, N., Studer, L., Auerbach, J.M., McKay, R.D. (2000). "Efficient generation of midbrain and hindbrain neurons from mouse embryonic stem cells." *Nature Biotechnology* 18: 675-679
71. Lei, Y., Gojgini, S., Lam, J., Segura, T. (2011). "The spreading, migration and proliferation of mouse mesenchymal stem cells cultured inside hyaluronic acid hydrogels." *Biomaterials* 32: 39-47
72. Lendahl, U., Zimmerman, L.B., McKay, R.D. (1990). "CNS stem cells express a new class of intermediate filament protein." *Cell* 60(4): 585-595
73. Levitan, I.B., Kaczmarek, L.K. (2002) "The Neuron: Third Edition." Oxford University Press, New York, USA, pp. 230-235, 375-387
74. Lewis, J.P., Trobaugh, F.E. (1964). "Haematopoietic Stem Cells." *Nature* 204: 589-590
75. Liepzig, N.D., Shoichet, M.S. (2009). "The effect of substrate stiffness on adult neural stem cell behaviour." *Biomaterials* 30: 6867-6878
76. Lo, C.M., Wang, H.B., Dembo, M., Wang, Y.L. (2000). "Cell movement is guided by the rigidity of the substrate." *Biophysics Journal* 79: 144-152
77. Lodish, H., Berk, A., Zipursky, S.L., Matsudaira, P., Baltimore, D., Darnell, J. (2004). "Molecular biology of the cell: 5th Edition." W.H. Freeman, New York, USA, pp.818
78. Lovett, D.B., Shekhar, N., Nickerson, J.A., Roux, K.J., Lele, T.P. (2013). "Modulation of Nuclear Shape by Substrate Rigidity." *Cellular and Molecular Bioengineering* 6(2): 230-238

79. Lu, T.Y., Lin, B., Kim, J., Sullivan, M., Tobita, K., Salama, G., Yang, L. (2013). “Repopulation of decellularised mouse heart with human induced pluripotent stem cell-derived cardiovascular progenitor cells.” *Nature Communications* 4:2307
80. Lu, Y.B., Franze, K., Selfert, G., Steinhäuser, C., Kirchhoff, F., Wolburg, H., Guck, J., Janmey, P., Wei, E.Q., Käs, J., Reichenbach, A. (2006). “Viscoelastic properties of individual glial cells and neurons in the CNS.” *Proceedings of the National Academy of Sciences USA* 103(47): 17759-1764
81. Lumelsky, N., Blondel, O., Laeng, P., Velasco, I., Ravin, R., McKay, R. (2001). “Differentiation of embryonic stem cells to insulin-secreting structures similar to pancreatic islets.” *Science* 292(5520): 1389-1394
82. Ma, W., Fitzgerald, W., Liu, Q.Y., O’Shaughnessy, T.J., Maric, D., Lin, H.J., Alkon, D.L., Barker, J.L. (2004). *Experimental Neurology* 190: 276-288
83. Ma, W., Tavakoli, T., Derby, E., Serebryakova, Y., Rao, M.S., Mattson, M.P. (2008). *BMC Developmental Biology* 8:90
84. Mason, C., Dunnill, P. (2008). “A brief definition of regenerative medicine.” *Regenerative Medicine* 3(1): 1-5
85. McMurray, R.J., Gadegaard, N., Tsimbouri, P.M., Burgess, K.V., McNamara, L.E., Tare, R., Murawski, K., Kingham, E., Oreffo, R.O.C., Dalby, M.J. (2011). “Nanoscale surfaces for the long-term maintenance of mesenchymal stem cell phenotype and multipotency.” *Nature Materials* 10: 637-644
86. Merryman, D., Engler, A.J. (2010). “Innovations in cell mechanobiology.” *Journal of Biomechanics* 43: 1
87. Migliorini, E., Grenci, G., Ban, J., Pozzato, A., Tormen, M., Lazzarino, M., Torre, V., Ruaro, M.E. (2011). “Acceleration of Neuronal Precursors Differentiation Induced by Substrate Nanotopography.” *Biotechnology and Bioengineering* 108: 2736-2746
88. Min, J.Y., Yang, Y., Converso, K.L., Liu, L., Huang, Q., Morgan, J.P., Xiao, Y.F. (2002). “Transplantation of embryonic stem cells improves cardiac function in postinfarcted rats.” *Journal of Applied Physiology* 92(1): 288-296
89. Minev, I.R., Moshayedi, P., Fawcett, J.W., Lacour, S.P. (2013). “Interaction of glia with a compliant, microstructured silicone surface.” *Acta Biomaterialia* 9(6): 6936-6942
90. Mokry, J., Nemecek, S. (1998) “Angiogenesis of extra- and intraembryonic blood vessels is associated with expression of nestin in endothelial cells.” *Folia biologica* 44(5): 155-161

91. Mondragon-Teran, P., Lye, G.J., Veraitch, F.S. (2009). "Lowering Oxygen Tension Enhances the Differentiation of Mouse Embryonic Stem Cells into Neuronal Cells." *Biotechnology Progress* 25: 1480-1488
92. Morizane, A., Li, J.Y., Brundin, P. (2008). "From bench to bed: the potential of stem cells for the treatment of Parkinson's disease." *Cells and tissue research* 331: 323-336
93. Moshayedi, P., Costa, L.F., Christ, A., Lacour, S.P., Fawcett, J., Guck, J., Franze, K. (2010). "Mechanosensitivity of astrocytes on optimized polyacrylamide gels analysed by quantitative morphometry." *Journal of Physics: Condensed Matter* 22: 194114
94. Murayama, Y., Mizuno, J., Kamakura, H., Fueta, Y., Nakamura, H., Akaishi, K., Anzai, K., Watanabe, A., Inui, H., Omata, S. (2006). "Mouse zona pellicula dynamically changes its elasticity during oocyte maturation, fertilization and early embryo development." *Human Cell* 19(4): 119-125
95. Myers, K.A., Applegate, K.T., Danuser, G., Fischer, R.S., Waterman, C.M. (2011) "Distinct ECM mechanosensing pathways regulate microtubule dynamics to control endothelial cell branching morphogenesis." *Journal of Cell Biology* 192(2): 321-334
96. Nakamura, A., Xie, C., Zhang, Y., Gao, Y., Wang, H., Ye, Li., Kishi, H., Okagaki, T., Yoshiyama, S., Hayakawa, K., Ishikawa, R., Kohama, K. (2007). "Role of non-kinase activity of myosin light-chain kinase in regulating smooth muscle contraction." *Biochemical and Biophysical Research Communications* 369: 135-143
97. Nelson, D., Cox, M. (2004) "*Lehninger Principles of Biochemistry: Fourth Edition.*" W.H. Freeman, New York, USA, pp. 182
98. Nichols, J., Zevnik, B., Anastassiadis, K., Niwa, H., Klewe-Nebenius, D., Chambers, I., Schöler, H., Smith, A. "Formation of pluripotent stem cells in the mammalian embryo depends on the POU transcription factor Oct4." *Cell* 95(3): 379-391
99. Nikkah, M., Edalat, F., Manoucheri, S., Khademhosseini, A. (2012). "Engineering microscale topographies to control the cell-substrate interface." *Biomaterials* 33: 5230-5246
100. Niwa, H., Burdon, T., Chambers, I., Smith, A. (1998). "Self-renewal of pluripotent embryonic stem cells is mediated via activation of STAT3." *Genes and Development* 12: 2048-2060

101. Okada, Y., Shimazaki, T., Sobue, G., Okano, H. (2004) "Retinoic-acid-concentration-dependent acquisition of neural cell identity during in vitro differentiation of mouse embryonic stem cells." *Developmental Biology* 275: 124-142
102. Okuda, A., Fukushima, A., Noshimoto, M., Orimo, A., Yamagishi, T., Nabeshima, Y., Kuro-o, M., Nabeshima, Y., Boon, K., Keaveney, M., Stunnenberg, H.G., Muramatsu, M. (1998). "UTF1, a novel transcription coactivator expressed in pluripotent embryonic stem cells and extra-embryonic cells." *The EMBO Journal* 17(7): 2019-2032
103. Pachernik, J., Esner, M., Bryja, V., Dvorak, P., Hampl, A. (2002). "Neural differentiation of mouse embryonic stem cells grown in monolayer." *Reproduction Nutrition Development* 42: 317-326
104. Parasiodou, L., Xie, C., Cho, H.J., Lin, X., Gu, X-L., Long, C-X., Lobbestael, E., Baekelandt, V., Taymans, J-M., Sun, L., Cai, H. (2009). "Phosphorylation of Ezrin/Radixin/Moesin Proteins by LRRK2 Promotes the Rearrangement of Actin Cytoskeleton in Neuronal Morphogenesis." *Journal of Neuroscience* 29: 13971-13980
105. Park, D., Xiang, A.P., Zhang, L., Mao, F.F., Walton, N.M., Choi, S.S., Lahn, B.T. (2009). "The radial glia antibody RC2 recognizes a protein encoded by nestin." *Biochemical and Biophysical Research Communications* 382(3): 588-592
106. Paszek, M.J., Zahir, N., Johnson, K.R., Lakins, J.N., Rozenburg, G.I., Gefen, A., Reinhardt-King, C.A. Marguiles, S.S., Dembo, M., Boettiger, D., Hammer, D.A., Weaver, V.M. (2005). "Tensional homeostasis and the malignant phenotype." *Cancer Cell* 8: 241-254
107. Pelham, R.J., Wang, Y. (1997). "Cell locomotion and focal adhesions are regulated by substrate flexibility." *Proceedings of the National Academy of Sciences USA*. 94: 13661-13665
108. Peyton, S.R., Putnam, A.J. (2005) "Extracellular matrix rigidity governs smooth muscle motility in a biphasic fashion." *Journal of Cellular Physiology* 204(1): 198-209
109. Pillarisetti, A., Desai, J.P., Ladjal, H., Schiffmacher, A., Ferreira, A., Keefer, C.L. (2011) "Mechanical Phenotyping of Mouse Embryonic Stem Cells: Increase in Stiffness with Differentiation." *Cellular Reprogramming* 13(4): 371-380
110. Poh, Y., Chowdhury, F., Tanaka, T.S., Wang, N. (2010) "Embryonic Stem Cells Do Not Stiffen on Rigid Substrates." *Biophysical Journal* 99: L19-L21

111. Pompe, T., Kaufmann, M., Kasimir, M., Johne, S., Glorius, S., Renner, L., Bobeth, M., Pompe, W., Werner, C. (2011). "Friction-Controlled Traction Force in Cell Adhesion." *Biophysical Journal* 101: 1863-1870
112. Prager-Khoutorsky, M., Lichtenstein, A., Krishnan, R., Rajendran, K., Mayo, A., Kam, Z., Geiger, B., Bershadsky, A.D. (2011). "Fibroblast polarization is a matrix-rigidity dependent process controlled by focal adhesion mechanosensing." *Nature Cell Biology* 13(12): 1457-1466
113. Previtera, M.L., Hui, M., Verma, D., Shahin, A.J., Schloss, R., Langrana, N.A. (2013). "The Effects of Substrate Elastic Modulus on Neural Precursor Cell Behavior." *Annals of Biomedical Engineering* 41(6): 1193-1207
114. Prosser, B.L., Ward, C.W., Lederer, W.J. (2011). "X-ROS signalling: rapid mechano-chemo transduction in heart." *Science* 333(6048): 1440-1445
115. Rao, M.S. (2006). "Neural Development and Stem Cells." Humana Press, Totowa, USA, pp. 54, 67-84
116. Rienzo, C.D., Jacchetti, E., Cardarelli, F., Bizzarri, R., Beltram, F., Cecchini, M. (2013). "Unveiling LOX-1 receptor interplay with nanotopography: mechanotransduction and atherosclerosis onset." *Scientific Reports* 3: 1141
117. Saha, K., Keung, A.J., Irwin, E.F., Li, Y., Little, L., Schaffer, D.V., Healy, K.E. (2008). "Substrate Modulus Directs Neural Stem Cell Behavior." *Biophysical Journal* 95: 4426-4438
118. Seuntjens, E., Umans, L., Zwijnen, A., Sampaolesi, M., Verfaillie, C.M., Huylebroeck, D. (2009). "Transforming Growth Factor typebeta and Smad family signalling in stem cell function." *Cytokine & Growth Factor Reviews* 20: 449-458
119. Skoglund, P., Rolo, A., Chen, X., Gumbiner, B.M., Keller, R. (2008). "Convergence and extension at gastrulation require a myosin II-b dependent cortical actin network." *Development* 135: 2435-2445
120. Smukler, S.R., Runciman, S.B., Xu, S., van der Kooy, D. (2006). "Embryonic stem cells assume a primitive neural stem cell fate in the absence of extrinsic influences." *The Journal of Cell Biology* 172(1): 72-90
121. Soria, B., Roche, E., Berná, G., León-Quinto, T., Reig, J.A., Martín, F. (2000). "Insulin-secreting cells derived from embryonic stem cells normalize glycemia in streptozotocin-induced diabetic mice." *Diabetes* 49(2): 157-162
122. Stadtfeld, M., Nagaya, M., Utikal, J., Weir, G., Hochedlinger, K. (2008). "Induced Pluripotent Stem Cells Generated Without Viral Integration." *Science* 322: 945-949

123. Stolberg, S., McCloskey, K.E. (2009). "Can Shear Stress Direct Stem Cell Fate?" *Biotechnology Progress* 25: 10-19
124. Sullivan, K.F., Cleveland, D.W. (1986). "Identification of conserved isotype-defining variable region sequences for four vertebrate beta tubulin polypeptide classes. *Proc Natl Acad Sci USA* 83(12): 4327-4331
125. Takahashi, K., Yamanaka, S. (2006). "Induction of pluripotent stem cells from mouse embryonic and adult fibroblast cultures by defined factors." *Cell* 126(4): 663-676
126. Takebe, T., Sekine, K., Enomura, M., Koike, H., Kimura, M., Ogaeri, T., Zhang, R., Ueno, Y., Zheng, Y., Koike, N., Aoyama, S., Adachi, Y., Taniguchi, H. (2013) "Vascularized and functional human liver from an iPSC-derived organ bud transplant." *Nature* 499(7459): 481-484
127. Tan, F., Naciri, M., Dowling, D., Al-Rubeai, M. (2012) "In vitro and in vivo bioactivity of CoBlast hydroxyapatite coating and the effect of impaction on its osteoconductivity." *Biotechnology Advances* 30(1): 352-362
128. Tee, S., Bausch, A.R., Janmey, P.A. (2009). "The Mechanical Cell." *Current Biology* 19: 745-748
129. Thomson, J.A., Itsovitz-Eldor, J., Shapiro, S.S., Waknitz, M.A., Swiergiel, J.J., Marshall, V.S., Jones, J.M. (1998). "Embryonic Stem Cells Derived from Human Blastocysts." *Science* 282: 1145-1147
130. Tsukita, S., Yonemura, S., Tsukita, S. (1997). "ERM proteins: head-to-tail regulation of actin-plasma membrane interaction." *Trends in Biochemical Sciences* 22: 53-58
131. Van Dyke, W.S., Sun, X., Richard, A.B., Nauman, E.A., Akkus, O. (2012). "Novel mechanical bioreactor for concomitant fluid shear stress and substrate strain." *Journal of Biomechanics* 45: 1323-1327
132. Wang, N., Tytell, J.D., Ingber, D.E. (2009). "Mechanotransduction at a distance: mechanically coupling the extracellular matrix with the nucleus." *Nature Review Mol. Cell Biol.* 10: 75-82
133. Wei, W.C., Lin, H.H., Shen, M.R., Tang, M.J. (2008). "Mechanosensing machinery for cells under low substratum rigidity." *American Journal of Physiology. Cell Physiology* 295(6): 1579-1589
134. Westfall, M.V., Paszk, K.A., Yule, D.I., Samuelson, L.C., Metzger, J.M. (1997). "Ultrastructure and cell-cell coupling of cardiac myocytes differentiating in embryonic stem cell cultures." *Cell motility and the Cytoskeleton* 36: 43-54

135. Wichter, H., Peljto, M. (2008). "Differentiation of Mouse Embryonic Stem Cells to Spinal Motor Neurons." *Current Protocols in Stem Cell Biology Chapter 1: Unit 1H.1.1-1H.1.9*
136. Wilkinson, D.G., Bhatt, S., Herrmann, B.G. (1990). "Expression pattern of the mouse T gene and its role in mesoderm formation." *Nature* 343: 657-659
137. Wolpert, L., Jessell, T., Lawrence, P., Meyerowitz, E., Robertson, E., Smith, J., (2007). "Principles of Development: Third Edition." Oxford University Press, New York, USA, pp. 332-334, 387-417
138. Yang, Y., Kulangara, K., Lam, R.T.S., Dharmawan, R., Leong, K.W. (2012). "Effects of Topographical and Mechanical Property Alterations Induced by Oxygen Plasma Modification on Stem Cell Behavior." *American Chemical Society: Nano* 6(10): 8591-8598
139. Yeung, T., Georges, P.C., Flanagan, L.A., Marg, B., Ortiz, M., Funaki, M., Zahir, N., Ming, W., Weaver, V., Janmey, P.A. (2005). "Effects of Substrate Stiffness on Cell Morphology, Cytoskeletal Structure and Adhesion." *Cell Motility and the Cytoskeleton* 60:24-34
140. Ying, Q., Stavridis, M., Griffiths, D., Li, M., Smith, A. (2003). "Conversion of embryonic stem cells into neuroectodermal precursors in adherent monoculture." *Nature* 21: 183-186
141. Young, T., Kelland, P. (1845). "A course of lectures on natural philosophy and the mechanical arts." Taylor and Walton, London, UK, Lecture XIII: pp.106
142. Yu, C.C., Woods, A.L., Levison, D.A. (1992). "The assessment of cellular proliferation by immunocytochemistry: a review of currently available methods and their applications." *The Histochemical Journal* 24(3): 121-131
143. Yu J, Vodyanik MA, Smuga-Otto K, Antosiewicz-Bourget J, Frane JL, Tian S, Nie J, Jonsdottir GA, Ruotti V, Stewart R, Slukvin II, Thomson JA. (2007). "Induced pluripotent stem cell lines derived from human somatic cells." *Science* 383: 1917-1920
144. Zatti, S., Zoso, A., Serena, E., Luni, C., Cimetta, E., Elvassore, N. (2012). "Micropatterning Topology on Soft Substrates Affects Myoblast Proliferation and Differentiation." *Langmuir* 28: 2718-2726
145. Zhang, K., Li, L., Huang, C., Shen, C., Tan, F., Xia, C., Liu, P., Rossant, J., Jing, N. (2010). "Distinct functions of BMP4 during different stages of mouse ES cell neural commitment." *Development* 137(13): 2095-2105

146.Zhao, L., Shim, J.W., Dodge, T.R., Robling, A.G., Yokota, H. (2013). "Inactivation of Lrp5 in osteocyte reduces Young's modulus and responsiveness to the mechanical loading." *Bone* 54: 35-43

147.Zhou, W., Freed, C.R. (2009) "Adenoviral gene delivery can reprogram human fibroblasts to induced pluripotent stem cells." *Stem Cells* 27(11): 2667-2674